UNIVERSITY OF LONDON THESIS

Degree PhD Year 2007 Name of Author SHAHRBAF DARVAZEHNOIE, Akbar

Stability of Ships with Forward Speed

by

Akbar Shahrbaf Darvazehnoie

A dissertation submitted for the degree of Doctor of Philosophy in the faculty of Engineering University of London

Department of Mechanical Engineering
University College London

March 2006

ProQuest LLC
789 East Eisenhower Parkway
P.O. Box 1346
Ann Arbor, MI 48106-1346

ABSTRACT

The initial stability of a ship is currently evaluated by empirical formula based largely on a static approach. Evidently stability is affected by speed that causes variation of pressure distribution on the wetted surface of a ship's hull, and generated waves on the surface of water by the vessel's motion. Forces and moments resulting from bottom pressures, as the speed of the ship changes, are significantly different for the ship at rest and in a seaway. The principal aim of the research is to investigate the effect of variations of forward speed on stability of a ship in calm water. The thesis presents theoretical and experimental approaches of the research. The novelty of the research results leads to the conclusion that although increasing speed may improve the stability of a ship in some cases, it also depends on heeling angle or on any asymmetry of the wetted area of a hull. Taking into account asymmetry effects, unbalanced pressure distribution acting on the wetted surface of the hull, in some cases, hence, decrease of stability is also possible.

On a moving, partially immersed body, hydrodynamic and hydrostatic forces predominate. These forces arise owing to interaction between the body's motion and its weight with respect to the surrounding water. In order to calculate these forces, the panel method of Computational Fluid Dynamics (CFD) has been applied to identify the velocity and pressure distribution on the wetted surface of a ship's hull. The mathematical model adopted is based on the source distribution on the ship's hull, known as the Kelvin source. The model for a body travelling with steady forward speed, where its motion does not disturb the free surface, is known as double body theory. For consideration of waves generated by the motion of the ship on the free surface, a three dimensional linearised potential flow solution has been utilised.

Comprehensive tests conducted in the UCL towing tank have established a better understanding of the significance of variation of ship's stability associated with forward speed in calm water. It is shown that an accurate judgement regarding the ship's stability cannot be made if only the effect of forward speed, as a single parameter, is considered. The heeling angle is another important parameter that must

also be taken into account. The effects of a combination of both variables have been investigated, and are reported herein.

The research is presented showing that the applied CFD method may be developed as an alternative method to assess stability of a ship in seaway, but there is a long way for the CFD approach to replace towing tank testing. At present, CFD may be used for consideration as a precursor to improve ship's stability during the design stage, for modification, and before operation. It is hoped that in future the findings of the experimental approach of this form of research could be used as additional guidance to be incorporated within the stability documentation for individual ships at the design stage, and ship trials.

ACKNOWLEDGMENTS

I wish to thank the Minister of Science, Research and Technology of Islamic Republic of Iran that provided this opportunity and financially supported this research for three years.

My gratitude goes to the late Prof. R K Burcher for encouragement and advice during the initial period of research.

I would like to thank Prof. G X Wu for his valuable suggestion and guidance in using the panel method and application of the Green's function.

My special thanks go to Dr. G J Lyons for encouragement and valuable supervision in replacement of Prof. Burcher, since before the transfer from MPhil to Ph.D.

I wish to express my appreciation firstly to Mr. D Fellows for great guidance and valuable comments, and all members of the Santa Fe lab, and the Fluid lab, Naval Architecture, and secretaries of the Department of Mechanical Engineering UCL.

I wish also to express my great appreciation firstly to Dr. Kara for great guidance and valuable comments, and all members of SSRC University of Strathclyde, Glasgow, Secondly Mr. Carter and all members of the School of Marine Science and Technology University of Newcastle upon Tyne.

I would like to draw attention to the efforts of the professional people, who have advised me in various conferences.

Finally I would also like to cordially express my sincere gratitude to my family for being extremely patient and strong through the tough times. I owe them a lot, as I could not properly accomplish my duties towards them throughout the work.

NOMENCLATURE

$a_{\varphi\varphi}$	Added mass
A_{ij}	Normal velocity coefficient
b	Breadth, beam, width
B, B_0, B_1	Centre of Buoyancy
B_{ij}	Component of velocity potential
B_{44}	Damping
BM	Vertical distance from the buoyancy centre to the metacentre point
C	Non-dimensional residuary stability coefficient
C_{44}	Restoring stiffness
CL	Centre line
d	Draft, Draught
D	Buoyancy force
f_{ik}	Force on each panel, i^{th}, in each direction k
F_k	Represents the x, y, and z components of the resultant force
Fn	Froude number
Fz	The vertical forces
$f_\varsigma(\xi,\eta)$	Source strength distributed on the body
G, G_1, g, g_1	Centre of gravity
$G(x,y,z;\xi,\eta,\zeta)$	Green's function for infinite depth with forward speed
ga	Gravity Acceleration
GM, H	Metacentric height
GZ	Righting arm or righting lever
I	Second moment of area
i_B	Gyration radius
I_{xx}	Inertia
K	Wave number
KB	Vertical distance from keel to the buoyancy centre
KG	Vertical distance from keel to the centre of gravity
KM	Vertical distance from the keel to the metacentre
L, l	Length

M	Metacentre point
Mh	Heeling moment
Mr	Righting moment
MS	Residuary stability lever
$\vec{n}$	Normal to the panel pointing out of the surface
n_x , n_y , n_z	Components of the normal
n_1 to n_6	Mode motion (Surge, Sway, Heave, Roll, Pitch and Yaw) respectively.
OX,Y,Z	Reference coordinate system
ox,y,z	Global coordinate system
P	Pressure
p(x,y,z)	Field point due to a source
$Q(\xi,\eta,\zeta)$	Source point over the boundary
r	Distance between a field point to a source point
r'	Distance between a field point image to a source point
r_0	The initial value of BM
Rw	Wave resistance
s_j	The j^{th} flat panel area
s_0	Underwater ship hull area
T_φ	Rolling period
u,v,w	Component of velocity
V(x,y,z)	Velocity vector
W, w	Weight
WL, W_0L_0, W_1L_1	Water line
X=(x,y,z)	A point from the Cartesian coordinate system origin fixed on the mid ship
ζ_w	Wave elevation on the free surface
ϕ	Inclination angle
Φ	Potential function
Φ_{body}	Potential due to steady forward speed of the ship
$\Phi_{body-image}$	Potential due to the effect of the mirror of the ship's hull
$\Phi_{freesurface}$	Potential due to free surface effect

$o\xi,\eta,\zeta$	Local coordinate system
ρ	Water density
σ	Source strength (intensity)
σ	Source strength in the case of the linearized problem, in the region below the equilibrium free surface boundary
σ_j	Source strength on the panel j^{th}
v	Volume of a wedge
∇	Under water volume of a vessel
Λ	Coefficient

ABBREVIATION:

BEM	Boundary Element Method
BK	Bilge Keels
BMT	British Maritime Technology
CAD	Computer Aided Design
CFD	Computational Fluid Dynamics
DNV	Det Norsk Veritas
DSP	Design Support Problem
GCS	Global Coordinate system
GL	Germanischer Lloyd
IMO	International Maritime Organisation
LR	Lloyds Register of Shipping
OFG	Overlay Frame Grabber
OSI	Operational Ship Inclining
PDE	Partial Differential Equations
PRS	Polski Rejesetr Statkow
RANS	Reynolds Averaged Navier Stokes
RHS	Right Hand Side
RINA	The Royal Institution of Naval Architects
SNAME	Society of Naval Architects and Marine Engineers
SSRC	Ship Stability Research Centre University of Strathclyde in Glasgow
UCL	University College London
2D	Two dimensional
3D	Three dimensional

To my family

FIGURES

TABLES

1. INTRODUCTION

Vast ranges of ships are continuously needed to be designed and constructed, either for profit or pleasure. They are required to carry commercial cargoes, people, or both. Geometry, space, and necessary equipment, according to the type of vessel, are all fundamental factors that need to be considered when designing and constructing a ship. In addition, an authority must certify the design and construction. The appropriate authority is an accepted source of expert information so as to satisfy given regulations and registration requirements. Vessels must comply with international or local regulations of the authority, where they may operate. This is known as a vessel's class. This arrangement should lead to an acceptable level of safety. However the definition of an acceptable level of safety is a contentious issue since increased safety implies increased cost.

One of the most important issues for ship safety is its ability to resist capsizing, otherwise referred to as its stability. The stability should be considered at the design stage, as well as during construction, or as a consequence of any modification, throughout the lifetime of the ship. Traditional ship stability criteria are based on the analysis of the static roll moment curve. Although this curve is an important ship characteristic in assuring ship safety, Falzarano and Troesch (1990), Burcher (1990), other ship characteristics are also significant. These include effects of hydrodynamic forces on the ship's hull as a consequence of ship speed.

Increasing demands for speed in marine transports have expanded the interest in vessels having some part of their weight supported by dynamic forces. The emphasis on speed results in development of hydrodynamic efficiency, lightweight, safe hull forms and a large increase in production cost. In this regard, ships hull forms may be categorized as displacement, semi-displacement and planing. Hence, very detailed design and engineering attention are required to ensure success to make reduced risk decisions relative to the design, and development of production of a high speed ship.

Generally, it is assumed that the stability of a vessel to be independent of speed. However, in case of small high speed craft it is becoming progressively evident that

this assumption is not valid, and it is given much thought. Small craft exhibit a loss of stability at high speed even though they possess adequate stability at rest. In some cases, instability can result in forceful and / or random motion which can lead to structural damage and crew injury; however, the problems are not readily apparent. Often they are uncovered after extended time in service and only after the regular explanations for unusual handling characteristics, such as inadequate operator quality and training, environment problem i.e. waves everywhere, and so on.

Despite the relatively serious problem, and massive attention has been paid on dynamic stability over the past, progress has been very limited, and very little is known about the fundamental characteristic and no guidelines presently exist to assure adequate dynamic stability Cohen S H, and Blount D L (1986), Burcher (1990), and Blount D L, Codega L T. (1992).

Through the years the level of designs has improved by application of some accepted empirical formula, and criteria. These criteria and empirical formula are successful to reduce accidents and incidents in their limitation conditions, especially for displacement hull. They have become stretched beyond their intended application for the new development of high speed craft. As an example, static stability criteria are based on technology that does not consider pressures generated by fluid velocity relative to the hull form.

Therefore, once speed is considered to be important, it is well known that in following, quartering, and head seas a high speed vessel can capsize by broaching, parametric rolling or stability reduction by waves Burcher (1990) and Dallinga et al (1998). Even in calm water a high speed craft can show unique motion characteristics, such as a chine walking, sudden large heel and porpoising, Ikeda and Katayama (2000). Some of these problems are known for both types of displacement and semi-displacement craft. However, due to demand of high speed marine transportation, and conventional mono-hull vessels, the transverse stability of a displacement type running in calm water at relatively high speed required review. Reduction in the stability may be caused by bottom pressure distribution and the wave pattern on the side of the hull. Among the literature there is very little about

effects of hydrodynamic forces on stability, in other words, variation of stability of ship in seaway is poorly understood when speed is important.

The aim of the present research is investigation and analyses of variation of forward speed on the stability of ships in calm water. Therefore, the present work is divided into theoretical and experimental parts. In the theoretical part of the research a steady velocity potential of Computational Fluid Dynamic (CFD) method is applied for computing pressure distribution, and considering its effect on the wetted surface of the hull for a range of forward speeds. The computed bottom pressures and their vectors were then integrated to find the righting moments. For the experiment, rolling motion was examined in accordance with different forward speed a long towing of a model in a towing tank.

A brief review on key points and definitions relating to ship motion, metacentric height, stability, and effects of ship dimension and loading on ship stability are presented in the Appendix A of current thesis as basic definitions, and conventions. The structure of the research conducted, is also described in this chapter.

1.2 PRINCIPAL AXES AND CORRESPONDING MOTIONS

In an arbitrary three-dimensional co-ordinate system, a ship can have up to six degrees of freedom. Three orthogonal axes may thus define any movement of a ship. These movements include three translations along axes, x, y and z, and three rotations about the same axes. Translations along the axes are referred to as 'surge', 'sway', and 'heave'. The corresponding rotations are denoted as 'roll', 'pitch', and 'yaw'. Figure 1.1 shows the principal axes with their origin at mid-ship and the corresponding motions related to the axes.

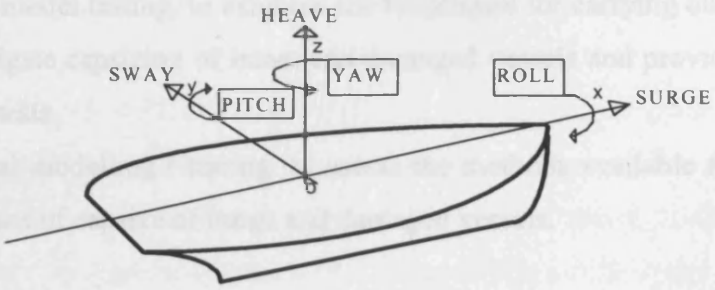

Figure 1.1 Principal axes and the corresponding motions of a ship

1.3 PROBLEM, LIMITATION AND SCOPE OF THE RESEARCH

The number of casualties and stability problems with fishing vessels, pleasure and small craft, conventional and unconventional ships with respect to speed show requirement of improving methodologies and international contribution efforts on stability assessment. In spite of the fact that several investigations associated with motion of a ship may be found in the literatures, that attention has been paid on stability in which dynamic forces are involved, but very little can be found on effects of solely forward speed on the stability.

Lundgren and Storch (1984) shown that initial static metacentric height (GM) is not a completely adequate measure of stability. In an extensive research plan for the investigation of dynamic instability of small high speed craft organised by Cohen et. al. (1986), they showed small high speed craft lose stability while underway even though they possess adequate stability at rest. Dynamic stability of planing boats has been investigated very well by Blount and Codega (1992). They showed nonoscillatory instability of planing boats for expected operating conditions. Through the years it became clear that dynamic instabilities are varied and depend upon a number of factors, including speed, displacement and hull forms.

More importantly, there are long term programmes that have started world wide, and associations between researchers are being formed in the ITTC to ensure continuous progress of development and ship safety utilises state-of-the-art knowledge, as is reported in 21st session of the ITTC. The ITTC (1996) recommended the following tasks to the executive specialist committee on ship stability:

- Physical model testing, to examine the techniques for carrying out model tests to investigate capsizing of intact and damaged vessels and provide guidelines for such tests.
- Numerical modelling / testing, to assess the methods available for numerical simulations of capsize of intact and damaged vessels.

As model testing is more or less a part of ship design today, the result of the physical modelling test, guidelines, may improve level of stability for high speed demand of today's transportation. In parallel, a proper numerical modelling may reduce significantly time and cost of a new design and / or any modifications on an existing ship.

Therefore, the principal aim of the research was to investigate the effects of variation of forward speed itself on the ship stability in calm water, without considering any excitation forces or moments. Then the variation of the GM was studied at different forward speeds theoretically and experimentally.

The main aim of the theoretical part of the work is to calculate the total reaction of the contribution of hydrostatic and hydrodynamic forces acting on the wetted surface of a hull. These forces are, in fact, the interaction between the immersed part of the vessel with surrounding water in a seaway. In conjunction with the above, the effect of different speeds is also examined.

Most previous numerical studies have used simple shapes such as a sphere or an ellipsoid, whereas in the work presented here a real ship shape is considered. A real ship shape has two associated problems regarding grid generation. Firstly, each cross section curve has to be defined by offsets individually, as there is no mathematical formula to express them. Secondly, the real bow and stern should not be ignored, and their offsets need to be taken into account. Then in theoretical consideration a mesh generation computer code and a panel method computer solver have been developed.

Over the years, several potential flow methods (analytical and numerical) have been developed to calculate hydrodynamic forces acting on bodies in a flow field. Analytical solutions however have been applied for only a limited number of shapes

such as spheroids, ellipsoids, etc, for more detail refer to Evans (1992). On the other hand, numerical solutions have been developed for both simple and complex shapes. For most practical hydrodynamic and aerodynamic problems, the panel method is a very good approach to identify the forces on the body in a flow field. This methodology has been used successfully for many marine vessel designs. Some of them are mentioned by Larsson (1998), and some research in this regard as respond to the recommended task of 21st ITTC presented in 22nd and 23rd sessions of ITTC.

The experiments carried out consisted of model testing conducted in the towing tank at UCL. The aim has been to investigate the behaviour of a ship's stability in calm water experiencing forward speed. A number of experimental publications exist, which consider the effect of environmental conditions on stability of a ship in a seaway in the presence of waves for following, beam, and quartering seas Kirsi and Paulling (1990) and Dudziak (1975). Some experiments have demonstrated unexpected capsizing for heading seas Burcher (1990), and Dallinga et al. (1998).

However, to date, the severity of the effect of speed on the stability of a ship has been poorly understood. In fact, locations of vessel centroids, such as centre of buoyancy (*C* of *B*) and metacentric height (G*M*), change by the contribution of hydrostatic and hydrodynamic forces and consumables loads that change the location of centre of gravity (C of G). In other words, it is clear that once a partially immersed body moves, its stability characteristics will be different compared with when the body is stationary. Most empirical formulae and criteria in use, regarding ship stability that are proposed by classification societies and IMO, merely estimate the static condition either for intact or damage stability.

The drawbacks, suggestions (on stability calculation), and progressive demand of high speed ship design have been the main incentives for conducting a series of experiments, aiming of provide a better understanding of the subject. In addition, the suitability of the numerical and mathematical modelling, which can be examined in comparison with the experimental data, leads to a new method for preliminary stability assessments of a ship in a seaway at the design stage and for operational condition for voyage.

The work was initially managed under the supervision of the late professor Burcher, and for the theoretical part supervised by professor Wu. Relevant articles on the subject were very limited particularly in open libraries and not available to this work compared with those which were available in research centres not otherwise. Anther very important note is that although, CFD methods computer programs were advancing in many research centres and universities, for the current research it is only a tool for investigation of effects of speed on the stability of ships. Nothing was available for this research as a suitable tool or source of basic validated program to modify for the purpose of the research. Hence, most parts of the research herein were developed from scratch with rather basic instrumentation, equipment and supervision.

1.4 STRUCTURE OF THE THESIS

In Chapter 1, some general information together with relative key points in Appendix A and their concepts are presented. In addition, the scope of the work and brief reasons of using the experimental as well as theoretical methodology are given.

Chapter 2 describes both theoretical and experimental more relevant works in this field. There is relatively little work published in this area and most of them are experimental. Whereas, theoretical research papers generally consider either powering (resistance of a ship) or optimisation of bodylines. Therefore more related papers on the subject are discussed.

General details of the mathematical formulae, including the theory, are discussed in Chapter 3. In particular, the mathematical modelling of the problem, plus the solution of the boundary element method (BEM) for three dimensions is presented. The solution adapted for triangular panel is presented too.

The numerical implementation of the solution is addressed in Chapter 4, and includes some procedures of the computer code, and discussion about the algorithms used in the programme. Also preliminary results and validation of the code are presented.

The mesh generation computer code is presented in Chapter 5. The code is able to generate a mesh not only over the wetted surface of a ship in any loading condition, but also is able to generate a mesh for any specified inclination angle. A few typical examples regarding application of the code are presented.

The experimental part of the research is explained in Chapter 6. The scaled model that was used in the theoretical approach, as the computational domain, as was previously constructed at UCL, has been used. The experiments have been conducted in a towing tank at UCL. Although it is relatively small in length and not very modern, very useful and advanced results have been obtained by users, the results can be found through years in their researches. The experimental data are shown in this chapter.

Discussions as well as comparison between the theoretical results and the experimental data are presented in Chapter 7. Although, in Chapter 4 theoretical results and validation of the steady potential code on the test case and the wigley hull form have been presented, and in Chapter 6 the experimental data have been discussed. However, focus on the validation of the steady potential and comparisons with the experimental data of the model are explained in Chapter 7.

Finally, general conclusions of the main findings of the research are given in Chapter 8, followed by suggestions and comments for future work. This work may be very useful for designers and operators, if it is continued to evolve as it is pointed in future work.

2. REVIEW OF PREVIOUS WORK

Disaster at sea has not been fully eliminated, as recent catastrophes clearly show. There are many recorded instances of ships, which have been properly surveyed and operated by competent crews, which have foundered. The number of serious casualties for RO-RO vessels alone still averages one per week, the stability problems with fishing vessels, pleasure and small craft are still at large and new challenging problems appear with the remaining of unconventional high speed ship designs flooding the market at an ever increasing rate, Vassalos (1996).

One of the historical tragedies that force designers to apply and be very careful for the application of stability criteria is the sinkage of Titanic and following incidents. It is thought that she was unsinkable, but she sank in her first voyage. Since this tragedy it has been understood that ships must be divided into compartments and they should be watertight. Under this arrangement many ships have been designed and built and operated safely. The criterion was forgotten during advance in ferries technology design with a very wide and long opening deck being the car deck. The problem was the same as before, violent free surface flow and the dynamic effect of flow on the inner deck were not considered. Many lives and ships were lost until the same resolution was applied to act for the ferries. That is to divide the car deck into watertight sections to make it safer.

In order to avoid re-examination of known phenomena of instability for high technological designs of today, it is necessary to investigate the critical modes leading to capsize. Simply, it can be said, predicting danger before happening, and not let it happen as in the tragedy of Titanic regardless of damage, a free surface flow in a very wide opening, as happened 86 years later to the Estonia involving the loss of 852 lives, BMT (1994).

The purpose of developing criteria is to improve the safety of ships against loss and capsizing. The criteria consist of a set of minimum values of stability parameters. These minimum values may appear as a result of certain calculation procedures or as data from model tests performed according to certain specified procedures.

Pierre Bouguer in France explained, for the first time in 1746, the mathematical properties of the metacentric height, *GM*, Vassalos (1998). Any criteria, which were used, were based on experience. It was clear that this was a poor guide, later, the value of *GM* was increasingly used as a criterion. For many years it was assumed that adequate matacentric height could be used as the sole measure of the stability safety for all angles of heel and all conditions of loading, even though *GM* is only an indicator of static upright stability.

The stability of a ship is normally assessed in two ways regarding the limitation of inclination angle. An initial assessment of stability may use the parameter *GM*, which gives an indication of the ship stability for small heel angles, assumed less than 10°. The limitation of these angles may vary depending on hull form. The *GM* value is derived from the following expression:

$$GM = KB + BM - KG \qquad (2\text{-}1)$$

where the terms have their usual meanings. Bearing in mind that *KG* is determined from the ship's weight and its load distribution, whereas *KB* and *BM* are calculated from the ship's geometry.

Large inclination angle stability however is measured by the curve of righting levers that is the so-called *GZ* curve. So the representative quantity of stability is derived from the couple formed by the action of weight and buoyancy, once a ship is heeled in still water as discussed briefly in appendix A. Then the *GM* does not remain constant, and it is preferable to measure the stability in terms of the *GZ* since this is very convenient for making a comparison between different loading conditions of the same ship. It must be noted that the GM value is the slope of GZ curve.

$$GZ = \sin\varphi(GM + \frac{BM}{2}\tan^2\varphi) \qquad (2\text{-}1a)$$

However, these curves were not originally easy to obtain at that time. Proshaska (1947, 1951) showed how values for *GZ* could be obtained more quickly for a normal type of vessel. He postulated the formula:

$$GZ = GM \sin\varphi + MS \qquad (2\text{-}2)$$

where MS is the residuary stability lever such that, $MS = Cr_0$, C is a non-dimensional residuary stability coefficient, and r_0 is the initial value of BM.

The value of C depends largely on the ratios of depth to beam and draught to beam, and so it is strongly dependent upon the geometrical form of the vessel. Further information can be found in references Lewis (1988), and Bhattacharyya (1987).

In the UK, Atwood developed a formula in 1796 for the calculation of the righting lever GZ curve. The concept of dynamic stability referring to the area under the GZ curve was introduced by Canon Moseley in 1850. He studied the unforced, undamped, single degree of freedom, roll equation of motion, and equated the overturning energy and the restoring energy in order to evaluate vessel safety.

In 1939 Rahola in his doctoral dissertation, analysed the righting arms of a number of capsized fishing vessels to determine what the important external forces are, and what should be the required righting arm curve to ensure vessel safety. It formed the current intact stability evaluation criterion by the International Maritime Organisation (IMO) and most of other classifications. It is interesting to note, however, that the great majority of ship designers and shipbuilders at the beginning of the 19th century regarded these developments as highly theoretical and they were initially ignored. In fact, the US Navy in the latter part of the 20th century adopted the first criteria involving Moseley's concept.

Nowadays, there are many stability criteria, which are useful to both designers and operators. Most of them are based on static stability which is however a questionable feature in assessing safety. Making a choice of stability criteria depends on the type of ship and the region where the vessel will be operated. Generally, international rules are issued by International Maritime Organisation (IMO), as well as national rules by the national flag state. Examples of these criteria can be found under selected

classifications societies such as Lloyds Register of Shipping (LR), Germanischer Lloyd (GL), Det Norsk Veritas (DNV), Polski Rejesetr Statkow (PRS), and others.

The preliminary ship design process involves satisfying each design requirement sequentially, modifying the dimensions and repeating the process until all requirements are met. The spiral diagram in Figure 2.1 shows the usual practical design sequence.

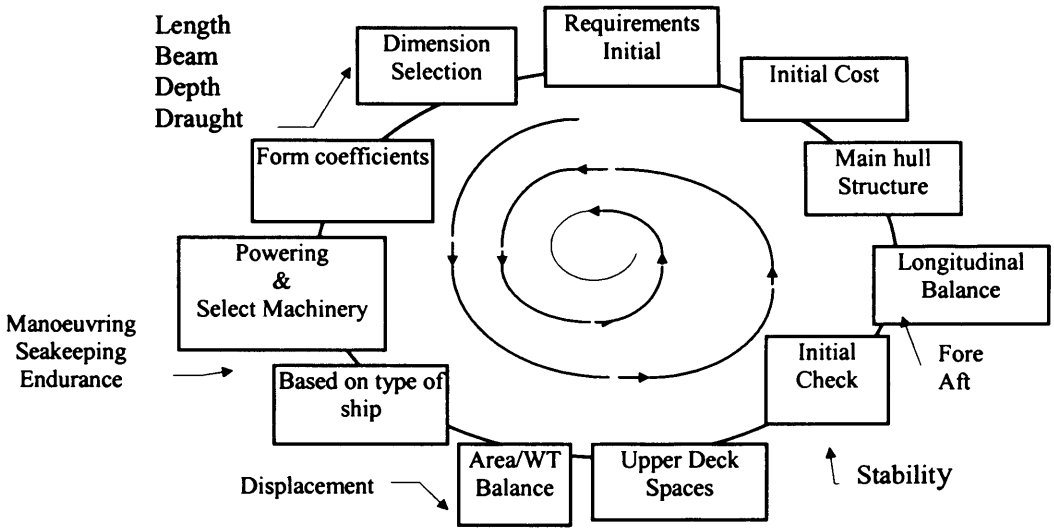

Figure 2.1 Spiral diagram showing usual procedure in a ship design

In accordance with the usual procedure of a ship design one important step is her stability estimation. There are several reliable computer programes for stability evaluation on the market which calculate the ship static stability conditions to a high level of reliability for intact ships. Examples of these software have been presented for ship design at RINA workshops every year since 1996. The procedure of softwear usually is the same that according to selected class for stability evaluation of a ship, users are able to apply stability criteria from the software's library. Although the data of a ship hull form and load conditions are high in accuracy and graphical presentation or tabulated results are fabulous, they are unable to deal with dynamic stability of a ship in seaway. This weakness in the software can be attributed to the absence of dynamic characteristic which influence the ships' stability. Problems are also noted by Kaps and Kastner (1990) showing how some uncorrected data are supplied for the stability evaluation.

There is evidence that marine stability criteria have improved levels of safety. However, capsizing in intact and damage conditions are very complex phenomena for displacement, semi-displacement, and planing ships. In a practical sense some accidents, and incidents, which still occur indicate that there are some unknown parameters in stability assessment. For example there is no agreement on the dynamic stability criteria, and the role of variations of speed on the stability is not fully clear. This is what makes it necessary to investigate unknown parameters for the critical modes leading to capsize. In other words, as a result of recent events and disasters it can said that stability appears to have been reborn as a subject. As has been mentioned by Vassalos, it warns the whole industry and researchers, regulations, administrators, designers, operators, and others relative to marine transport.

Clearly, the ship motions and the resulting loads acting on the ship, cargos, and crews depend on her operational stability. The operational stability is different from minimum stability requirement which is purposed by classification societies. The latter are seen as a guideline for operators, whereas, the former is set by operators. Those minimum requirements for stability constitute the minimum set standard, in order to allow the ship to sail. The minimum stability must allow the ship to overcome regularly encountered situations. If minimum levels are set too high, in order to cope with very extreme sea condition, the main disadvantages are:

- worse ship behaviour in seaway
- unnecessary high motion
- more securing and lashing for cargos

as well as, at very low setting of the minimum stability levels the ship might not be able to resist a severe environment or any other disturbances. It has been the subject of research for many years in a very wide scope of researchers. Some examples are presented in the following.

2.1 EXPERIMENTAL INVESTIGATIONS

As a prototype approach experiment, Kaps and Kastner (1990) studied the methods of calculation and measurement of ship stability, and their accuracy, in particular during service. They found that the input data on loading was very often inaccurate. In this instance measuring the actual stability status by means of the Operational Ship Inclining (OSI) experiment is recommended. The feasibility of such an approach is shown with different container vessel tests in different harbours. In general, the OSI can be also extended to other types of vessels with critical stability as well. However, the method has shown some inaccuracies of the input loading data. Also application of the method can confirm only the stationary accuracy of the stability, in absence of speed and any disturbances in a seaway. Moreover, these inaccuracies of input loading data may affect the results of advanced software used for stability evaluation.

Kastner (1986) in his research noted that safe sea transportation of cargo is not just a matter of safe stowage and securing of cargo, but is strongly related with the design and construction of the ship, and her outfit, as well as the way the ship is being operated at sea in different environmental conditions. Although minimum stability requirements by classification societies can not include any risk, they are as a guideline and they can not show clearly on which operational conditions they have been based upon. Then, the ship master is concerned about safety from capsizing, about low motion acceleration on the cargo, and its feedback to ship behaviour. Mostly, the ship master judges and decides on his own experience. Therefore, it is required a practical setup of developing necessary information and data on board to improve operational stability of ships.

The actual stability status of a ship during her voyage varies in time due to changes in cargo and ballast of the ship, and due to the changing environmental conditions at sea. On the other hand, minimum stability proposed by authorities reflects the intact stationary stability of a ship not the state of stability of ship in seaway. In order to ensure safety of a ship from capsizing, the actual stability status must be compared with the minimum stability requirements set by classifications. During the last twenty years most of the efforts focus on stability of a ship in seaway. Many useful

experimental researches investigated wave effect on manoeuvring and sea-keeping of a ship in a seaway. Available papers discuss stability of a ship in following, quartering and head seas.

However, the role of speed has been shown to have a very significant effect on stability of planing type, and it is the subject of many researches theoretically and experimentally, as reported in ITTC 21st, 22nd, and 23rd, Fast Ship, and other professional conferences.

Since in marine transportation users seek to reduce travelling time, then increasing speed and improving of comfort and safety are vital. In this respect many types of vessels have been designed, constructed, and operated having an operational speed higher than that normally associated with a conventional ship. It is useful to look at the main information that are classified by Kuo (1997).

The catamaran, having two hulls joined by a structure spending the breath of the vessel, is one type. In recent years, size of the catamaran for passenger transport has been steadily increasing. The Small Waterplan Area Twin Hulls (SWATH) is similar to the catamaran except the shape of the hulls have a torpedo like, but the former is made of slender hulls. Reduction of required power for reaching high speed, and better stability compared to the monohull are advantages of this type. They represent about 34% of the world High Speed Craft (HSC) population.

Hydrofoils attached to the sides of another class of monohull generate lifting force when the vessel gains speed. Operation of a very large hydrofoil craft is not cost effective, and there is restriction of depth of water where they operate, but they represent 26% of the world HSC population.

The principle for Surface Effect Ship (SES) is to create a cushion of pressurised air between the bottom of the hull and the water surface. Therefore, there is no displaced water and no water resistance. Another advantage is the possibility of operating over solid surfaces. This type of the HSC represents about 11% population of the HSC. Other types of crafts that represent only 1.5% of the population are not discussed further here.

However, a more important type of HSC that is similar to conventional ship and represent 27% of the population of HSC is mono-hull. The percentage continues to grow, and is considered in many recent investigations. The principle is that the hull form has been designed to assist the achievement of high speed i.e. a planing hull. Therefore, hydrodynamic lift force increases as speed increases. The resulting lifted hull has a reduced wetted surface leading to lower wave making resistance and viscous pressure drag. Another advantage of this type is that considerable operational experience is available. The observations and findings of this type of vessel are relevant to the aim of the current research if obtained for calm water.

Lundgren and Storch (1984) observed the irregular stability of a small fishing boat. They rang the bell that attention must be paid to the fact that initial static metacentric height (GM) is not a completely adequate measure of stability. Through the years it became clear that dynamic instability varies and depends upon a number of factors, including speed, displacement and hull forms.

It became increasingly evident that the assumption that vessel stability is independent of speed is not valid. It has been shown that although small craft may possess adequate stability at rest they exhibit a loss of stability at high speed. The technical literature is scattered with example of high speed vessels stability in seaway. Cohen and Blount (1986) presented one of the best papers that provides a general technical overview of the problem and highlights relevant research. The primary purpose of the paper is to extend this knowledge into a proposed plan and objective of developing technical guidelines to prevent dynamic instability problem.

At zero speed, stability is of course governed entirely by hydrostatics. As the Froude number increases, the hydrodynamic effects come into play and are considered to comprise two separate components, one due to the *hull wave* and the other due to *hydrodynamic pressure* distributions along the wetted surface of the hull.

The hull wave causes more of the vessel to be supported at the bow and the stern and less along the midhull. Then redistribution of the buoyancy can lead to a reduction in the metacentric height, resulting in a loss of stability of finely shaped high speed hulls

operating relatively at, or slightly above, low speed. Hydrodynamic bottom pressure effects can also come into play under this condition.

Beyond the cited speed, the influence of bottom pressures tends to dominate, and the hull wave effect diminishes. Generally, instability at high speed can be characterized as being oscillatory and nonoscillatory. The former type includes periodic transverse roll oscillations known as *chine walking,* and *porpoising* the equivalent situation with longitudinal pitch oscillations. Both are usually associated with high speed hard chine planing craft operating in calm water, generally, on relatively heavily loaded craft (that is low projected chine area for a given displacement), the nonoscilaatory instability can occur at more moderate speed than that associated with oscillatory instability. Unstable nonoscillatory behaviour has been reported in both the transverse and longitudinal direction with motions ranging from a rapid loss in running trim, progressive heeling to port or starboard, or a combined roll-yaw motion. General types of instabilities have been summarised by Cohen and Blount are shown in Table 2.1.

	HYDROSTATIC ← → HYDRODYNAMIC			
	DISPLACEMENT	SEMI DISPLACEMENT		PLANING
	INCREASING FROUDE NUMBER →			
TRANVERSE	TRANSVERSE HYDROSTATICS $GM_T \leq 0$	LOSS OF GM_T DUE TO WAVE EFFECT 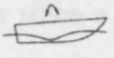	ROLL INSTABILITY NON ZERO HEEL NON OSCILLATORY 	"CHINE WALKING" DYNAMIC ROLL OSCILLATION 
LONGITUDINAL	LONGITUDINAL HYDROSTATICS $GM_L \leq 0$	LOSS OF GM_L DUE TO WAVE EFFECT 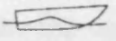	TRIM INSTABILITY BOW DROP NON OSCILLATORY 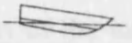	"PORPOISING" DYNAMIC PITCH-HEAVE OSCILLATION 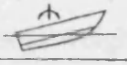
COMBINED	COMBINED $GM_T \leq 0$ $GM_L \leq 0$	COMBINED WAVE EFFECT 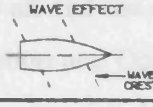	BROACH NON OSCILLATORY 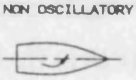	"CORKSCREW" PITCH-YAW-ROLL OSCILLATION 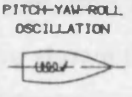

Table 2.1 General type of instabilities ref. Cohen and Blount (1986)

Nonoscillatory instabilities commonly occur at speeds lower than those associated with oscillatory instabilities and are found on relatively heavy loaded craft travelling at moderately high speeds. For this condition unstable behaviour can occur about the yaw, pitch and roll axes represented by a loss in running trim, progressive heeling motion, bow steering or a combination of rotations. A new stable operation may result

from these motions, and the craft may be operated with some degree of control for an extended time with this new approach. There also may be secondary results, such as broaching or unpredictable steering response.

Oscillatory instabilities include roll oscillations (chine walking), and pitch and heave oscillations (porpoising). There are some common factors in both oscillations that are associated with high speed. The amplitude of oscillation is related to boat speed, and oscillations occur without any warning and any excitation from environment or operator. In some cases, the oscillations increase while the craft is at constant speed. There is an accepted guideline for prediction and avoiding porpoising, but no accepted guideline is available for predicting the conditions which result in chine walking Blount and Codega (1992).

The underwater shape has a great effect on the tendency for nonoscillatory dynamic instabilities. Although the literature on the subject is very limited usually it can be found that forming of low pressure areas on the wetted hull depends upon:

- In the case of planing hull, unfairness of shell plating where it is welded to frames that is shown by Clement (1982) caused local low pressure area as the boat heeled or encountered a wave, and a heeling moment was being formed.
- In the case of fast flat bottom boat with buttocks shaped like half of an airfoil, as weight is shifted forward or when a wave strikes the bow, the more highly curved forward sections become immersed. These forward sections may develop pressure lower than static. As pressure forward drops, the pressure aft must increase to compensate for the support of the total boat weight. Further shifting of centre of pressure aft and the centre of gravity fore, thus a dynamic instability can be created. Abbott and Doenhoff (1959) have shown that higher thickness to chord (t/c) ratio develop lower local pressure than a lower t/c ratio.
- Any asymmetric port and starboard wetted surface or a change in trim (caused by shift in weight or sea state) changes the pressure distribution. In the case of a vee-bottom hull having buttocks shaped as two airfoil sections joined at the keel, a boat with a high t/c ratio is more prone to develop the local low pressure areas that lead to instabilities.

In addition, ventilation may produce a lift force, and ventilation off centreline will induce a roll moment. As dynamic pressure is a function of speed squared, the extreme dependence on speed is clear. Therefore, any source of rapidly changing pressure distribution under a hull, including shape of the hull, ventilation of a portion of the hull bottom and / or appendages, may lead to a dynamic instability.

Ikeda and Katayama (2000) investigated transverse and longitudinal instability of the motion of a high speed planing craft. They experimentally confirmed that the transverse stability significantly decreases at high speed and it causes large heel of a craft. The stability loss which depends on trim angle also generates roll motion when a craft has pitching motion. It is reported that porposing (unstable heave and pitch coupling motion) of the craft is a self exciting motion due to the different sign of the coupling restoring coefficients between pitch and heave motions. Prediction methods are proposed for evaluation of the roll and heave damping including vertical lift force contribution.

Walkeling et al (1984) measured a series of pressures on a model with adequate stability at rest, to investigate the loss of transverse stability of a round bilge hull at speed in a seaway. They reported that the model would only remain stable up to a critical speed, consequently, it would take on a steady heel angle, because the pressure measurements revealed that the behaviour was due to negative pressure developed along the aft body and was attributed to the hull form. This is a fundamental difference between the two hull forms (the planing and the round bilge) showing that the round bilge hull is an unsatisfactory hull shape for high speed. In fact, the planing hull forms, unlike round bilge hulls, are always associated with large positive bottom pressures.

Tim et al. (1985) introduced a computer-based approach to design a ship, which improves both the efficiency and effectiveness of the design process. They formulated the problem in a structured mathematical form and also, in order to modify a designed ship applied a design support problem (DSP), which is applicable in the design of all engineering systems. According to Kupras (1981) there are two types of DSP; selection and compromise. Selection entails choosing one alternative from a number of feasible alternatives without modification, whereas compromise overcomes

improving a feasible alternative. The compromise DSP method was chosen by Tim et al. to develop their computer programme to modify the design. The righting arms are calculated based on the regression analysis carried out for ship forms; Series 60. The method is explained in Kupras (1981). The programme output for ship stability is linked to a table of righting arms for angles 0 to 60 degrees. These may be used to check the final design against the stability regulations established by IMCO. The role of a computer at this stage has been limited to reducing the time and effort involved in design calculations.

Other computer programmes are relatively similar to Tim et al's code in implementation of stability criteria to evaluate stability of either a ship design, modifying or to check stability of an existing ship. Major differences of recent programmes are that they apply stability criteria of all classifications in their library, they provide very well graphical presentation of the results, and are very user friendly, such as those software presented in the RINA workshops (1996 to 2001). Significant decrease of time for stability evaluation is an advantage of CAD. These software are not able to deal with dynamic stability.

For new design of a ship or modification of an existing ship, it is of great practical interest to know the flow and the resulting forces on the wetted surface of a body due to the steady motion of the hull. In this regard serious efforts of numerical prediction methods started with the novel work of Michell (1898).

2.2 MATHEMATICAL INVESTIGATIONS

In 1898 the Australian mathematician J H Michell published a paper on the calculation of the wave resistance of ships, well ahead of his time, he introduced thin ship theory. In this theory, the vessel is assumed to be thin, which means the beam of the vessel is small compared with all other characteristic lengths (vessel length, wave length ...). In general, it is known that Michell's approach gives a reasonable prediction of the ship resistance at higher Froud number (Fn). The paper was forgotten, until Havelock (1923) discovered it to extend the theory in his research over three decades later.

Havelock used a Green's function method instead of the Fourier integral method used by Michell. Typical of the Michell approach is the use of analytical methods to the largest possible extent. Without computers only the methods with a small number of elements, or simple shapes, could be used.

Ursell (1949) employed a series of multipoles to present the radiation potential for the heaving motion of a half immersed circular cylinder in deep water. By applying a transformation to the results of Ursell's circular cylinder, this method was extended to the other ship-like sections later.

A theoretical basis of solving the linearised ship motion problem was published by Haskind (1953). He made use of Green's theorem to construct the velocity potential due to the presence of a ship hull and derived the necessary Green's function. The resulting integral equation was solved by adopting the thin ship idealisation. An important feature of the analysis was widely spread procedure of separating the linearised problem so that the diffraction and radiation problem could be solved independently. Haskind also mentioned that it is possible to estimate the diffraction forces acting on ship due to an incident wave from the solution of the radiation problem. The idea was developed further by Newman (1962, 1965). Then the numerical solutions of a simpler class of two dimensional problem for free floating bodies without forward speed have been developed.

The very practical tool called Strip Theory through solving the coupled heave and pitch motions of a ship in regular waves was provided by Kroukovsky (1955) and Jacops (1957). They assumed that the hydrodynamics associated with a ship could be represented by a series of two dimensional elements, usually known as strips. The two dimensional boundary value problem was solved to obtain the hydrodynamic forces for each strip. Then the three dimensional hydrodynamic forces of a ship were to be taken through the lengthwise integration of the two dimensional forces. The procedure did not take into account interaction effects between different strips along the ship length.

The strip theory has been found to give good agreement with model tests in predication of heave and pitch and roll motions for high frequencies and moderate Froude numbers. The strip theory may, however, give inadequate predictions of local effects like pressure distributions over the hull surface. In spite of the successful application, the strip theory does not account for three dimensional interactions between sections comprising the hull surface nor do any forward speed effects on the free surface, although Ogilive and Tuck (1969) introduced a higher order approximation for the forward speed effect.

To complement the shortcomings, Newman (1978) and Newman and Sclavounos (1980) introduce the unified strip theory in which the two dimensional near field solution of the strip theory is corrected by the three dimensional far field solution. Based on the strip theory simplifications adopted in the formulation of the theories, inadequate consideration is given to the three dimensional flow effects and the effect of the forward speed.

This situation changed dramatically with the introduction of the computer in the 1960s, and a new type of method, more numerical in nature, started to appear. The basic approach was the method for non-lifting potential flow without a free surface. It was first introduced by Hess and Smith (1962) and later developed in several papers by Hess and Smith (1964, 1967). At this time, Ursell's method was extended to the other ship like sections by Frank (1967) and other researchers. Frank used the source distribution method to obtain two dimensional hydrodynamic forms for any cross sectional shape, which is known as Frank-Close Fit method.

The common method of Hess and Smith uses plane quadrilateral panels with constant source strength of each and control points in a suitably defined centre of each panel. During the latter part of the 1960s modern research in viscous flows was also initiated, and in 1968 several different methods for two dimension boundary layers were developed. This research was continued for three dimension boundary layers in the 1970s and in 1980 the first workshop devoted to ship boundary layers, was held in Gothenburg.

The wavelike disturbance as is generated due to heading of ship in calm water was first established by Lord Kelvin (1887). A classical investigation of this is given in detail by Wehausen and Laitone (1960), Emerson (1967), Ogilvie (1968), Chen and Noblesse (1983) and others. It may be seen from their expressions that the dominant waves generated by the moving sources are restricted into a sector making an angle of $\text{arccot}(2\sqrt{2}) \approx 19.5°$ with the downstream sailing line. Also the wave energy flux is minimal near the borderlines of this sector. A more detailed analysis shows that within the sector there occur two separate (distinct) wave systems of transverse and diverging wave patterns with a common angle of $\arctan(\sqrt{2}) \approx 55°$ near the cusp lines, as shown in Figure 2.2.

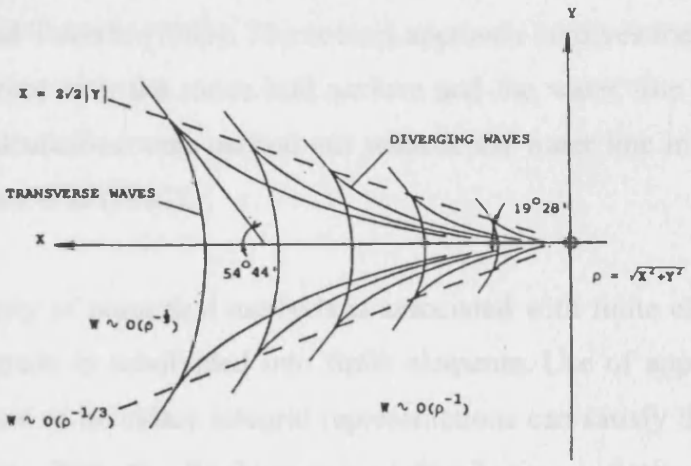

Figure 2.2 Sketch of the Kelvin ship wave pattern from ref. Baar and Price (1988)

The past thirty years have witnessed a rapid growth in the development of three dimensional panel methods capable of simulating steady and unsteady free surface potential flows past conventional ships, high speed vessel and yachts. These methods extend significantly the capabilities of strip and slender body theories and are progressively finding routine use in practice because of their robustness, reliability and efficiency. Several methods with this capability were now available. Application of the methods for design and modification of ship and boat may be divided into four different areas such as:

- resistance and flow
- propellers and cavitation
- seakeeping
- manoeuvring.

For their solution numerical methods generally can be classified into two categories, a singularity distribution, and finite element methods. The bases of the methods will be briefly described here, although, the latter method may be subdivided into several categories such as finite difference (forward, backward and centre). Singularity distribution methods are based on boundary integral identities for the velocity potential obtained by applying Green's second formula to the potential and an appropriate Green's function. The Green's function may be chosen as either a fundamental Rankine source or the potential of a translating submerged source satisfying the free surface and radiation conditions. The latter Green's function is referred to as the Kelvin wave source potential. In the first approach, the Rankine source is distributed over both the mean free surface and the hull surface, see Dawson (1977), Adachi and Taheshi (1983). The second approach involves the distribution of Kelvin wave sources over the mean hull surface and the water line contour, Brard (1972). Earlier calculations were carried out without the water line integral by Gadd (1975), and Andrew et al (1987).

The second category of numerical methods is associated with finite elements. In this case the fluid domain is subdivided into finite elements. Use of appropriate eigen-function expansions or boundary integral representations can satisfy the downstream radiation condition. Both the Rankine source distribution and the finite element methods require discretization of the free surface and suffer from difficulties in applying the proper radiation condition. The Kelvin wave source distribution technique has no such disadvantages but the evaluation of the Kelvin wave source potential is more involved due to its complicated mathematical formulation, Noblesse (1981), and Baar and Price (1988). In the current research, the Kelvin source distribution technique is applied, which has provided reasonably accurate results for linear free surfaces.

Seakeeping (ship behaviour in the longitudinal plane "heave and pitch motions" in head seas), Manoeuvring (ship behaviour on the horizontal plane "surge, sway and yaw motions" in still water), and Stability (extreme ship behaviour in the transverse plane "roll motion" in wave) are very important issues of past and present research. Seakeeping has attracted most effort, and has progressed very rapidly, due to being more appropriate to analysis by linear theory. Two examples of the development on

the subject are theses by Ha (2000) and Kara (2000). Ha developed a three dimensional ship motion program to predicate seakeeping performance of a high speed marine vessel in seaway for steady and unsteady problems. Another example of numerical development is a time domain hydrodynamic and hydroelastic analysis of floating bodies with forward speed by Kara.

The other two subjects, due to severe non-linearities in the force mechanisms leading ship behaviour, depend heavily on support from experimental work using model testing. A study for predication of intact and damaged stability in a seaway was organized by ITTC 1999, mathematically and experimentally. Some mathematical and experimental results are presented as a benchmark in ITTC 23rd. It is well accepted that hull resistance and propulsive performance and wave induced surge force are very important data for prediction of capsizing of intact ships. However, since such data are not available, an accurate prediction method is still desirable. Then, obtaining intact stability at speed is clearly an area of research, which needs more investigation.

3. THEORETICAL APPROACH

For the purposes of stability, a ship may be regarded as a rigid body, with six degrees of freedom. These are three translation (surge, sway, heave) parallel to the Cartesian axes (x,y,z), and (roll, pitch, yaw) three rotations about the same axes respectively. Figure 3.1 shows a right handed co-ordinate system in which the origin is assumed at the mid-ship, with positive z vertically upward and positive y towards the port side of the ship. Equations of motion are derived by equating the external hydrodynamic force and moment to the inertial force and moment associated with the ship's mass. These modes of motions are denoted by the indices (j=1..6) respectively.

$$\sum_{j=1}^{6}(A_{ij}\ddot{X}+B_{ij}\dot{X}+C_{ij}X)=F_{wi} \qquad (3.1)$$

where $A_{ij}=m_{ij}+a_{ij}$ for i=1..3 and j=1..3 relate to translation motion ($i=j$),

$A_{ij}=I_{ij}+a_{ij}$ for i=4..6 and j=4..6 relate to rotational motion ($i=j$).

A_{ij} for i=4..6 and j=1..3 relate to the effects of translation on rotation, whilst A_{ij} for i=1..3 and j=4..6 relate to the effects of rotation on translation.

F_{wi} can be exciting forces and moments due to waves, towing, pulling, mooring, environment etc.

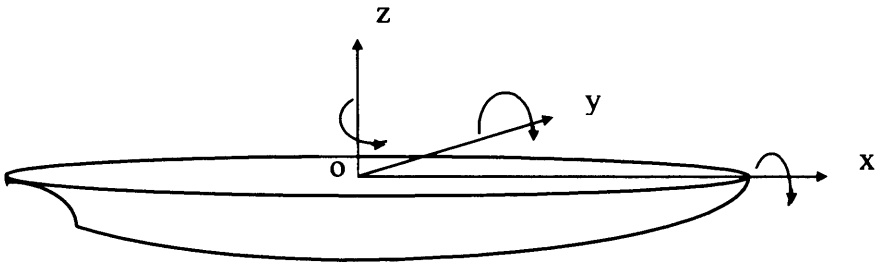

Figure 3.1 Definition of ship motions and the co-ordinate system

To simplify the equations of motion, it may be assumed that the ship is heading in calm water at constant speed u along the x-axis, with no external forces acting. Hence the right hand side (RHS) of the equation of motion (3.1) is zero. Although the roll and the pitch are both rotating motions of any floating bodies, which become more important when analysing the stability of a ship, for simplification of equation (3.1), it is assumed that neither of these modes has an effect upon the other. Consequently

considering one degree of freedom only for the dynamics of rolling, then the equation of motion can be written as:

$$A_{44}\ddot{\varphi} + B_{44}\dot{\varphi} + C_{44}\varphi = 0 \qquad (3.2)$$

where: $A_{44} = I_{xx} + a_{\varphi\varphi}$

I_{xx} is the inertia moment, $a_{\varphi\varphi}$ the added moment, B_{44} the damping and C_{44} the restoring stiffness. For a small heel angle (where $tan\varphi \approx sin\varphi \approx \varphi$) the restoring coefficient can be written as:

$$C_{44} = \frac{\rho g \nabla GM_0 \varphi}{\varphi} = \rho g \nabla GM_0 \qquad (3.3)$$

As we can see, inertia should play some part in assessing the stability of floating bodies. The rolling period can be written as:

$$T_\varphi = \frac{2\pi}{\omega} = 2\pi\sqrt{\frac{A_{44}}{C_{44}}} \qquad (3.4a)$$

where: $\omega = \sqrt{\frac{C_{44}}{A_{44}}}$ is the rolling frequency.

In this form second moments appear as part of A_{44}. Because the dynamic problem of a vessel rolling near capsizing is highly non-linear, it is impossible to solve the problem exactly in closed form. Consequently some approximations must be made. Eliminating A_{44} and C_{44} from equations (3.2) and (3.3), where $I_{xx} = i_B + a_{\varphi\varphi}$ we can obtain the roll period from:

$$T_\varphi = 2\pi\sqrt{\frac{i_B^2 \rho \nabla + a_{\varphi\varphi}}{\rho g \nabla GM_0}} \qquad (3.4b)$$

where: i_B is gyration radius, and the component of added mass is $a_{\varphi\varphi}$.

Added moment in rolling motion depends on form of the body and appendages, if there is no fin stabilizer or other effective parts that create the rolling added mass then it may ignored from the equation (3.4b). The roll motion period then can be simplified as follows:

$$T_\varphi = 2\pi\frac{i_B}{\sqrt{gGM_0}} = \Lambda\frac{1}{\sqrt{GM_0}} \qquad (3.5)$$

where the added mass is very small then: $\Lambda = 2\pi \frac{i_B}{\sqrt{g}}$

Another alternative procedure for the uncoupled natural period in roll, which is relatively the same as (3.5), was introduced by Faltinsen (1990) as:

$$T_{44} = 2\pi \sqrt{\frac{Mr_{44}^2 + a_{44}}{\rho g \nabla GM}} \qquad (3.6a)$$

where: r_{44} is the roll radius of gyration with respect to an axis parallel with the x axis through the C of G, and r_{44} is the same as i_B and typically it is assumed to be 0.35 times the beam.

If the added mass is very small then the above equation simplified as:

$$T_{44} = \frac{2\pi(0.35b)}{\sqrt{g}} * \frac{1}{\sqrt{GM}} \qquad (3.6)$$

Consequently from equation (3.5) or (3.6), it can be seen, that the period of rolling rises as the *GM* becomes small or vice versa the period of rolling motion decreases as the GM becomes large. Both of these GM levels have some disadvantages, which are discussed before in Chapter 2.

Neither of these *GM* levels is recommended by classification authorities for design and navigation of a ship. Typical examples of *rolling period* values are shown in Table 3.1.

Type of vessel	T_{44} [sec]
small fishing vessels	4-6
conventional merchant vessels	8-12
specialised heavy lift vessels	20-25
semi-submersible	35-50

Table 3.1 Typical example of natural roll period according to Faltinsen (1990)

Therefore the *GM* is very important and it must be controlled during design a ship, and the ship's lifetime. It is possible to calculate the *GM* in any operational condition of a voyage for a ship in a seaway.

In order to estimate *GM* of a ship in a seaway, from equation (3.5), a stopwatch can measure the roll period of a ship in a seaway. Knowing the value of Λ of the equation, for the ship as given in her documents, therefore the *GM* may be obtained. Typical examples of the coefficient Λ values are presented in Table 3.2.

Type of vessels	Λ
Coasters – empty or ballast condition	0.88
loaded, 20% of full	0.78
with tanks 10% full	0.75
filled to 5%	0.73

Table 3.2 values of coefficient Λ approximated from Kobylinski (1990)

At the design stage the exact value of *GM* of a ship can be determined through either model test or a large calculation, which may be beneficial using commercial software.

There are numerous commercial marine software packages which can calculate ship's stability statically. Using commercial software offers easy calculation of *GM* for a range of particular loading conditions. The restoring moment of a ship at the design stage can be calculated from the traditional method, which is introduced in most Naval Architecture text books and it is indicated in Appendix A. As these methods are implemented into commercial software they consider the restoring moment of a ship in statically conditions not on a sea-way.

The current research attempted to check whether CFD is able to evaluate *GM* for a ship in all conditions including sailing in calm water, once its bodylines have been designed, and so, investigated effects of variation of forward speed on *GM* of the ship sailing in calm water.

The success of the research gives an alternative approach to enable estimation of restoring force or moment of a ship at the design stage for different loading conditions, as well as for navigation in calm water. The detail of the methodology and its procedure are presented in the following sections in this chapter and the next.

3.1 METHODOLOGY OF THE THEORETICAL APPROACH

The panel method or boundary integral method may be applied to identify the pressure distribution on the wetted surface of a ship's hull. The calculation of velocity and pressure on an immersed body surface in the fluid around the body may be described as external flow. Such a flow is concerned with the pattern of streamlines surrounding a solid body moving in the fluid. The concept of a boundary layer deals with the effect of viscosity of fluid flow. Viscosity has an effect on a fluid adjacent to a solid surface, with the calculation of forces acting on the surface due to fluid friction. The frictional forces are not of interest in the present study, moreover if the damping force of rolling motion is negligible, then the viscosity may be neglected. In this case, velocity, and pressure are affected by the physical presence of the body's surface.

Seawater is assumed incompressible, inviscid, and the fluid flow irrotational. Therefore knowledge of potential flow is applied to describe the fluid velocity vector V(x,y,z)=(u,v,w) at the point X=(x,y,z) from the Cartesian co-ordinate system origin fixed on the mid ship. The ship moves with forward speed u, along the positive x axis, and the plane of undisturbed free surface is on the Oxy plane. Based on the above assumptions, the fluid flow around the ship's hull is characterised by the potential function Φ. Generally the total potential function can be written as:

$$\Phi = \Phi_{body} + \Phi_{free-surface} \tag{3.7}$$

where: Φ_{body} is the potential due to steady forward speed of the ship without the wave effect, and $\Phi_{freesurface}$ is the effect of the wave generated due to forward speed of the ship on the surface of the water.

The problem has been divided into two parts, firstly it was considered in calm water without the free surface effect, and secondly, with the effect of the free surface.

Identification of either pressure or velocity distribution on a solid body is the goal of CFD methods. For potential flows it is possible to derive a simple expression for the

fluid pressure by the well known Bernoulli equation. Potential flows, and their characterisation using the Laplace equation, have many important and useful properties that can be used in the formulation of numerical solutions. The use of the divergence theorem by Gauss (to convert volume to surface integrals), Green's theorem (to convert a surface integral to a line integral), and principle of superposition of solutions, all provide the means to formulate boundary element solution methods. The panel method is discussed in more detail below and is applied to the research as the theoretical approach.

Firstly, the body must be discretized into small elements, here referred to as panels; the procedure of discretization is discussed in Chapter 5. Then, the velocity potential constructed from distributions of sources on each panel of the discretized boundary surface and the strengths of the singularities are assumed to be constant on each panel. These must be evaluated at suitable nodal points on every panel. Hence when the boundary integral equation is discretized in the physical domain i.e. with N panels being used to describe the body surface, the result is a linear system of N algebraic equations. The Gaussian Elimination method or any factorisation method may be applied to solve the system of equations. This system includes an N by N matrix of coefficients and N unknown source strengths, which are different from panel to panel but constant over each panel, and N unknown velocity potentials due to distribution of sources.

Once the source strength on each panel is obtained, then the velocity potential can be calculated. Consequently from Bernoulli's equation N pressures can be evaluated on N panels. Once the pressure on the panels is computed, forces and moments can be determined.

As a result in calm water, when the ship's speed is zero, the hydrostatic force acts on the wetted surface of ship hull, which is the buoyancy force. This can be estimated and the centre of the resultant force (the buoyancy centre '*B*') can be calculated. When the speed of the ship is non zero, due to forward speed of a ship, waves are generated on the calm water surface, which affect the pressure distribution on the wetted surface of the ship's hull and the surface of the water.

It is known that the pressure must remain constant on the free surface of the calm water. To compensate for the changes of the pressure, due to generated waves, a redistribution of the normal pressure occurs about the hull and so variations on the surface of the calm water height occur. This effect must be considered when evaluating the pressure distribution for which the free surface is disturbed. Accordingly, the buoyancy force consists of hydrostatic and vertical components of hydrodynamic force on each panel. Once the force on each panel is determined, the restoring moment can be calculated for any inclination angle or any unbalanced wetted surface of the ship hull at any given speed.

3.2 MATHEMATICAL BASIS

Before discussing the methodology further in detail some fundamental definitions and references of mathematical formulas of the panel method are given and explained in the following section.

3.2.1 SOURCE PANEL METHOD

Linear partial differential equations such as Laplace's equation in terms of velocity potential are often used to model both the internal and external fluid flows in an inviscid, incompressible and irrational fluid flow. It is required that the velocity potential Φ satisfy Laplace's equation:

$$\nabla^2\Phi = 0 \tag{3.8}$$

where :

$$\nabla^2 = \frac{\partial^2}{\partial X^2} + \frac{\partial^2}{\partial Y^2} + \frac{\partial^2}{\partial Z^2} \tag{3.9}$$

in the domain of interest for a three dimensional (3D) case.

The basic concept of the panel method is to replace the required solution in the domain with a surface integral equation by the application of Gauss theorem to the domain of interest.

A source is a point from which fluid is imagined to flow out uniformly in all directions. If the total flux outwards across a small closed surface surrounding the point is σ, then σ is the strength of the source. For a three dimensional case, $\phi(p)$, the velocity potential at any field point p(x,y,z), due to source at point $Q(\xi,\eta,\zeta)$ over the boundary surface for a three dimensional body can be written as:

$$\phi(p) = \frac{1}{4\pi} \int_{s_0} \sigma \frac{1}{r} ds \tag{3.10}$$

where: r is the radial distance from the source point to the field point

s_0 is a solid body boundary.

Figure 3.2 shows a sketch for source point Q and field point p. For a general body in an infinite stream, there is an infinite number of sources distributed on the body surface. The surface of the body is first modelled as a finite number of panels in the panel method. Each panel is associated with the strength to deflect the oncoming flow. The resultant flow can be made tangential to the panel surface around the body by regulating the source strength.

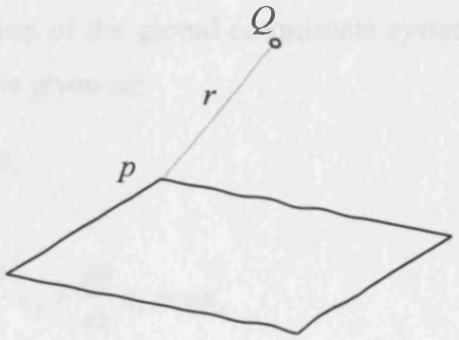

Figure 3.2 Sketch for source and field point

The requirement that the oncoming flow should be tangential to every panel at a particular location gives a set of simultaneous equations for source strength computation. The source at any point p_i will impose a velocity vector on all the other panels. Therefore the velocity potential at each panel i^{th} is the sum of the contribution from all the panels, $\phi(p_i)$. Approximating the body surface s_o with N flat panels, equation (3.10) becomes:

$$\phi(p_i) = \frac{1}{4\pi} \sum_{j=1}^{N} \int_{s_j} \sigma_j \frac{1}{r} ds \tag{3.11}$$

where: s_j is the j[th] flat panel area.

The physical meaning of the Laplace's equation requires that no mass flow is created or destroyed from a body. There should be no net flow across the closed body surface. If the body is moving in a fluid, then the uniform stream will have a velocity direction component normal to the body surface.

The problem in using the source panel is to determine the source strength σ_j. This is accomplished by selecting a control point on each panel and requiring that there is no flow across the panel at this point. The control point is selected as the centre point of each panel. Here it is assumed that the source strength and velocity potential are constant over each panel.

To satisfy the boundary condition there must be no flow across the body at the control points. Then the velocity of the fluid normal to the panels must be equal to the velocity of the body in the same direction i.e. for a body moving with constant speed u is in the x direction of the global co-ordinate system (GCS). Therefore the boundary condition on s_0 is given as:

$$\nabla\phi \cdot \vec{n} = un_x \tag{3.12}$$

or:

$$\frac{\partial\phi}{\partial x}n_x + \frac{\partial\phi}{\partial y}n_y + \frac{\partial\phi}{\partial z}n_z = un_x \tag{3.13}$$

where: $\vec{n}$ is the normal to the panel pointing out of the surface,

n_x, n_y and n_z are its components.

Equation (3.11) should fulfil the boundary condition (3.12) on each panel, then:

$$\frac{\partial\phi}{\partial n} = \frac{1}{4\pi}\sum_{j=1}^{N}\sigma_j \int_{s_j}\frac{\partial}{\partial n}\frac{1}{r}ds \tag{3.14}$$

or:

$$\frac{\partial\phi}{\partial x}n_x + \frac{\partial\phi}{\partial y}n_y + \frac{\partial\phi}{\partial z}n_z = \frac{1}{4\pi}\sum_{j=1}^{N}\sigma_j \int_{s_0}\frac{\partial}{\partial n}\frac{1}{r}ds \tag{3.15}$$

Thus:

$$\frac{\partial \phi}{\partial n} = \frac{1}{4\pi}\sum_{j=1}^{N}\sigma_j \int_{s_j}\left[\frac{\partial}{\partial x}\left(\frac{1}{r}\right)\cdot n_x + \frac{\partial}{\partial y}\left(\frac{1}{r}\right)\cdot n_y + \frac{\partial}{\partial z}\left(\frac{1}{r}\right)\cdot n_z\right]ds \quad (3.16)$$

The right hand side of equation (3.16) shows components of the normal velocity at the i^{th} panel. Then equation (3.16) can be written as:

$$\left(\frac{\partial \phi}{\partial n}\right)_i = \frac{1}{4\pi}\sum_{j=1}^{N}\sigma_j \mathrm{A}_{ij} \quad (3.17)$$

where:

$$\mathrm{A}_{ij} = \int_{s_j}\left[\frac{\partial}{\partial x}\left(\frac{1}{r}\right)\cdot n_x + \frac{\partial}{\partial y}\left(\frac{1}{r}\right)\cdot n_y + \frac{\partial}{\partial z}\left(\frac{1}{r}\right)\cdot n_z\right]ds \quad \text{for } i \neq j$$

$$A_{ij} = \frac{1}{2} \quad \text{for } i = j \quad (3.18)$$

In summary the velocity potential and the potential function (3.10) and (3.17) can be written as:

$$un_x(P_i) = \frac{1}{4\pi}\sum_{j=1}^{n}\mathrm{A}_{ij}\sigma_j \quad (3.19)$$

$$\Phi(P_i) = \frac{1}{4\pi}\sum_{j=1}^{N}\mathrm{B}_{ij}\sigma_j \quad (3.20)$$

where $B_{ij} = \int_{s_i}\frac{1}{r}ds$

respectively.

The source strength σ_j is obtained from the above linear algebraic equation (3.19). It can be used to calculate the velocity potential at any control point i from equation (3.20), with B_{ij} which will be considered later. Figure 3.2 shows the generalised source panel configuration.

3.2.2 PRESSURE AND FORCE

The total pressure, P, can be presented from Bernoulli's equation:

$$P = -\rho\left(\frac{\partial \Phi}{\partial t} + \frac{1}{2}\nabla\Phi\nabla\Phi\right) - \rho g z \quad (3.21)$$

For steady state, where potential does not change with time, equation (3.21) can be written as:

$$P = -\frac{\rho}{2}\nabla\Phi\nabla\Phi - \rho gz \tag{3.22}$$

or:

$$P = \rho(-\frac{1}{2}\nabla\phi\nabla\phi + u\phi_x - \frac{1}{2}u^2 - gz) \tag{3.23}$$

where: $\Phi = \phi - ux$

and: $\nabla\Phi = \frac{\partial\Phi}{\partial x}\vec{i} + \frac{\partial\Phi}{\partial y}\vec{j} + \frac{\partial\Phi}{\partial z}\vec{k}$

Then the dynamic pressure on each panel can be written as:

$$P_i = \rho(-\frac{1}{2}\nabla\phi_i\nabla\phi_i + u\phi_{xi} - \frac{1}{2}u^2) \tag{3.24}$$

After evaluating the dynamic pressure from Bernoulli's equation, the hydrodynamic force components acting on each panel may be obtained by integration of the pressure over the corresponding panel surface. Then the force on each panel, f_i, can be evaluated in each direction k from:

$$f_{ik} = \int_{s_i} P_i \cdot n_{ik}\, ds \qquad k=\text{x,y,z} \tag{3.25}$$

The pressure distribution over a panel s_i can be approximated as constant and equation (3.25) may lead to:

$$F_k = \sum_{i=1}^{N} f_{ik} = \sum_{i=1}^{N} P_i n_{ik} s_i \qquad \text{k=x,y,z} \tag{3.26}$$

F_k represents the x, y, and z components of the resultant force respectively. For a symmetrical body moving forward along the x direction in an ideal fluid, the lateral hydrodynamic force on the body is zero. Only the vertical and resistance forces remain.

3.2.3 DOUBLE BODY THEORY

To compute velocity over the wetted surface of a partially immersed body in calm water where the free surface effects are small or simply not of interest the water-plane can also be assumed to be a symmetry plane so-called the double-body. Therefore, the mirror image of the body is assumed on the body itself, and the horizontal plane or the free surface is assumed as a plane of symmetry. The symmetry boundary condition for

the velocity components tangential to these boundaries is that their gradients normal to the boundaries are zero. Then the velocity potential, Φ, can be written as:

$$\Phi = \Phi_{body} + \Phi_{body-image} \tag{3.27}$$

where: Φ_{body} is the potential due to steady forward speed of the ship in calm water and $\Phi_{body-image}$ is the potential due to the effect of the mirror of the ship's hull below the free surface.

Both the body and its image are assumed to be moving together in the unbounded fluid domain. Based on these assumptions, the velocity potential can be written as:

$$\Phi = \frac{1}{4\pi}\sum_{j=1}^{N}\sigma_j \int_{s_j}(\frac{1}{r}+\frac{1}{r'})ds \tag{3.28}$$

where: r is distance between field point to source point and
r' is distance between field point image to source point.

Figure 3.3 shows the vector of co-ordinates joining the field point (x,y,z) to the image of the source point. Therefore the Φ in equation (3.28) simply corresponds to a superposition of a unit Rankine source at the source point (ξ,η,ζ) and its mirror image about the free surface at point $(\xi,\eta,-\zeta)$.

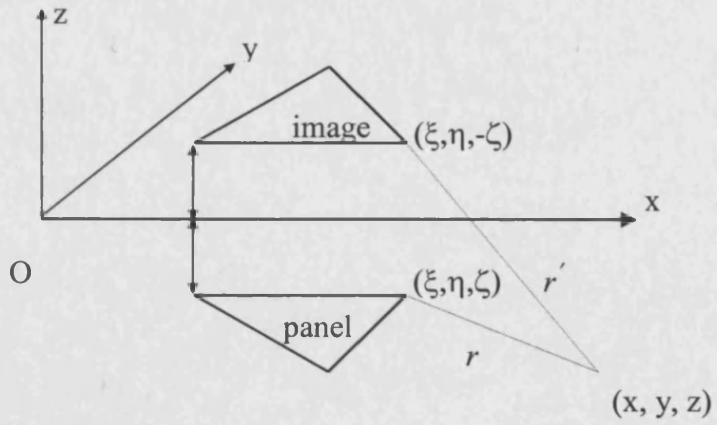

Figure 3.3 Sketch of source and field point for both panel and its image

3.2.4 FREE SURFACE EFFECT

Waves considered here regard those being generated due to an object moving on the surface of a fluid. A relevant flow model for study is the linearized wave disturbance generated by a submerged source, hereafter referred to as the Kelvin source. It is subject to the Laplace equation in the fluid domain and is written as Wehausen and Laitone (1960):

$$\Phi = \phi_{body} + \phi_{mirror-image} + \phi_{free-surface} \tag{3.29}$$

As usual in this method it relies upon being able to construct a function of form:

$$\Phi(x,y,z) = -\frac{u}{2\pi}\int_{s_0}\int f_\varsigma(\xi,\eta)G(x,y,z;\xi,\eta,\zeta)d\xi d\eta \tag{3.30}$$

where: $f_\varsigma(\xi,\eta)$ is the source's strength distributed on the body, or as $\sigma = uf_\varsigma(\xi,\eta)$ in the case of the linearized problem, in the region below the equilibrium free surface boundary.

Here we assume a horizontal bottom at $z=-h$, $h \le \infty$ and h is the water depth. Then we may obtain the following G for infinite depth. From Wehausen and Laitone (1960) it can be written as:

$$\begin{aligned} G(x,y,z;\xi,\eta,\zeta) = {} & \frac{1}{r} - \frac{1}{r'} \\ & -\frac{4}{\pi}K\int_0^{\frac{\pi}{2}} d\theta \sec^2\theta \int_0^{\infty} dk \frac{\exp k(z+\zeta)}{k - K\sec^2\theta} \\ & \quad * \cos(k(x-\xi)\cos\theta) * \cos(k(y-\eta)\sin\theta) \\ & -4K\int_0^{\frac{\pi}{2}} d\theta \sec^2\theta \exp(K(z+\zeta)\sec^2\theta)\theta) \\ & \quad * \sin(K(x-\xi)\sec\theta)\cos(K(y-\eta)\sin\theta\sec^2 \end{aligned} \tag{3.31}$$

where: $r = [(x-\xi)^2 + (y-\eta)^2 + (z-\zeta)^2]^{\frac{1}{2}}$

$r' = [(x-\xi)^2 + (y-\eta)^2 + (z+\zeta)^2]^{\frac{1}{2}}$

$K = g/u^2$

Figure 3.4 shows the geometric relation between the axis system, a source point, a field point, and an image of the source point.

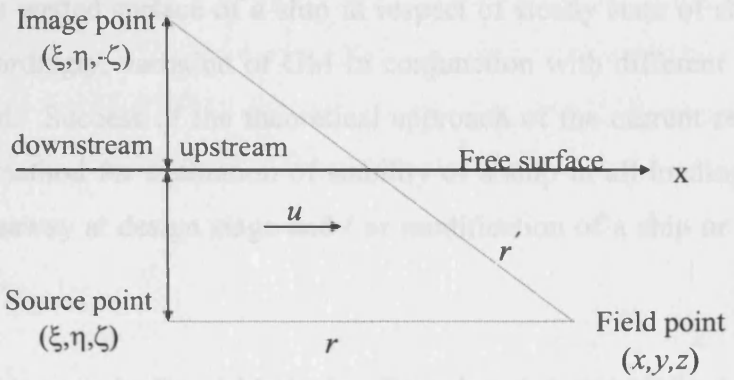

Figure 3.4 Sketch of source and field point for both the panels on the wetted ship's hull and its image

3.3 IMPLEMENTATION OF THEORETICAL APPROACH

Earlier, in section 3, the GM of a ship in a seaway has been evaluated by using the equation 3.5 for an existing ship in a voyage. The variation of the GM in respect to inclination angle and the loading conditions have been indicated in Appendix A, and can be found in many naval architecture text bookss for a stationary ship. The aim of theoretical approach of the current research is to investigate the effect of different forward speed on the GM of a ship in steady state condition in calm water.

Pressure distributed on the wetted surface of a ship hull may be change in respect to ship speed. Then, heave, pitch and rolling motions may occur owing to the difference of pressure distributed on the hull. Unbalanced pressure distributed on the hull will result in a heeling or pitching or yawing moment or a combination of these.

In the research, it is assumed that unbalanced pressure occurred only in respect to the CL of the hull. It means only heave, pitch and rolling motion may occur, and the yaw motion is avoided. To simplify the problem, for modelling of unbalanced pressure distributed on the wetted of a ship hull, it is assumed a ship hull is transversely inclined in different small inclination angles for mesh generation, the procedure is explained in Chapter 5.

This section explains application of the panel method for evaluation of pressure distributed on the wetted surface of a ship in respect of steady state of ship speed in calm water. Accordingly, variation of GM in conjunction with different ship speeds may be computed. Success of the theoretical approach of the current research may establish a new method for evaluation of stability of a ship in all loading and speed conditions in a seaway at design stage and / or modification of a ship or for existing ships in a voyage.

The method used here is the Panel Method or Boundary Integral Method. The steady linear free surface flow around a hull placed in a uniform stream is determined by integration of the Green's function for steady state. To solve the problem the mathematical modelling is divided into two parts. The procedure starts from the solution of double model linearization such as Dawson's problem (double body as a basis flow for linearization). An advantage of this method is that the results from other researchers have been shown to be very accurate, such as Hunt (1995). Also an analytical expression can be given for the solution at the final stage to compare results, as is presented herein as a test case in Chapter 4. Additionally from the computational point of view it is adequately efficient.

In the second part (once the source strength on each panel is known), the process is followed by adding the free surface effect. For 2D originally Ogilvie (1968) suggested the idea, and application to the 3D case has been discussed by Baba (1975). Dawson (1977) proposed a purely numerical method to solve the boundary value problem with the free surface condition. This provides the distribution of Kelvin sources over the immersed body and its mirror image together with the disturbed free surface effect. Several studies have been developed based on the above technique for arbitrary or mathematical shapes, Andrew et al. (1987), Shuanxing et al (1999), and others.

The following explains step by step the method which has been applied in the research in two parts; steady potential, and steady potential with respect to the free surface effect.

3.3.1 STEADY POTENTIAL WITHOUT FREE SURFACE EFFECT

Based on the assumption of inviscid, incompressible and irrotational flow around a ship's hull with constant speed u in the x-direction the potential flow is expressed as equation (3.7). For the first part of the research the ship's hull is assumed as moving through calm water where it can not disturb the free surface. Thus the potential flow associated with double body theory can be presented as:

$$\Phi = \Phi_{body} + \Phi_{body-image} \tag{3.32}$$

To satisfy Laplace's equation (3.8) and applying Green's identity, the potential at any field point due to a source point over the boundary surface for three dimensional body can be written as equation (3.10). In the equation, s_0 is the wetted surface of a ship's hull. It is approximated by N triangular flat panels, as explained in detail in Chapter 5. Here it is assumed that the ship moves in the horizontal plane where its motion can not disturb the free surface. The corresponding boundary condition (3.34) is satisfied by adding an image to the submerged portion of the hull. The resulting "double body" is symmetrical about the plane of the free surface, and the potential velocity can be written as:

$$\Phi = \frac{1}{4\pi}\sum_{j=1}^{N}\sigma_j \int_{s_j}\left(\frac{1}{r}+\frac{1}{r'}\right)ds \tag{3.33}$$

where: r is distance between field point to source point and

r' is distance between field point image to source point

s_j is the j^{th} flat panel area.

As mentioned earlier, Laplace's equation requires that no mass flow is created or destroyed from a body. For the body moving with speed u in the x-direction, the body boundary condition can be written as:

$$\nabla\phi \cdot \vec{n} = un_x \qquad \text{on } s_0 \tag{3.34}$$

or:

$$\frac{\partial\phi}{\partial x}n_x + \frac{\partial\phi}{\partial y}n_y + \frac{\partial\phi}{\partial z}n_z = un_x \tag{3.35}$$

where: $\vec{n}$ is the normal of the panel pointing out of the surface,

n_x, n_y and n_z are its components.

To satisfy the above boundary condition at control points, the velocity of the body normal to the panels must be equal to the velocity in the same direction of the fluid. Then for the body and its mirror image we can obtain:

$$\frac{\partial\phi}{\partial n} = \frac{1}{4\pi}\sum_{j=1}^{N}\sigma_j \int_{s_j}\frac{\partial}{\partial n}(\frac{1}{r}+\frac{1}{r'})ds \tag{3.36}$$

or:

$$\frac{\partial\phi}{\partial x}n_x + \frac{\partial\phi}{\partial y}n_y + \frac{\partial\phi}{\partial z}n_z = \frac{1}{4\pi}\sum_{j=1}^{N}\sigma_j \int_{s_0}\frac{\partial}{\partial n}(\frac{1}{r}+\frac{1}{r'})ds \tag{3.37}$$

Thus:

$$\frac{\partial\phi}{\partial n} = \frac{1}{4\pi}\sum_{j=1}^{N}\sigma_j \int_{sj}\left[\frac{\partial}{\partial x}\left(\frac{1}{r}+\frac{1}{r'}\right)\cdot n_x + \frac{\partial}{\partial y}\left(\frac{1}{r}+\frac{1}{r'}\right)\cdot n_y + \frac{\partial}{\partial z}\left(\frac{1}{r}+\frac{1}{r'}\right)\cdot n_z\right]ds \tag{3.38}$$

The right hand side of equation (3.38) shows components of the normal velocity at the i^{th} panel. Then equation (3.38) can be written as:

$$\left(\frac{\partial\phi}{\partial n}\right)_i = \frac{1}{4\pi}\sum_{j=1}^{N}\sigma_j A_{ij} \tag{3.39}$$

where:

$$A_{ij} = \int_{sj}\left[\frac{\partial}{\partial x}\left(\frac{1}{r}+\frac{1}{r'}\right)\cdot n_x + \frac{\partial}{\partial y}\left(\frac{1}{r}+\frac{1}{r'}\right)\cdot n_y + \frac{\partial}{\partial z}\left(\frac{1}{r}+\frac{1}{r'}\right)\cdot n_z\right]ds \qquad \text{for } i \neq j$$

$$A_{ij} = \frac{1}{2} \qquad \text{for } i = j \tag{3.40}$$

In summary, the velocity potential and the potential function can be written as:

$$un_x(Q_i) = \frac{1}{4\pi}\sum_{j=1}^{n} A_{ij}\sigma_j \tag{3.41}$$

$$\Phi(Q_i) = \frac{1}{4\pi}\sum_{j=1}^{N} B_{ij}\sigma_j \tag{3.42}$$

respectively.

The component of A_{ij} can be obtained according to the method used by Hess and Smith (1967), Bai and Young (1974), and Katz and Plotkin (1991). They chose a quadrangular panel, but here the triangular flat panel has been chosen, because a ship's hull is a very complex shape. The following equations therefore are obtained based upon the above references, and they are worked out for the triangular panel. Hence the component of normal velocity can be written as:

$$A_{ij} = un_x + vn_y + wn_z \tag{3.43}$$

where: u, v and w are velocity components such as:

$$u = \frac{\sigma}{4\pi}\left[\frac{y_2 - y_1}{d_{12}}\ln\frac{r_1 + r_2 - d_{12}}{r_1 + r_2 + d_{12}} + \frac{y_3 - y_2}{d_{23}}\ln\frac{r_2 + r_3 - d_{23}}{r_2 + r_3 + d_{23}} + \frac{y_1 - y_3}{d_{31}}\ln\frac{r_3 + r_1 - d_{31}}{r_3 + r_1 + d_{31}}\right]$$

(3.44)

$$v = \frac{\sigma}{4\pi}\left[\frac{x_1 - x_2}{d_{12}}\ln\frac{r_1 + r_2 - d_{12}}{r_1 + r_2 + d_{12}} + \frac{x_2 - x_3}{d_{23}}\ln\frac{r_2 + r_3 - d_{23}}{r_2 + r_3 + d_{23}} + \frac{x_3 - x_1}{d_{31}}\ln\frac{r_3 + r_1 - d_{31}}{r_3 + r_1 + d_{31}}\right]$$

(3.45)

$$w = \frac{\sigma}{4\pi}\left[\tan^{-1}\left(\frac{m_{12}e_1 - h_1}{zr_1}\right) - \tan^{-1}\left(\frac{m_{12}e_2 - h_2}{zr_2}\right) +\right.$$

$$\tan^{-1}\left(\frac{m_{23}e_2 - h_2}{zr_2}\right) - \tan^{-1}\left(\frac{m_{23}e_3 - h_3}{zr_3}\right)\Bigg] +$$

$$\tan^{-1}\left(\frac{m_{31}e_3 - h_3}{zr_3}\right) - \tan^{-1}\left(\frac{m_{31}e_1 - h_1}{zr_1}\right)\Bigg] \qquad (3.46)$$

where:

$$d_{12} = \sqrt{(x_2 - x_1)^2 + (y_2 - y_1)^2}$$

$$d_{23} = \sqrt{(x_3 - x_2)^2 + (y_3 - y_2)^2}$$

$$d_{31} = \sqrt{(x_1 - x_3)^2 + (y_1 - y_3)^2}$$

$$m_{12} = \frac{y_2 - y_1}{x_2 - x_1}$$

$$m_{23} = \frac{y_3 - y_2}{x_3 - x_2}$$

$$m_{31} = \frac{y_1 - y_3}{x_1 - x_3}$$

$$r_k = \sqrt{(x - x_k)^2 + (y - y_k)^2 + z^2} \qquad k=1,2,3$$

$$e_k = (x - x_k)^2 + z^2$$

$$h_k = (x - x_k)(y - y_k)$$

Once the components of A_{ij} are known, the source strength σ_j can be computed from linear algebraic equation (3.41).

To compute the velocity potential from equation (3.42), the component of B_{ij} can be obtained according to the above references. For the triangular panel we can write:

$$B_{ij} = \int_{s_j} \frac{ds}{\sqrt{(x - x_0)^2 + (y - y_0)^2 + z^2}} \qquad (3.47)$$

which gives:

$$B_{ij} = \left\{\left[\frac{(x - x_1)(y_2 - y_1) - (y - y_1)(x_2 - x_1)}{d_{12}} \ln\frac{r_1 + r_2 + d_{12}}{r_1 + r_2 - d_{12}}\right.\right.$$

$$+\frac{(x-x_2)(y_3-y_2)-(y-y_2)(x_3-x_2)}{d_{23}}\ln\frac{r_2+r_3+d_{23}}{r_2+r_3-d_{23}}$$

$$+\frac{(x-x_3)(y_1-y_3)-(y-y_3)(x_1-x_3)}{d_{31}}\ln\frac{r_3+r_1+d_{31}}{r_3+r_1-d_{31}}\Bigg]$$

$$+|z|\cdot\Bigg[\tan^{-1}\left(\frac{m_{12}e_1-h_1}{zr_1}\right)-\tan^{-1}\left(\frac{m_{12}e_2-h_2}{zr_2}\right)$$

$$+\tan^{-1}\left(\frac{m_{23}e_2-h_2}{zr_2}\right)-\tan^{-1}\left(\frac{m_{23}e_2-h_2}{zr_3}\right)$$

$$+\tan^{-1}\left(\frac{m_{31}e_3-h_3}{zr_3}\right)-\tan^{-1}\left(\frac{m_{31}e_1-h_1}{zr_1}\right)\Bigg]\Bigg\} \qquad (3.48)$$

It should be noted that the derivation is performed in a local frame of reference on each panel (LCS). For the global co-ordinate system (GCS) a co-ordinate transformation is used to transfer data between two systems of co-ordinates.

The procedure described above is for velocity potential of the body $\Phi_{body}=\frac{1}{4\pi}\int_{s_0}\sigma\frac{1}{r}ds$ the same can be followed for the image of the body $\Phi_{body-image}=\frac{1}{4\pi}\int_{s_0}\sigma\frac{1}{r'}ds$, when in all equations (3.43) to (3.48) instead of the value of the r, the value of r' is used.

3.3.2 STEADY POTENTIAL WITH FREE SURFACE EFFECT

When a ship has forward speed, the free surface of the calm water is disturbed due to movement of the ship's hull, and a wave is generated. The problem has attracted many theoretical investigations by mathematicians. Despite this considerable effort a satisfactory solution of the steady ship motion problem with free surface effect has not been achieved so far. Extensive literature on the subject has been produced. The experimental and theoretical investigation of the problem is complicated considerably by the dependence of the ship's resistance on both viscous and gravitational effects.

It is assumed that the seawater is an ideal fluid and flow is irrotational in predicting wave-making resistance, in agreement with Froude's hypothesis (1868) concerning the separation of viscous flow and wave-making resistance. This implies that the effects of viscosity on the formation of ship waves are negligible.

A point of some current academic interest concerns the free surface effect on the pressure distribution on the body. The Neumann-Kelvin condition linearized the wave disturbance on the mean position of the free surface generated by a submerged source, hereafter referred to as the Kelvin source, and has been used extensively with panel methods utilizing the Kelvin wave source as a Green's function. It is subject to the Laplace equation in the fluid domain, and a radiation condition of no waves upstream. According to the international workshop held on the prediction of ship wave resistance, at the 1979 meeting in Washington DC, and recently a paper by Larsson (1998), this method is an extremely useful complement to the design tools of modern naval architects and is essential for modification of body line.

Assume that the right-handed co-ordinate system Oxyz moves with steady speed u in the same direction of the positive x-axis, as illustrated in Figure 3.1. The sea water is regarded as ideal (incompressible, inviscid and homogeneous) and irrotational flow, then the effects of surface tension, wave breaking and spray formation at the bow are not existant, and there are no external forces acting on the ship. The method applied here is a boundary integral method with Kelvin source, in an infinitely deep unbounded water, for which Havelock introduced the method of Green's functions, and can be found in Wehausen and Laiton (1960).

Green's functions are known for several important physical situations. Many of these are given in Wehausen and Laitone (1960). Consequently for 3D the potential function can be written as equations (3.29), (3.30) and (3.31). The parameters of these equations have the same meaning as presented elsewhere herein. The steady linear free surface flow around a hull is determined in the frequency domain so as to fulfil the linear free surface condition, and the hull surface condition. For the infinite fluid case the velocity potential associated with the flow about a body can be described by either a simple source or doublet distribution over the body surface, but here we chose

source distribution. The source distribution produces normal velocities which are discontinuous across the surface s_o. Moreover this will not cause a problem, because the flow on one side only is of interest, and this is usually the case. Thus the source distribution appears to be a convenient method and is applied as follows.

A potential at some point (x, y, z) in the fluid region may be expressed in terms of a surface distribution of sources as:

$$\Phi = \frac{1}{4\pi}\iint_{s_o}\sigma(\xi,\eta,\zeta)G(x,y,z;\xi,\eta,\zeta)ds \tag{3.49}$$

where: (ξ,η,ζ) denotes a point on s_0 and $\sigma(\xi,\eta,\zeta)$ denotes the unknown source distribution.

For steady motion in the x-direction, with velocity u, the $G(x,y,z;\ \xi,\eta,\zeta)$ is given by:

$$G(x,y,z;\xi,\eta,\zeta) = -\frac{4K}{\pi}\int_0^{\frac{\pi}{2}}\frac{1}{\cos^2\theta}d\theta\int_0^{\infty}\frac{e^{k(z+\zeta)}}{k-\frac{K}{\cos^2\theta}}\cos[k(x-\xi)\cos\theta]\cos[k(y-\eta)\sin\theta]dk$$

$$-4K\int_0^{\frac{\pi}{2}}\frac{1}{\cos^2\theta}e^{\frac{K(z+\zeta)}{\cos^2\theta}}\sin\left[K\frac{x-\xi}{\cos\theta}\right]\cos\left[K\frac{(y-\eta)\sin\theta}{\cos^2\theta}\right]d\theta$$

where $$K = \frac{g}{u^2} \tag{3.49a}$$

The explanation is this has always the form of the infinite fluid with an additional term, consisting of a double integral over an oscillating integrand, which has to be evaluated numerically. The integral is carried out over the complete immersed surface of the object. The Green's function source potential $G(x,y,z;\ \xi,\eta,\zeta)$ satisfies all the boundary conditions of the problem apart from that on the body surface. Based on the assumption of the linearized theory, the steady potential must satisfy continuity:

$$\nabla^2\Phi = 0 \tag{3.50}$$

and on the body under the free surface Φ must be satisfied:

$$\nabla\phi\cdot\vec{n} = un_x \qquad \text{on } s_o \tag{3.51}$$

then the free surface boundary condition can be written as:

$$K\frac{\partial \Phi}{\partial z}+\frac{\partial^2 \Phi}{\partial x^2}=0 \qquad \text{on z=0} \qquad (3.52)$$

By definition of the Neumann-Kelvin problem, the free surface condition is linearized, but no restrictions are imposed on the shape of the hull surface. Some justification for adopting the linear free surface condition of the type expressed in equation (3.52) may be derived from experimental evidence which suggests that ship generated waves have relatively small amplitude over a large portion of the free surface, Baar (1987). More precisely, the wave elevation, ζ_w, can be written as:

$$\zeta_w = K(\frac{\partial \Phi}{\partial x}-\frac{1}{2}|\nabla \Phi|^2) \qquad \text{on free surface} \qquad (3.53)$$

Furthermore, in order to ensure that the velocity potential has the correct behaviour in the far field the source does not generate waves upstream or far in front of the ship. In this case the waves follow the ship and there are no upstream waves.

Source strength density on each panel calculates in the same way as before (in the section 3.3.1). The calculation follows by solution of the last part of Green's function equation (source potential), as Wehausen has pointed for exact ship boundary condition without trim and squat this can be written as equation (3.31).

Serious drawbacks of the method are associated with CPU time as well as accuracy. Most computational schemes of the Green's function are not fast enough and validity of the numerical solution may be uncertain. Despite several attempts having been made to develop a reliable, fast enough and more accurate scheme for the numerical solution, further research is still needed to improve it. More detail can be found in Iwashita and Ohkusu (1989), Baar and Price (1988), Wehausen and Laitone (1960) and others.

4 NUMERICAL PROCEDURE OF THE THEORETICAL APPROACH

Throughout the previous chapter the fundamental mathematical formulae and their application of the potential flow were discussed. In this respect, it is assumed that, sea water is inviscid, incompressible, irrotational with a constant density, while atmospheric pressure is assumed at the free surface. The right handed co-ordinate system is fixed on the mid-ship at the free surface level, which is moving forward in the positive x-direction at constant speed (u, 0, 0) and there are no external forces or moments acting on the ship.

This chapter discusses the procedure for implementation of the theoretical approach of the current research to analyse the stability of a ship with forward speed. Although the stability in nature is an unsteady problem, in the research it is assumed that for a ship sailing in the steady state with a constant forward speed in calm water the effects of different speeds on the intact GM are sought. In fact, hydrostatic pressure acts on the wetted surface of a stationary floating body in calm water, where there are no current and external forces or moments acting on the body, only the weight of the body equals to the buoyancy force. The situation is very different for the body sailing in calm water, there is a contribution of hydrostatic and hydrodynamic forces acting on the wetted surface of the body in the same water. The buoyancy force includes hydrostatic and hydrodynamic forces, which depend upon the shape and speed of the body. Sinkage of the body shows the effect of contribution of the forces on the body against gravitational force on the body. An example is lifting of a high speed ship in a speed range. In addition, any inclination angle transversely and / or longitudinally of the sailing body depends on location of the centre of gravity (G) and location of the residual forces acting on the body (B). Hence, unbalanced pressure distribution on the wetted surface related to the CL and / or related to the mid-ship section creates inclination angle (heel and/or trim, and may contribute to yaw). Therefore, action of the unbalanced pressure distribution on the wetted surface of the sailing body may increase or decrease these angles. The work presented herein uses the panel method of CFD to compute pressure distribution on a ship hull form to investigate the aim of the research.

The technique was first developed in aeronautical engineering for analysing arbitrary body shapes such as wing sections by Hess and Smith (1967). Generally, the flow around an arbitrary three dimensional body may be analysed using the boundary integral equation method replacing the boundary value problem as an integral equation that was established by Hess and Smith. The arbitrary three dimensional body surface is approximated by using either quadrilateral or triangular panels. The method has been successfully applied in many applications by other researchers, and was well documented by Katz and Plotkin (1991).

The mathematical model adopted is based on Kelvin source distributed on a ship's hull. For a ship travelling with steady forward speed at the free surface the wave-making solution was derived from a Neumann-Kelvin formulation by means of a three dimensional linearised potential flow theory.

To solve the linear hydrodynamic problem in three dimensional analysis one may use the Neumann-Kelvin formulation, which is one of the most popular methods. In the method the free surface boundary condition is linearised using the free stream potential at the mean position of the free surface and the body boundary condition at the mean position of the body surface. Then the geometry of body form is arbitrary, and discretization of the body surface satisfies the body boundary condition at the collocation points.

Mainly, the method is used to calculate the pressure distribution on the wetted hull surface at certain loading conditions of the ship. Then the actions of forces on the wetted hull surface are computed corresponding with variation of forward speed of the ship. The location of the centre of gravity of a ship may not exactly be on the centre plane (OXZ) as shown by Kap and Kastner (1990). Therefore, there exists unbalanced pressure distribution related to the centre plane, which may cause inclination of the ship. Hence, the variation of the GM, since it is indication of the stability of a ship, may be evaluated by equating the inclination moment with the righting moment, in a sea-way. Here, it is assumed the unbalanced pressure is only related to the x axis and not to y axis, and the yaw angle or motion does not occur.

For the purpose of the research a CFD potential computer code, based on the discussed theoretical method has been developed. Through the last three decades many CFD code have been developed to compute hydrodynamic forces on a partially floating body for steady and unsteady flow and also for viscous and non-viscous flow problems. Some of them were introduced by Larrsan (1998) and also research presented at ITTCs, stability workshops and RINA conferences. However, due to unavailability of validated CFD computer code for the research at UCL as a tool, the presented potential CFD code started from a very basic stage and was developed as described in the following.

4.1 INPUT DATA

The computational domain is the wetted surface of a ship's hull. It is divided into N triangular panels. As mentioned above there may be very powerful mesh generation computer codes available in many other research centres, but due to unavailability of such a tool a mesh generation computer code was also developed for the purpose of the research. The procedure of the mesh generation is discussed in Chapter 5 in detail. However, Figure 4.1 shows the system of co-ordinates, and brief definitions of node and panel numbering on the immersed part of a ship's hull.

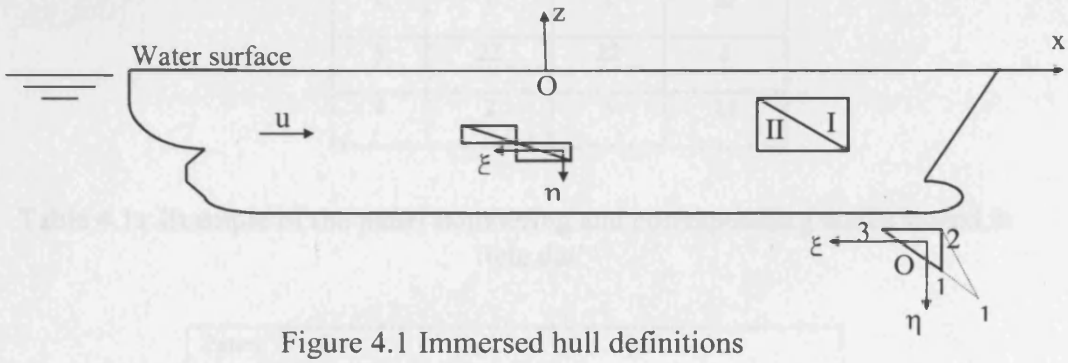

Figure 4.1 Immersed hull definitions

Where:

Oxyz is the global co-ordinate system (GCS) fixed at mid-ship

Oξη is the local co-ordinate (LCS) system on the element

1, 2 and 3 show the local node's number of an element

I and II show the element's numbering.

The mesh generation computer code prepares two data files. One of them includes the node number and its specification in the Global Cartesian Coordinate System (GCS), the file is called '*fnod.dat*'. The other one named '*tele.dat*' includes the element and its corresponding nodes. Examples of these data files are shown in Tables 4.1 and 4.2 respectively.

Node	x	y	z
1	0.13436650E+03	0.000000E+00	0.0000E+00
2	0.12790000E+03	0.145500E+01	0.0000E+00
3	0.12150000E+03	0.267225E+01	0.0000E+00
4	0.11510000E+03	0.389400E+01	0.0000E+00
38	0.25500000E+02	0.607000E+01	-0.3500E+00
39	0.19100000E+02	0.344000E+01	-0.3500E+00

Table 4.1 Example of the node numbering and co-ordinates in the GCS stored in 'fnod.dat'

Panel	Corresponding Nodes		
	1	2	3
1	22	21	1
2	1	2	22
3	23	22	2
4	2	3	23

Table 4.1a Example of the panel numbering and corresponding nodes stored in 'tele.dat'

Panel I		
Nodes	1	X1,Y1,Z1
	2	X2,Y2,Z2
	3	X3,Y3,Z3
Panel II		
Nodes	1	X1,Y1,Z1
	2	X2,Y2,Z2
	3	X3,Y3,Z3

Table 4.2a Examples of panel numbering and corresponding nodes specifications

These data files, which define the wetted surface of ship's hull, have suitable input format for the CFD computer code. In addition, input data files, with panel number and coordinates of three corresponding corners in format as shown in Table 4.2a is used for validation of the CFD code. The original of the file for quadrangular panel on the wetted surface of a Wigley hull was provided by the Ship Stability Research Centre of University of Strathclyde.

For visual checks of the generated panel on the wetted surface of the model some graphical examples are shown in Figures 4.2 to 4.4. More information and validation of the code may be found in Chapter 5.

Cross sections of the physical model are shown in Figure 4.2. It shows how the cross sections of the model change from bow to stern. Whereas, figures 4.3 and 4.4 show the arrangement of the triangular panels that are fixed on the wetted surface of the model.

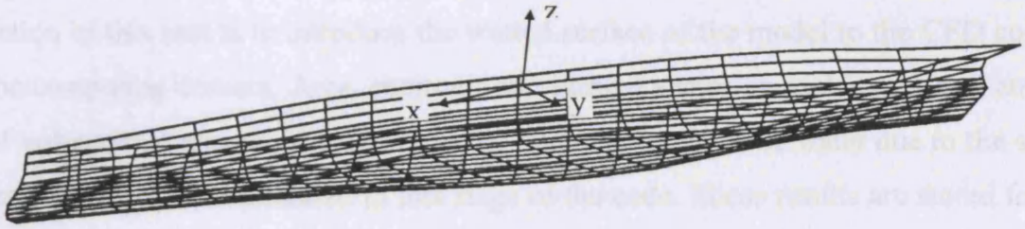

Figure 4.2 View of the ship, showing body curves, and cross sections from bow to aft

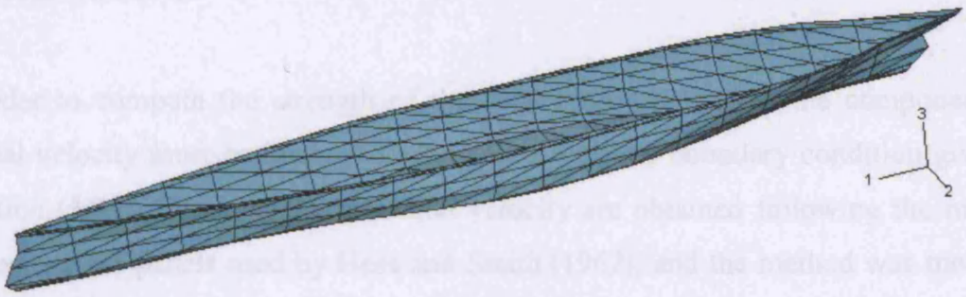

Figure 4.3 View of the immersed part of ship by the triangular panels

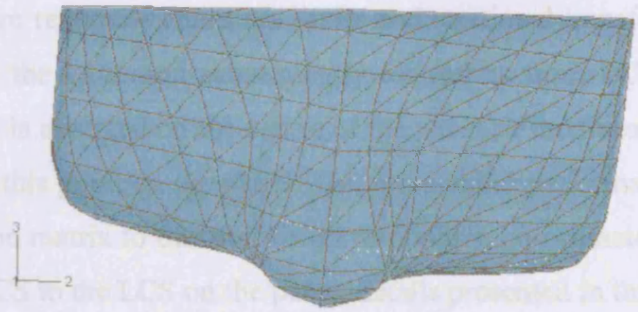

Figure 4.4 Front view of an inclined ship wetted part

The CFD code has three parts: pre-processing, processing, and results. These are applied to implement the theory in Section 3.3. More detail is described in the following sections including how they link together for the purpose of the research.

4.2 PRE-PROCESSING

The pre-processing of data for steady potential flow (the CFD code) works such that data are read from input files as described in detail in the above section. The first action of this part is to introduce the wetted surface of the model to the CFD code as the computing domain. Area, centroid, unit normal vector on each panel, and amount of volume that a panel contributes to the total displacement of water due to the ship's immersed hull are calculated in this stage of the code. These results are stored for the following calculation.

4.3 PROCESSING

In order to compute the strength of the source on each panel, the components of normal velocity must be known in accordance with the boundary condition given in equation (3.34). Components of normal velocity are obtained following the method for rectangular panels used by Hess and Smith (1967), and the method was modified for the triangular panel in the theoretical formula as shown in equations (3.43) to (3.48) for the current panel form.

Equations (3.35) to (3.40), and (3.43) to (3.48) are referenced to the local co-ordinate system (LCS) of each panel. Therefore, in order to use equations (3.43) to (3.48),

transformations are required. There are linear and rotational transformations for data from the GCS to the LCS, and subsequently for results from LCS to GCS. As the origin of the LCS is assumed on the centre of the panel so the linear transformation is from the GCS to this point on the panel. The rotational transformation is in the form of a transformation matrix to transfer the corresponding co-ordinates of all nodes of a panel from the GCS to the LCS on the panel, details presented in the Appendix B.

In order to shift the data from the GCS (x, y, z) to the LCS (ξ, η, ζ), the linear transformation of data is from the GCS to the centre of each panel. Therefore, nodal coordinates of a panel are used to find this origin. The corresponding nodes of each panel are used to establish the rotational transformation since rotations are not available as angles as discused in Appendix B. Once the transformation matrix {t} is calculated for a panel, the corresponding coordinate of each corner of the panel on the LCS may be computed as shown in equation (4.1).

$$\begin{Bmatrix} \xi \\ \eta \\ \zeta \end{Bmatrix} = \begin{Bmatrix} x_p - x_c \\ y_p - y_c \\ z_p - z_c \end{Bmatrix} \begin{Bmatrix} t_{11} & t_{12} & t_{13} \\ t_{21} & t_{22} & t_{23} \\ t_{31} & t_{32} & t_{33} \end{Bmatrix} \tag{4.1}$$

where: ξ, η, and ζ are co-ordinates of a node on the LCS

x_p, y_p and z_p are co-ordinates of a node of an element from the GCS

x_c, y_c and z_c are co-ordinates of centroid of an element from the GCS

t_{ij} $i=1..3, j=1..3$ are coefficients of transformation matrix.

Hence, the data are ready for equation (3.43) to calculate N by N coefficients of A_{ij}. To estimate strength of source on each panel, the RHS of equation (3.34), which is the boundary condition, must be calculated. Then with N panels on the wetted surface of the hull there exists a linear system of N equations, which can be solved simultaneously to obtain the source strength on panels:

$$\begin{Bmatrix} a_{11} & .. & .. & a_{1N} \\ : & .. & .. & : \\ : & .. & .. & : \\ a_{N1} & .. & .. & a_{NN} \end{Bmatrix} \begin{Bmatrix} \sigma_1 \\ \sigma_2 \\ : \\ \sigma_N \end{Bmatrix} = \begin{Bmatrix} un_{x1} \\ un_{x2} \\ : \\ un_{xN} \end{Bmatrix} \tag{4.2}$$

Once the strengths of the sources have been obtained, in order to evaluate the velocity potential on each panel, the component of B_{ij} is calculated using equation (3.48):

$$\begin{Bmatrix} \phi_1 \\ \phi_2 \\ \vdots \\ \phi_N \end{Bmatrix} = \begin{bmatrix} b_{11} & .. & .. & b_{1N} \\ \vdots & .. & .. & \vdots \\ \vdots & .. & .. & \vdots \\ b_{N1} & .. & .. & b_{NN} \end{bmatrix} \begin{Bmatrix} \sigma_1 \\ \sigma_2 \\ \vdots \\ \sigma_N \end{Bmatrix} \tag{4.3}$$

Now, having obtained the velocity on each panel, the pressure distribution on each panel can be calculated using equation (3.23).

In order to confirm that the code developed was functioning correctly it was necessary to validate the results against a known result. Therefore a hemi-sphere and a Wigley hull were chosen as test cases.

4.4 RESULTS

In order to solve the problem numerically and verify the results, firstly it is assumed that the motion of the model does not disturb the water surface (double body). Then, contribution of the pressure distribution of generated wave, due to steady forward speed of the model on the free surface, on the wetted surface of the model is added to evaluate the total velocity potential. In other words, the velocity potential can be computed in accordance with the flowchart shown in Figure 4.5 for steady state condition, once applying the formulae as discussed in section 4.3 and 3.3.

The generated waves on the free surface for deep and unbounded water can be modelled mathematically by the Green's function as equation (3.49), which is used to evaluate the small amplitude waves generated due to motion of the body on the free surface (surge). More detail about the Green's function can be found in "Surface wave" by Wehausen and Laitone (1960). The evaluation of the Green's function was found to be very sensitive to position of the panel in particular near to the free surface, as is reported in valuable papers by Newman (1987), Ursell (1960, 1988), Baar and Price (1988), and others.

Accordingly, Bernoulli's equation is used in order to compute pressure distribution on the wetted surface of the hull once the velocity potential is obtained from the above

methodology. Forces and moments can be then computed for the prescribed loading condition and given forward speed.

Results of the code must be validated before any effort for the aim of the research, therefore, a Wigley ship hull form and a hemi-sphere are chosen as a test case for the validation of the code.

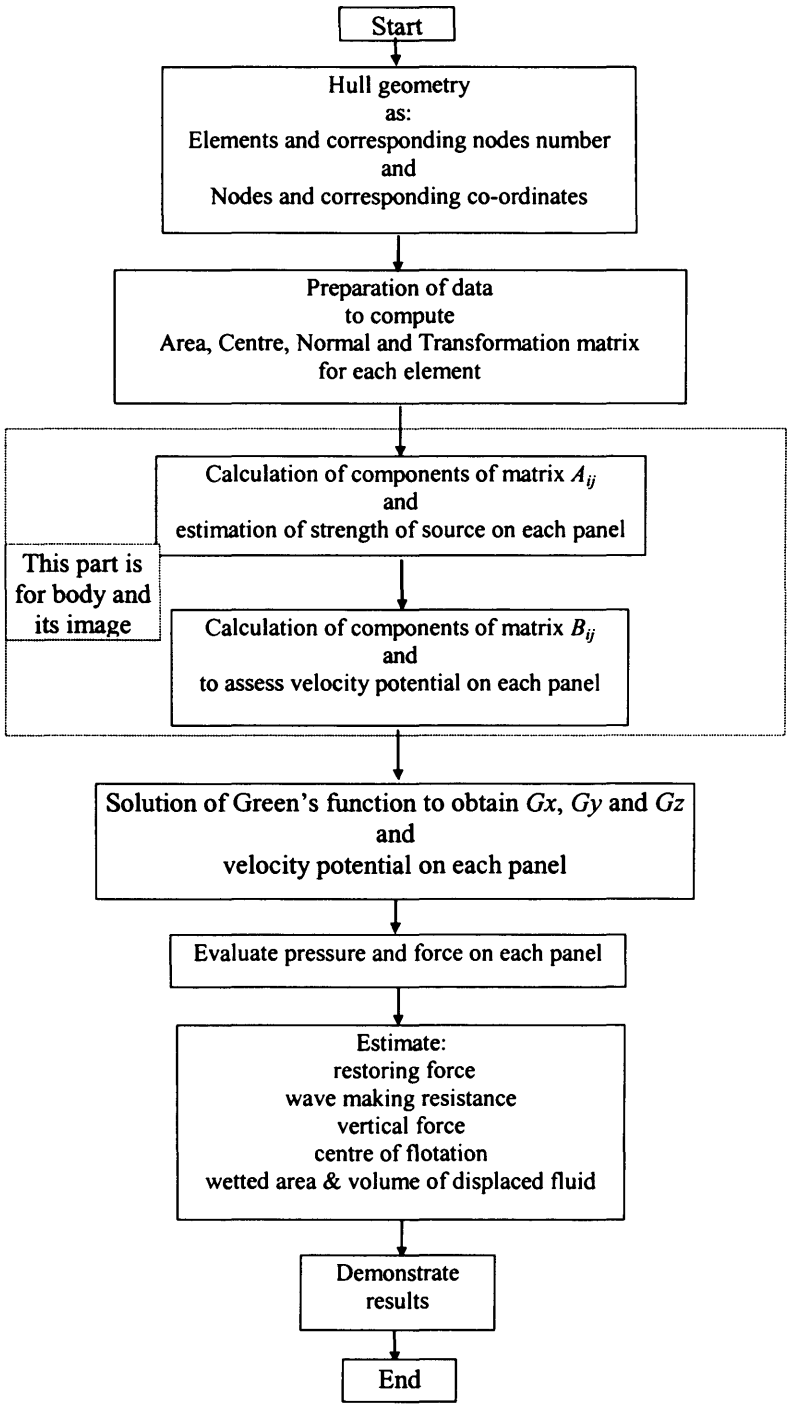

Figure 4.5 Complete CFD computer code flow chart

4.4.1 VALIDATION OF THE CFD POTENTIAL CODE

It is assumed that a hemi-sphere is immersed in calm water. It moves in the x-direction with speed u, as for the ship model and for the Wigley hull. The new mesh generation computer code was developed to create triangular panels on the hemi-sphere surface. The shape of a hemi-sphere is geometrically regular, and can be created with respect to its radius and using mathematical formule. The subdivision is chosen with the GCS origin of the hemi-sphere in the z direction, as its water line level, and on each circumference of a water line as water plane. Some graphical results of the mesh generation code are shown in Figures 4.6 to 4.9.

On completion of the mesh generation two output files are generated *'fnod.dat'* and *'tele.dat'*. These are input data to the CFD code. The results of running the code can be pressure distribution, resistance, sinkage and trim moment, the area of the immersed part of sphere and volume of the displaced water or other requirements.

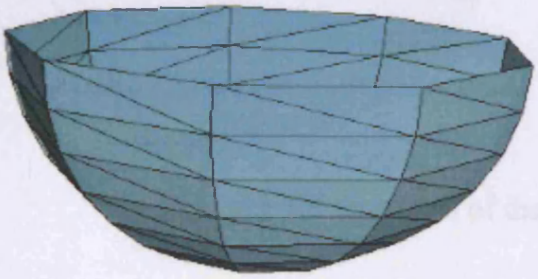

Figure 4.6 Perspective view of the hemi-sphere

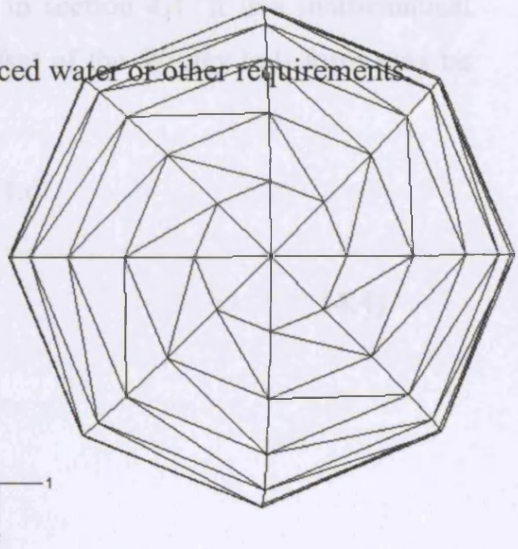

Figure 4.7 Plan view of the hemi-sphere

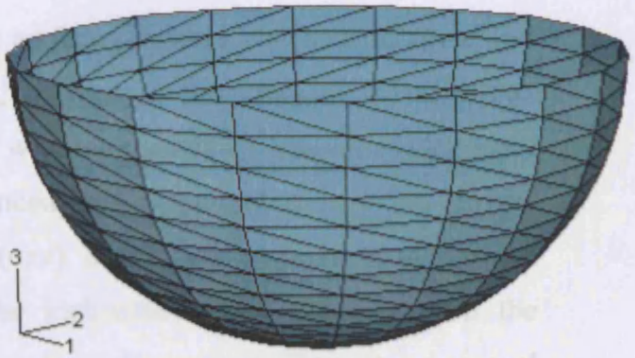

Figure 4.8 Perspective view of the hemi-sphere

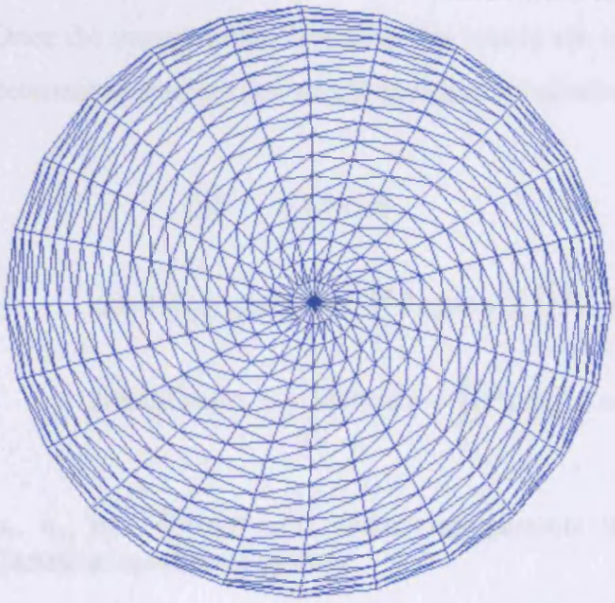

Figure 4.9 Plan view of the hemi-sphere

The other test case is a Wigley hull introduced in section 4.1. It is a mathematical form of model for research purposes, and the offset of the Wigley hull form may be described as follow:

Where: $\frac{L}{B}=10$ and $\frac{B}{T}=1.6$

$$\frac{2Y}{B}=\left\{1-\left(\frac{Z}{T}\right)^2\right\}\left\{1-4*\left(\frac{2X}{L}\right)^2\right\} \tag{4.4}$$

B is beam of the Wigley hull form

T is draft of the Wigley hull form

L is length of the Wigley hull form

The pressure distribution on the wetted hull surface produces a steady lift force and trim moment. The force leads to sinkage, as well as the moment to trim. The importance of the trim and sinkage of a ship was investigated by Vassalos (1996) and Ikeda and Katayama (1996). If an unbalanced pressure distribution exists on the wetted ship hull referenced to the CL plan (oxz), it produces an inclination moment that inclines the ship. Development of the inclination angle depends upon the equilibrium sign which either increases the angle or decreases it. Here, it is assumed that there is no unbalanced pressure distribution referenced to the mid cross section of the ship (oyz) plan.

Once the pressure distributed on the panels are computed, forces and moments can be determined through the steady pressure integration over the wetted hull surface.

$$Lift = -\iint_S Pn_z ds \tag{4.5}$$

$$restoringMoment = -\iint_S Pn_4 ds = -\iint_S P.(yn_z - zn_y)ds \tag{4.6}$$

$$TrimMoment = -\iint_S Pn_5 ds = \iint_S P.(zn_x - xn_z)ds \tag{4.7}$$

n_x, n_y, n_z Normal unit vector components in three directions according to the Cartesian coordinate system.

$n_{1\ to\ 6}$ Modes of motion: Surge, Heave, Yaw, Roll, Pitch, and Sway respectively.

The numerical results of the current research are presented in the following figures as University College London (UCL-ASD). For validation of the results the steady state wave resistance, sinkage force and trim moment are chosen. For comparison between the results with other research in this area it is assumed that the model is running in surge mode in calm water at constant forward speed where forces and moment on the body take constant values. Comparison between the CFD results with the results of Kara and Vassalos (2005) show good agreement. Figure 4.10 shows the steady wave resistance of the Wigley hull form, the wetted surface of the body is discretized with 144 panels on the half of the body surface. Sinkage force and trim moment are shown in Figures 4.11 and 4.12

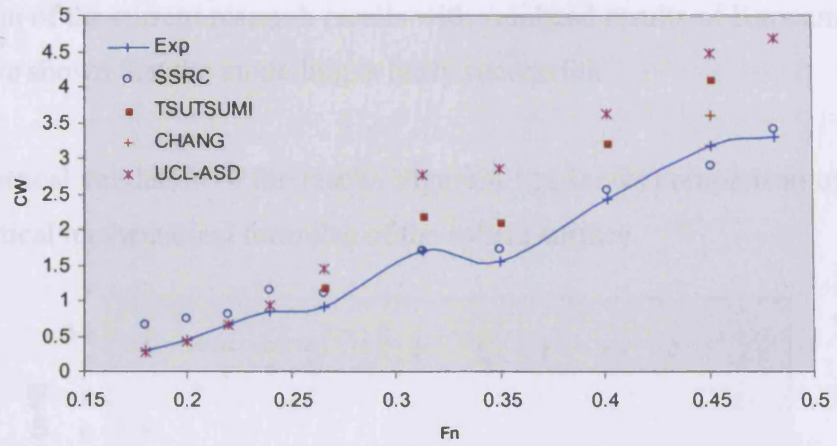

Figure 4.10 Comparison of wave resistance of Wigley hull at different Froude number for validation of the code

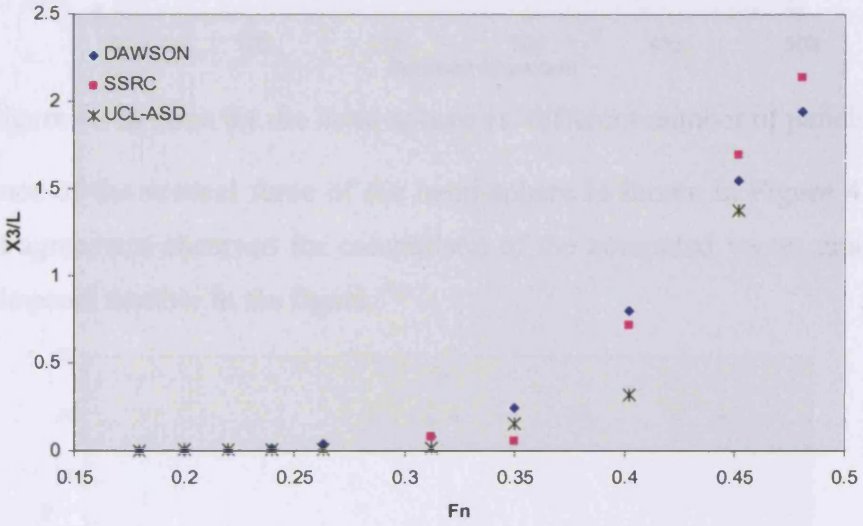

Figure 4.11 Comparison of Sinkage of Wigley hull at different Froude number for validation of the code

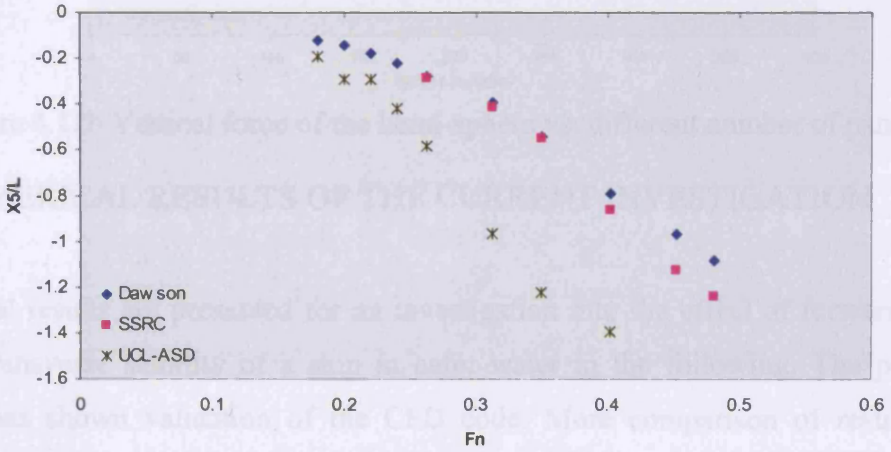

Figure 4.12 Comparison of Trim of Wigley hull at different Froude number for validation of the code

Comparison of the current research results with validated results of Kara and Vassalos (2005) have shown that the modelling is fairly successful.

For geometrical validation of the results Figure 4.12a shows comparison of the code with analytical mathematical formulae of the sphere surface.

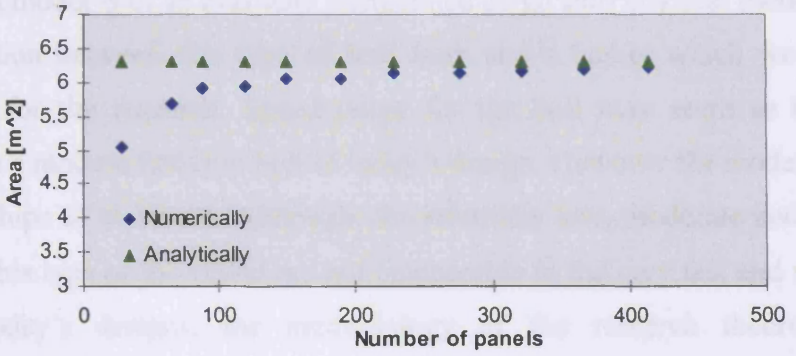

Figure 4.12a Area for the hemi-sphere vs. different number of panels.

Convergence of the vertical force of the hemi-sphere is shown in Figure 4.12b with very good agreement observed for comparison of the computed verses analytical *Fz* for suitable panel number in the figure.

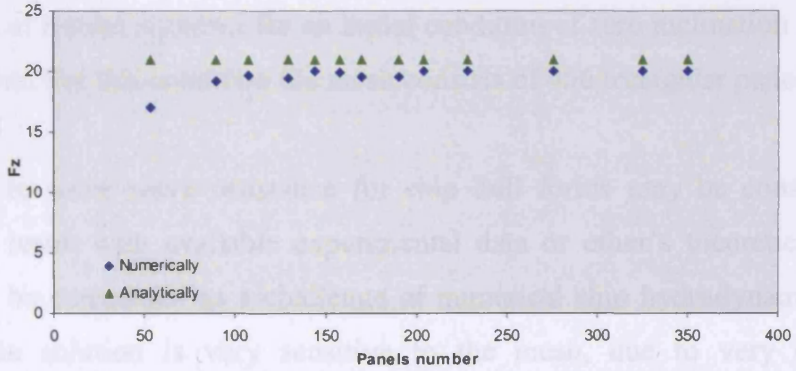

Figure 4.12b Vertical force of the hemi-sphere vs. different number of panels

4.5 NUMERICAL RESULTS OF THE CURRENT INVESTIGATION

Numerical results are presented for an investigation into the effect of forward speed on the transverse stability of a ship in calm water in the following. The previous section has shown validation of the CFD code. More comparison of results will confirm the approval of the code in the following section. Various parameters were computed over the prescribed speed range, and inclination angles in the range of small inclination angle. These parameters or results included sinkage and trim moment,

pressure distribution on the hull, wave making resistance and forces on the hull. Different numbers of the triangular panels for different loading conditions representing the wetted hull surface of the ship as the computer domain are shown as examples in Figures 4.2, 4.3 and 4.4, and in more detail in the Chapter 5.

The selected model is of an available refrigerated cargo ship physical model. This was the best option between this type of hull form and a tanker which were available alternatives for the research. Speed range for the hull may seem to be not high compared to a modern fast ship hull of today's design. However the model was one of the fastest ships of that time. Although, the relatively low, moderate and high speed referred to this type of the vessel are not comparable to the very fast and modern ship hulls of today's designs, the methodology of the research theoretically and experimentally have shown good results on the Wigley hull form in section 4.4 and 4.5.2.

4.5.1 INITIAL CONDITION

The first set of results is shown for an initial condition of zero inclination angle, and a draft of 7.55m. For this condition the mesh consists of 456 triangular panels.

The ability to solve wave resistance for ship hull forms may be considered as a comparable result with available experimental data or other's theoretical methods, then it may be considered as a challenge of numerical ship hydrodynamic research. However the solution is very sensitive to the mesh, due to very complicated mathematical formulae, as some computed results have shown e.g. Liangzi and Hsiung (1990). Figure 4.13 shows the computed wave resistance for the range of speeds of the ship. In fact, once the vessel begins to move from the stationery condition, due to the induced motion of surrounding water, at very low speeds the wave making resistance starts rising as speed increases, and at some level of speed it begins to decrease. In reality, total resistance of a body moving in a fluid depends upon wave making resistance and viscosity term of the fluid, the viscous term may be evaluated from extrapolation of resistance method for three dimensions introduced in ITTC 72 and 78 or other methods, but it is not considered here.

As it is assumed the fluid is inviscid the CFD code computes the wave making term of resistance. Generally, in a speed range of a body moving in calm water for the wave making resistance plot some hollows and humps appear, which are very important for evaluation of powering and propulsion system. Figure 4.13 shows an estimate (using a coarse mesh) of wave resistance for the initial condition. The pattern of the plot shows behaviour, which is possibly correct. Due to unavailability of experimental results for the model it is not possible to make comparison. However, the results of the code are validated for the Wigley hull form. Moreover, the quality of the prediction of wave resistance and other forces is dependent on the fineness of the mesh, but in some range of grid size results must show independence on the grid size. This is examined in the next section (4.6.2) with an increased number of panels.

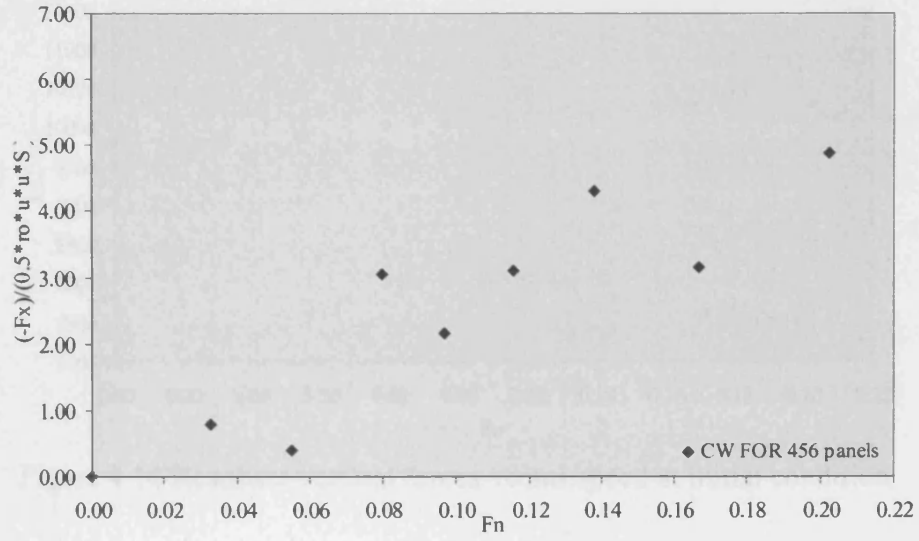

Figure 4.13 Wave resistance versus speed at initial condition

On the free surface for moderate and high speed ranges relatively larger wave amplitudes are generated than for the low speed range relatively. This shows that the wave resistance depends upon the hull form, the maximum cross sectional area of the hull normal to the direction of motion, and speed.

The resultant force of the vertical pressure is the buoyancy force, and at equilibrium condition this equals the weight of a ship when stationary and there are no external forces and moment acting on the ship. Owing to forward speed this force varies. If this force is greater than the ship's weight it causes the ship to rise (reducing draft).

Conversely if this force is less than the ship's weight the ship must be sink lower in the water (increases the draft).

Figure 4.14 shows the resultant vertical force on the hull for a range of speeds at the initial condition. The plot shows that for a small number of panels at low speed the computed *Fz* is less than the ship's displacement. It increases slightly for moderate and high speed range, in other words it is oscillating near and above the ship's displacement with speed. Generally, it is seen that the variation of speed modifies vertical force, demonstrating the role of the computed pressure distribution. These effects are presented in Figures 4.15 and 4.16 as sinkage and trim respectively.

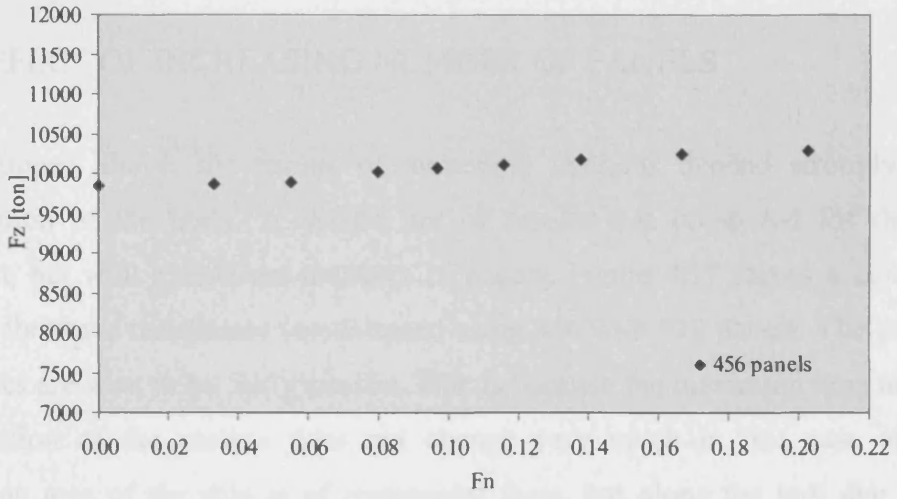

Figure 4.14 Resultant vertical forces versus speed at initial condition

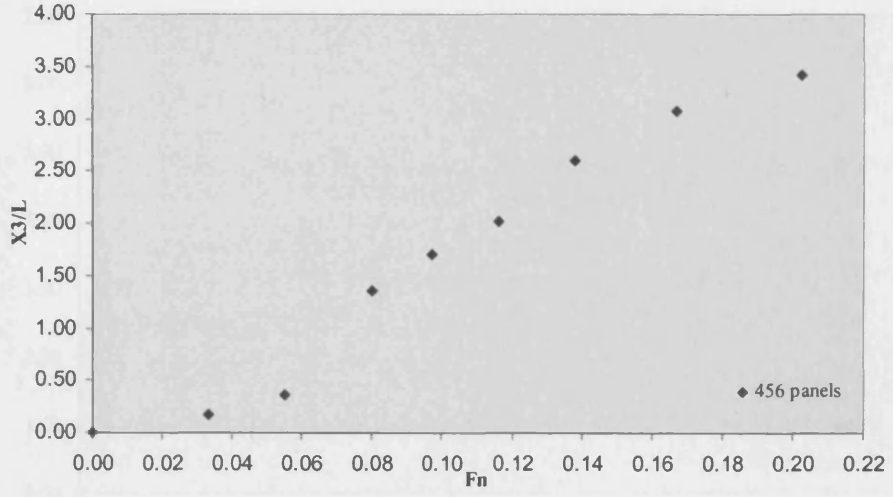

Figure 4.15 Sinkage forces versus speed at initial condition

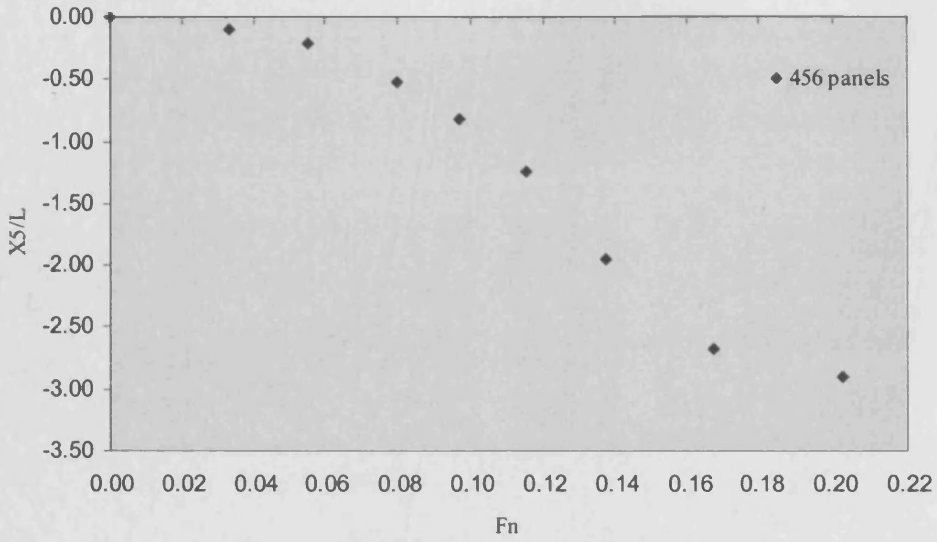

Figure 4.16 Trim moment versus speed at initial condition

4.5.2 EFFECT OF INCREASING NUMBER OF PANELS

As mentioned above, the results of numerical methods depend strongly on the discritisation of the body. A second set of results was computed for the initial condition, but with a different numbers of panels. Figure 4.17 shows a comparison between the wave resistances versus speed using 456 with 912 panels. The computed resistances are seen to be fairly similar. This is because the maximum area normal to the direction of the motion does not change very much in this case since the midsection area of the ship is of rectangular form, but along the hull due to more realistic hull shape this affected the results in particular for the high speed range.

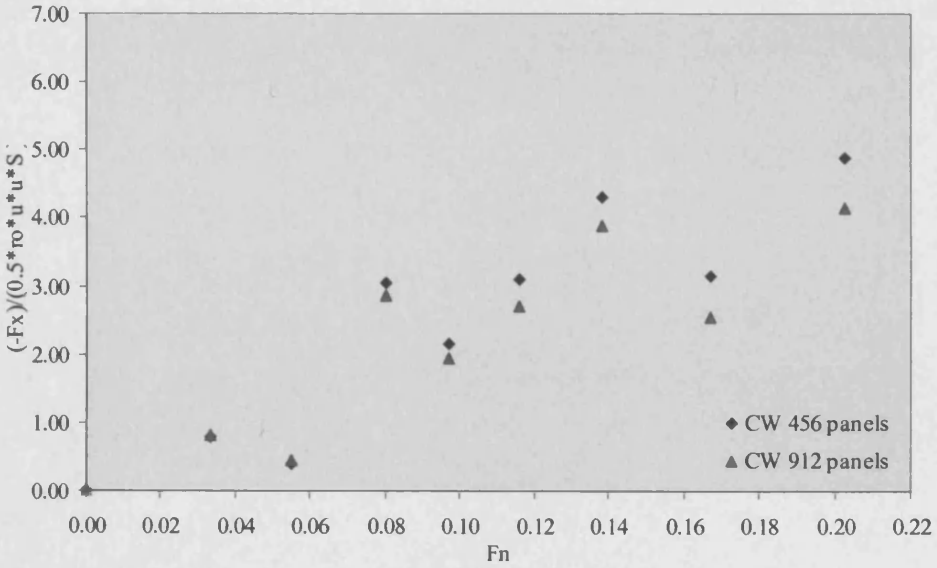

Figure 4.17 Wave resistances versus speed at initial condition for two sets of panel size

However, increasing the number of panels shows significant effects on wave resistance, forces and moments. Figure 4.18, using the model with 456 and 912 panels, shows a significant effect on the resultant vertical forces on the hull across the speed range. The figure shows that for both sets of panels, the buoyancy force oscillates about the weight of the ship although the oscillation for higher number of the panels is closer to the ship weight than lower number of the panels. The slope of the plot for the higher number of panels increases smoothly. Generally, it can be seen from the figure that vertical force varies due to forward speed, and the choice of the number of panels in the mesh has significant consequence on the computed results.

For a ship sailing in unbounded and calm water, the vertical resultant force is expected to increase in the same way as speed of the ship increases, as shown in Figure 4.18. But sometimes it is not true, if a low pressure region exists on the underwater area, which depends on many parameters such as trim angle, smoothness of surface of the wetted hull, appendages and so on as mentioned in Chapter 2.

Increasing the number of panels on the wetted hull surface shows a significant influence on the computed results as shown in Figure 4.17 to 4.20.

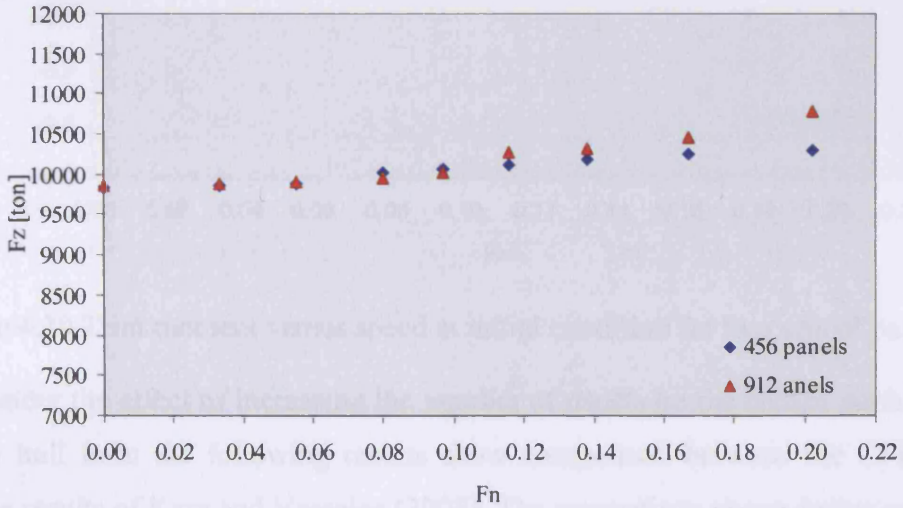

Figure 4.18 Vertical forces versus speed at initial condition for two sets of panel size

In the low speed part of the plots the results coincide more or less for both the lower and higher number of panels up to Fn ≈ 0.1, although evidently for better simulation

and meaningful results more panels or more accurate form of the hull are required. In some papers it is suggested more than 3000 panels are required but it depends on ability of computer, the computer program and implemented method of computing.

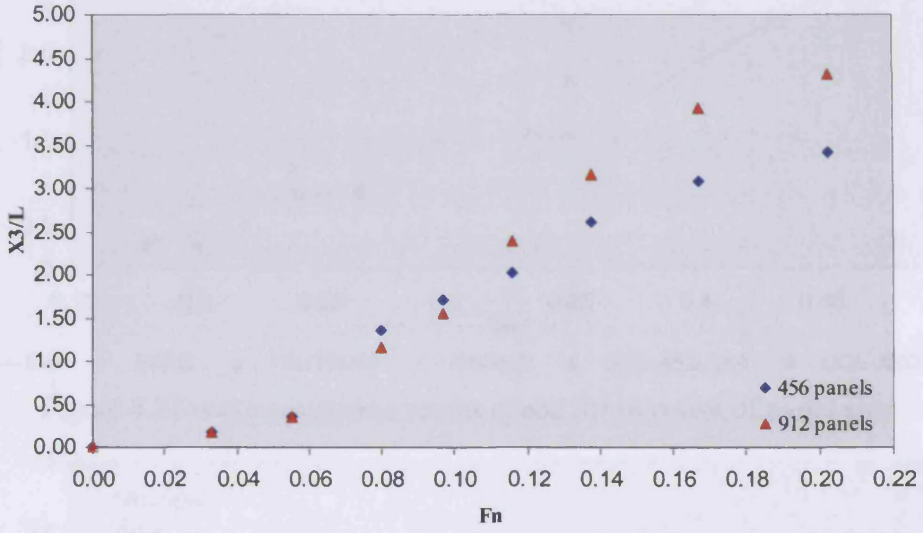

Figure 4.19 Sinkage versus speed at initial condition for two sets of panel size

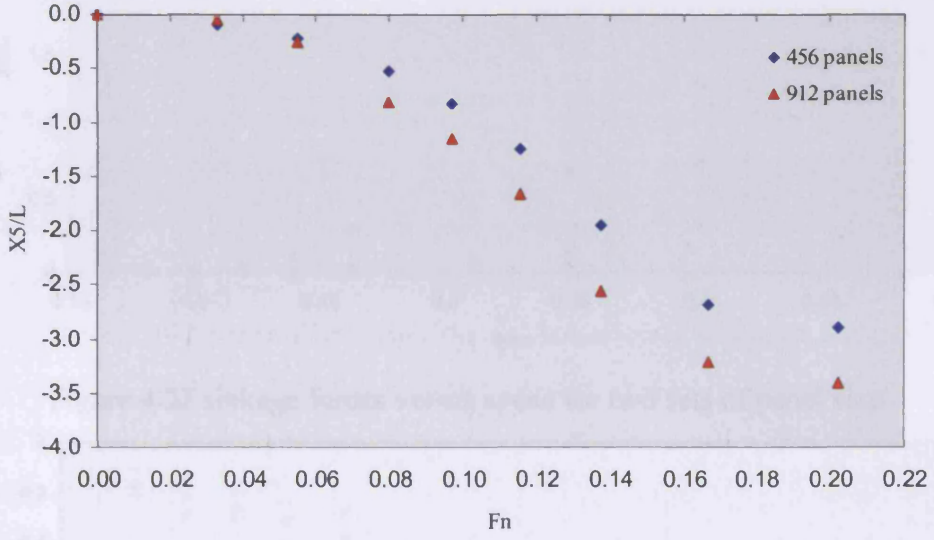

Figure 4.20 Trim moment versus speed at initial condition for two sets of panel size

To consider the effect of increasing the number of panels on the wetted surface of the Wigley hull form the following results show comparison between the CFD results with the results of Kara and Vassalos (2005). The comparison shows better agreement with increased number of panels. Figure 4.21 shows the steady wave resistance of the Wigley hull form, the wetted surface of the body is discretized with 144 and 256 panels on the half of the body surface. Sinkage force and trim moment are shown in Figures 4.22 and 4.23.

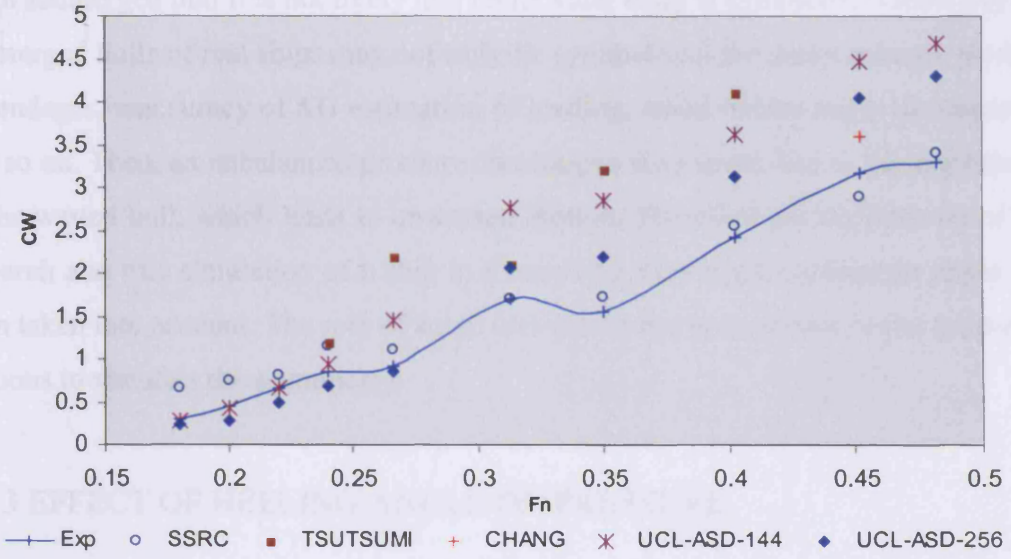

Figure 4.21 wave resistance versus speed for two sets of panel size

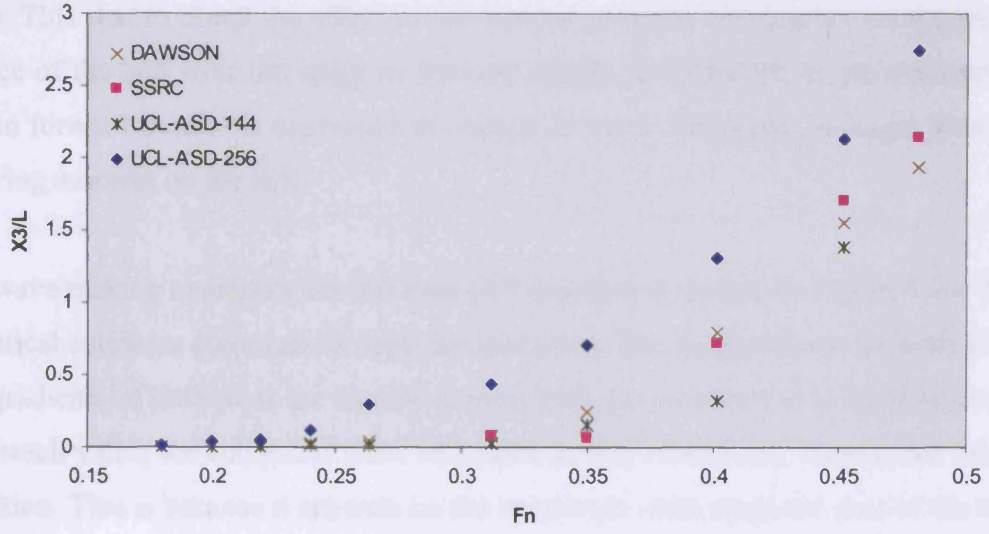

Figure 4.22 sinkage forces versus speed for two sets of panel size

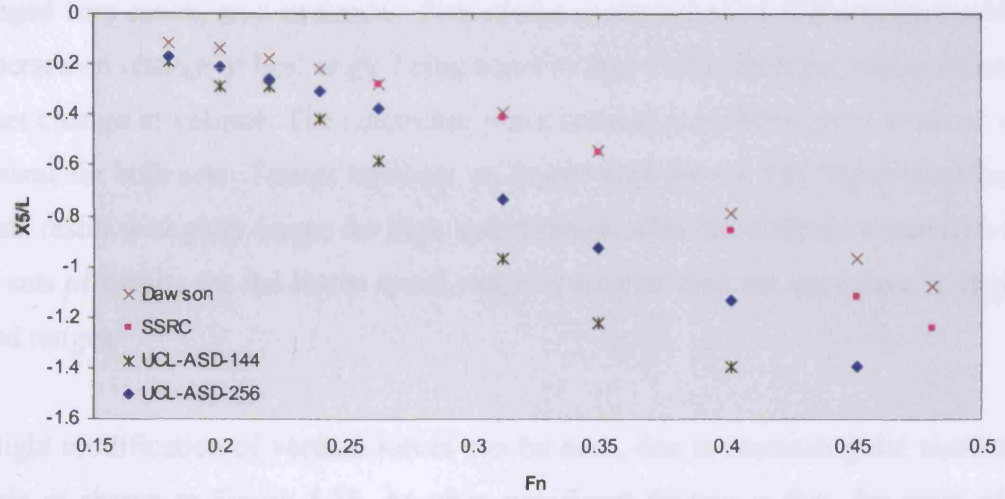

Figure 4.23 Trim moment versus speed for two sets of panel size

For a submerged hull it is not likely that underwater body is symmetric. Generally the submerged hulls of real ships may not truly be symmetrical for many reasons, such as appendages, inaccuracy of *KG* estimation of loading, small rudder angle in a seaway, and so on. Then, an unbalanced pressure distribution may occur due to the asymmetry of the wetted hull, which leads to unwanted motion. Therefore for the purpose of the research and true simulation of a ship in a seaway a very small inclination angle has been taken into account. The role of small inclination has been shown in the following sections to simulate the asymmetry.

4.5.3 EFFECT OF HEELING ANGLE ON PRESSURE

The third set of theoretical results was computed for the model with 2.5° inclination angle. This was to check the effect of unbalanced pressure distribution on the wetted surface of the hull over the range of forward speeds. Distribution of pressure on the hull in forward motion is expressed as change in wave resistance, sinkage, trim and restoring moment on the hull.

The wave making resistance for this case (2.5 degrees) is shown on Figure 4.24. The numerical solutions converge for both the grid sizes. The figure shows for both grids that gradients of both plots are similar in most part. In this case the inclination angle is of small value, the computed wave resistance is very close to its value at the initial condition. This is because it depends on the maximum cross sectional area of the hull normal to the direction of motion, as long as the area of cross section has not changed very much, so it is similar. This is also a consequence of the volume which immerses on change in heel angle being equal to that which emerges, and so there is no net change in volume. The calculated wave resistance in this case is more or less the same for both sets of panel numbers, as Figure 4.24 shows. The higher number of panels result is slightly larger for high speed range. Also the difference between the two sets of results for the lower speed range is smaller than the moderate or higher speed ranges.

A slight modification of vertical forces can be seen, due to increasing the number of panels as shown in Figure 4.25. Another significant finding is that, for most of the range of speeds, the resultant forces for both sets of panels vary in a similar way with

very small differences due to grid quality. The gradients of both plots are mostly smooth particularly in the low speed range.

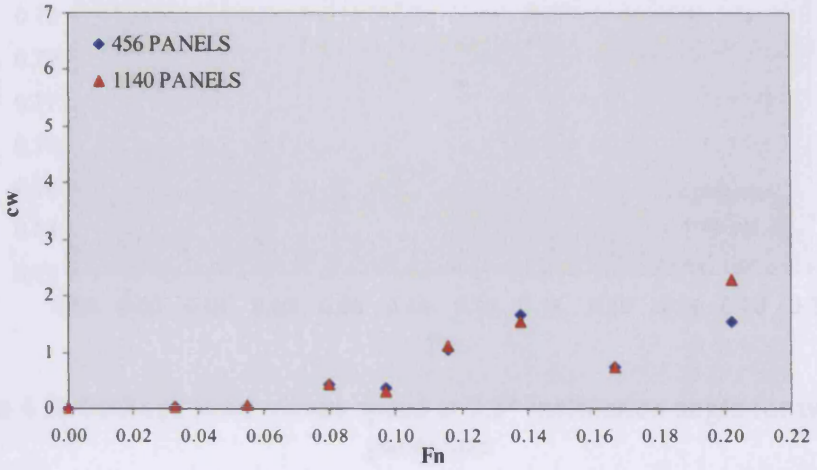

Figure 4.24 Wave resistances versus speed at 2.5° inclination angle for two sets of panel size

Figures 4.26 and 4.27 show the sinkage forces and trim moment for the case of 2.5° inclination angle. There are very significant findings from the results on these plots, showing that in lower speed range the effect of the inclination angle is not significant but increasing speed introduces the heave forces and the trim moments which are very different compared with the initial condition in Figures 4.19 and 4.20 respectively. Performance of the force and the moment are very impotent. To make this more clear, it was decided to increase inclination angle. The following results show better understanding of effects of unbalanced pressure distribution.

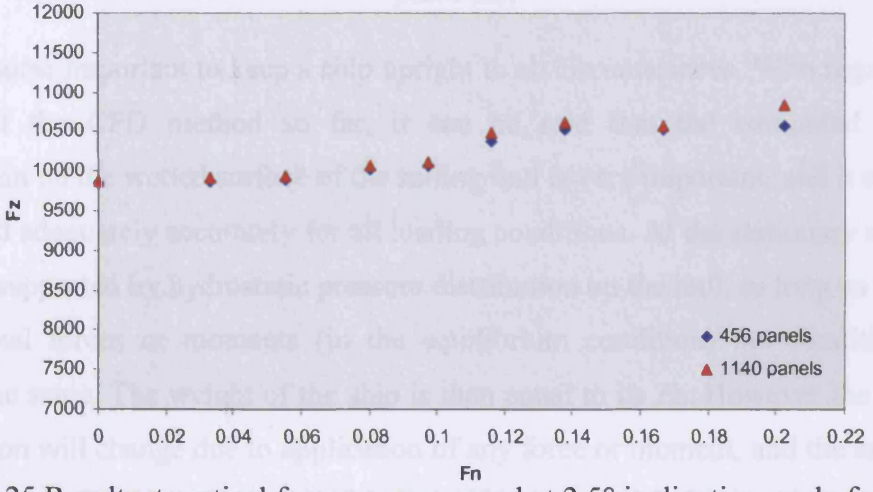

Figure 4.25 Resultant vertical forces versus speed at 2.5° inclination angle for two sets of panel size

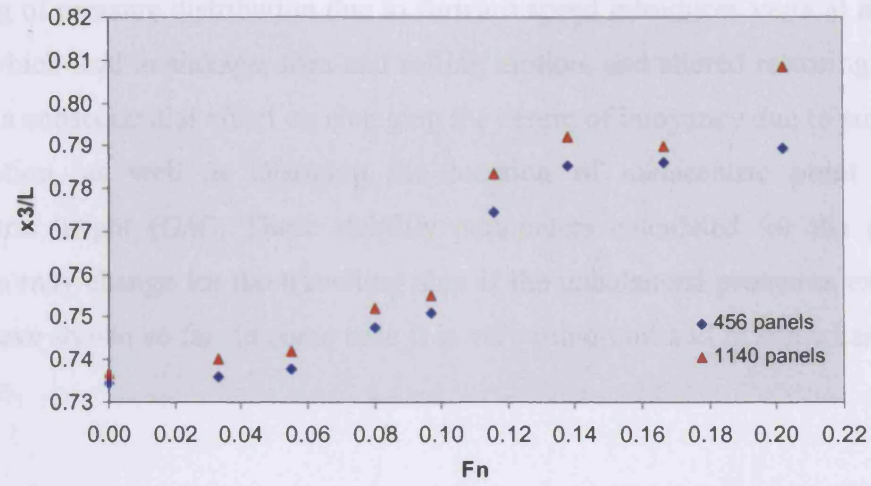

Figure 4.26 Sinkage force versus speed at 2.5° inclination angle for two sets of panel size

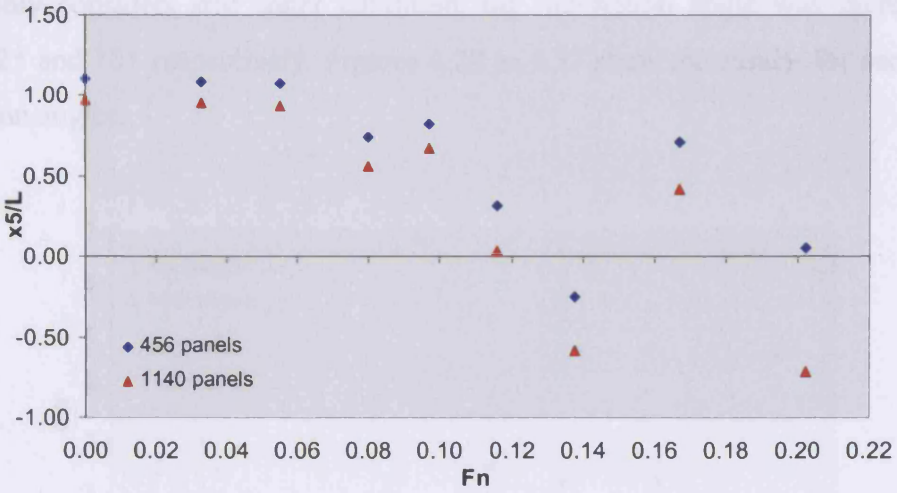

Figure 4.27 Trim moment versus speed at 2.5° inclination angle for two sets of panel size

It is of course important to keep a ship upright in all circumstances. With regard to the results of the CFD method so far, it can be said that the computed pressure distribution on the wetted surface of the sailing hull is very important, and it should be calculated adequately accurately for all loading conditions. At the stationary condition a ship is supported by hydrostatic pressure distribution on the hull, as long as there are no external forces or moments (in the equilibrium condition) the condition must remain the same. The weight of the ship is then equal to its *Fz*. However the pressure distribution will change due to application of any force or moment, and the associated hydrodynamic pressure can be positive or negative, which is very important in a seaway for safety of a ship. Consequently, motions may occur in reaction to an unbalanced pressure on the hull.

Changing of pressure distribution due to forward speed introduces vertical and lateral forces, which lead to sinkage, trim and rolling motion, and altered restoring moment. There is a consequential effect on changing the centre of buoyancy due to sinkage and trim motion, as well as changing the location of metacentric point affecting metacentric height (*GM*). These stability parameters calculated for the stationary condition may change for the travelling ship if the unbalanced pressures exist as the results have shown so far. In some case it is very important and in some cases it may be less so.

The risk of capsizing for any circumstance is not immediately apparent. To examine further the effect of variation of pressure distribution on the ship hull, in this research which only considers still water condition, the inclination angle was increased to 5.4°, 7.2° and 10° respectively. Figures 4.28 to 4.37 show the results for each set of inclination angles.

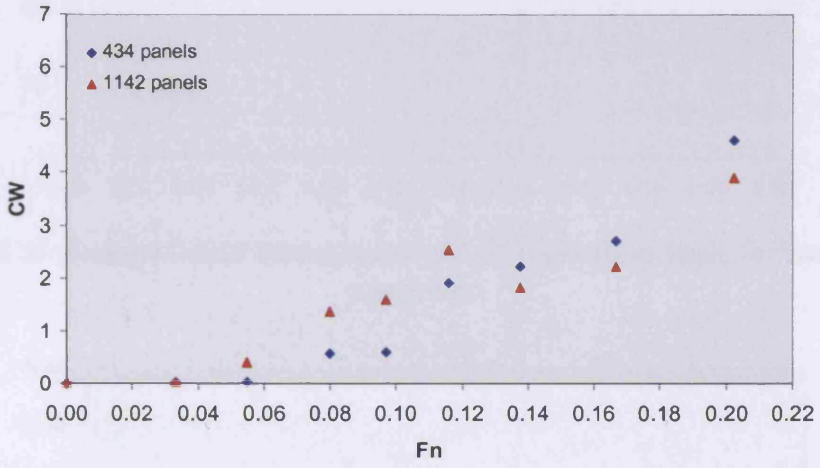

Figure 4.28 Wave resistances versus speed at 5.4° inclination angle for two sets of panel size

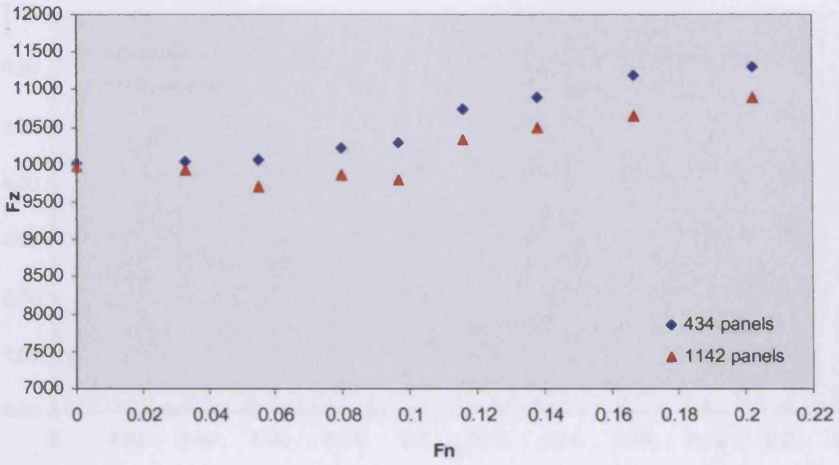

Figure 4.29Vertical forces versus speed at 5.4° inclination angle for two sets of panel size

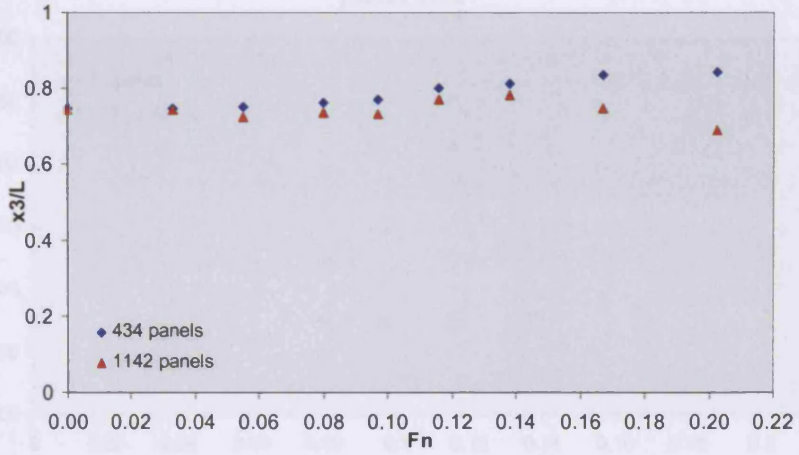

Figure 4.30 Sinkage forces versus speed at 5.4° inclination angle for two sets of panel size

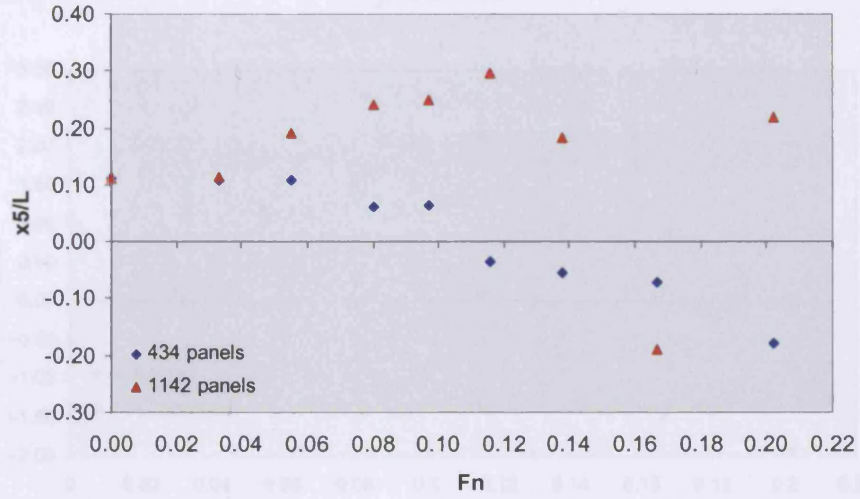

Figure 4.31 Trim moment versus speed at 5.4° inclination angle for two sets of panel size

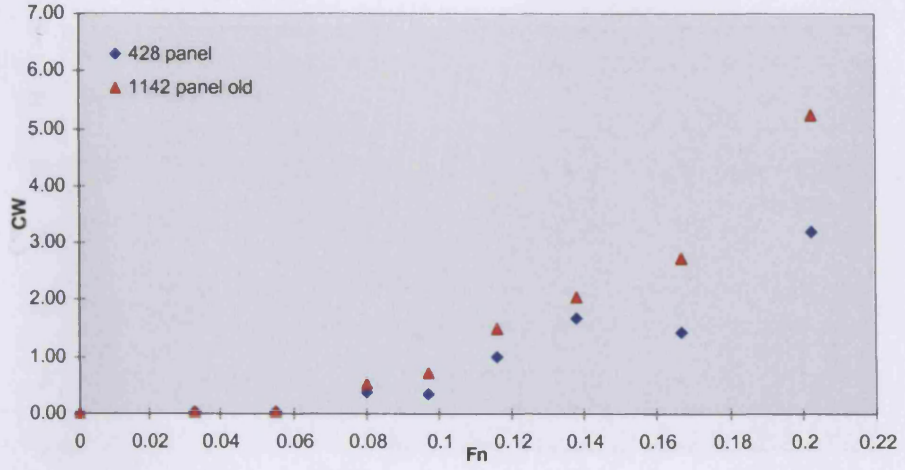

Figure 4.32 Wave resistances versus speed at 7.2° inclination angle for two sets of panel size

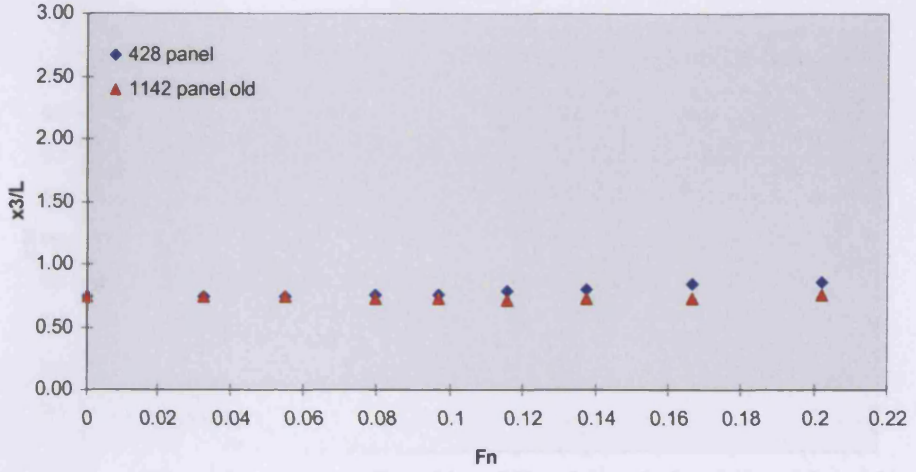

Figure 4.33 Sinkage forces versus speed at 7.2° inclination angle for two sets of panel size

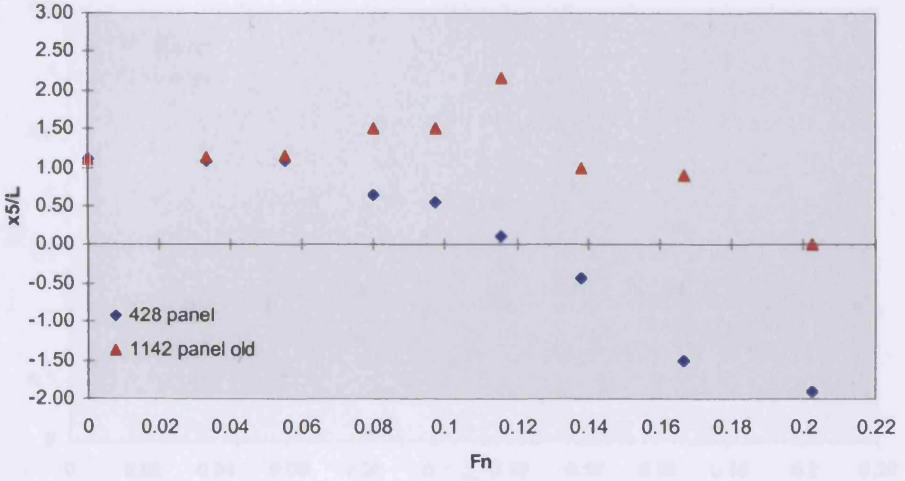

Figure 4.34 Trim moments versus speed at 7.2° inclination angle for two sets of panel size

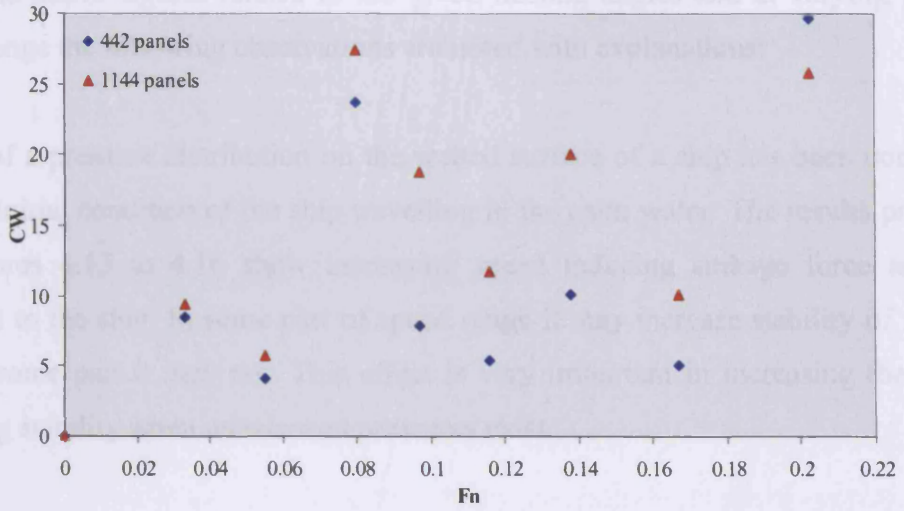

Figure 4.35 Wave resistances versus speed at 10° inclination angle for two sets of panel size

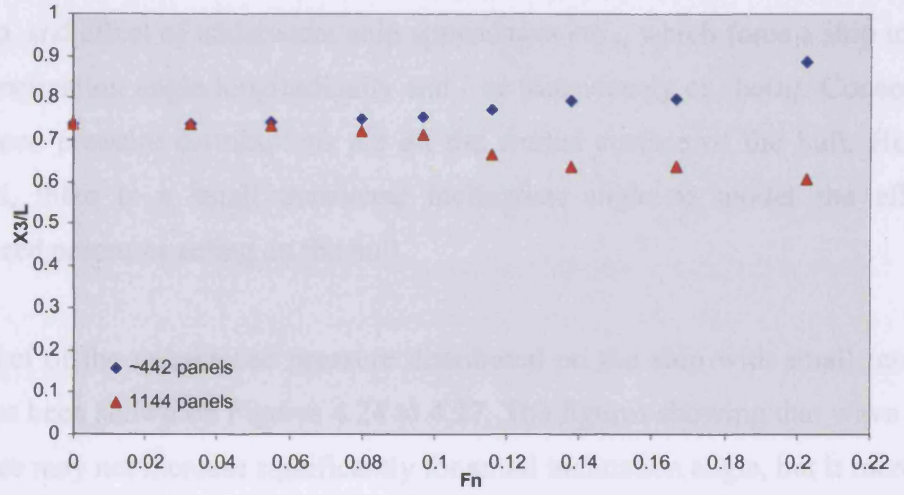

Figure 4.36 Sinkage forces versus speed at 10° inclination angle for two sets of panel size

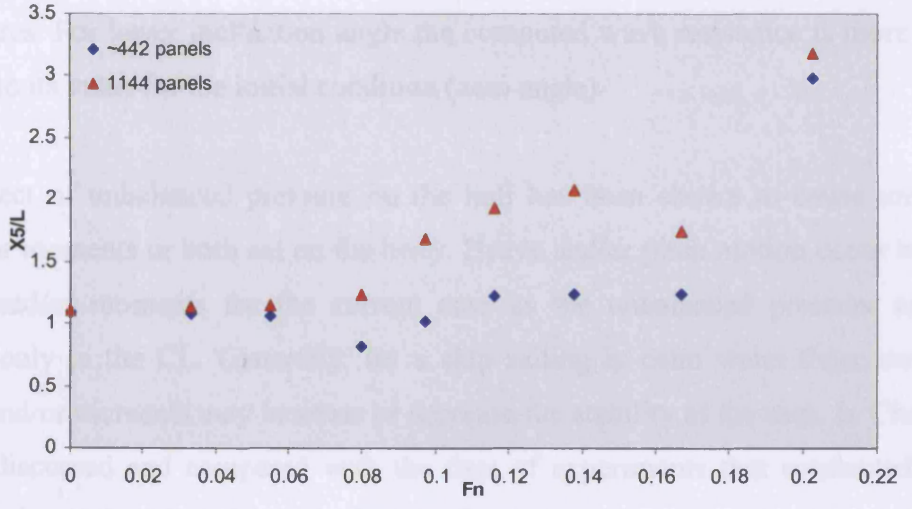

Figure 4.37 Trim moments versus speed at 10° inclination angle for two sets of panel size

From the above figures related to the given heeling angles and at varying forward speed range the following observations are noted with explanations:

Effect of a pressure distribution on the wetted surface of a ship has been considered for the initial condition of the ship travelling in the calm water. The results presented on Figures 4.13 to 4.16 show increasing speed inducing sinkage force and trim moment to the ship. In some part of speed range it may increase stability of the ship and in some part it may not. This effect is very important in increasing the risk of reducing stability when unbalanced pressures exist.

As discussed in Chapter 2 there are some disturbances, such as error of KG estimation of loading, external forces or moments such as wind pressure acting on the upper part of a ship, and effect of underwater ship appendages etc.., which force a ship to incline (small inclination angle longitudinally and / or transversely or both). Consequently, unbalanced pressure distributions act on the wetted surface of the hull. Here, it is assumed, there is a small transverse inclination angle to model the effects of unbalanced pressures acting on the hull.

The effect of the unbalanced pressure distributed on the ship with small inclination angle has been shown on Figures 4.24 to 4.27. The figures showing that wave making resistance may not increase significantly for small inclination angle, but it increases as inclination angle increases. This observed from comparison of wave making resistance of the initial condition with other higher inclination angles than shown in the figures. For lower inclination angle the computed wave resistance is more or less similar to its value for the initial condition (zero angle).

The effect of unbalanced pressure on the hull has been shown to cause unwanted forces or moments or both act on the body. Heave and/or pitch motion occur by these forces and/or moments for the current case as the unbalanced pressure assumed related only to the CL. Generally, for a ship sailing in calm water these unwanted forces and/or moments may increase or decrease the stability of the ship. In Chapter 7, this is discussed and compared with the data of experiments that conducted in the UCL towing tank and explained in Chapter 6.

5. MESH GENERATION

5.1 INTRODUCTION

Partial differential equations (PDEs) are normally used to describe certain physical phenomena. In the cases where no analytical solution can be adopted, numerical methods are typically required to solve these. The latter leads to discretisation in the physical domain, and either the geometry (topology) of the region or a mathematical formula might be used to describe the domain. Discretisation of a three-dimensional geometry is not a straight-forward technique, particularly if the geometry is of a complex shape such as a ship's hull that is the domain in the current study. The surface of a ship's hull may be defined from either body curves or from a tabulated offset, both of which can be determined at the design stage. They form the configuration of the hull, which itself has to be subdivided (discretised) into cells.

A computer program has been developed to generate the mesh on the ship's hull, for the theoretical part of the research. The mesh generation technique, that is used to divide the ship's hull into panels, is discussed in the following sections. Brief reviews associated with significant points of mesh generation techniques are also presented.

5.2 BACKGROUND

Hendrix and Noblesse (1995), studied free-surface potential flow about a mathematically defined hull form called the Wigley hull. This hull form was approximated by means of flat triangular panels within which the source strength was piecewise constant. The flow was defined using the slender ship approximation. They concluded that convergence of the computed velocity potential with respect to hull discretisation (i.e. size and aspect ratio of panels) may require a large number of panels. They also indicated that the Froude number could have a considerable influence on accuracy of the results. Moreover, it was found that error variations regarding different arrangements that are characterised by the aspect ratio of a relatively small number of panels are fairly large.

Hendrix and Noblesse also suggested "the errors due to hull discretisation, as well as other numerical inaccuracies, clearly must be demonstrated to be small enough to confidently ascertain the relative quality of different mathematical models".

For the Wigley hull, at a Froude number of 0.25, Dommermuth et al (1988) showed that the Neumann-Kelvin source strength that depends on the Froude number and the hull geometry varies much more rapidly than the slender ship source strength. Hence, a greater number of panels is likely to be required if an integral equation is to be solved.

Generally for most numerical methods, the discretisation of the domain is very important and has a direct effect on the accuracy of the results. It is generally much easier to generate a mesh for a typical geometrical form such as a sphere or an ellipsoid or even a Wigley hull than for an irregular form like a true ship's hull. In this work, the real configuration of a ship's hull is considered. The hull form can be defined from design offsets appearing either in tabulated or in graphical form.

5.3 PHYSICAL MODEL GEOMETRY

The geometry of hull of a ship has been chosen from the offsets of a refrigerated container ship "M V Baltic Trader", as shown in Figure 5.1, which shows the body lines. The configuration of the hull used in the numerical model, and for the model tests. The cross-section curves, in the figure, show stations from the bow to the stern for the half body. The curves form the right side of the figure to the centre line, CL, have been numbered from 10 to 20 showing the station of the mid-ship to the bow. As well as number 10 to 0 showing stations of the mid-ship to the stern on the other side of the figure from CL to the left. These curves form the shape of the hull, and are used to determine the offsets, and hereafter are used as initial offsets. For a given draft, a wetted surface may be obtained from the initial offsets from the keel, base line, to a chosen water line.

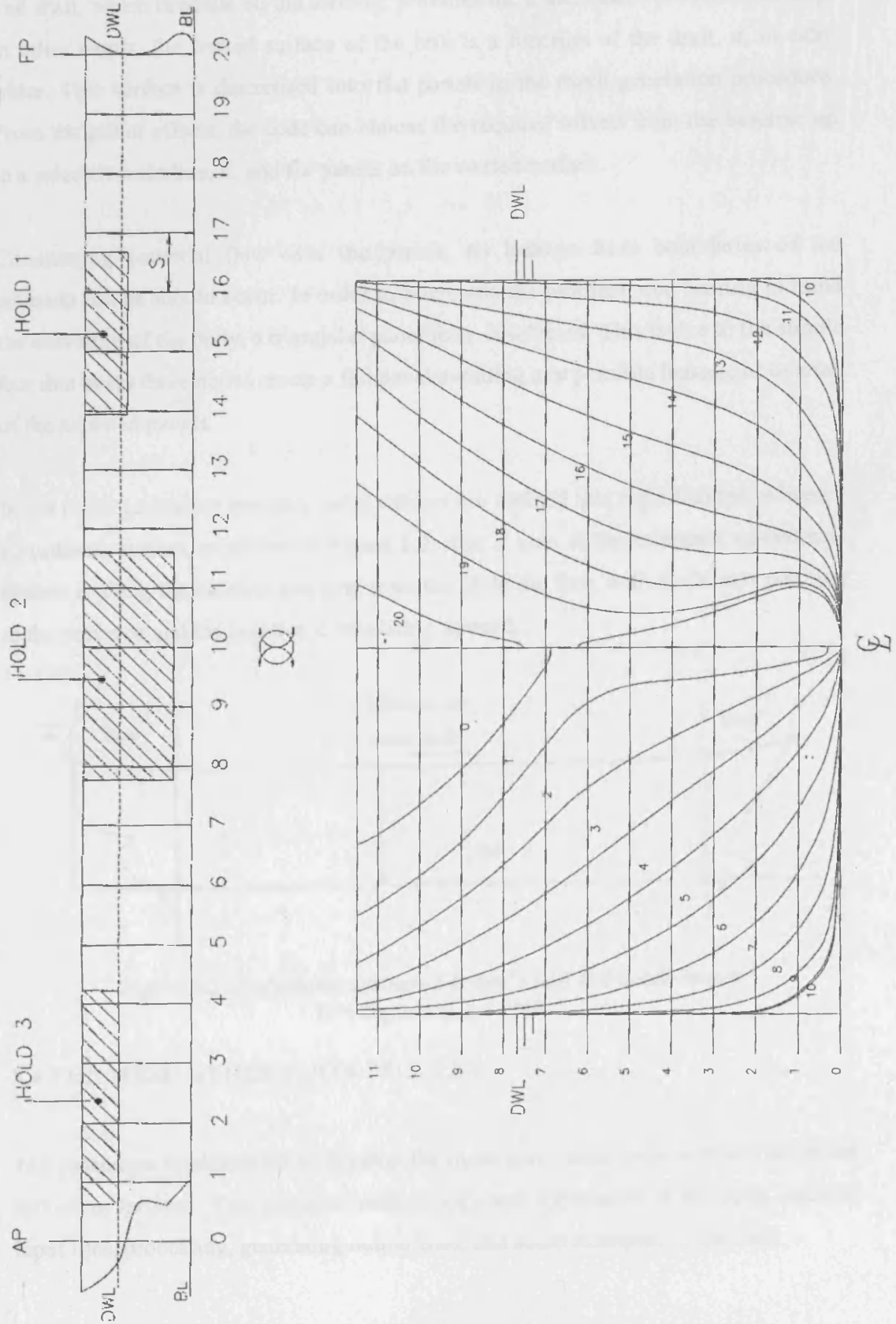

Figure 5.1 "M V Baltic Trader" body lines

The draft, which depends on the loading, provides the underwater volume of the ship. In other words, the wetted surface of the hull is a function of the draft, *d*, in calm water. This surface is discretised into flat panels in the mesh generation procedure. From the initial offsets, the code can choose the required offsets from the baseline up to a selected waterline, d, and fix panels on the wetted surface.

Considering potential flow over the panels, no leakage from boundaries of the adjacent panels should occur. In order to overcome the problem, and bearing in mind the curvature of the body, a triangular panel form is selected. This is due to the simple fact that every three nodes create a flat panel avoiding any possible leakage or overlap of the adjusted panels.

In the mesh generation process, panel corners are defined in a right-handed reference co-ordinate system, as shown in Figure 5.2. The X axis of the reference co-ordinate system is along the baseline pointing from the aft to the fore, with the Y axis pointing to the port side and the positive Z axis being upward.

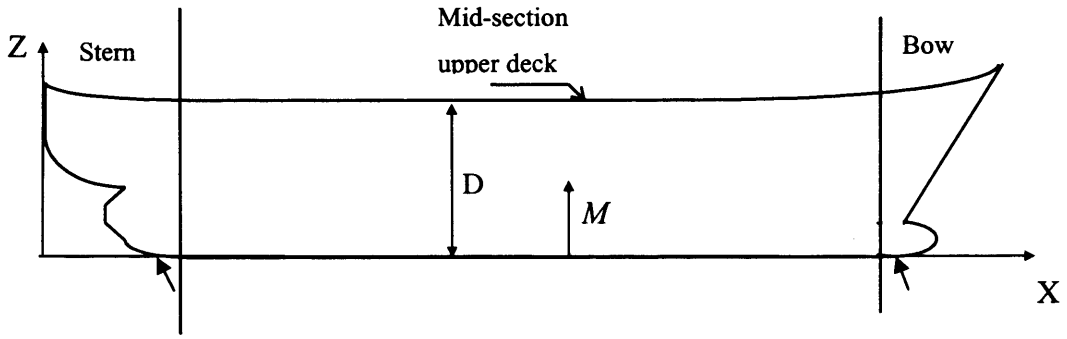

Figure 5.2 Co-ordinate system of a ship's hull and subdivisions
D = depth and d = draft

5.4 THE MESH GENERATION PROCESS

The procedure implemented to develop the mesh generation code is described in the following sections. This includes methodology and application of the code, such as input files, processing, generating output files, and some examples of the code.

5.4.1 INPUT FILES

There are three input data files for the offsets, as the hull is divided longitudinally into three parts. These are the bow, mid, and stern parts as shown in Figure 5.2. The hull must then be divided into a number of horizontal lines parallel to the water line. It is assumed that the centreline (CL) is in the plane OXZ. Therefore the offsets can be read from the intersection of each horizontal line (waterline) and vertical curves at either bow, stern, or each cross section curves in between. Figure 5.3 shows the detail of all parts. For reading of the offsets, it is assumed that the ship has no inclination angle either longitudinally, trim, or transversally, heel.

In order to insert the tabulated offsets into input data files it is necessary to know the above offsets for the bow, mid, and stern parts. For the case that there are no such tabulated data, these must be worked out from its bodylines. Alternatively, tabulated data should be classified as the following procedures.

In order to classify the tabulated data, or to read offsets using a body curves as in Figure 5.1, and as was mentioned previously in Section 5.4, additionally it is shown in graphical form in detail in Figure 5.3. The small arrows on the curves show location of offset values for reading. The following set of procedures explains how to read it from the bodylines, and how to arrange it for putting in each input file:

- Firstly, the bow curve is separated at the intersection of the keel (baseline) with the bow curve up to the upper deck. The bow curve is assumed to be on the OXZ plane, and therefore the length of each node on this curve at any waterline level can be read from the reference co-ordinate system. Hence, on the bow curve any node has length (X), Y = 0, and height value Z = wl_i as is shown in Figure 5.3a. This value must be arranged from the baseline, where Z=0.0, up to maximum depth (D) as below:

  (X_{base}, Y=0, Z= wl_{base}) Z is almost equal to zero for first node.

  (X_1, Y=0, Z= wl_1) Z is equal to draft of first waterline.

  :

  (X_{dwl}, Y=0, Z= wl_d) Z is equal to draft at design waterline

:

(X_D, Y=0, Z= D) Z is equal to depth of the hull for last node.

In the 'bow.dat' input file, the arrangement of the data is from lower waterline to upper waterline. But before entering the data the number of waterlines should be introduced, then the level of each waterline, and the length of each node on the bow curve must be inserted after the maximum waterline level, as below:

*Number of waterlines;

*Waterlines wl_0 (wl_0 is usually zero, because it is assumed on baseline)

: (Waterline's level that is selected between wl_0 and wl_d)

*Design waterline wl_d (Level of design waterline from the baseline)

: (Waterline's level that is selected between wl_d and wl_D)

*Height of the deck D (Level of depth from the baseline)

*Length of each node on the bow curve:

X_0 (Length of intersection of wl_0 with the bow curve)

: (Length of intersection of wl_i with the bow curve)

X_d (Length of intersection of wl_d with the bow curve)

: (Length of intersection of wl_k with the bow curve)

X_D (Length of intersection of wl_D with the bow curve)

The number of lengths of nodes (X) is equal to the number of waterlines.

- Secondly, the midsection of the ship is selected as a part of the body between the bow curve and the stern curve, the mid-part includes many curves (cross-sections). The distance from the reference co-ordinate system to any station is of constant length for all nodes lying on the curves. The offsets for each cross-section where X is constant can be read on the plane OYZ as shown in Figure 5.3b. The first curve or station is assumed to be the nearest to the bow curve. Then the Y co-ordinate from the centre plane or the OXZ plane can define nodes on that cross section at each water level. The co-ordinates of these nodes must be arranged from the nearest curve of the bow to the aft for the mid input file named 'mid.dat'.

To store the data in the "mid.dat" input file, the number of all stations between the bow and stern curve must be introduced first. Then the length of each station (cross

section) from the reference co-ordinate for the station, followed by the Y values for nodes lying on the same station, must be inserted. After that the length of the next station and Y values for nodes on this station put in the file, and so on. This procedure is begun from the nearest curve from the bow to the stern. The number of Y values on each station must be equal to the number of waterlines. The number of stations, between the bow and the stern curves, must be equal to number of length of station from the origin reference, OXYZ.

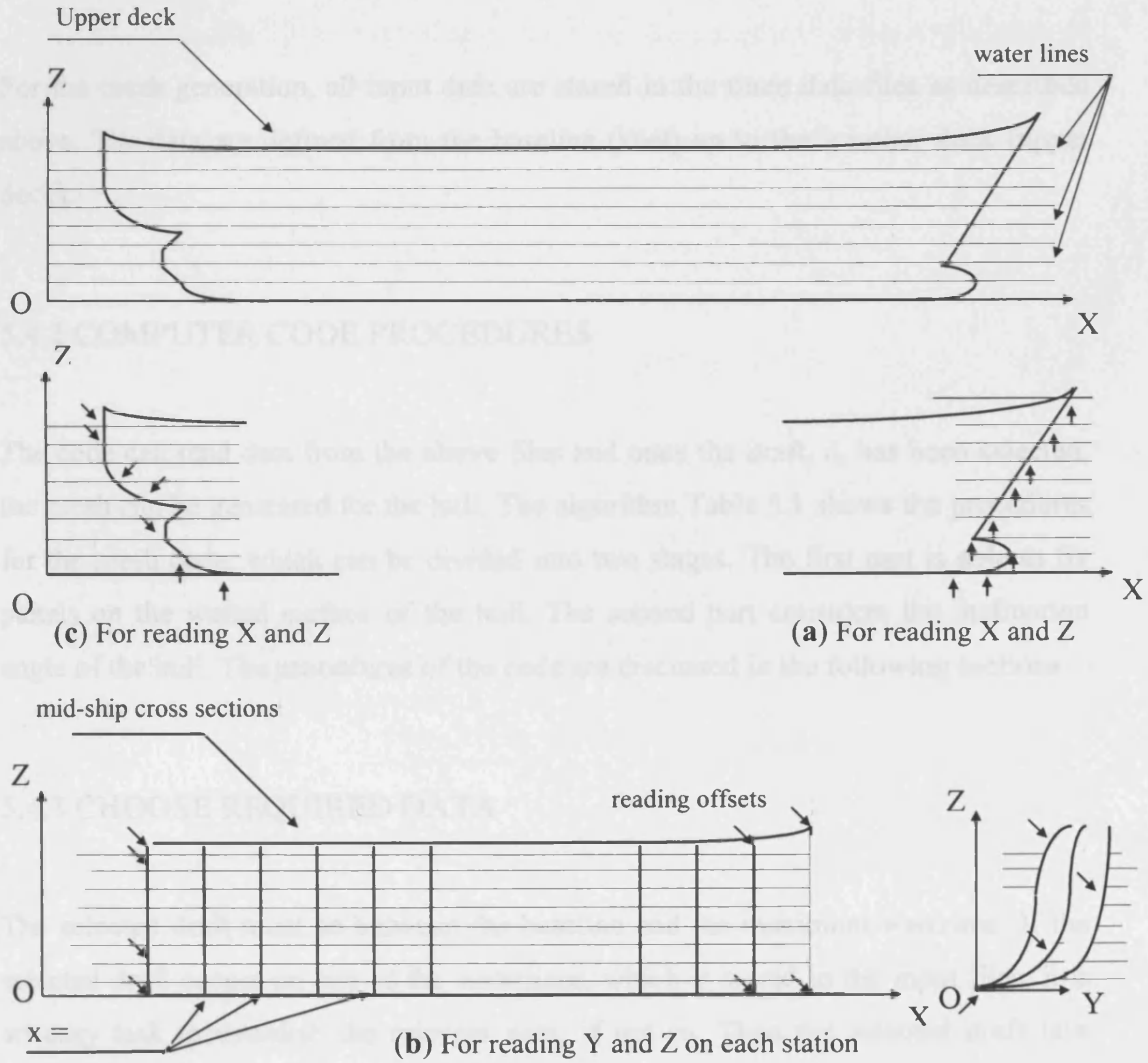

(**c**) For reading X and Z

(**a**) For reading X and Z

(**b**) For reading Y and Z on each station

Figure 5.3 Subdivision and how to read offsets from body lines, bow(**a**) mid (**b**) and aft(**c**), with XYZ as reference co-ordinate

- Finally, the stern curve is separated at the intersection of the keel or the baseline with the stern curve, using the same method discussed above for the bow curve. The offset is a point on the stern curve of intersection of the curve at each waterline division on the centre plane OXZ. It can be defined by length and height as (X, Y=0, Z= wl). Figure 5.3c shows an example of these data. These points' co-ordinates are inserted to the 'stern.dat' input file using a process similar to that used for the bow, except for the first part of the data that specifies the waterline numbers and their levels from the baseline.

For the mesh generation, all input data are stored in the three data files as described above. The data are defined from the baseline (keel) up to the weather deck (upper deck).

5.4.2 COMPUTER CODE PROCEDURES

The code can read data from the above files and once the draft, d, has been selected, the mesh can be generated for the hull. The algorithm Table 5.1 shows the procedures for the mesh code, which can be divided into two stages. The first part is able to fix panels on the wetted surface of the hull. The second part considers the inclination angle of the hull. The procedures of the code are discussed in the following sections.

5.4.3 CHOOSE REQUIRED DATA

The selected draft must be between the baseline and the maximum waterline. If the selected draft occurs on one of the waterlines, which is stored in the input files, it is an easy task to establish the relevant data, if not so. Then the selected draft lays somewhere between two waterlines, which are stored in the input data files. Therefore on each curve the required data is between two adjacent waterlines, the computer code can find it by interpolation between the adjacent offsets on each curve. In order to find data on each curve, which depends on the bow, stern, and midsection curves, the following formulae are applied for interpolation:

- On the bow or stern curves for an X value between two adjacent waterlines above and below of the chosen draft, d, the X value can be calculated from:

$$X_d = X_1 + \frac{X_2 - X_1}{Z_2 - Z_1}(d - Z_1) \qquad (5.1)$$

where d is the selected draft, and subscripts 1 and 2 denote the vertical co-ordinate of the waterline below and above the chosen waterline respectively.

- On the midsections, curves are located on the constant X values, therefore Y values must be interpolated. To compute a Y value of a node between two adjacent waterlines with respect to the chosen d the following formula is applied:

$$Y_d = Y_1 + \frac{Y_2 - Y_1}{Z_2 - Z_1}(d - Z_1) \qquad (5.2)$$

Notation and subscripts have the same meaning as above.

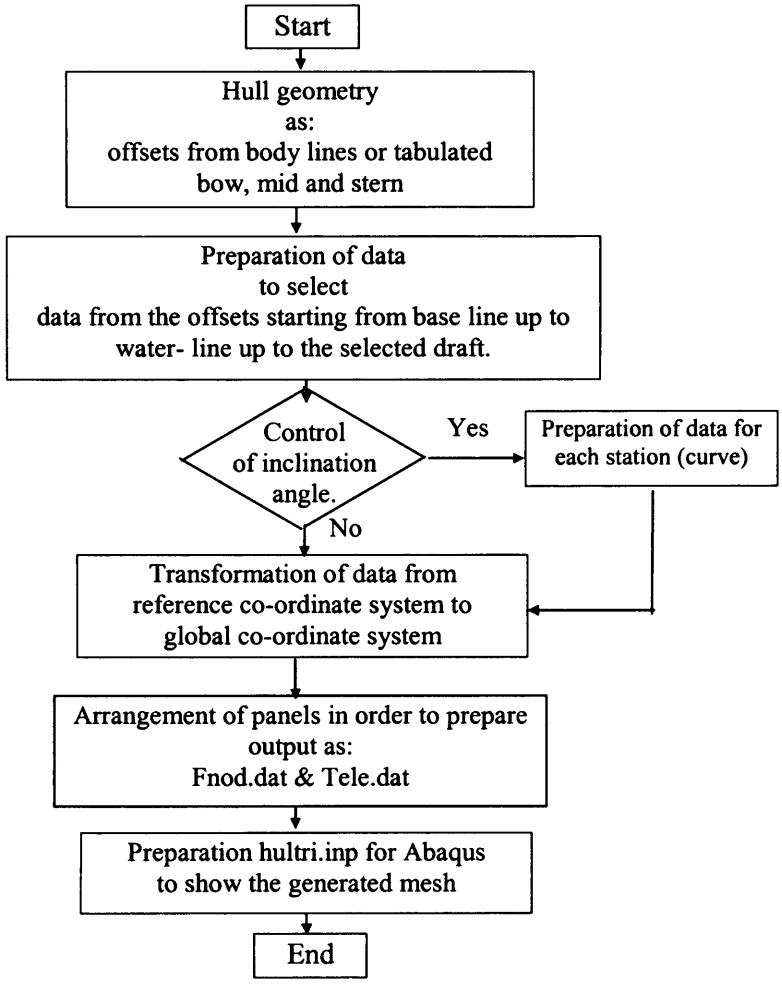

Table 5.1 Algorithm showing key procedures in the mesh generation code

The data in the three input files are arranged in two-dimensional form, but up to this level of the code, the required data in respect of the chosen draft are separated from input files data. They are then arranged in three-dimensional form associated with the position of nodes in space on the hull surface. Hence the real underwater form of the ship's hull may be represented from selected data in 3D shape for the chosen draft. The numbering of nodes, elements and the graphical mesh generation are discussed in Sections, 5.4.5 to 5.4.8, and 5.5.

Up to this stage, the mesh can be generated based on the selected draft without any longitudinal (trim) and transverse (heeling) inclination angle. Considering the transverse inclination angle, which is very important in the stability of a ship, the code is able to select the required data within the original offsets. Although in general, a ship when heeled will also trim to maintain its longitudinal equilibrium, it is assumed that there is no contribution from roll and pitch motion. Therefore due to the transverse inclined angle, the resultant immersed volume wedge remains equal to the emerged volume wedge. For selection of the required data at the chosen draft and heel angle, the algorithm in Table 5.1 shows that the code advances to the second stage, which begins with the inclination condition.

5.4.4 APPLYING INCLINATION ANGLE

The heel angle is defined in such a way that a positive angle indicates that the port side is immersed. Firstly the level of the waterline (d_n) for the inclined ship must be found on each curve (sections). Secondly the required data must be selected from the initial offsets (input files). Therefore data on each curve selects from the baseline up to the relative waterline on the n^{th} curve. The relative waterline level d_n with regard to the heel angle and the draft on each curve can be obtained from:

$$d_n = Z_0 + (Y_{dn} - Y_1)\frac{Z_2 - Z_1}{Y_2 - Y_1} \tag{5.3}$$

or relatively:

$$d_n = d + (Y_{dn} - Y_0)\tan(\varphi) \tag{5.4}$$

where: d_n and Y_{dn} indicate values of draft and half beam on the n^{th} curve for the inclination angle φ. Subscript 2 indicates the level of the waterline at the initial condition (φ = 0), and subscript 1 indicates the nearest waterline below the 2 at initial condition. Subscript 0 indicates the position of the node on the centre plane for each curve. The detail is shown in Figure 5.4.

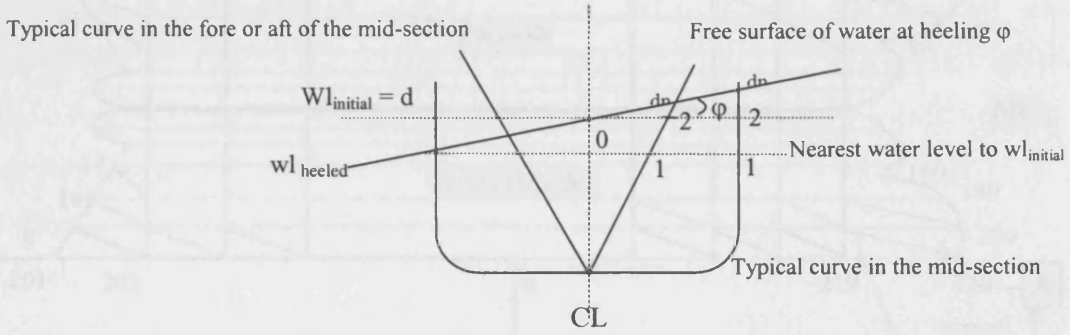

Figure 5.4 Position of the waterlines and nodes on the free surface for an inclined ship

5.4.5 NODE NUMBERING

The last stage of the above process involves node numbering, which begins with each node on the upper waterline on the port side, from the fore to aft, then moving to the next waterline, and so on until the baseline. From the baseline the node numbering continues on the starboard side to the upper waterline. The numbering is shown in Figure 5.5.

5.4.6 ELEMENT NUMBERING

In a similar fashion to the node numbering, the element numbering begins on the port side from the top of the bow to top of the stern, between two adjacent waterlines and continues down to the baseline, as shown in Figure 5.5. Then the next row of elements is numbered by a similar procedure on the same side of the hull. Once the keel or baseline has been reached the elements on the other side of the hull are addressed, whereby the same process of numbering, but in the reverse direction (from bottom to top) is followed. This is also shown in Figure 5.5.

It should be noted that in this stage, the reference coordinate system (OXYZ) is transferred from the baseline to the upper waterline on the mid-ship section of the underwater part of the hull (oxyz). Hereafter it is referred to as the Global Coordinate System (GCS). It is now on the free surface, and is shown in Figure 5.5.

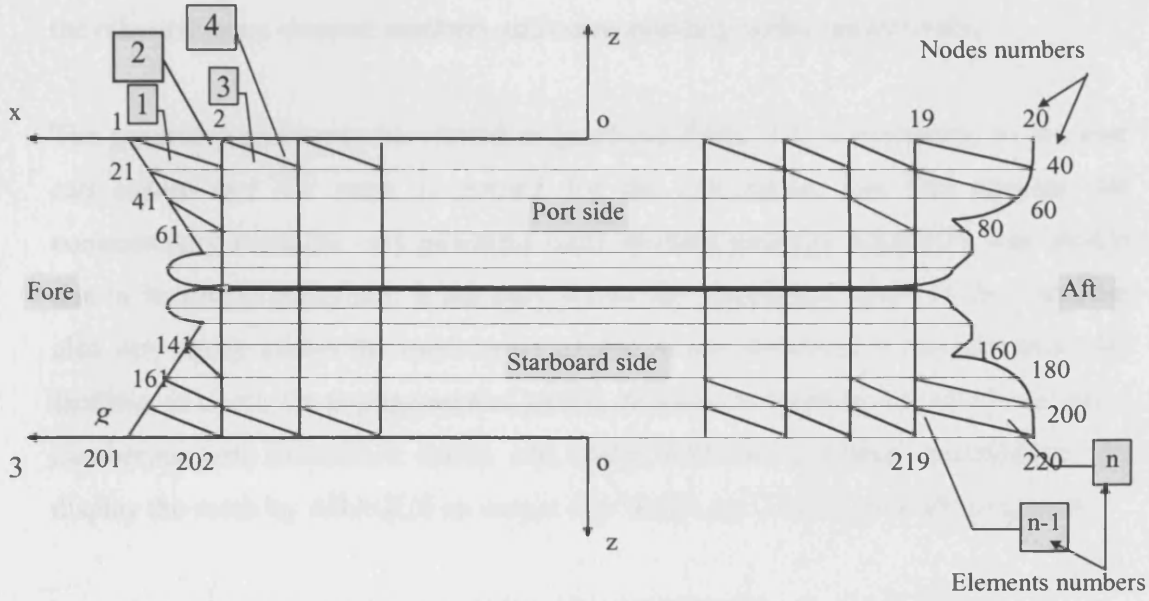

Figure 5.5 Node and element numbering on both sides of the ship and repositioning of the coordinate system

5.4.7 TRANSFORMATION

For the transformation of coordinate systems, two linear transformations are involved. Firstly in the vertical direction from the original location of the reference coordinate system to the upper waterline which is dependent on the selected draft. Secondly horizontal transformation from the previous position at the stern of the hull to the half-way position of the chosen upper waterline, which is about 0.5 L_{WL} from the reference coordinate system origin to the mid-ship.

For the inclined case a rotational transformation is required. In this case it is assumed that in any condition the free surface is in the plane oxy of the global coordinate system (GCS). Then the GCS must rotate in the same way as inclination angle and by that value.

5.4.8 OUTPUT FILES

The output of the above process is fed into two data files *'fnod.dat'* and *'tele.dat'*. The former data file includes nodes and corresponding coordinates (x,y,z), whereas the other contains element numbers and corresponding nodes respectively.

The generated mesh may be viewed in graphical form, if it is necessary, so the user can ensure that the mesh is correct for the calculation. For this purpose the commercially available very powerful finite element package ABAQUS was chosen due to its robust behaviour. It not only shows the perspective view of the mesh but also very easily allows the mesh to be rotated in any direction. It has also powerful facilities to check the arrangement of panels, and also to interactively check the panel numbering with associated nodes, and nodes with corresponding coordinates. To display the mesh by ABAQUS an output file *'hultri.inp'* is automatically prepared.

5.5 SOME EXAMPLES OF MESH GENERATION

Some results are shown here firstly for different drafts for zero initial heeling angles, and then for some transverse inclination angles.

Figure 5.6 shows the perspective view of the bodylines from bow to stern. In this figure the rectangular panel is fixed on the wetted surface of the hull, without any heeling angle.

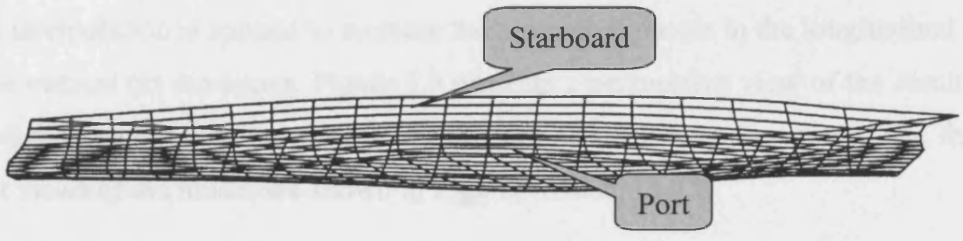

Figure 5.6 View of ship bodylines showing bodylines from fore to aft

Figure 5.7 shows the perspective view of the ship with a small angle of rotation. These two perspectives show body curves along the ship's hull, and how they vary along the ship's length

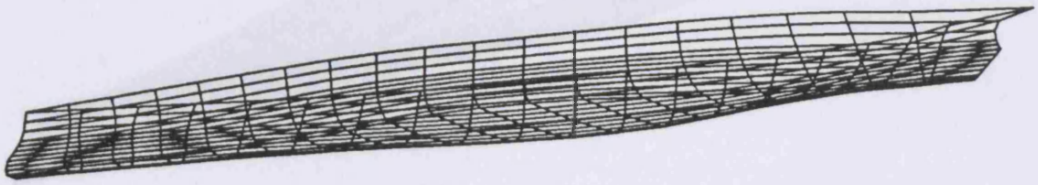

Figure 5.7 View of the ship hull, showing a small of rotation

The shape of the triangular panel mesh is shown in Figure 5.8. This figure presents structural triangular panels, which are fixed on the wetted surface of the model.

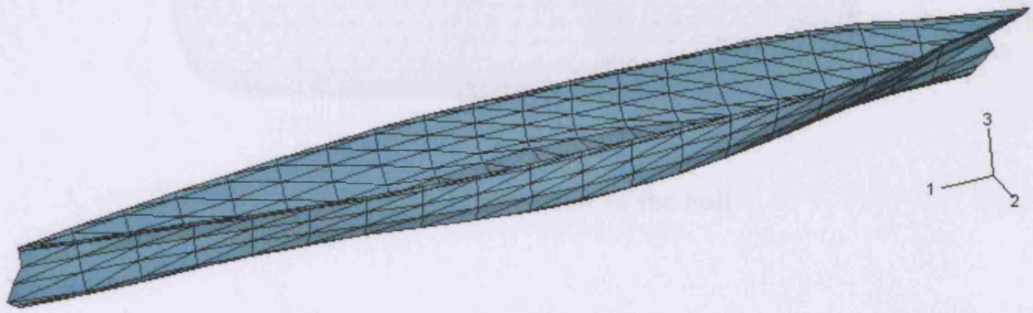

Figure 5.8 View of the hull, showing the triangular panel on wetted surface from bow to aft

Spline interpolation is applied to increase the number of panels in the longitudinal (x) and the vertical (z) directions. Figure 5.9 presents a perspective view of the result of one subdivision between two nodes in the x and also in the z directions. The front and aft views of the model are shown in Figures 5.10 and 5.11.

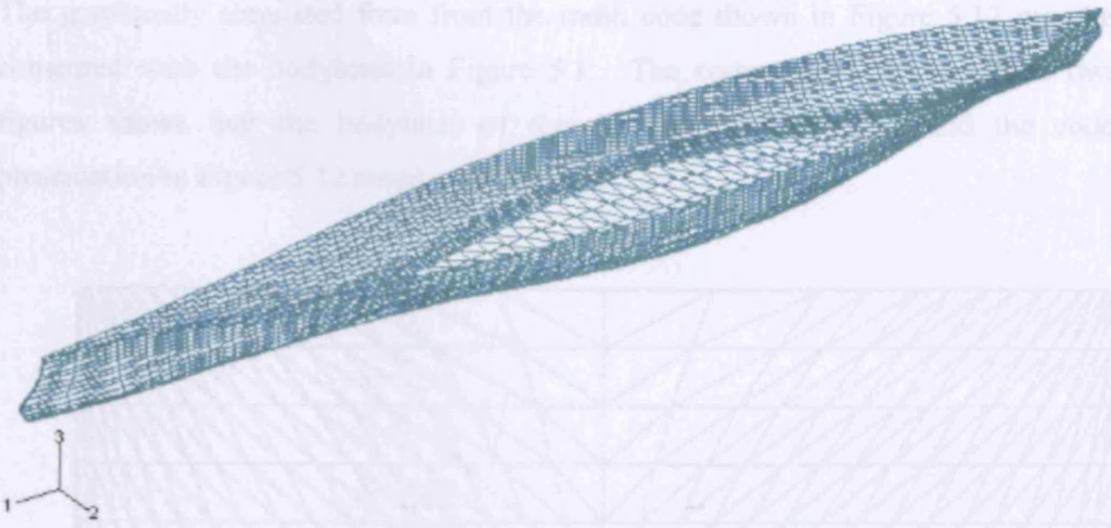

Figure 5.9 View of the hull, showing increased number of the triangular panel on wetted surface from bow to aft

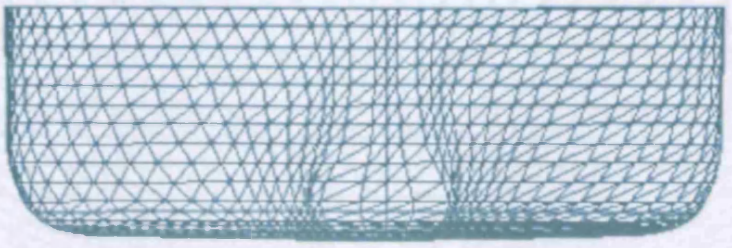

Figure 5.10 Front view of the hull

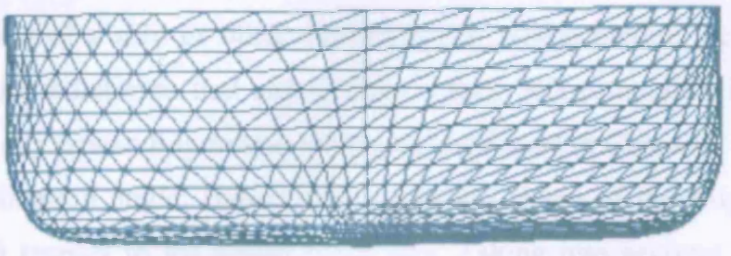

Figure 5.11 Aft view of the hull

The graphically simulated form from the mesh code shown in Figure 5.12 may be compared with the bodylines in Figure 5.1. The comparison between these two figures shows that the bodylines of the drawing in Figure 5.1 and the code presentation in Figure 5.12 mostly are the same.

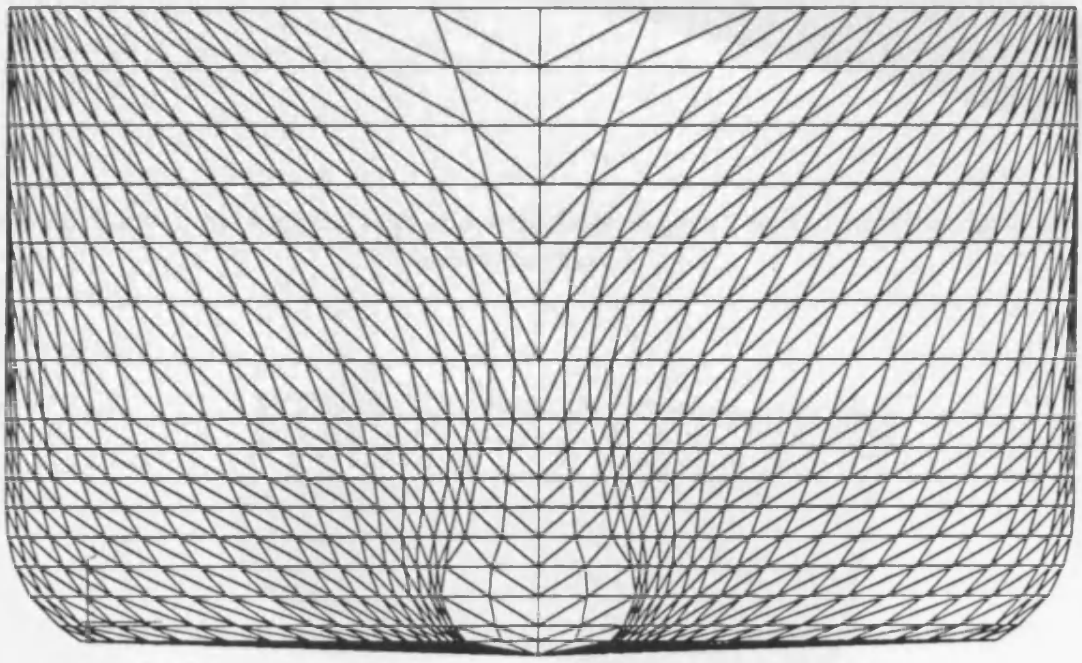

Figure 5.12 Body curves created by the mesh code from bow to the midship of the M V Baltic Trader

Another application of the code is to generate the mesh over an inclined ship. The results can accurately simulate an actual practical form of an inclined ship due to either the loading of a ship or other circumstances, which incline the ship during a voyage. The author believes that any mistake during KG estimation in loading and unloading, and any upstanding forces, which are explained in Chapter 1 cause the ship to have an inclination angle. Hence the underwater shape of the ship is no longer symmetric with respect to the centre plane oxz. Taking into account this effect the code has been improved, accordingly the front view, aft view, and perspective view of the inclined ship (by port side) are shown in Figures 5.13 to 5.15. Also views of higher resolutions of meshes for the inclined ship are possible as it shown on Figure 5.16

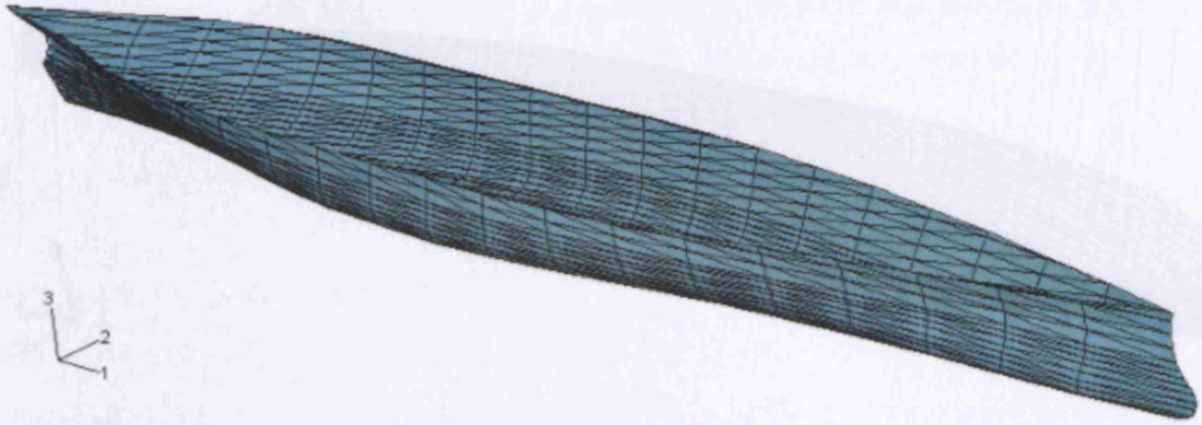

Figure 5.13 View of the inclined hull, showing the triangular panel, on wetted surface from bow to stern

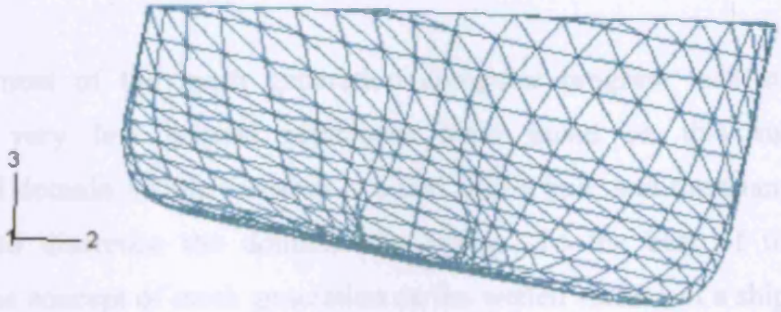

Figure 5.14 Front view of the inclined hull, wetted area

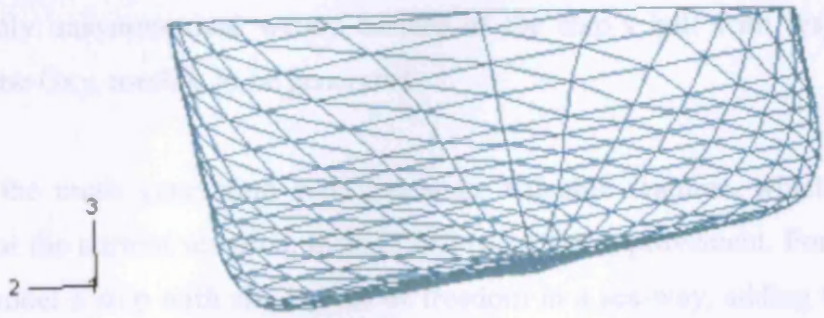

Figure 5.15 Aft view of the inclined hull, wetted area

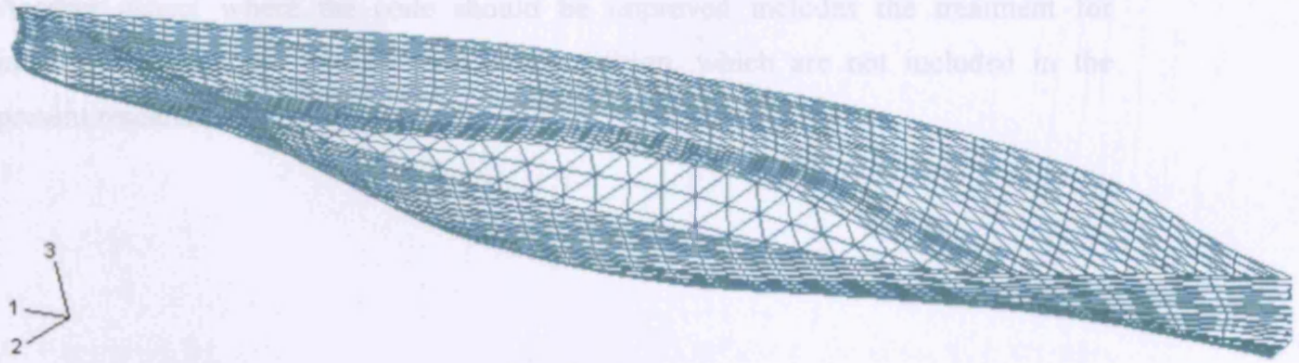

Figure 5.16 View of the inclined hull, showing increased number of triangular panels on wetted surface from bow to aft

5.6 SUMMARY

The development of the mesh generation computer program was started from scratch, but very few general references were found on this subject. The computational domain for the research is a real ship's hull, and the triangular panel was chosen to discretise the domain into panels. To the best of the author's knowledge, the concept of mesh generation on the wetted surface of a ship's hull due to loading conditions, in other words as a function of draft, is for the first time presented in this thesis. This allows the transverse inclination angle, and consequently unsymmetrical wetted surface of the ship's hull with respect to the central plane Oxy, meshes to be generated.

Although the mesh generation code has some valuable features, which have been required for the current research, there is still room for improvement. For example in order to model a ship with six degrees of freedom in a sea-way, adding the effect of trim angle, especially for large inclination angles in order to balance the ship, where heeling angle contributes with trim angle.

It would also be desirable to apply a more efficient method of controlling the number of panels in both vertical and longitudinal directions, and changing of panel size for better control of aspect ratios of panels.

Another aspect where the code should be improved includes the treatment for incoming waves, and extreme sea-state condition, which are not included in the present research.

6. MODEL EXPERIMENTS

6.1 INTRODUCTION

A number of publications exists which consider the effect of speed on stability of a ship in a seaway in the presence of waves for following and quartering seas, Dudziak (1975), Pulling and Wood (1975). However, some experiments have demonstrated unexpected capsizing due to a phenomenon, known as parametric resonance, for head seas. This phenomenon causes the ship to capsize in a head sea, if the natural period of roll motion of the ship is twice the wave natural period, and the wave's length is slightly greater than the ship's length. It is suggested that for a ship caught in this condition it is operationally better to speed up into the waves. Reducing the speed leads to a dangerous situation. More detail can be found in Burcher (1990), and Dallinga et al. (1998). Moreover most empirical formulae and criteria proposed by IMO and uses by classification societies regarding ship stability merely estimate the static condition.

Efforts of the specialist committee on ship stability of the ITTC have provided a central point for monitoring, reviewing, planning research, disseminating information, facilitating implementation and technology transfer since 1996. Although, the progress of the ITTC has shown success and very valuable papers may be found, stability inherently is a complex problem. Therefore, for any new improvement of design or any change in an existing ship, the stability must be carefully considered as a new born problem.

The role of speed has been shown to very significantly effect stability of planing craft, and it is the subject of much research theoretically and experimentally, as reported in ITTC 21st, 22nd, and 23rd, and other professional conferences. Since in marine transportation users seek to reduce travelling time, then increasing speed and improving of comfort and safety are of prime concern. It is clear that once a partially immersed body moves its stability characteristics will be different compared with

when the body is stationary. In particular the contribution of hydrostatic and hydrodynamic forces may change the location of vessel centroids such as centre of buoyancy and metacentre height *GM*. Hence experimental investigation of the effect of speed on the stability of a ship in calm water is important.

The static assessment of stability for relatively high speed ships today and the suggestion of speeding up to escape from parametric resonance have been the main incentives for conducting a series of experiments which will be seen to have been useful to improve our knowledge of the subject, and illuminate the role of speed on stability of a ship. In particular to show when speeding up can improve stability of a ship, and reducing speed can be dangerous.

6.2 APPARATUS AND MEASUREMENT EQUIPMENT

The following apparatus and equipment were used for the experiments:

6.2.1 TOWING TANK

A model was towed along in the UCL towing tank. This tank has a length of 21m, width 1.5m and depth of water 0.9m. It is equipped with an overhead towing carriage, and a flap type wave-maker at one end, which is able to generate regular waves, but was not used for the experiments. At the other end of the tank there is a slip type beach which can absorb the waves after travelling along the tank. Two safety switches at each end of the tank can stop the towing of the model to ensure no damage will occur to either the tank or the model. This safety feature limits the useful running length of the model along the tank to 12m. Speed and direction of the towing carriage are controlled by a rotary speed controller with a range of 0 to 100%. Figure 6.1 is a calibration plot associated with the dial speed of the carriage versus speed of the model in m/sec. Further details concerning the calibration procedure are given in Section 6.2.2.

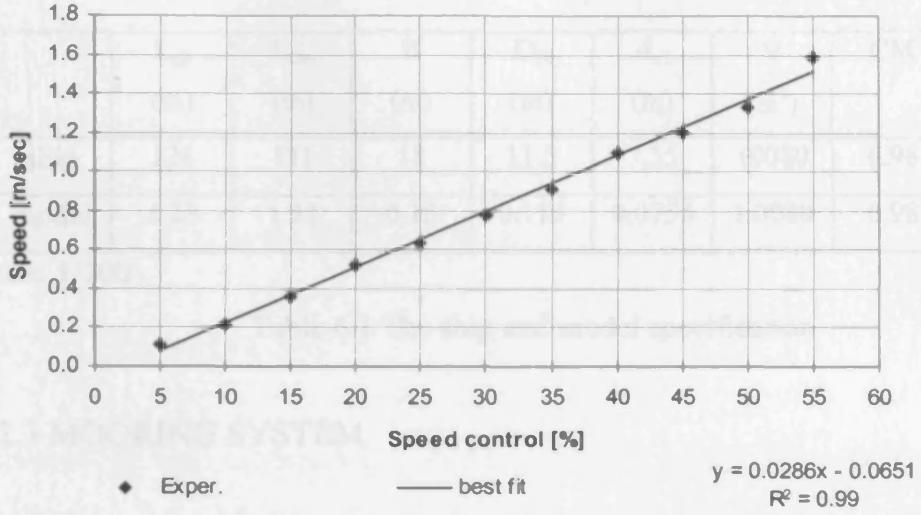

Figure 6.1 Speed calibrations for towing the model

6.2.2 MODEL

The model used for the experiments had the same configuration as that used for the mesh generation in Chapter 5 as well as for the numerical computation in Chapter 4. The "M.V. Baltic Trader" model previously constructed at UCL was used for the experiments. The actual dimensions of the ship and the corresponding figures for the model are presented in Table 6.1, that showing the scale coefficient of 1/100. The model has three compartments which may be used for loading and balancing to obtain the designed waterline (d_{wl}) at mid ship for the initial condition, where there is neither trim nor heel angle.

In order to heel the model, a small box was fixed on the upper deck above its *C* of *G*, and a small weight was located on the longitudinal centreline (CL). Therefore to heel the model the weight could be moved across the box to either the port or starboard side at a certain distance from the CL. A digital inclinometer was mounted on the deck to measure the heel angle at stationary condition, in other words to fix the desired inclination angle.

	L_{pp} (m)	L_{OA} (m)	B (m)	D_H (m)	d_{wl} (m)	∇ (m^3)	CM	CP
ship	128	131	18	11.5	7.55	10080	0.98	0.58
model	1.28	1.31	0.18	0.115	0.0755	1.0080	0.98	0.58

Scale: 1/100

Table 6.1 The ship and model specification

6.2.3 MOORING SYSTEM

The horizontal towing system comprised two sets of fishing lines, one attached fore and the other aft of the model. This line was able to provide adequate force for towing and was able to avoid transfer of unacceptable forces to the model and the measurement equipment. The position of the towing system was close to the waterline to avoid unwanted loads acting on the model and restraining the model completely from lateral motions. Then the model with the towing system was free for rolling, pitching and yaw motions. The model and test arrangement are shown on Figure 6.41.

6.2.4 MEASUREMENT INSTRUMENTS

Three rotary potentiometers were chosen to measure motions during towing of the model. Two of them were connected at midship on each side of the model, and the other one was connected at the bow. A simple arrangement with strings was fitted on the model to transfer the motion of the model to the potentiometers. The potentiometers gave analogue signals proportional to the absolute motions of the model, where they were connected. Those potentiometers located in midship measured heeling angle, and in combination with the bow potentiometer the heave and the pitch were also obtained. The procedure is discussed later.

In order to supply power and to transmit the response of the potentiometers' output, existing instrumentation arrangements on the towing tank were used. These included:

- voltage power supply ± 5 volts dc
- a pair of input and output cases mounted on the carriage and on the tank side wall
- the control panel for speed, (and the wave maker that was not used).

6.2.5 DATA RECORDER

A data acquisition system was used in the experiments, which comprised:

- a data logger (OASIS4) distributed by Data Harvest Ltd. and its software (3D)
- a laptop PC to run the 3D software for recording the data.

6.3 TEST PROCEDURE

General schematic of the setting of the model and relative equipment are shown in Figure 6.41. The tests were carried out in two stages consisting of inclination test and rolling motion.

6.3.1 INCLINATION TEST

The static *GM* was investigated by an inclining experiment. Tests were then completed for a range of heeling angles from 0° to ~12°. In order to incline the model the small weight *w* was moved to different positions to both port and starboard of the model. For each movement of the weight across the deck its distance from the centre line (CL) and the associated heeling angle were recorded. Hence a curve of change in angle of heel over a range of heeling moments was established from the static condition, as shown in Figure 6.2.

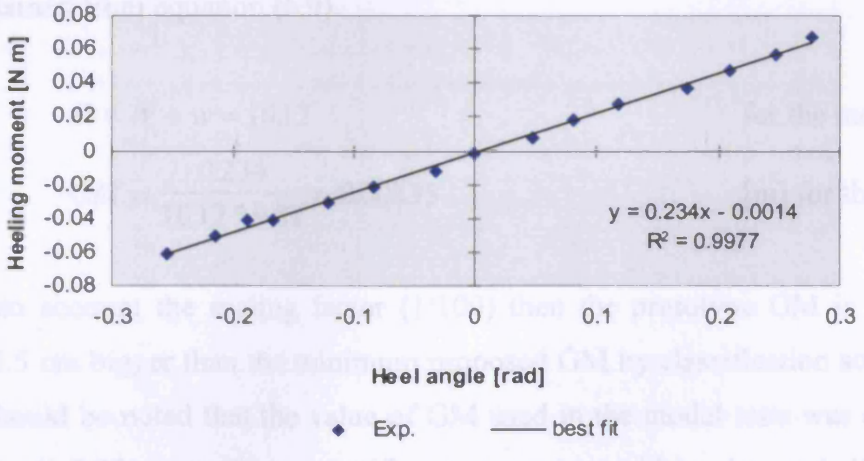

Figure 6.2 Inclination Experiment

The equilibrium condition for static stability is shown in Figure 6.3. As long as heeling moments are equal to righting moments, the ship is stable. According to the above configuration for this situation then it can be written as:

$$M_h + M_r = 0 \tag{6.1}$$

with $$M_r = D * g * GZ \tag{6.2}$$

and $$M_h = w * g * y\cos\varphi \tag{6.3}$$

where $$GZ = GM\sin\varphi \tag{6.4}$$

and $$D = -(W + w) \tag{6.5}$$

substitution (6.4) and (6.5) into (6.1) gives

$$w * g * y\cos\varphi - D * g * GM\sin\varphi = 0 \tag{6.6}$$

therefore $$\tan\varphi = \frac{w * y}{D * GM} \tag{6.7}$$

Hence the initial metacentric height can be calculated from the slope of the inclining test data, Figure 6.2, thus

$$GM = \frac{w * y}{D * \tan\varphi} \tag{6.8}$$

For very small heeling angles we can approximate $\sin\varphi = \tan\varphi = \varphi$ then:

$$GM = \frac{w}{D} * \frac{y}{\varphi} \tag{6.9}$$

where $\frac{w * y}{\tan\varphi}$ or $\frac{w * y}{\varphi}$ is the slope of the inclining test curve (φ in radians).

According to Figure 6.2 the slope for the model is 0.234 Nm rad^{-1}, therefore the *GM* can be obtained from equation (6.9)

Where $D = W + w = 10.12$ for the model [kg]

$$GM = \frac{0.234}{10.12 * 9.81} = 0.00235$$ [m] for the model

Taking into account the scaling factor (1/100) then the prototype GM is 23.5 cm, which is 3.5 cm bigger than the minimum proposed GM by classification societies or IMO. It should be noted that the value of GM used in the model tests was chosen to be very small 2.35mm so that a significant response could be detected. Whilst the value is small it has been accurately determined from an inclining experiment in which it was possible to accurately control the values of mass and linear dimension to achieve the GM to the accuracy indicated.

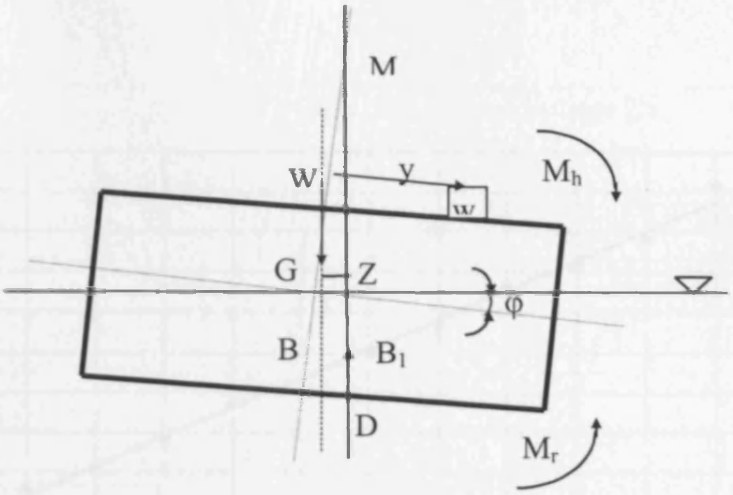

Figure 6.3 Equilibrium of static stability

6.3.2 ROLLING MOTION

In the second part of the experiments the model was towed along the tank at different speeds varying from 0 to 1.67 ms^{-1}, and inclination angles from 0 to 10°. Table 6.2 shows the speed of the model as well as the corresponding speed of the ship and Froude number (Fn). The values of the model speed are calculated on the basis of towing time and the useful length of the tank. The useful length of the tank is the length between where the model reached the required speed and the second limit switch. The corresponding values of speed controller are also presented in the Table 6.2. Moreover Figure 6.4 shows the variation of Froude number (Fn) with respect to the rotary speed controller.

% speed controller	Running time [sec]	model m/sec	ship m/sec	Fn
5	36.13	0.111	0.6	0.017
10	18.27	0.219	1.2	0.034
15	11.2	0.357	1.9	0.055
20	7.62	0.525	2.9	0.081
25	6.31	0.634	3.52	0.098
30	5.18	0.772	4.2	0.119
35	4.41	0.907	5	0.140
40	3.67	1.090	6.05	0.168
45	3.33	1.201	6.66	0.186
50	3.02	1.325	7.34	0.205
55	2.52	1.587	8.8	0.245

Table 6.2 Speed calibration of the rotary controller switch and speed for both the model and the ship

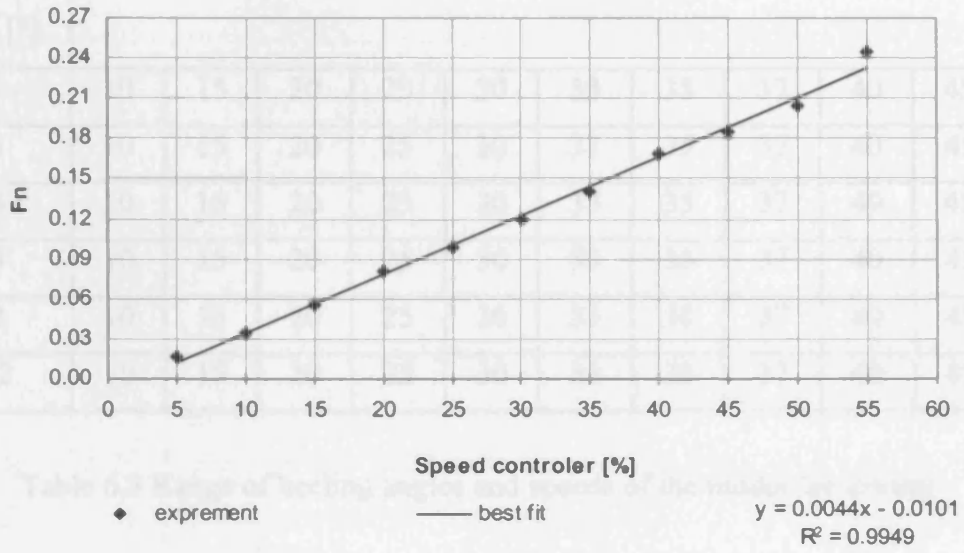

Figure 6.4 Speed calibration of the rotary controller switch

It is very difficult to be sure that the wetted part of a ship's hull is exactly symmetric. In other words, its *C* of *G* may not be exactly located on the CL nor in the plane Oxz. In fact, environmental condition in a seaway, any inaccuracy for *KG* evaluation in loading and unloading, and underwater appendages of a ship even a very small angle of rudder may force the ship to heel to one side. These may generate unbalanced pressure distribution on the wetted surface of the hull. Then the purpose of introducing heeling angle to the model was to simulate a practicable form of non-symmetric underwater body surface. Therefore, a known heeling moment was applied to give a small heel angle in the static condition, and this condition was kept during a set of the speed range for collection of variation of heeling motion along the test.

The model was towed while various heeling angles were set so as to consider dynamic development of rolling motion and *GM*. Table 6.3 shows inclination angles of the model as well as associated speeds used during the tests.

Heeling angle [°]	speed of the carriage percentage [%]										
0	10	15	20	25	30	33	35	37	40	45	50
2.5	10	15	20	25	30	33	35	37	40	45	50
5.4	10	15	20	25	30	33	35	37	40	45	50
7.3	10	15	20	25	30	33	35	37	40	45	50
8.2	10	15	20	25	30	33	35	37	40	45	50
10.2	10	15	20	25	30	33	35	37	40	45	50

Table 6.3 Range of heeling angles and speeds of the model for towing

Practically, application of the equation 3.5 is discussed for evaluation of GM of a ship in a seaway in Chapter 3. GM of the model for static condition at the design waterline is obtained as discribed in section 6.3.1. To consider the effect of forward speed on the GM of the model, varation of the heel angle was measured along the towing tank for a given forward speed in accordance with Table 6.3. Therefore, for each recorded inclination angle the along towing tank, once knowing the weight of the model and the prescribed applied inclination moment, the GM of the model may be evaluated using equation 6.8. The results of tests and the GM evauation are presented in the following sections.

6.4. RESULTS

In this section certain circumstances of the tests and the observed results are presented and discussed.

6.4.1 FREE ROLLING MOTION

To obtain free rolling decay for a stationary condition, the model was heeled to the port side and then released. Figure 6.5 shows the behaviour of the model concerning variation of rolling decay versus time. It can be verified that although the rolling decay dies out after a few seconds, the trend maintains a very small port angle. This might be due to the fact that the model could not initially be set to a truly zero angle. Best efforts were made and the digital inclinometer could not be adjusted to a figure better than 0.1°, so this was inevitably taken as zero level for all subsequent experiments.

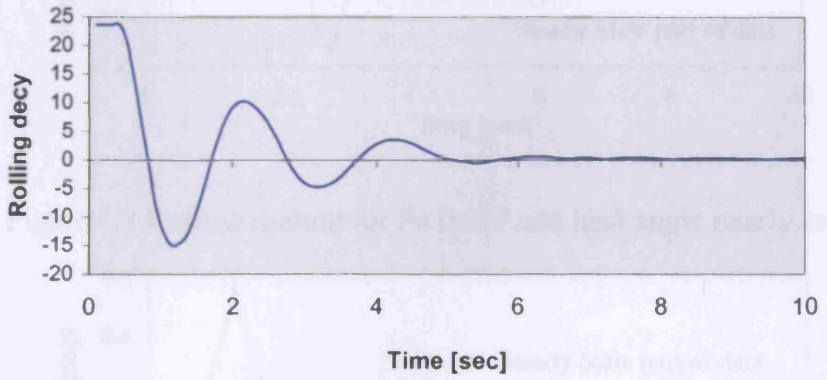

Figure 6.5 Free rolling motion

6.4.2 ROLLING MOTION BY DIFFERENT SPEEDS

The same arrangement (zero inclination angle) was utilised for running the model using various ranges of speed as shown in Table 6.2. Variation of rolling motion in association with speeds 0.634, 0.772 and 1.090 ms^{-1}, that are equivalent to Fn = 0.098, 0.119 and 0.168 respectively, are selected as typical examples for further discussion.

It is important to note that although no initial heeling angle was applied to the model, it demonstrates an irregular rolling motion along the towing tank. The corresponding results are shown in Figures 6.6 to 6.8.

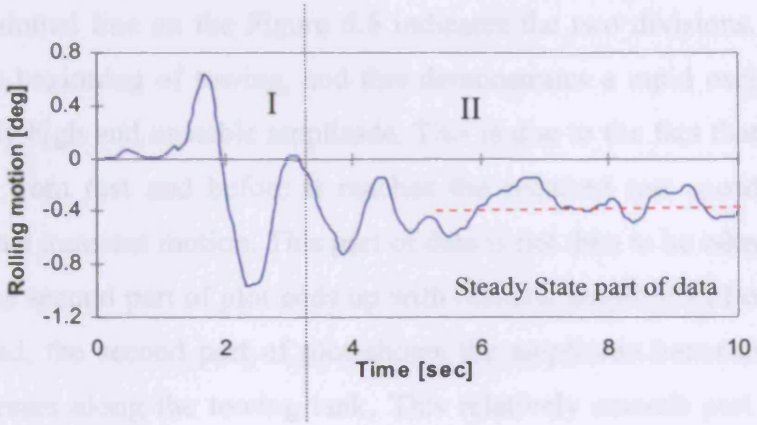

Figure 6.6 Rolling motion for Fn 0.098 and heel angle nearly zero

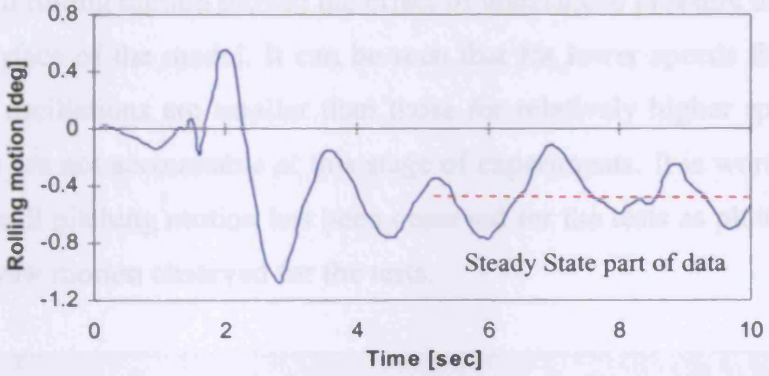

Figure 6.7 Rolling motion for Fn 0.119 and heel angle nearly zero

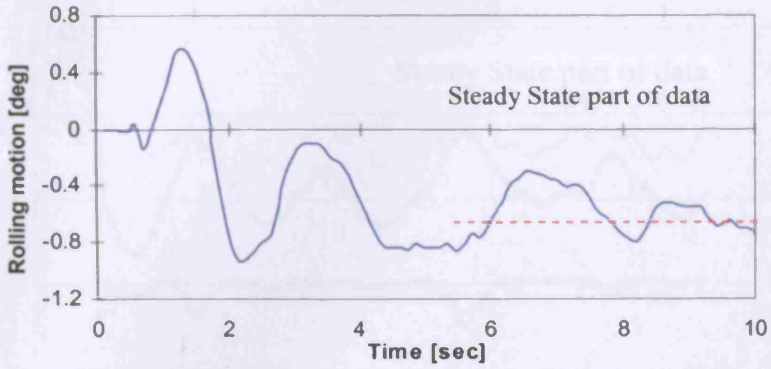

Figure 6.8 Rolling motion for Fn 0.168 and heel angle nearly zero

Referring to the above figures, an unexpected rolling motion occurred associated with model towing at various speeds, when zero heeling moment was applied. On each figure, it can be seen that the plot is typically divided into two distinct parts (I and II). The vertical dotted line on the Figure 6.6 indicates the two divisions. The first part related to the beginning of towing, and this demonstrates a rapid oscillatory motion with relatively high and unstable amplitude. This is due to the fact that towing of the model starts from rest and before it reaches the required test speed, it inevitably passes though a transient motion. This part of data is not then to be taken into account. Eventually the second part of plot ends up with realistic amplitude of oscillations. On the other hand, the second part of plot shows the amplitude becomes stable as the model progresses along the towing tank. This relatively smooth part of the data is referred to as steady state motion of the model.

The very small rolling motion proved the effect of unbalanced pressure distribution on the wetted surface of the model. It can be seen that for lower speeds the period and amplitude of oscillations are smaller than those for relatively higher speeds, though the variations are not accountable at this stage of experiments. It is worth to mention that a very small pitching motion has been observed for the tests as plotted on Figure 6.6a, and no yaw motion observed for the tests.

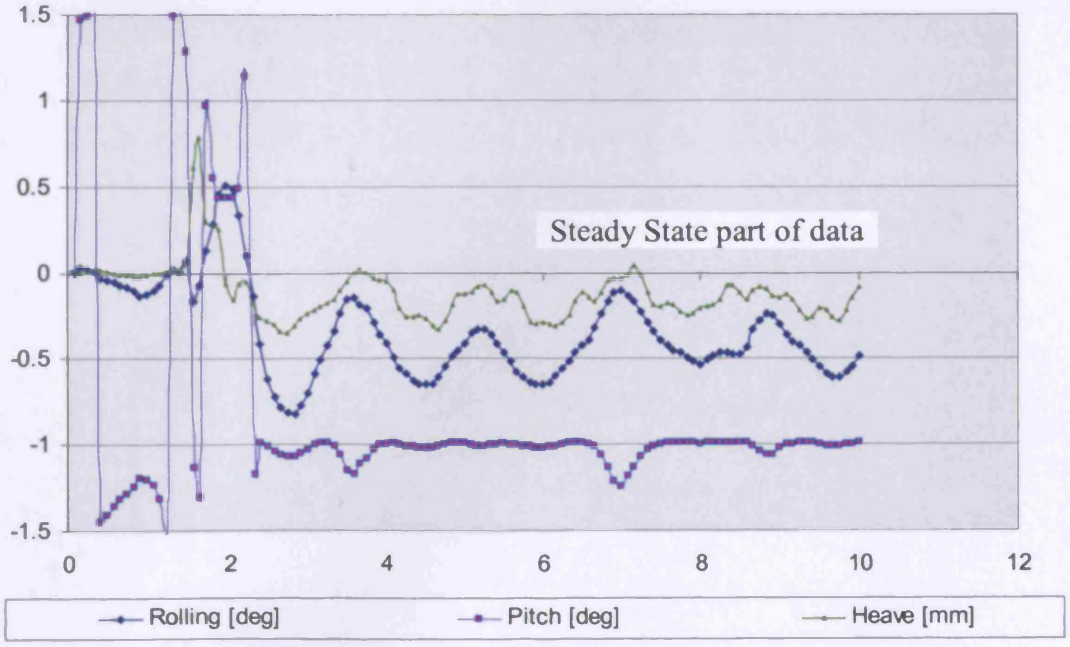

Figure 6.6a Heave, Roll and Pitch Motions for Fn 0.098 and heel angle nearly zero

6.4.3 ROLLING MOTION AFFECTED BY HEELING ANGLE

In the previous section an unexpected rolling motion associated with the model towed was observed for nearly zero inclination angle. In order to make sure that the variation of unbalanced pressure distribution on the wetted surface of the model was the main source of the rolling motion, and to consider the effect of the variation of speed on the rolling motion the following tests were conducted. In this section the observed rolling motion when the model has an initial heeling angle for certain speeds will be presented. The result of the steady state part of each plot is the part of data used as initial data to determine *GM* of the model at any instance of rolling motion.

Due to the vast number of tests which were conducted according to Table 6.3, just a few runs are selected for further discussion. The selected tests are chosen with respect to heeling angle and speed. The selected heeling angles are 2.5°, 5.4°, 7° and 10°, for these angles the experimental results for different selected forward speeds Fn = 0.034, 0.098, 0.119 and 0.168 are presented. Furthermore, in all results produced only the rolling motion will be examined, and no argument will be made concerning the transient part nor the effect of oscillating amplitude and period.

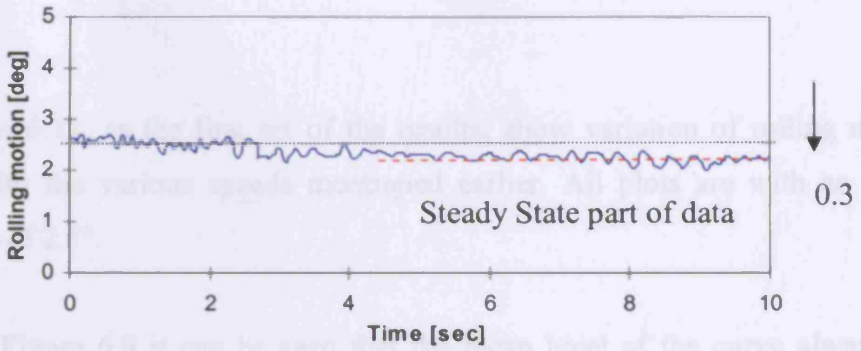

Figure 6.9 Rolling motion for Fn 0.034 and heel angle 2.5 °

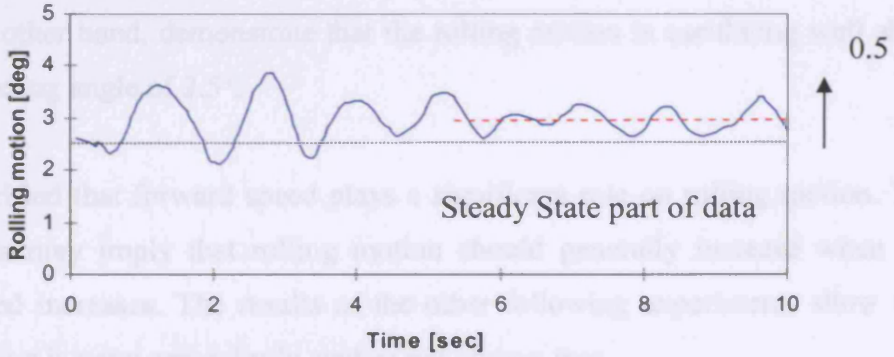

Figure 6.10 Rolling motion for Fn 0.098 and heel angle 2.5 °

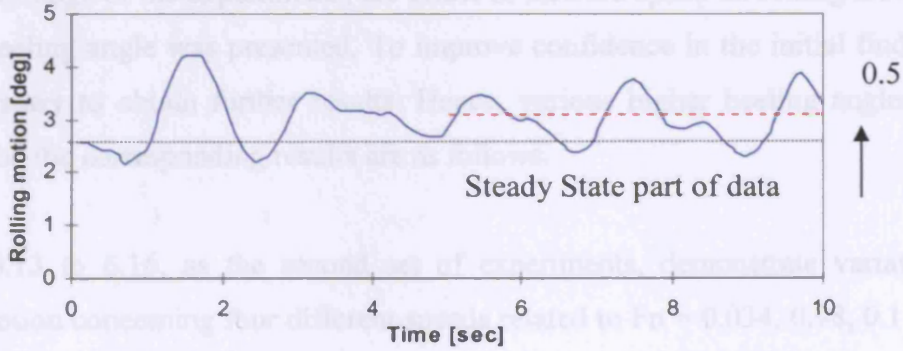

Figure 6.11 Rolling motion for Fn 0.119 and heel angle 2.5 °

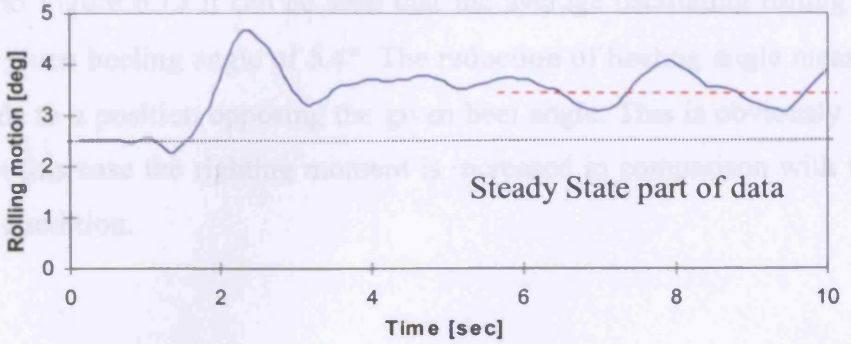

Figure 6.12 Rolling motion for Fn 0.168 and heel angle 2.5 °

Figures 6.9 to 6.12, as the first set of the results, show variation of rolling motion associated with the various speeds mentioned earlier. All plots are with an initial heeling angle of 2.5°.

Referring to Figure 6.9 it can be seen that the mean level of the curve always has values less than the given heeling angle. While, Figure 6.10 shows that the rolling motion is oscillating almost uniformly around the initial given angle. Figures 6.11 and 6.12, on the other hand, demonstrate that the rolling motion is oscillating well above the initial heeling angle of 2.5°.

It can be verified that forward speed plays a significant role on rolling motion. The above results may imply that rolling motion should generally increase when the forward speed increases. The results of the other following experiments show that this implication is not a general rule, and so not always true.

At an early stage of the experiments, the effect of forward speed on rolling motion for a small heeling angle was presented. To improve confidence in the initial findings it was necessary to obtain further results. Hence, various higher heeling angles were applied and the corresponding results are as follows.

Figures 6.13 to 6.16, as the second set of experiments, demonstrate variation of rolling motion concerning four different speeds related to Fn = 0.034, 0.98, 0.119 and 0.168. For all these speeds the initial heeling angle is fixed at 5.4°.

Referring to Figure 6.13 it can be seen that the average oscillating rolling motion is below the given heeling angle of 5.4°. The reduction of heeling angle means that the model tends to a position opposing the given heel angle. This is obviously due to the fact that in this case the righting moment is increased in comparison with that of the stationary condition.

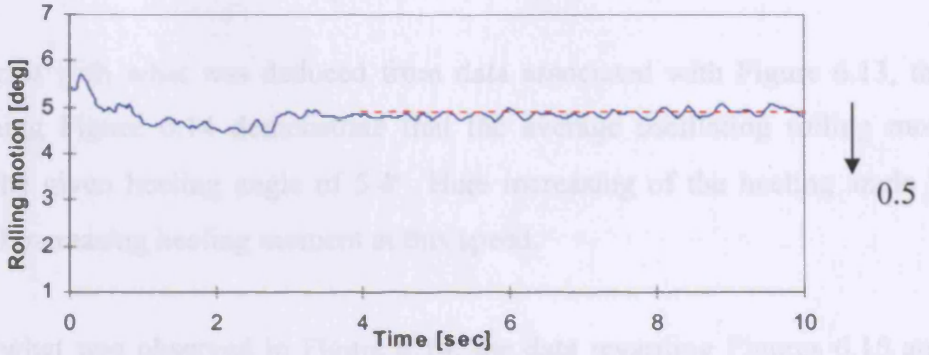

Figure 6.13 Rolling motion for Fn 0.034 and heel angle 5.4 °

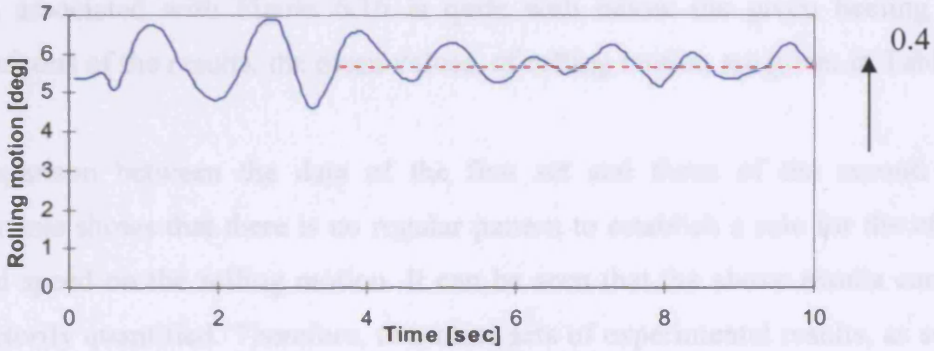

Figure 6.14 Rolling motion for Fn 0.098 and heel angle 5.4 °

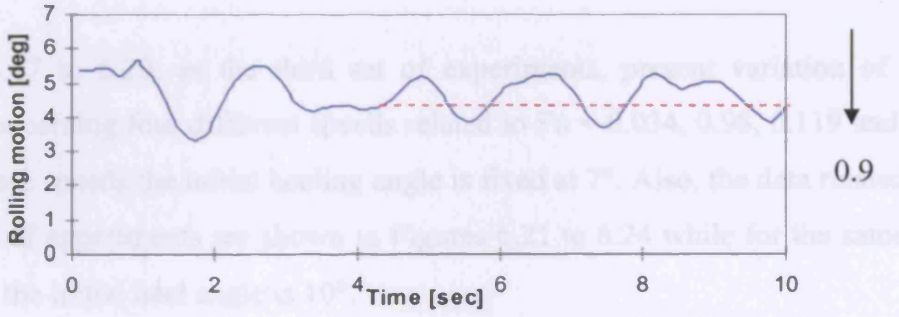

Figure 6.15 Rolling motion for Fn 0.119 and heel angle 5.4 °

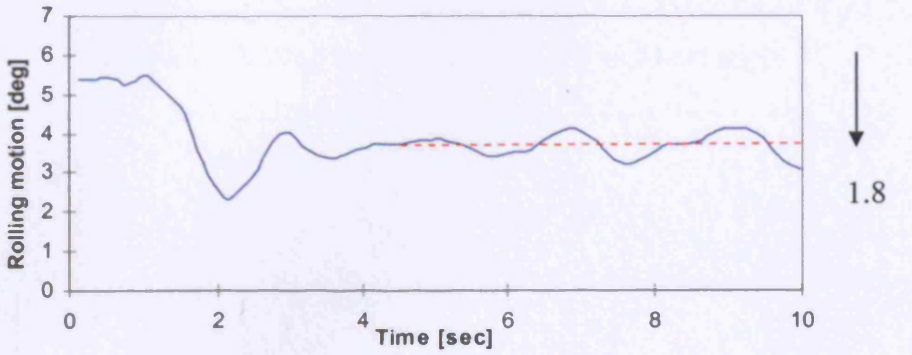

Figure 6.16 Rolling motion for Fn 0.168 and heel angle 5.4 °

In contrast with what was deduced from data associated with Figure 6.13, the data concerning Figure 6.14 demonstrate that the average oscillating rolling motion is above the given heeling angle of 5.4°. Here increasing of the heeling angle is as a result of increasing heeling moment at this speed.

Unlike what was observed in Figure 6.14, the data regarding Figures 6.15 and 6.16 show similar patterns to Figure 6.13 though the mean value of oscillating rolling motion associated with Figure 6.16 is quite well below the given heeling angle. Comparisons of the results, the mean values, of rolling motion are given in Table 6.4.

A comparison between the data of the first set and those of the second set of experiments shows that there is no regular pattern to establish a rule for the effect of forward speed on the rolling motion. It can be seen that the above results cannot be satisfactorily quantified. Therefore, two more sets of experimental results, as selected earlier, are presented and discussed here.

Figures 6.17 to 6.20, as the third set of experiments, present variation of rolling motion concerning four different speeds related to Fn = 0.034, 0.98, 0.119 and 0.168. For all these speeds the initial heeling angle is fixed at 7°. Also, the data related to the fourth set of experiments are shown in Figures 6.21 to 6.24 while for the same range of speeds the initial heel angle is 10°.

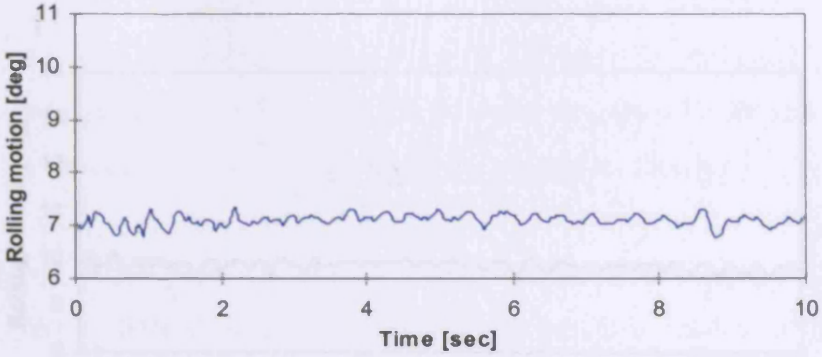

Figure 6.17 Rolling motion for Fn 0.034 and heel angle 7°

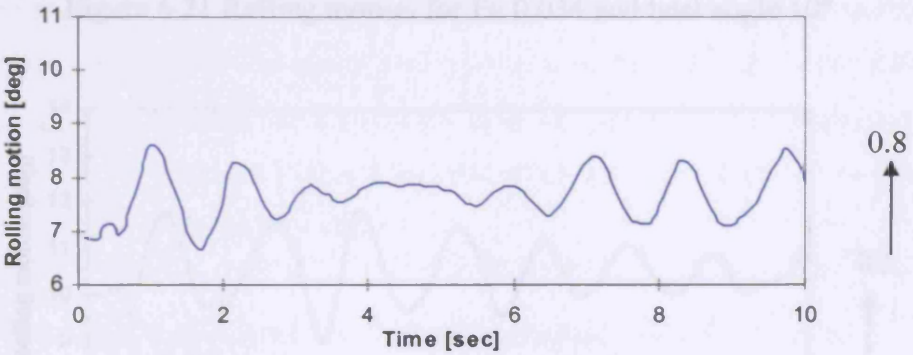

Figure 6.18 Rolling motion for Fn 0.098 and heel angle 7°

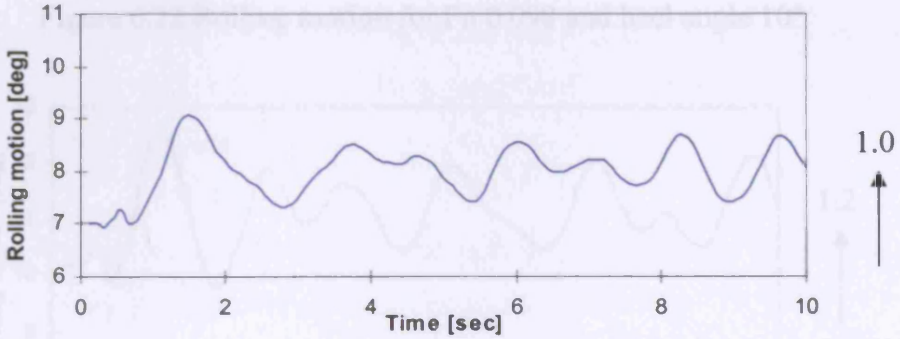

Figure 6.19 Rolling motion for Fn 0.119 and heel angle 7°

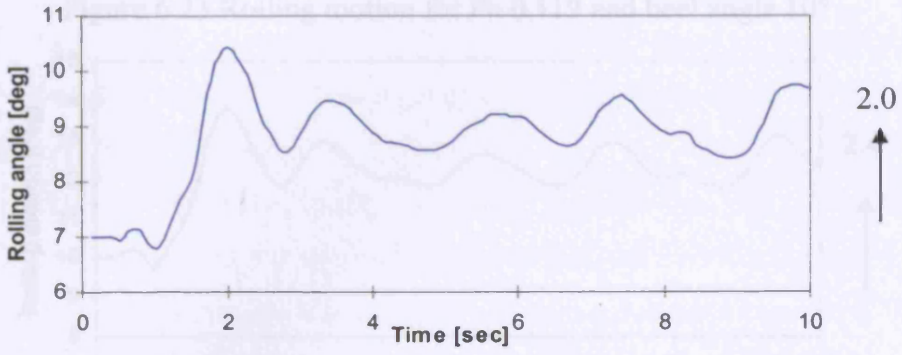

Figure 6.20 Rolling motion for Fn 0.168 and heel angle 7°

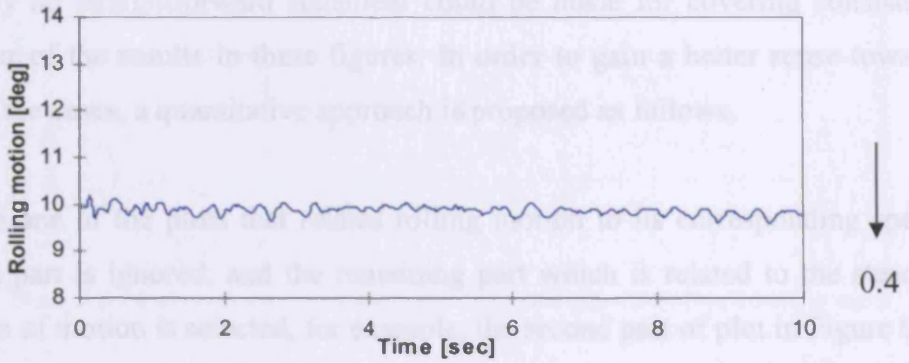

Figure 6.21 Rolling motion for Fn 0.034 and heel angle 10°

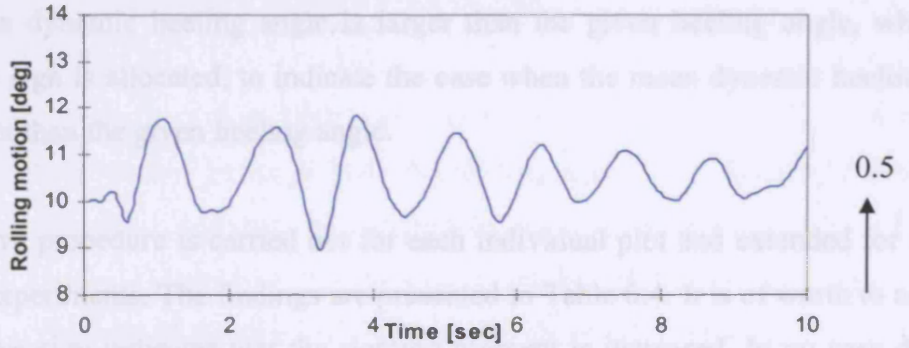

Figure 6.22 Rolling motion for Fn 0.098 and heel angle 10°

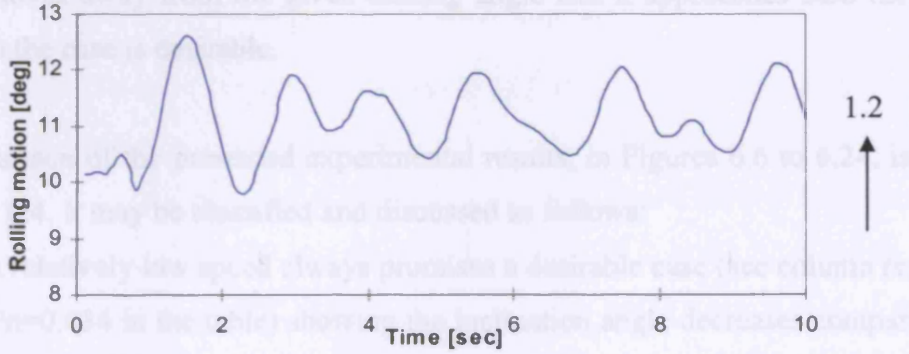

Figure 6.23 Rolling motion for Fn 0.119 and heel angle 10°

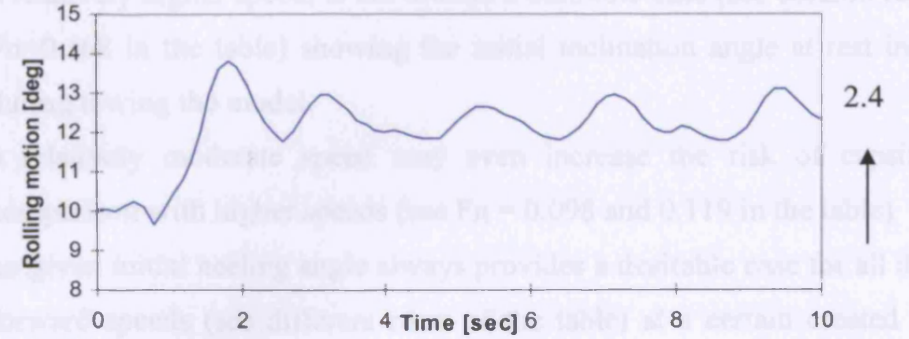

Figure 6.24 Rolling motion for Fn 0.168 and heel angle 10°

Generally no straightforward statement could be made for covering consistency of behaviour of the results in these figures. In order to gain a better sense towards the study of the cases, a quantitative approach is proposed as follows.

For each one of the plots that relates rolling motion to its corresponding speed, the transient part is ignored, and the remaining part which is related to the steady state condition of motion is selected, for example, the second part of plot in Figure 6.6. The average value of the rolling motion is calculated for the selected part of recorded data and compared with the initial given heeling angle. A positive sign is assigned when the mean dynamic heeling angle is larger than the given heeling angle, whereas a negative sign is allocated, to indicate the case when the mean dynamic heeling angle is smaller than the given heeling angle.

The above procedure is carried out for each individual plot and extended for all four sets of experiments. The findings are presented in Table 6.4. It is of worth to note that a negative sign indicates that the righting moment is increased. In no case does the negative figure exceed the corresponding initial heeling angle. This means that the model moves away from the given heeling angle and it approaches zero inclination angle, so the case is desirable.

A comparison of the presented experimental results, in Figures 6.6 to 6.24, is shown in Table 6.4. It may be classified and discussed as follows:

- a relatively low speed always promises a desirable case (see column regarding Fn=0.034 in the table) showing the inclination angle decreases compared with the given initial inclination angle at rest.
- a relatively higher speed, is not always a desirable case (see column regarding Fn=0.168 in the table) showing the initial inclination angle at rest increased during towing the model.
- a relatively moderate speed may even increase the risk of capsizing in comparison with higher speeds (see Fn = 0.098 and 0.119 in the table)
- no given initial heeling angle always provides a desirable case for all different forward speeds (see different rows of the table) at a certain created heeling angle, an individual /or a zone regarding forward speed may be considered as a desirable case.

Fn		0.034	0.098	0.119	0.168
Inclination angle	2.5°	-0.3	+0.5	+0.5	+0.9
	5.4°	-0.5	+0.4	-0.9	-1.8
	7°	0	+0.8	+1	+2
	10.0°	-0.4	+0.5	+1.2	+2.4

Table 6.4 Difference of mean dynamic rolling angle and given heeling angle

6.5 EFFECT OF FORWARD SPEED ON *GM*

In the previous section a desirable case was referred to as a case when the negative sign of rolling motion indicated that the heeling decreased, therefore, the righting moment is increased. Although an undesirable case may be referred to the case when the heeling angle is increasing, this does not necessarily mean a risk of capsizing. It is showing actual role of forward speed on the GM variation. Consequently, an adequate study of *GM* requires small heeling angle and / or in general unbalanced pressure distributed on the wetted surface of a hull.

In this section variation of the *GM* in terms of forward speed is studied, due to the effect of heeling angle. The values selected for heeling angle as well as forward speed are the same as described in the previous section. Then on the basis of previous results the GM is calculated for each instant inclination data. It is worth mentioning that the value of *GM* changes during towing. Therefore, an instantaneous *GM*, denoted as GM_d, will also be dealt with. In all subsequent presentations a ratio of GM_d/GM will be indicated as a generalised measure rather than *GM* itself. This suggests that a ratio of 1 should refer to as a reference indicating that the static *GM* has not changed.

The results produced are shown in Figures 6.25 to 6.40. These are classified in the form of four inclination angles of which each includes four different speeds. Figures 6.25 to 6.28, which are associated with a fixed heeling angle of 2.5° are selected as a typical example for discussion. Bearing in mind that the steady state part of the data is the main part of the concern, where the model reaches a given forward speed.

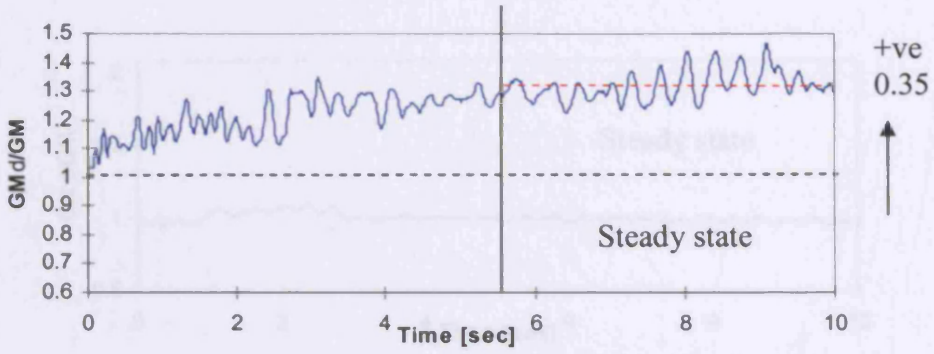

Figure 6.25 GM ratio for Fn 0.034 and heel angle 2.5°

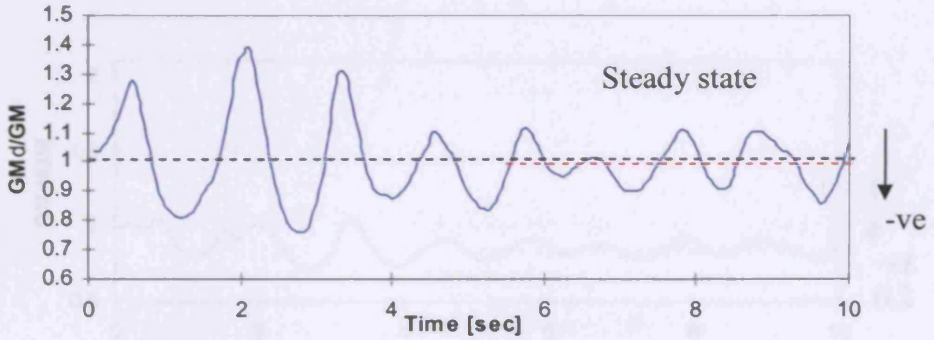

Figure 6.26 GM ratio for Fn 0.098 and heel angle 2.5°

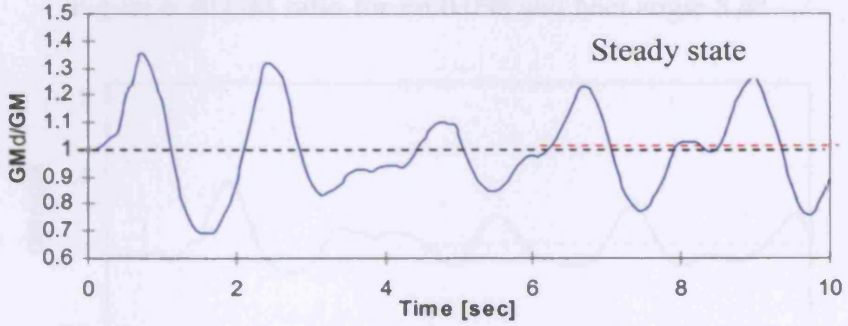

Figure 6.27 GM ratio for Fn 0.119 and heel angle 2.5°

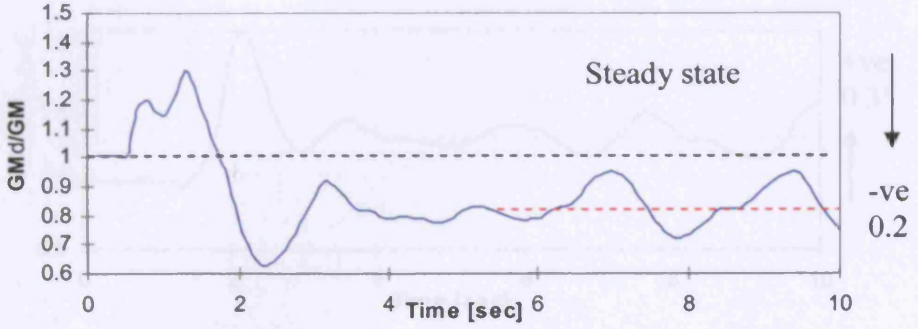

Figure 6.28 GM ratio for Fn 0.168 and heel angle 2.5°

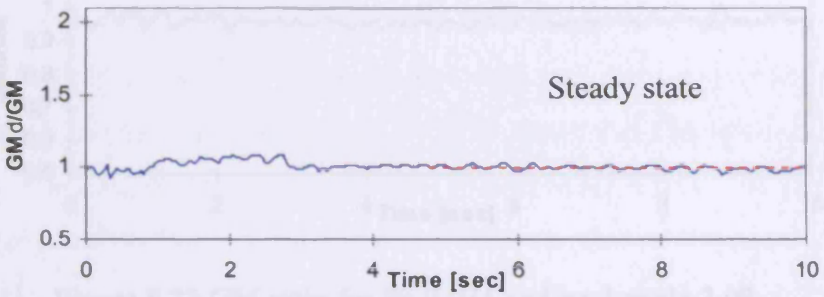

Figure 6.29 GM ratio for Fn 0.034 and heel angle 5.4°

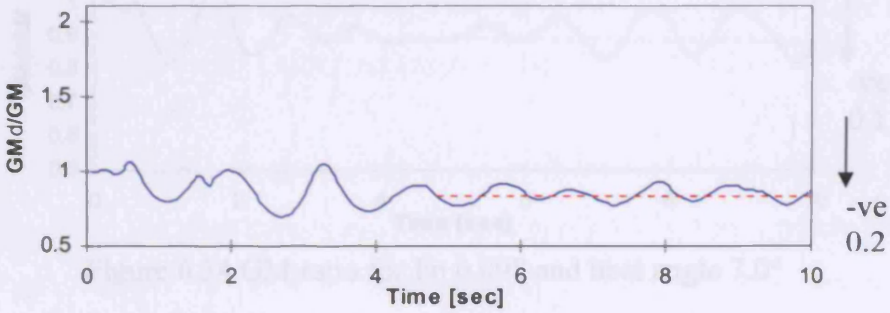

Figure 6.30 GM ratio for Fn 0.098 and heel angle 5.4°

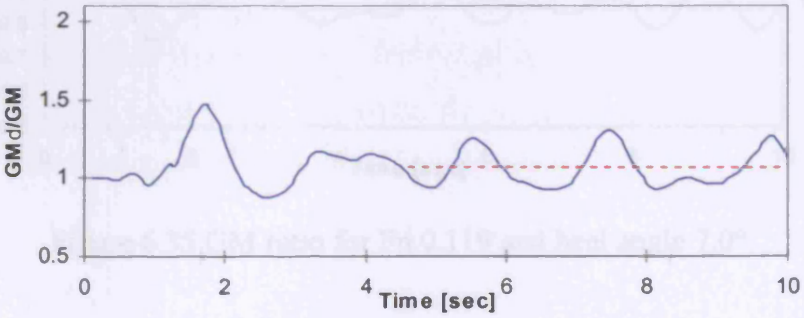

Figure 6.31 GM ratio for Fn 0.119 and heel angle 5.4°

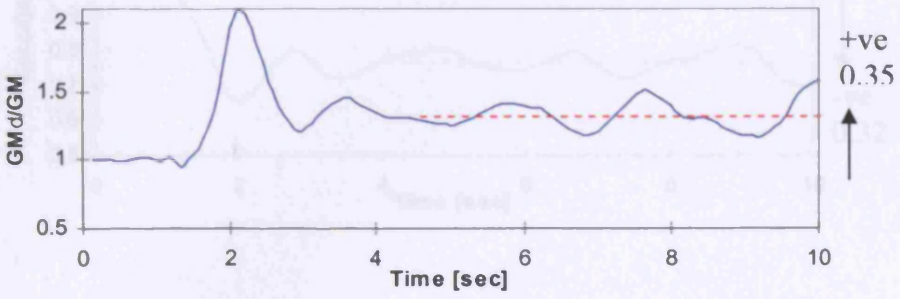

Figure 6.32 GM ratio for Fn 0.168 and heel angle 5.4°

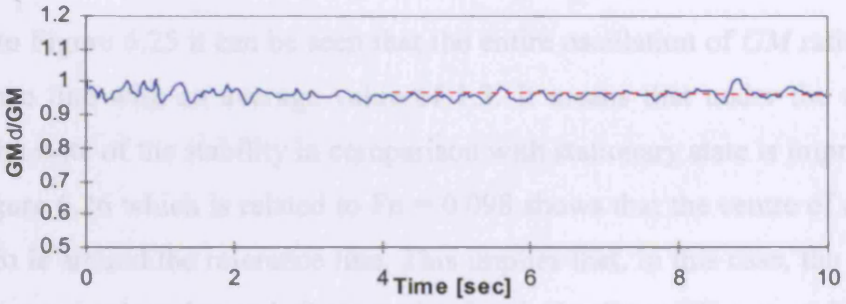

Figure 6.33 GM ratio for Fn 0.034 and heel angle 7.0°

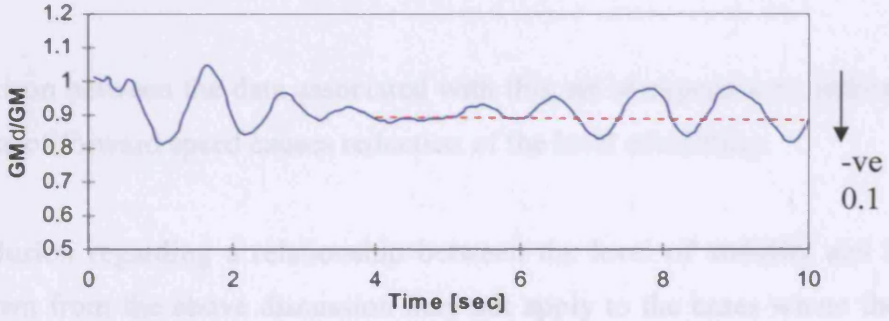

Figure 6.34 GM ratio for Fn 0.098 and heel angle 7.0°

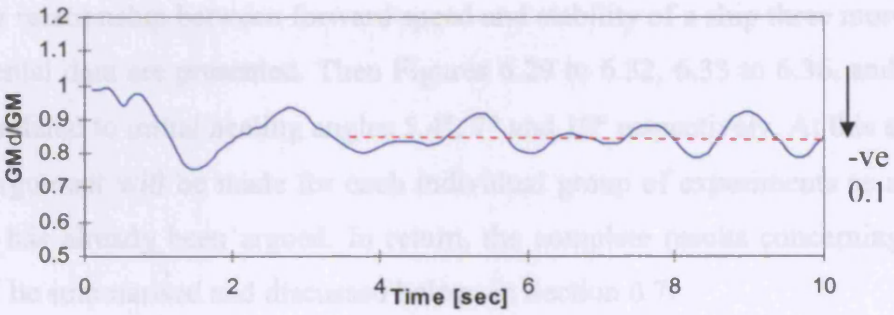

Figure 6.35 GM ratio for Fn 0.119 and heel angle 7.0°

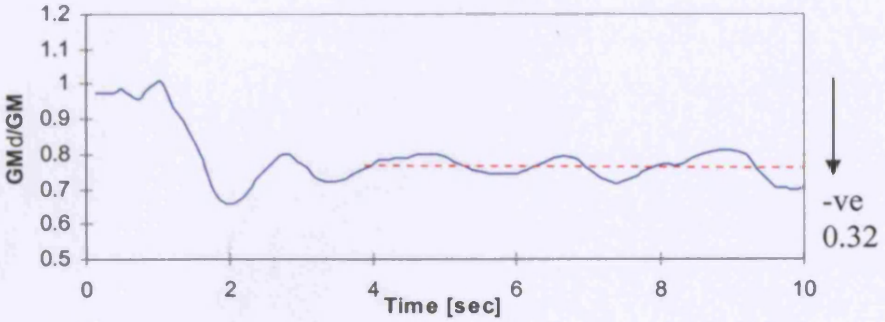

Figure 6.36 GM ratio for Fn 0.168 and heel angle 7.0°

Referring to Figure 6.25 it can be seen that the entire oscillation of *GM* ratio is above the reference line with an average value of 1.3. It means that under the conditions provided the state of the stability in comparison with stationary state is improved. The data of Figure 6.26 which is related to Fn = 0.098 shows that the centre of oscillation of *GM* ratio is around the reference line. This implies that, in this case, the static *GM* has almost remained unchanged. On the other hand, the data of Figures 6.27 and 6.28 which are respectively related to Fn = 0.119 and 0.168 demonstrate that the *GM* ratio oscillation is below the reference line with average values of 0.9 and 0.8.

A comparison between the data associated with this set of experiments indicates that an increase of forward speed causes reduction of the level of stability.

The conclusion regarding a relationship between the level of stability and forward speed drawn from the above discussion may not apply to the cases where the initial heeling angle changes. In order to investigate the existence of any general rule or particular relationship between forward speed and stability of a ship three more sets of experimental data are presented. Then Figures 6.29 to 6.32, 6.33 to 6.36, and 6.37 to 6.40 are related to initial heeling angles 5.4°, 7° and 10° respectively. At this stage, no further argument will be made for each individual group of experiments as a typical example has already been argued. In return, the complete results concerning all the tests will be summarised and discussed below, in Section 6.7.

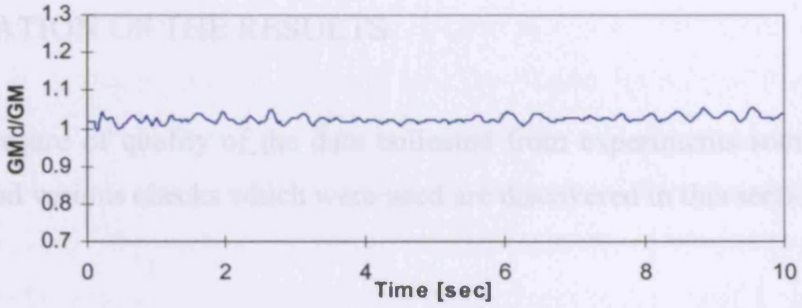

Figure 6.37 GM ratio for Fn 0.034 and heel angle 10°

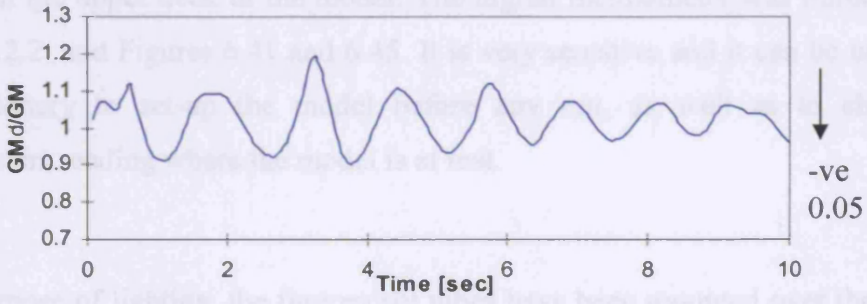

Figure 6.38 GM ratio for Fn 0.098 and heel angle 10°

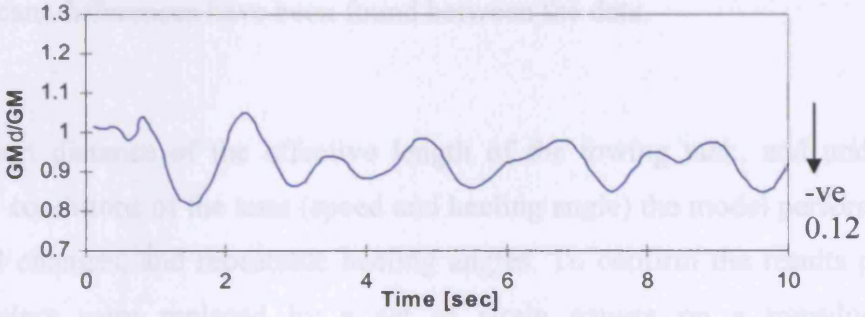

Figure 6.39 GM ratio for Fn 0.119 and heel angle 10°

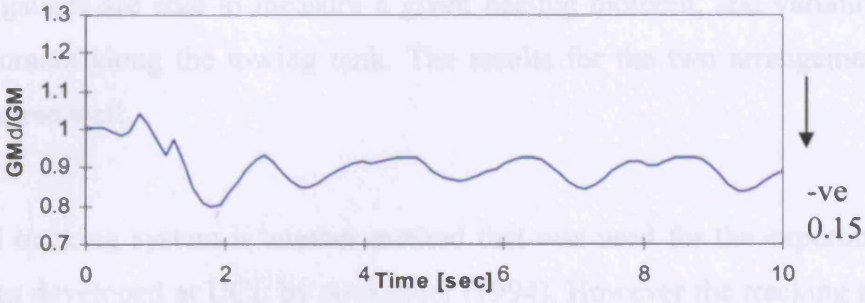

Figure 6.40 GM ratio for Fn 0.168 and heel angle 10°

6.6 VALIDATION OF THE RESULTS

In order to ensure of quality of the data collected from experiments some auxiliary instrument and various checks which were used are discovered in this section.

The initial inclination angle was checked for any run by the digital inclinometer mounted on the upper deck of the model. The digital inclinometer was introduced in Sections 6.2.2, and Figures 6.41 and 6.45. It is very sensitive and it can be used only when stationery to set-up the model before any run, as well as to check the potentiometers reading where the model is at rest.

For the purpose of lighting, the fluorescent tubes have been mounted over the towing tank. To avoid noise effect of electromagnetic fields of the lighting the experiments were conducted with the lighting on. Some were repeated when the lighting was off. No significant differences have been found between the data.

Due to short distance of the effective length of the towing tank, and under some prescribed conditions of the tests (speed and heeling angle) the model performed with very small changes, and repeatable heeling angles. To confirm the results produced potentiometers were replaced by a set of strain gauges on a transducer. The potentiometer is able to measure angle, and difference between the initial setup with variation of heeling angle along the towing that were used in the tests. Alternatively the strain gauges are able to measure a given heeling moment, and variation of the heeling moment along the towing tank. The results for the two arrangements were shown to agree well.

An optical tracking system is another method that was used for the experiment. The method was developed at UCL by Alexander (1994). However the tracking system is not suitable as a general package to offer user any straightforward results, it can be used as a very good guideline. General idea is to record the performance of the model and developing image processing in C program language to detect the positions of

model lights and references for subsequent motions analysis. Tests were recorded on the video tapes, and a suitable C program was developed (as port of this research). However, owing to unavailability of a camcorder to replay the recorded tests and malfunction of the image processing system, only one of the recorded tests was processed manually. To analyse one of the recorded data tapes the package Arcview Geographic Information System (GIS), of the Department of Geomatic Engineering at UCL, was used. Comparisons between the data of the tracking with the data presented in this chapter for low speed showed similar behaviour. Schematic set-up of the tracking system and its required facilities for image processing are shown in Figures 6.43 and 6.44.

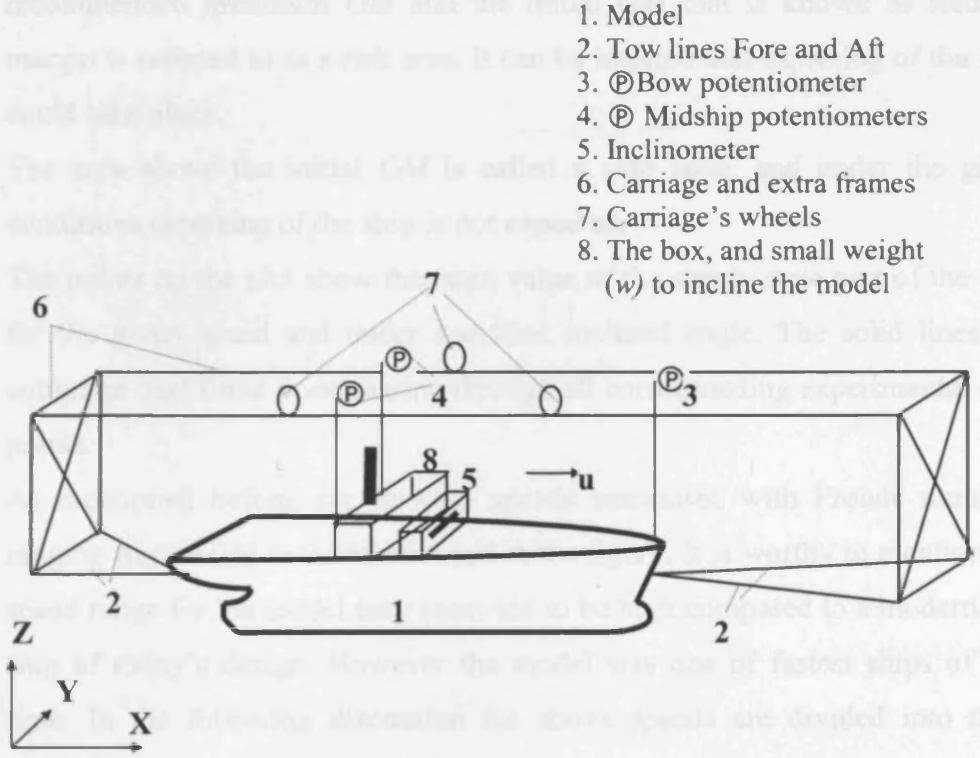

Figure 6.41 The schematic arrangement of the test

6.7 CONCLUSION

Before presenting any conclusion, a few guide points associated with Figure 6.42 are introduced here as follows:

1. The horizontal dashed line refers to the recommended minimum *GM* which according to many classification societies is 0.2 m for ships, and consequently is 0.002 m for the model due to scaling coefficient (1/100). The region below this line is indicated as an unsafe zone. In fact, risk of capsizing of the ship will take place.
2. The initial *GM* of the model, that was calculated previously, is 0.235 m and presented by the dotted line. The reason for very small GM chosen for the model is to demonstrate any arbitrary motions and to be very sensitive, because of the model towed in calm water condition. The area between recommended minimum *GM* and the initial *GM* that is known as stability margin is referred to as a risk area. It can be implied that capsizing of the ship could take place.
3. The area above the initial *GM* is called a safe zone, and under the given conditions capsizing of the ship is not expected.
4. The points on the plot show the main value of the steady state part of the data for the given speed and under specified inclined angle. The solid lines are computer best fitted lines passing through all corresponding experimental data points.
5. As mentioned before, six forward speeds associated with Froude numbers ranging from 0.034 to 0.168 are used in the figure. It is worthy to mention the speed range for the model may seem not to be high compared to a modern fast ship of today's design. However the model was one of fastest ships of that time. In the following discussion the above speeds are divided into three groups in an increasing order. The first group corresponding to Fn =0.034 and 0.081 will be referred to as low speeds, while the next following groups will be referred to as moderate and high speeds respectively. The definition of low, moderate and high for the speeds are of course relative.

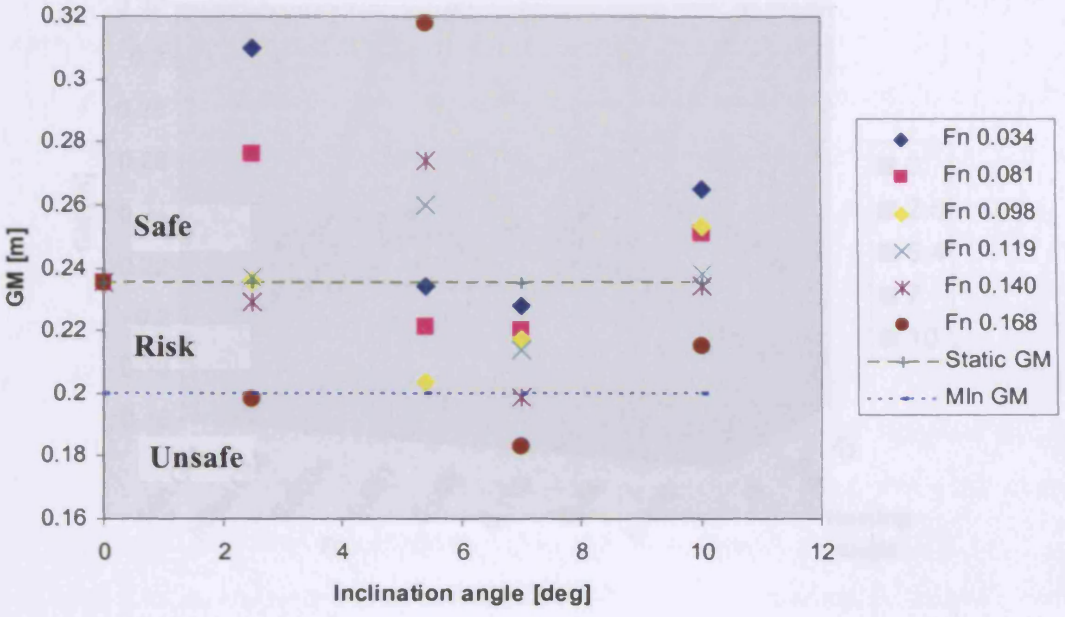

Figure 6.42 Variation of GM in terms of inclination angle for the model, the data also relate to various forward speeds

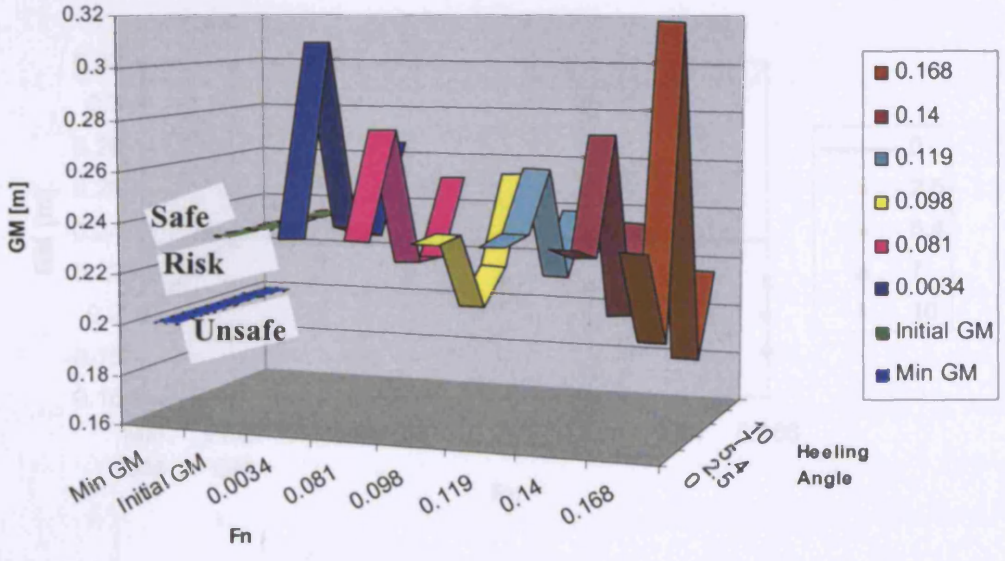

Figure 6.42a A 3D view of GM variation in terms of inclination angle for different forward speeds

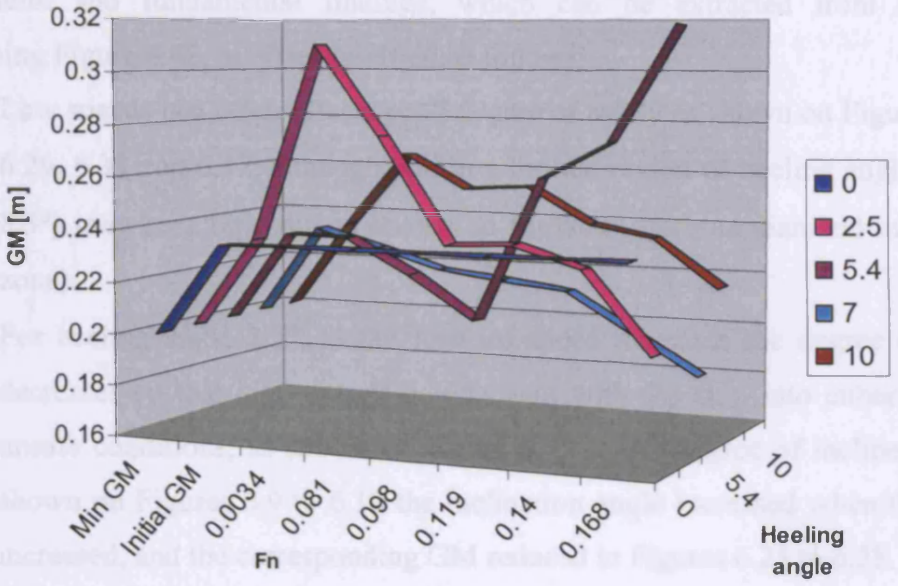

Figure 6.42b A 3D view of GM variation in terms of various forward speeds at prescribed inclination angle

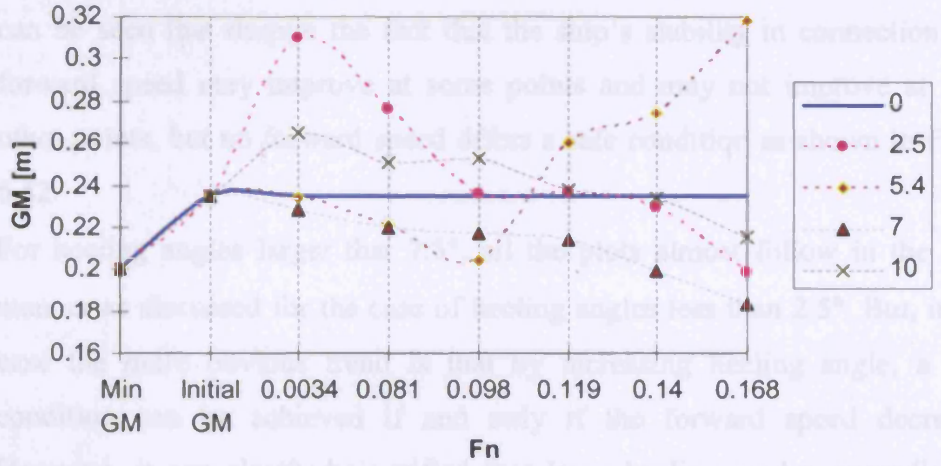

Figure 6.42c GM variation in terms of various forward speeds at prescribed inclination angle the dotted line shows best fit to each set of the inclination angle

The useful and fundamental findings, which can be extracted from the data concerning Figure 6.42, may be classified as follow:

- Low speeds can often offer a good degree of safety as shown on Figures 6.25, 6.29, 6.33 and 6.37, although within a limited region of heeling angle (4.5°to 8.5°) may be a bit risky as shown on Figure 6.42 (blue diamond in the risk zone).
- For heeling angle 2.5°, as the forward speed increases the degree of safety decreases so that high speeds could result with the ship into either risky or unsafe conditions, as shown on Figure 6.42 at 2.5 degree of inclined and as shown on Figures 6.9 to 6.12 the inclination angle increased when the speed increased, and the corresponding GM reduced in Figures 6.25 to 6.28.
- For heeling angles varying from 2.5° to 7.0° the plots repeatedly intersect each other so that no certain rule for variation of *GM* can be deduced. For example at heeling angel of 5.5° although high speeds lead to a safe condition, and low speeds to just risky condition, for moderate speeds no clear justification can be made (the plot concerning Fn =0.098 is in the risky zone while for Fn =0.119 is in the safe zone) see Figures 6.42 and 6.42c.
- The heeling angle domain 6.5° to 7.5° may be considered as the worst zone. It can be seen that despite the fact that the ship's stability in connection with forward speed may improve at some points and may not improve at some other points, but no forward speed offers a safe condition as shown in Figure 6.42.
- For heeling angles larger that 7.5°, all the plots almost follow in the same manner as discussed for the case of heeling angles less than 2.5°. But, in this case the more obvious trend is that by increasing heeling angle, a safer condition can be achieved if and only if the forward speed decreases. However, it can clearly be verified that large heeling angles, regardless of forward speed, could endanger the ship's stability and so should be avoided.
- Stability in connection with forward speed and heeling angle is complex. However, maximum confidence of stability can be achieved at Fn =0.119 for a wide range of heeling angles. In fact, an optimum profile of *GM* is related to a moderate speed.

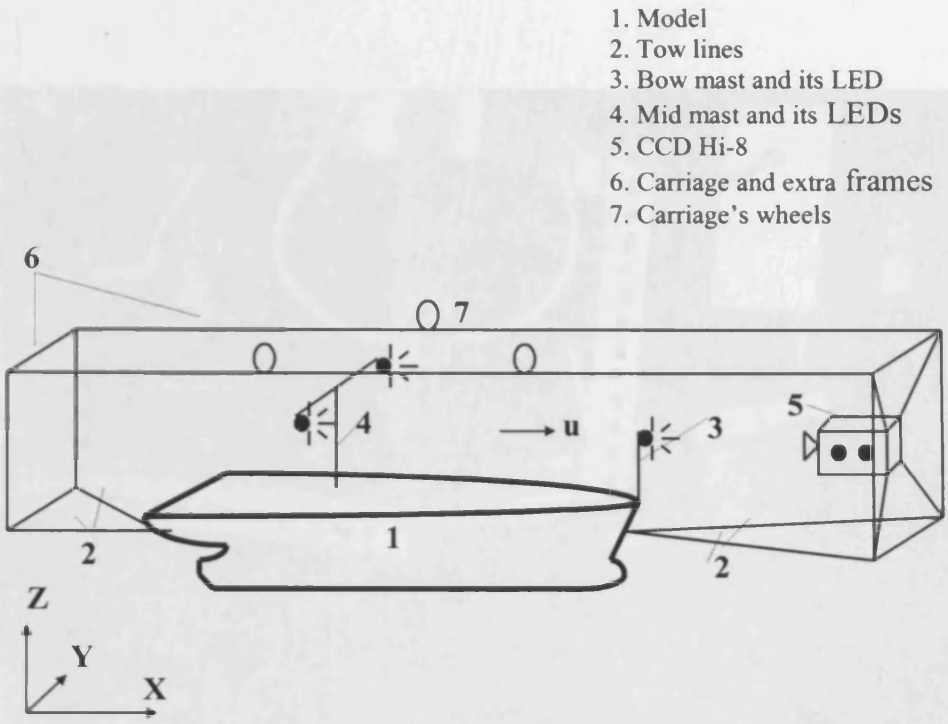

Figure 6.43 The Optical tracking system arrangements in the towing tank

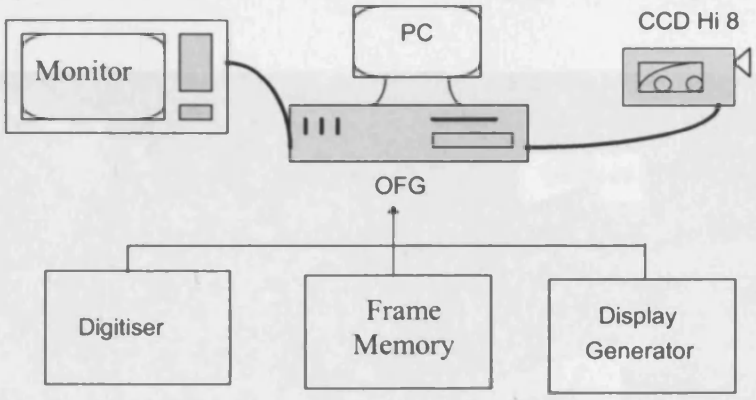

Figure 6.44 The set-up required for analysis of the video recorded tape using the Overlay Frame Grabber (OFG)

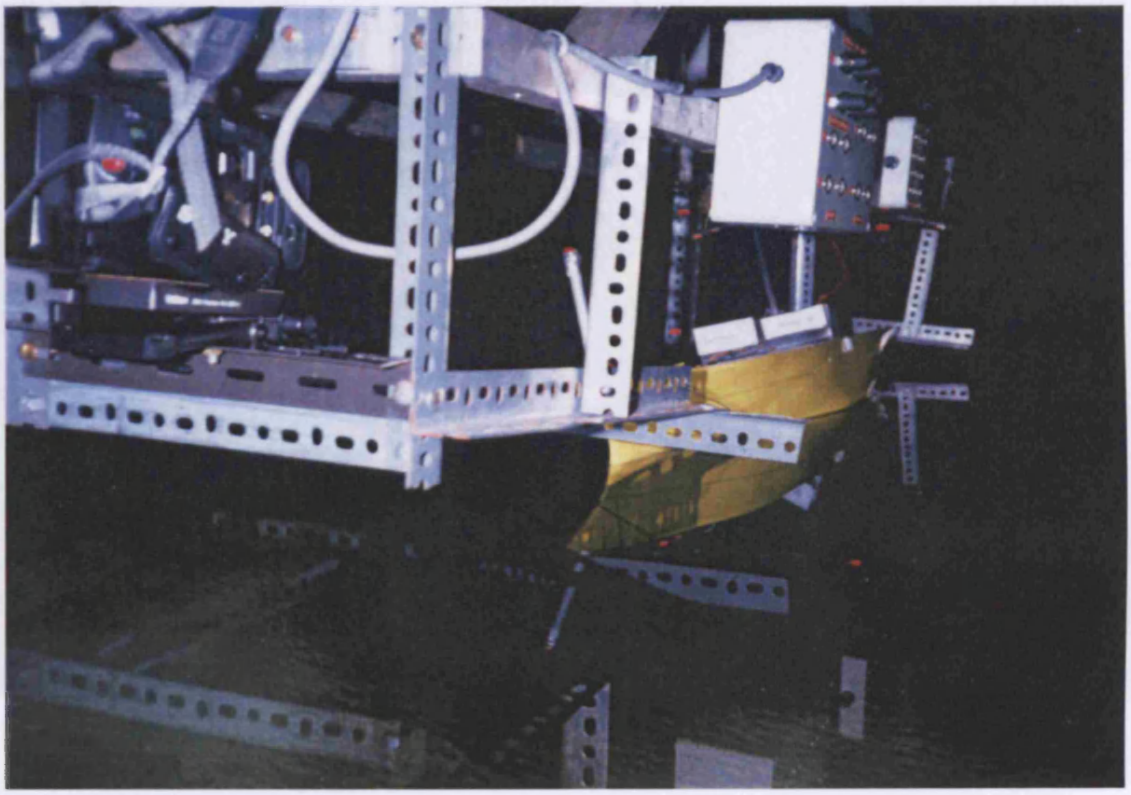

Figure 6.45 Photo of the Optical tracking system arrangement

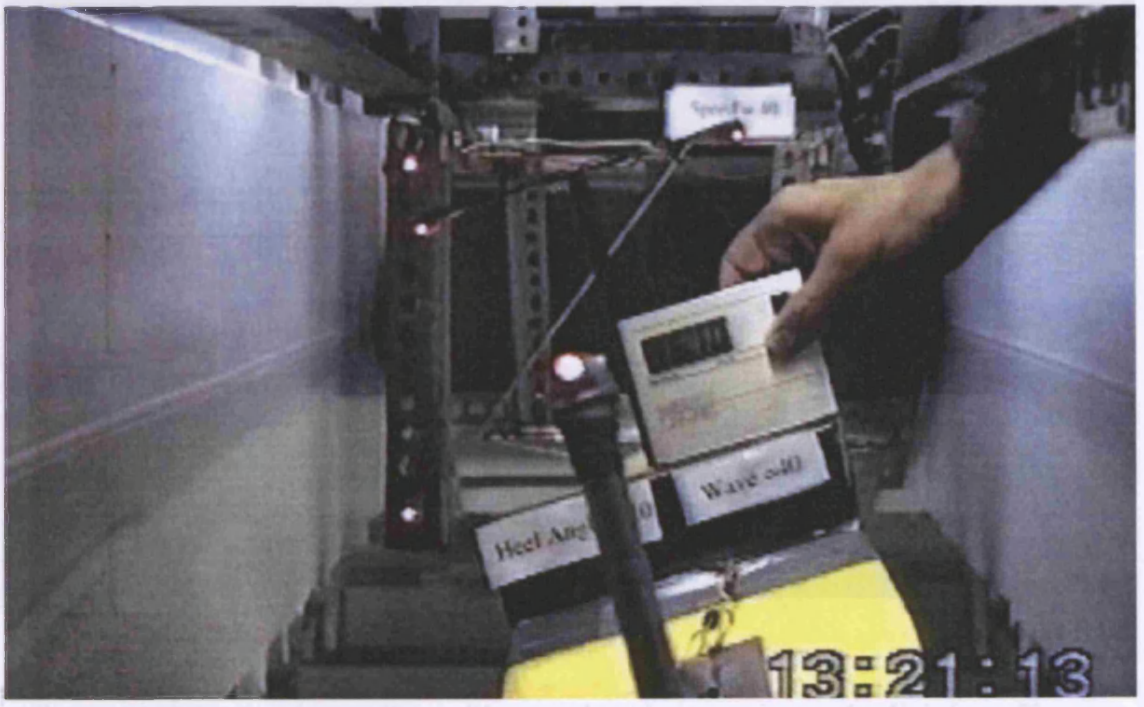

Figure 6.46 Photo of inclination angle setting and checking under lighting on

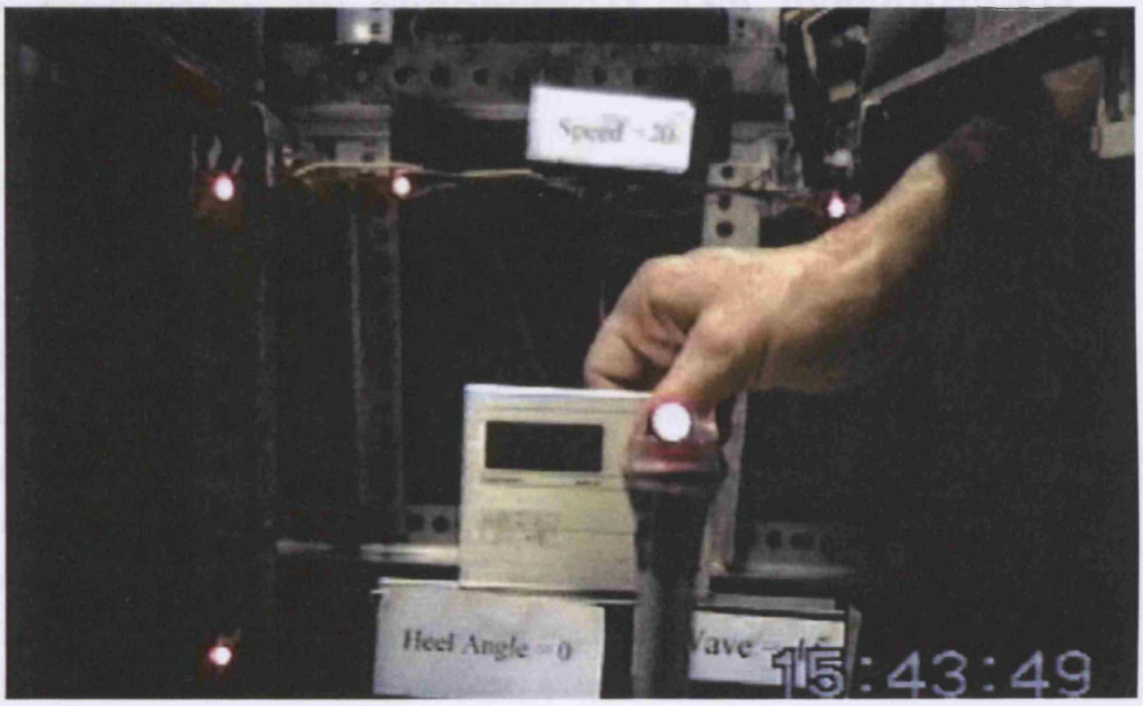

Figure 6.47 Photo of inclination angle setting-up for 2.5° under lighting off

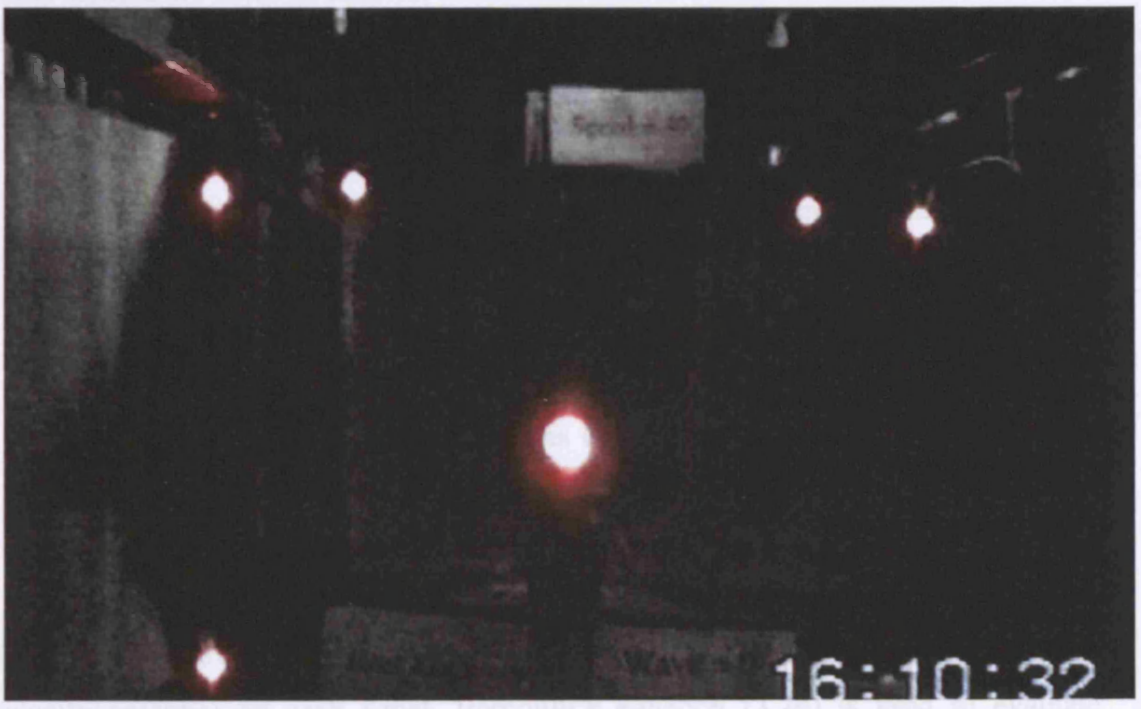

Figure 6.48 Photo of recording rolling motion along towing under lighting off

7. DISCUSSION ON THEORETICAL AND EXPERIMENTAL RESULTS

7.1 THEORETICAL APPROACH

A summary of the CFD method that has been applied for theoretical investigations in the research is reported herein. The wetted surface of a ship's hull has been assumed as a computational domain. In order to subdivide the domain into a large number of triangular panels a computer code was developed. The computer code generates a grid (mesh) on the wetted part of the ship, as explained in more detail in Chapter 5. The mesh generation is able to create the triangular panels on the wetted surface of a hull for any loading condition and inclination angle, and the result of the code is used by the steady CFD panel method. The panel method has been coded to provide velocity potential distribution on the wetted surface of the ship's hull on each panel. Chapters 3 and 4 discussed the technique and the methodology in detail. Some elements of the panel method are listed as follows:

- Normal component of the velocity of equation (3.43), described in detail in Section 3.3 as steady potential
- The value of constant source strength on each panel is assumed in equation (3.41), the matrix equation (4.2) is solved using Gaussian Elimination which is discussed in detail in Section 4.4
- The component of B_{ij} is obtained from equation (3.48)
- Velocity potential is computed from equation (3.42)
- The effect of small amplitude waves constructed on the free surface (due to ship forward speed) is simulated, using Green's function that it is given in equation (3.49) in the second part of the Section 3.3.

The output of the computer program yields information such as strength of source and velocity potential on each panel. Bernoulli's equation (3.24) is used to evaluate pressure distribution on the wetted surface of the hull. Thus forces and moments, shown in Figure 1.1 and given in equation (3.1), can be computed in accordance with the pressure distribution. Although the program is able to analyse all motions of a ship, for the main purpose of the research, more attention has been focused on the

variation of vertical force and corresponding restoring moment at certain loading conditions at prescribed forward speeds. Then using equation (4.5) and (4.6) vertical force and restoring moment respectively have been calculated.

The analytical solution of a hemi-sphere and the validated results of the Wigley hull form are compared with the computed results of the CFD code for validation of the code. The comparisons show a good agreement as discussed in Chapter 4. The results of running the CFD code on the generated meshes of the model are discussed in Chapter 4, and in following sections. Here, most concern is focused on the quality of meshes of the model, and proof of meaningful results of the CFD code. Finally, there are some comparisons of the theoretical and the experimental data of the research.

7.2 MESH GENERATION ACCURACY

The mesh generation code has been validated in two parts, firstly visual presentation of the panels fixed on a wetted surface of a body and then properties of the panel as to the mesh's quality. In order to display and aid visual validation of the generated mesh graphically, the robust commercial software Finite Element package ABAQUS was used. ABAQUS has been used only for displaying, random check of the panel numbering, node numbering and rotating the mesh for a visual checking in any directions. The shape and arrangement of the triangular panels shows the ability of the mesh generator consistency to map the prototype. Some examples of the generated meshes have been shown in Chapters 4 and 5. Therefore, the graphical agreements of the generated meshes with bodylines of the prototype have validated the output of the meshing computer code successfully. Then, here more attention has been paid on the panel's properties and quality of mesh.

The displacement of the prototype ship at initial loading condition is selected for comparison. The initial displacement at 7.55m draft is 10080m^3. The pre-processing of the CFD code computes volume of the wetted hull at particular loading conditions for which the mesh is generated. The computed displacement at the initial loading condition has then been used to check the geometrical accuracy of this part of the

meshing code. Therefore volume and wetted area of the generated mesh are examined further here.

Two sets of different numbers of panels, fixed on the wetted surface of the hull, at the design waterline (7.55m) with different inclination angles range (from zero to 10.0°) are selected to consider verification of the mesh geometry. The CFD code has computed displacement for both sets of the meshes at zero speed. It is expected that the computed volumes of two sets of the meshes to be equal with the prototype, but there is a little difference. A discrepancy of the computed volume with the prototype's volume is estimated as an error. Then percentage of the displacement error has been calculated for the computed displacements of the meshes with the initial displacement of the prototype ship from equation (7.1), as shown in Figure 7.1. Although, the discrepancy is small, it is variable. In some part of the plots the difference is not very large, and it seems that the difference may not have a significant effect on the computed results (forces and moments). Where the error between the higher and lower number of panels is small, it may be believed that the results of the CFD code in Chapter 4 and the current Chapter are reliable.

$$error\nabla = \frac{(original\nabla - computed\nabla) \times 100}{Original\nabla} \qquad (7.1)$$

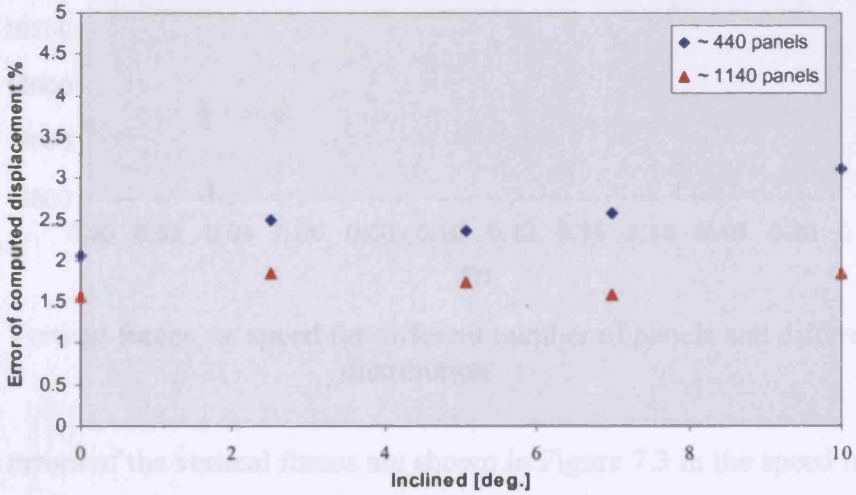

Figure 7.1 Validation in calculated displacement of two meshes at different inclination angles

It has been reported in many CFD research papers, such as Hershey (1975), Hunt (1995) and others, that the mesh has a significant effect on the convergence, accuracy and meaningfulness of the computed result.

Figure 7.1 shows the percentage error of the static status, where speed is zero, of the computed displacement. For better convergence of the results or to reduce the errors, a suitable number of the panels are required. To observe quality of computing results when speed is greater than zero on the generated meshes, some results have been presented in Chapter 4, and are given in this chapter. However, comparisons between the results of the CFD code with the validated results of Kara and Vassalos (2005) have confirmed the accuracy of the CFD code results on the same meshes in Figures 4.21, 4.22 and 4.23.

There is a comparison of computed vertical forces at different speeds for different grid sizes and grid arrangements of the model shown in Figure 7.2, and for the test case hemi-sphere shown in Figure 4.12b.

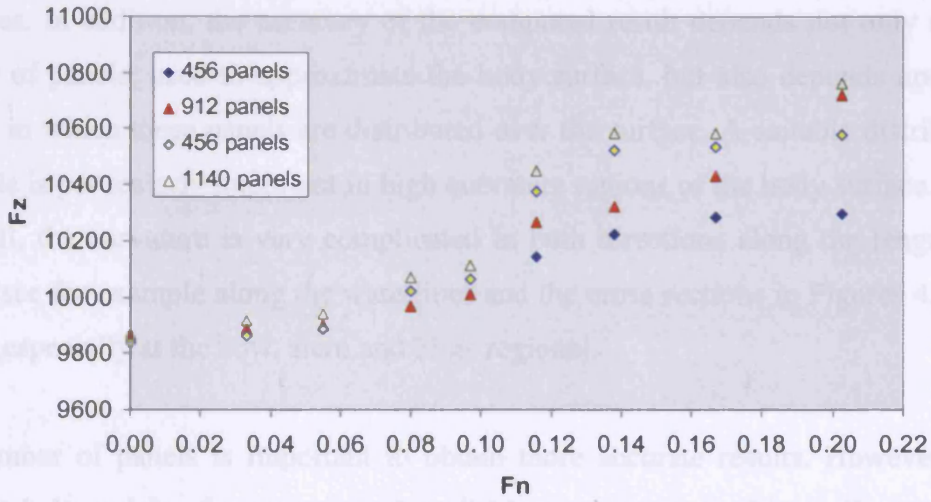

Figure 7.2 Vertical forces vs. speed for different number of panels and different panel distribution

Percentage errors of the vertical forces are shown in Figure 7.3 in the speed ranges for different sets of panel numbers of the model with different arrangements. The result confirming that for low speed range and moderate speed, there is independency on the meshes for the CFD code, but more discrepancies of the result are observed in higher speed range than Fn ≈0.1 for two sets of the meshes.

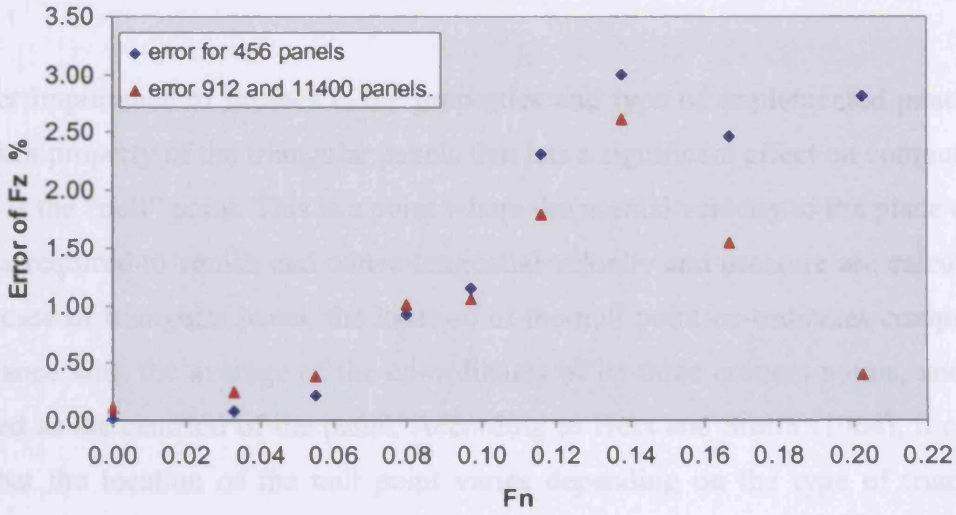

Figure 7.3 Percentage error of vertical force between different number of panels and different panel distribution

The difference between the prototype displacement with the computed displacement and the *Fz* for the model are related to patches (panels). In other words, the panels put together to provide the computational domain for the CFD code are not fine enough to create a smooth hull surface. As the number of the panels increases the difference decreases. In addition, the accuracy of the computed result depends not only on the number of panels, used to approximate the body surface, but also depends upon the manner in which these panels are distributed over the surface. A suitable distribution of panels is particularly important in high curvature regions of the body surface. For a ship hull, the curvature is very complicated in both directions along the length and height (see for example along the waterlines and the cross sections in Figures 4.2, 4.3 and 4.4 especially at the bow, stern and bilge regions).

The number of panels is important to obtain more accurate results. However, this must be balanced by the capacity of available computing machines. Comparisons between the results of the Wigley hull form from the CFD code with the validated numerical results of Kara and Vassalos (2005) in Figures 4.10, 4.11 and 4.12, and the results for the hemi-sphere with the analytical solution in Figures 4.12a and 4.12b have shown a good agreement with very small difference for a large number of panels. Therefore, as with most CFD applications, it is necessary to use as many panels as allowed by the program and the available computing time to obtain more likely meaningful results.

Another importance of meshes is the properties and type of implemented panel. An important property of the triangular panels that has a significant effect on computation results is the "null" point. This is a point where the normal velocity to the plane of the panel is required to vanish and where tangential velocity and pressure are calculated. In the case of triangular panel, the location of the null point co-ordinates compute in accordance with the average of the co-ordinates of its three corners points, and it is assumed as the centriod of the panel. According to Hess and Smith (1964), it can be seen that the location of the null point varies depending on the type of triangular panels with a small base or large base. Then the null point and the centroid are thus not particularly close together on triangular panels. They of course coincide on an equilateral triangle (base to height ratio of 1.15) as shown in Figure 7.4 b.

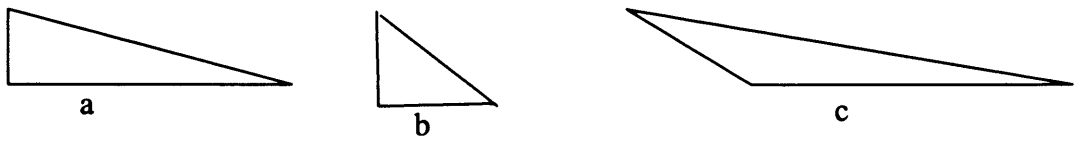

Figure 7.4 Three different examples of triangular types

In accordance with these very important issues, particular attention must be paid to base to height ratio of triangular panels, aspect ratio, and density of the panels in curvature regions for modification of the mesh generation computer code.

7.3 DETERMINING HYDRODYNAMICS ACCURACY

It is valuable to consider the accuracy of the theoretical results in respect of dynamic characteristics such as pressure distribution, resultant forces, and moments. Some dynamics characteristics are very difficult to compute accurately, particularly due to variable speed. The more important dynamics characteristics are discussed as follows.

At zero speed, stability is of course governed entirely by hydrostatics. As the Froude number increases, the hydrodynamic effects come into play and are considered to

comprise two separate components, one due to the *hull wave* and the other due to *hydrodynamic pressure* distributions on the wetted surface of the hull.

The hull wave causes more of the vessel to be supported at the bow and the stern and less along the mid-ship. Then redistribution of the buoyancy can lead to a reduction in the metacentric height, consequential in a reduction of stability of the hull operating relatively at, or slightly above, low speed. Hydrodynamic bottom pressure effects can also come into play under this condition.

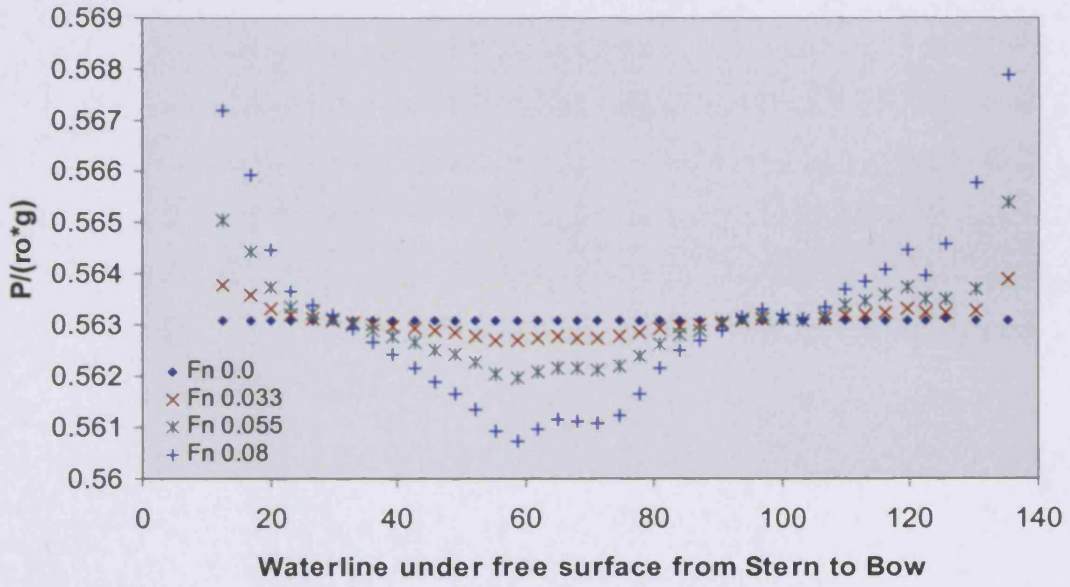

Figure 7.5 Computed pressures on the centre of panels along the waterline below the free surface for low and moderate speed

The experimental investigations have shown the reduction of transverse stability of the model in some towing cases for the model with adequate stability at rest. For example the model has demonstrated a very small heeling angle in Figures 6.6, 6.7 and 6.8 at different speed. It can be found for other loading conditions in Chapter 6.

The pressure distributions on the bottom of the model have revealed that the behaviour was due to variation of pressure developed along the wetted area of the hull for the given speed, as the computed results have shown the same phenomena. Beyond the low speed range the results show that the influence of bottom pressures tends to dominate.

The pressure distribution on each panel has been evaluated at different inclination angles and for a range of speeds as presented as forces in Section 4.5. The resultant vertical force (*Fz*) is chosen for further discussion here. It is discussed that at zero speed and no inclination angle it is expected that the computed *Fz* would be equal for both sets of meshes. In addition, the computed *Fz*, for these cases, must be equal to the prototype ship weight or the displacement of the prototype. Figure 7.6 shows the computed displacements for the two sets of the meshes at the draft 7.55m, and for the range of inclination angles, at zero speed. Differences between the computed displacements of the model with the initial displacement of the prototype are very small for both sets of the meshes at different inclination angle. The results of both sets of panels in the figure show underestimate of the *Fz* for the range of inclination angle, however the computed *Fz* shows improvement for high number of panel than the lower number set of meshes.

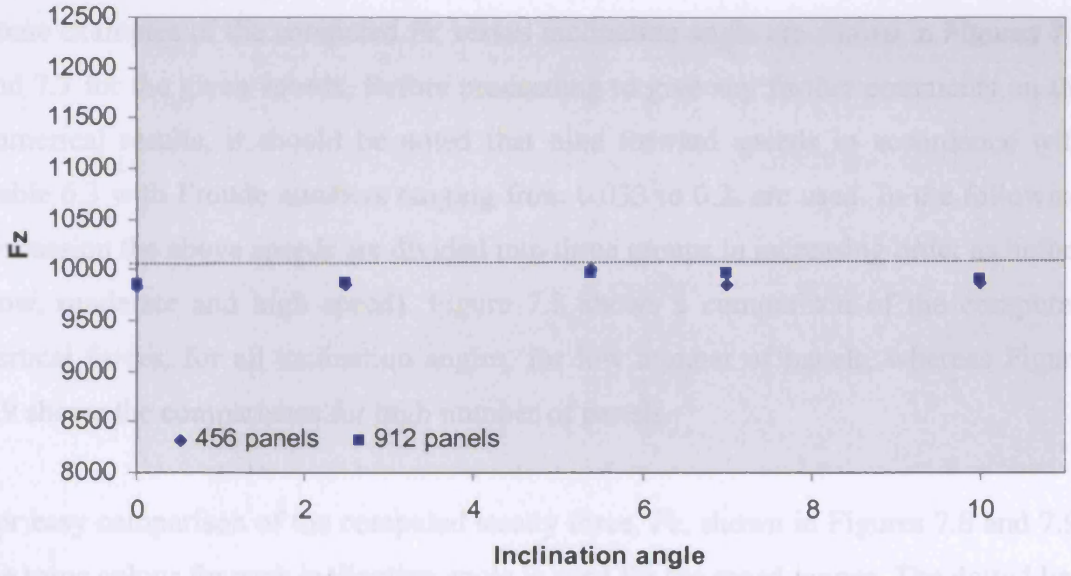

Figure 7.6 Variation of vertical forces vs. inclination angle for zero speed

The vertical forces, *Fz*, are computed for two grid sizes of pre-inclined angle 7°. Figure 7.7 shows the *Fz* variation versus speed range. The figure shows convergence of the results obtained at this loading condition for low and high number of panels fixed on the hull. Higher number of panels of the plot shows oscillation of the *Fz* in the speed range and it is underestimated, but with a small improvement of the *Fz* for higher Fn.

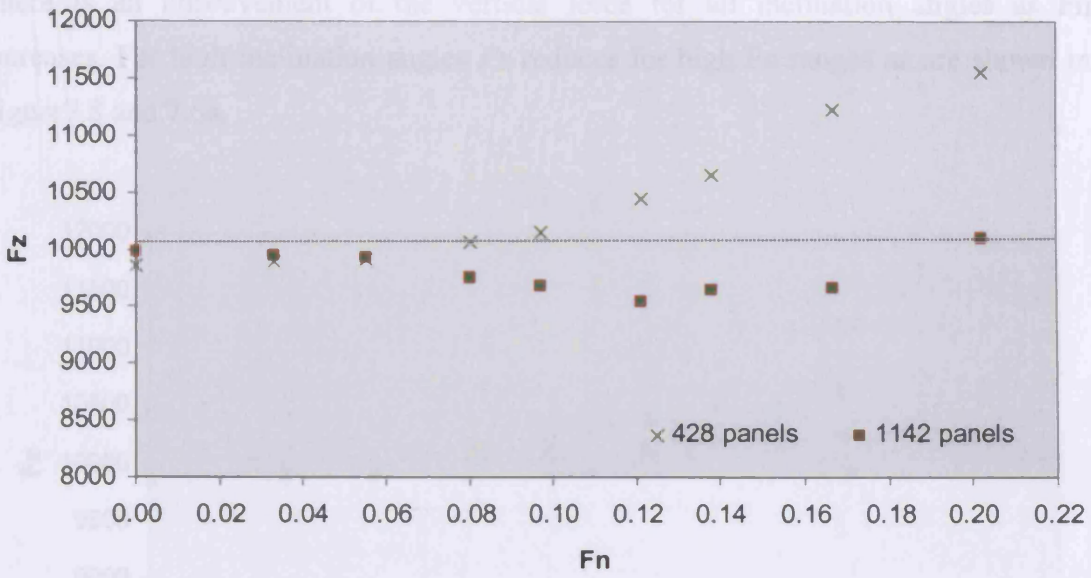

Figure 7.7 Variation of vertical forces vs. speed for 7° inclination angle

Some examples of the computed *Fz* versus inclination angle are shown in Figures 7.6 and 7.7 for the given speeds. Before proceeding to give any further comments on the numerical results, it should be noted that nine forward speeds in accordance with Table 6.3 with Froude numbers ranging from 0.033 to 0.2, are used. In the following discussion the above speeds are divided into three groups in increasing order as before (low, moderate and high speed). Figure 7.8 shows a comparison of the computed vertical forces, for all inclination angles, for low number of panels, whereas Figure 7.9 shows the comparisons for high number of panels.

For easy comparison of the computed steady force, *Fz*, shown in Figures 7.8 and 7.9, the same colour for each inclination angle is used for the speed ranges. The dotted line shows the prototype's displacement in the figures.

Comparison of forces in Figure 7.8 and / or 7.8a shows that as Fn increases the computed *Fz* increases, and inclination angle has an important role here. Differences of the computed *Fz* are very small for low and moderate speeds, but increase for high speed range. Computing meaningful result of the mathematical formulae of the theoretical method is not an easy task for variable speed, and it is sensitive to the mesh. A suitable mesh size is required for more accurate and meaningful results.

There is an improvement of the vertical force for all inclination angles as Fn increases. For high inclination angles *Fz* reduces for high Fn ranges as are shown in Figure7.8 and 7.8a.

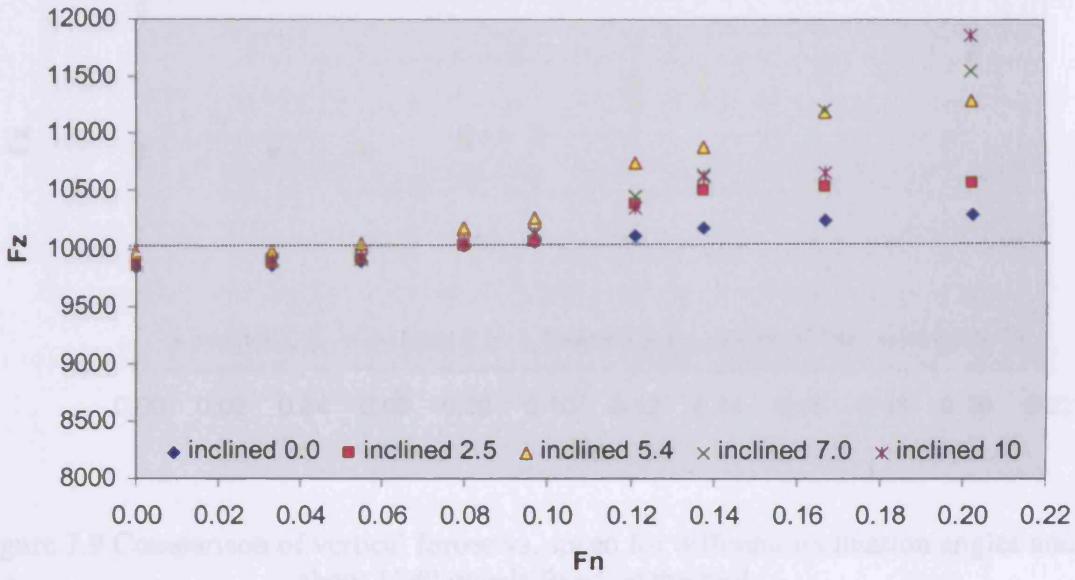

Figure 7.8 Comparison of vertical forces vs. speed for different inclination angles and about 456 panels fixed on the hull

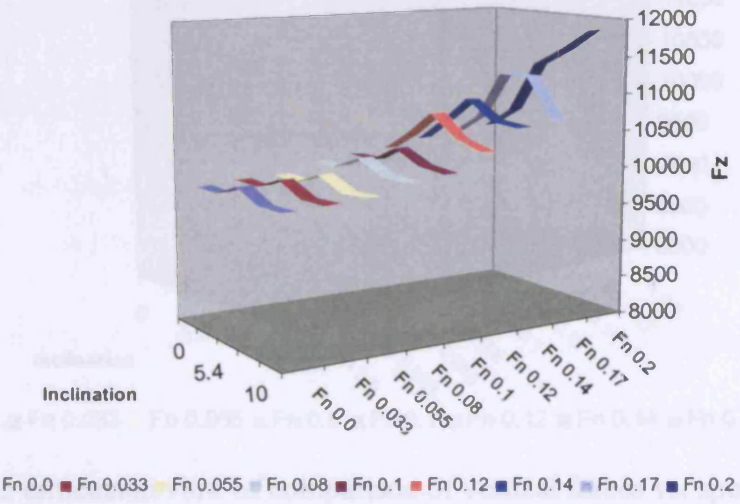

Figure 7.8a 3-dimension view of comparison of vertical forces vs. speed for different inclination angles and about 456 panels fixed on the hull

Figure 7.9 shows, for high number of panels, good convergence of the *Fz* for low inclination angle. The computed vertical forces, *Fz*, show significant drops for high

inclination angle in the moderate speed range and above. Consequently, showing that recovery of the *Fz* with speed depends critically on inclination angle range.

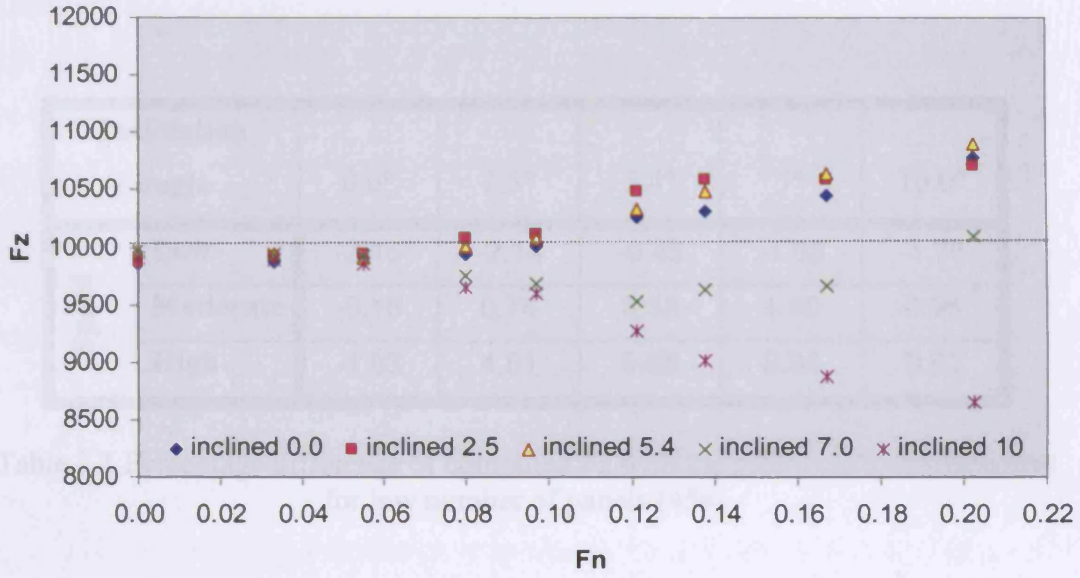

Figure 7.9 Comparison of vertical forces vs. speed for different inclination angles and about 1140 panels fixed on the hull

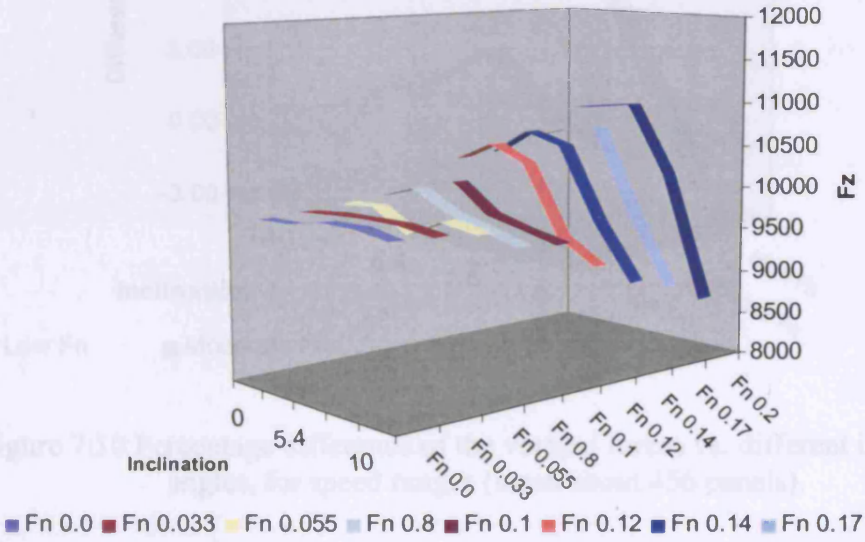

Figure 7.9a 3 dimension view of comparison of vertical forces vs. speed for different inclination angles and about 1140 panels fixed on the hull

The results of computed *Fz* are compared in Figures 7.8 and 7.9 for two sets of the meshes. A percentage difference of the computed results, *Fz*, with the prototype ship's displacement calculated is presented in Table 7.1 for the lower panel number,

and is shows in Figure 7.10. The positive sign shows increase and negative shows decrease of the computed *Fz* against the prototype's displacement at prescribed Fn.

Inclination angle		0.0°	2.5°	5.4°	7°	10.0°
Speed	Low	-2.16	-2.14	-0.43	-1.98	-1.76
	Moderate	-0.15	0.74	3.38	1.40	0.96
	High	-1.63	4.61	9.85	9.94	9.62

Table 7.1 Percentage difference of computed *Fz* with the prototype's displacement for low number of panels (456)

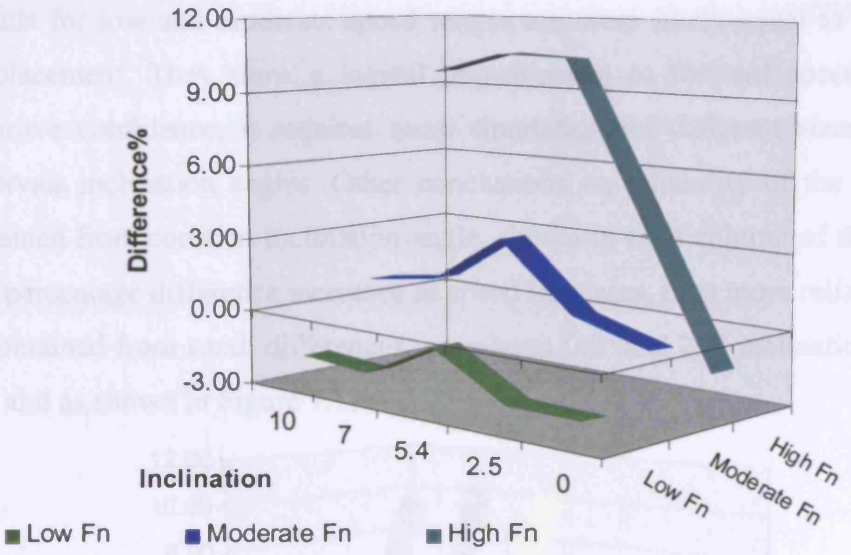

Figure 7.10 Percentage difference of the vertical forces vs. different inclination angles, for speed ranges (mesh about 456 panels).

Referring to Table 7.1; the percentage difference is not very large for low and moderate speed ranges, for all inclination angles. The computed *Fz* is more or less constant as inclination angle increases for the low speed range. Its value is underestimated by about 2% for the low speed range, which should as a minimum be equal to the prototype's displacement or a little above it.

For moderate speed range, the computed *Fz* oscillates about the prototype's displacement. The *Fz* increases compared with the low Fn results, as is expected. It decreases when inclination angle increases with the same trend as for the low Fn. A large difference is shown for the high speed range with the higher inclination angle. The story is different, as 3rd row of the table shows that percentage difference of the computed *Fz* with the prototype's displacement decreases for zero inclination angle, but the trend of the curve for high Fn is still the same as the other two. However its difference is large for all inclination angles. As discussed before it is the weakness of meshing particularly for high inclination angle, which is revealed in the high speed range.

One may consider the results so far that the results for low and moderate speed ranges may be accepted as preliminary results of the CFD code. This is because the results for low and moderate speed ranges are more likely equal to the prototype's displacement. They show a logical improvement as forward speed increases. To improve confidence, it requires more simulation for different sizes of mesh, and intervals inclination angles. Other conclusions on reliability of the results may be obtained from constant inclination angle, shown in each column of the table. Where the percentage difference increases as speed increases, then more reliable results may be obtained from small differences, as column 0.0° and 2.5° inclinations in the Table 7.1 and as shown in Figure 7.11.

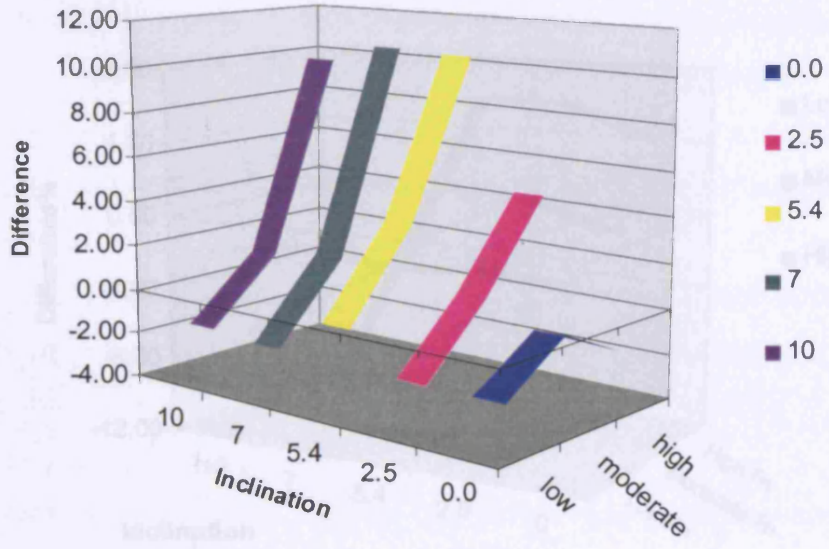

Figure 7.11 Percentage difference of the vertical forces vs. speed ranges, for different inclination angles (mesh about 456 panels).

A similar summary as for Table 7.1 has been made for the results of the high number of panels, in Figure 7.9. The percentage difference of the computed *Fz* with the displacement of the prototype is presented in Table 7.2 and Figure 7.12 for high number of panels. The difference for the low speed range in the table is very similar to the results in Table 7.1 for all inclination angle ranges. However, there is small improvement of the *Fz* in the speed ranges, in Table 7.2, when compared with the same inclination angles in Table 7.1. This feature shows the mesh may be sufficient for computed results for the low speed range. In addition, the effect of increasing speed clearly can be shown by the percentage differences of the computed *Fz* with the prototype's displacement which are greater than the equivalent data in Table 7.1. However, the results for high inclination angle and / or high speed range show the mesh may not sufficient for these conditions (high speed and inclination ranges).

Inclination angle		0.0°	2.5°	5.4°	7°	10.0°
Speed	Low	-2.01	-1.70	-2.11	-1.34	-1.89
	Moderate	-0.05	1.49	-0.54	-4.19	-5.71
	High	4.31	5.92	5.96	-2.65	-11.20

Table 7.2 Percentage difference of the computed *Fz* with the prototype's displacement for high number of panels (1140)

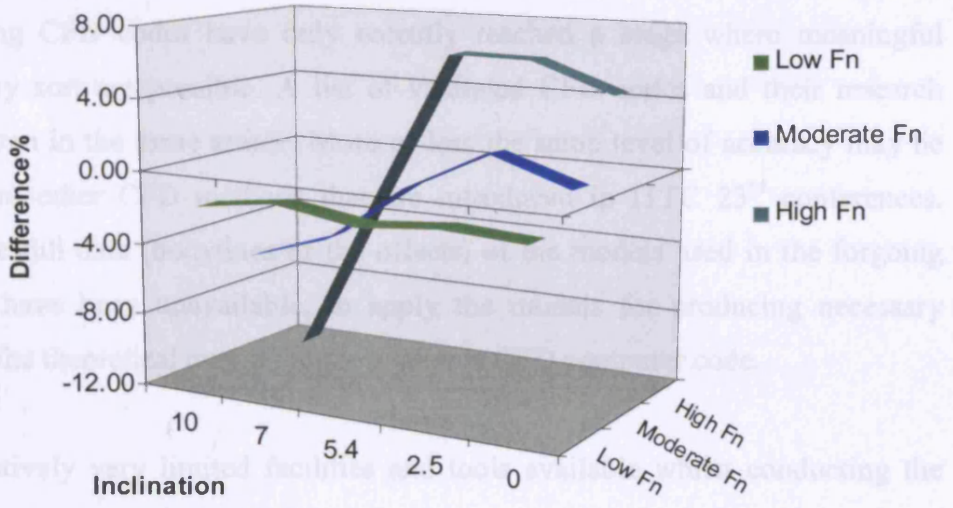

Figure 7.12 Percentage difference of the vertical forces vs. different inclination angles, for speed ranges (mesh about 1140 panels).

Comparison of the data in Tables 7.1 and 7.2 confirms that the computed results for the low and the moderate speed ranges are reliable. The computed results of very low inclination angle for the high speed range can be accepted too. One important feature of the results in Figure 7.10 for the speed range is oscillation of the results about the prototype ship displacement, which is usually expected for CFD simulation.

According to the computed results and the cost of computation, there are two major problems associated with the numerical method that must be considered in order to obtain more meaningful and accurate results. These are modification of the mesh generation code and the integral solution of the free surface, which affect the computation of the pressure distributed on the wetted hull area in particular near to the free surface. More detail is given in Section 8.2.

7.4 DISCUSSION OF THEORY AND EXPERIMENT APPLIED METHODS

After validation of the experimental data in Chapter 6, and proving the theoretical approach in Chapter 4 and this chapter, the current section discusses comparison between the theoretical results and experimental data of the model.

The accuracy of towing tank data is higher than accuracy of any existing CFD methods according to Larsson (1998). He has shown that research centres that have been applying CFD codes have only recently reached a stage where meaningful results of any sort are possible. A list of validated CFD codes and their research centres is given in the same article. More or less the same level of accuracy may be obtained from other CFD methods that are introduced in ITTC 23rd conferences. However, the full data (bodylines or the offsets) of the models used in the forgoing conferences have been unavailable, to apply the models for producing necessary results from the theoretical method in the available CFD computer code.

Due to relatively very limited facilities and tools available whilst conducting the research, there was not enough opportunity to test a wide range of operational conditions of the model such as speed, loading, and inclination angle, or to find an

alternative bodyline of a high speed ship with a suitable experimental data of the ship for comparison and validation purposes of the CFD, and the meshing code. Although, there are some experimental and numerical results in ITTC 23rd the greatest problem was unavailability of the offsets or whole bodylines of the model except for the Wigley hull form that has been used for validation of the CFD. Therefore, for the discussion the validated CFD results and the experimental data of the model of the current research are used. The presented results are chosen from both approaches, for nearly the same forward speeds, the same loading and inclination angle conditions as those discussed in Chapter 6, with reference to information of Table 6.1, 6.2, and 6.3. Figure 6.42 represents a summary of the chosen experimental data for the model scaled at 1: 100.

The theoretical results show a complicated variation as also exhibited by the model tests data. A better understanding of these variations would result from the availability of a significantly greater number of computed results. Additionally model tests for intermediate heel angle positions are required.

A comparison of the computed results for low number of panels (coarse mesh) and high number of panels (fine mesh) with the experimental data for four inclination angles is shown in Figures 7.13 to 7.16 for 2.5°, 5.4°, 7.0° and 10.0° inclination angles respectively. For each inclination angle there are two plots one showing the GM versus Fn, and the other comparing the GMs obtained from computation and experiment at constant forward speed. The minimum GM and the initial GM of the plots show the minimum level of accepted GM of most standards, and the evaluated static GM of the model. The other data show variation of the GM for the given speed in the same Fn range from 0.034 to 0.168 respectively. In the plot GM versus Fn, the Fn ranges from 0 to 8 showing the same information as shown on the lower diagram.

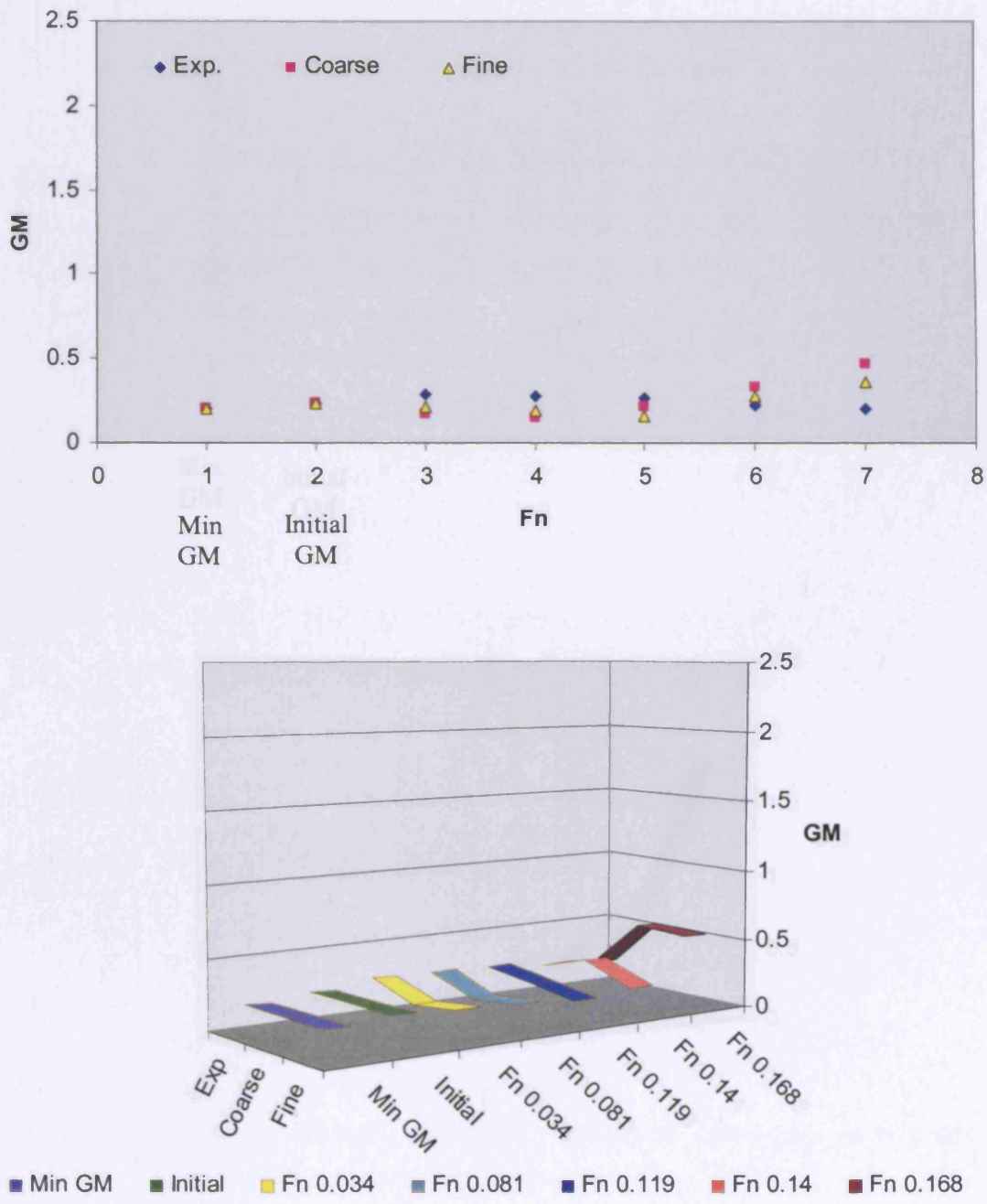

Figure 7.13 Comparison between experimental with theoretical results of GM variation in terms of forward speed ranges at 2.5° inclination angle

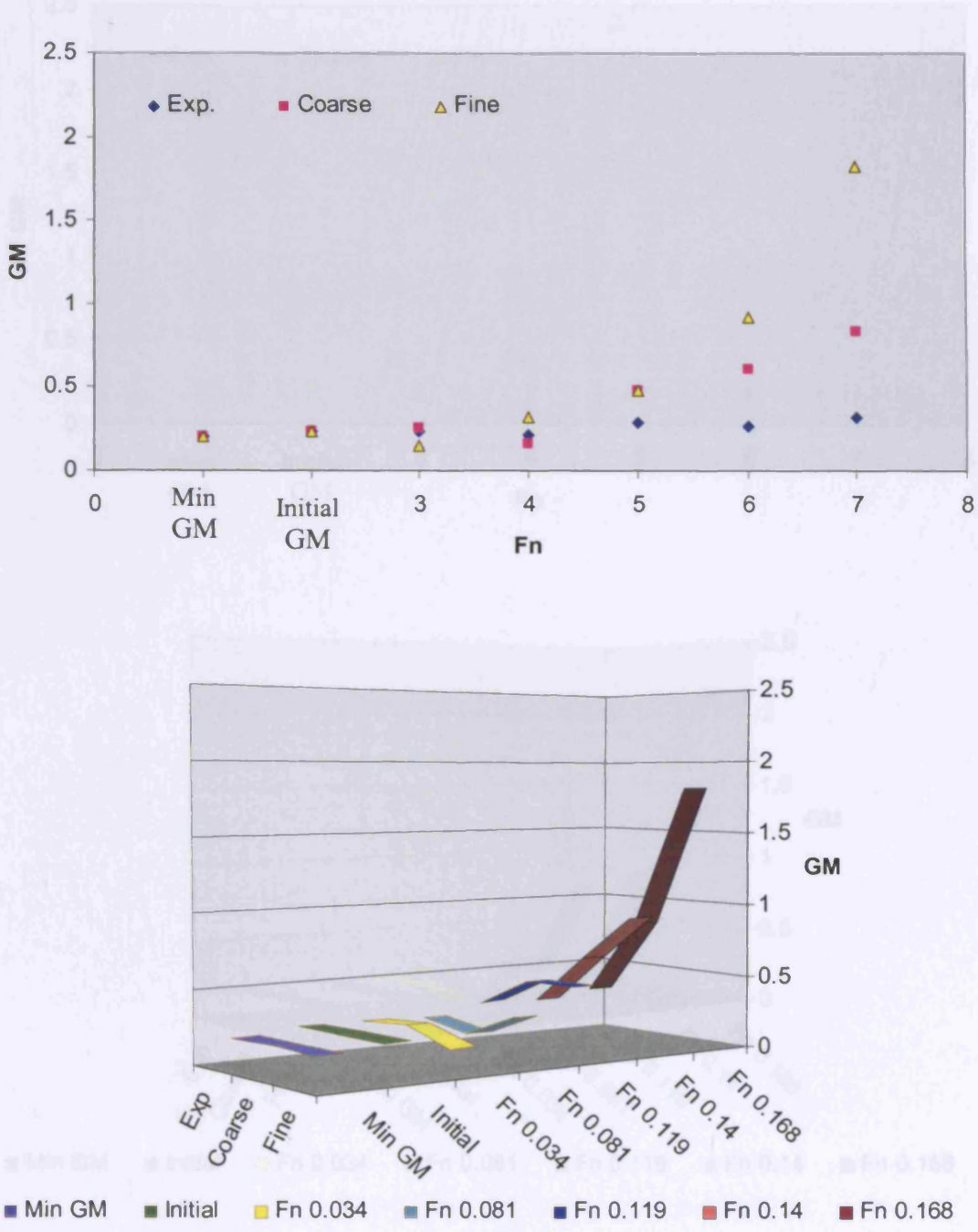

Figure 7.14 Comparison between experimental with theoretical results of GM variation in terms of forward speed ranges at 5.4° inclination angle

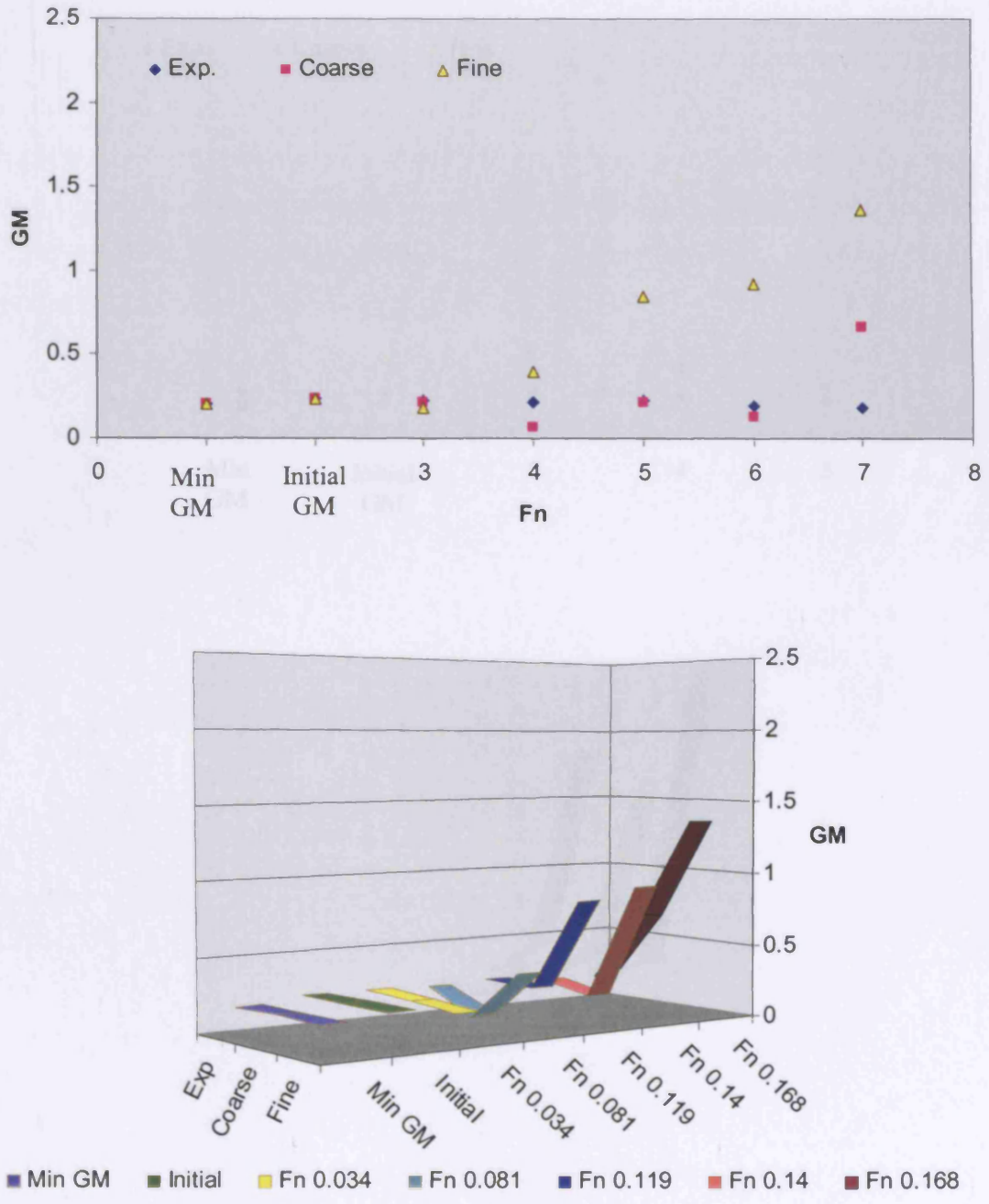

Figure 7.15 Comparison between experimental with theoretical results of GM variation in terms of forward speed ranges at 7.0° inclination angle

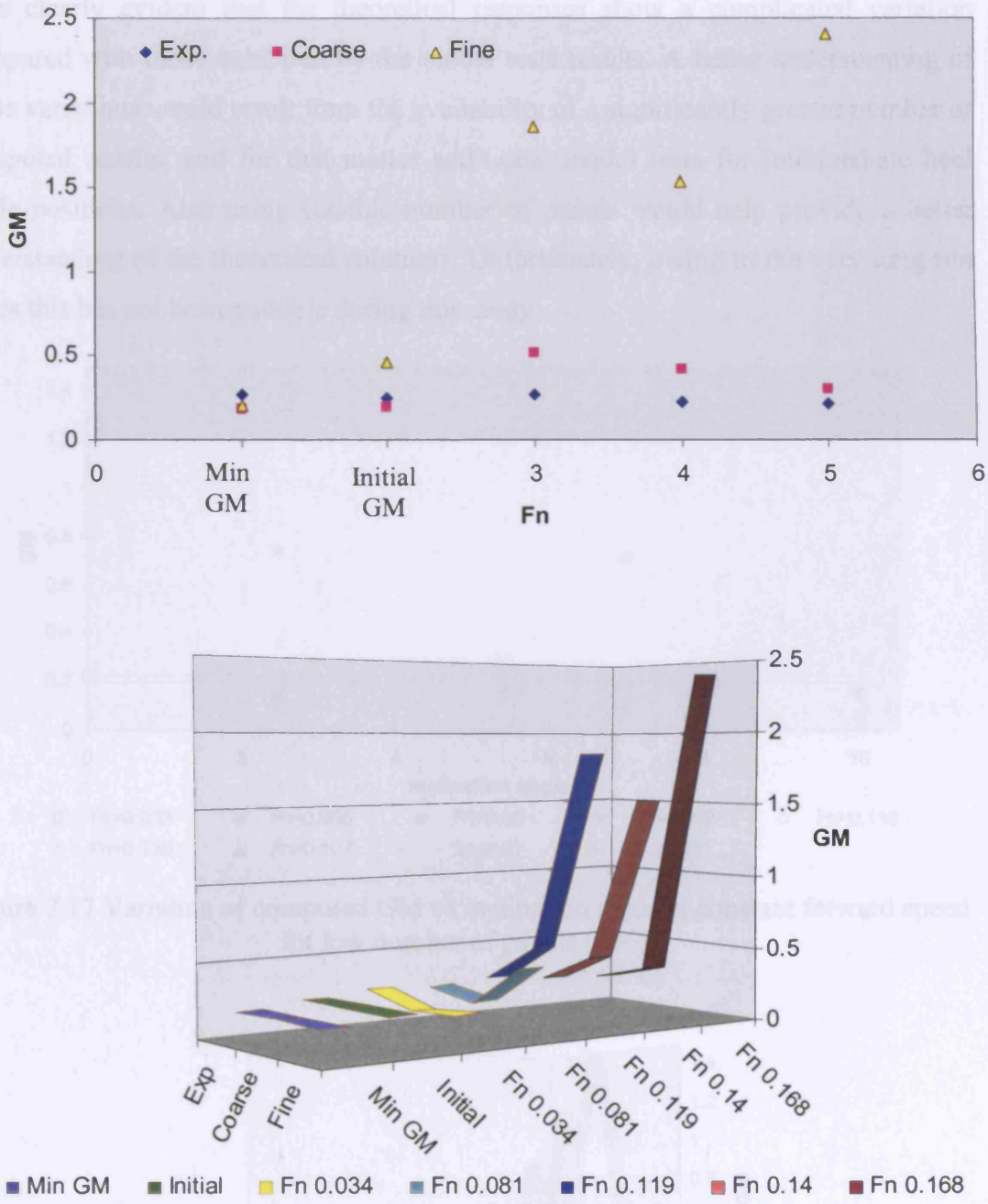

Figure 7.16 Comparison between experimental with theoretical results of GM variation in terms of forward speed ranges at 10.0° inclination angle

It is clearly evident that the theoretical responses show a complicated variation compared with those exhibited by the model tests results. A better understanding of these variations would result from the availability of a significantly greater number of computed results, and for that matter additional model tests for intermediate heel angle positions. Also using suitable number of panels would help provide a better understanding of the theoretical solutions. Unfortunately, owing to the very long run times this has not been possible during this study.

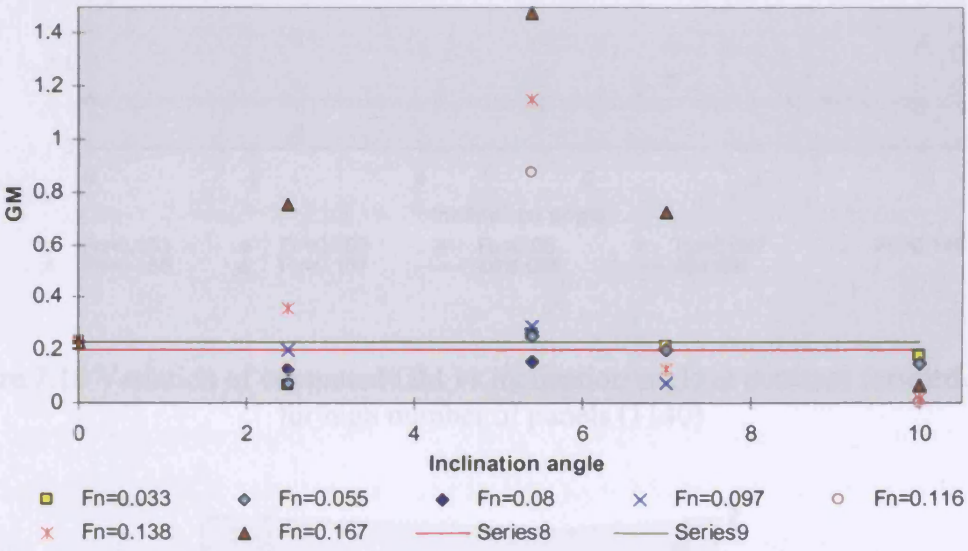

Figure 7.17 Variation of computed GM vs inclination angle at constant forward speed for low number of panels (456)

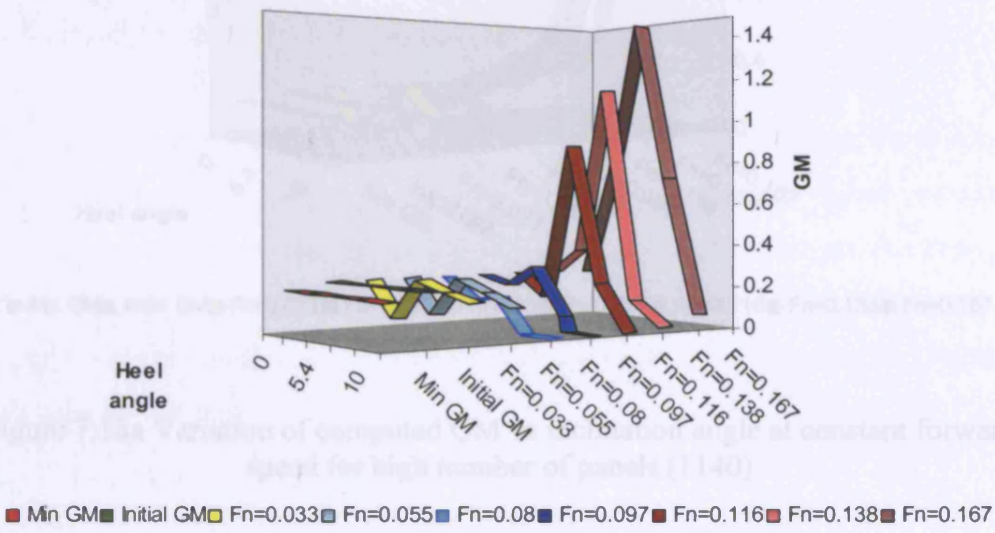

Figure 7.17a Variation of computed GM vs inclination angle at constant forward speed for low number of panels (456)

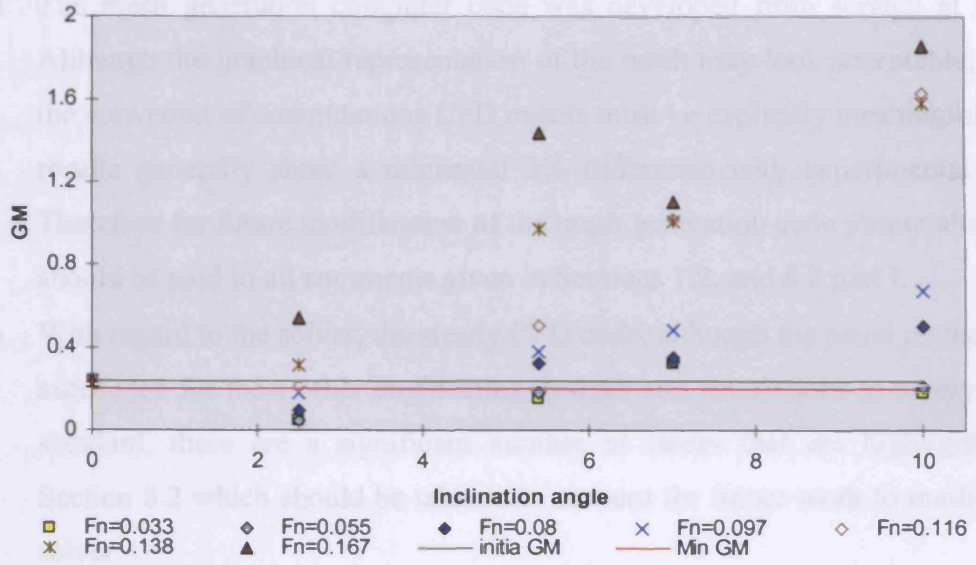

Figure 7.18 Variation of computed GM vs inclination angle at constant forward speed for high number of panels (1140)

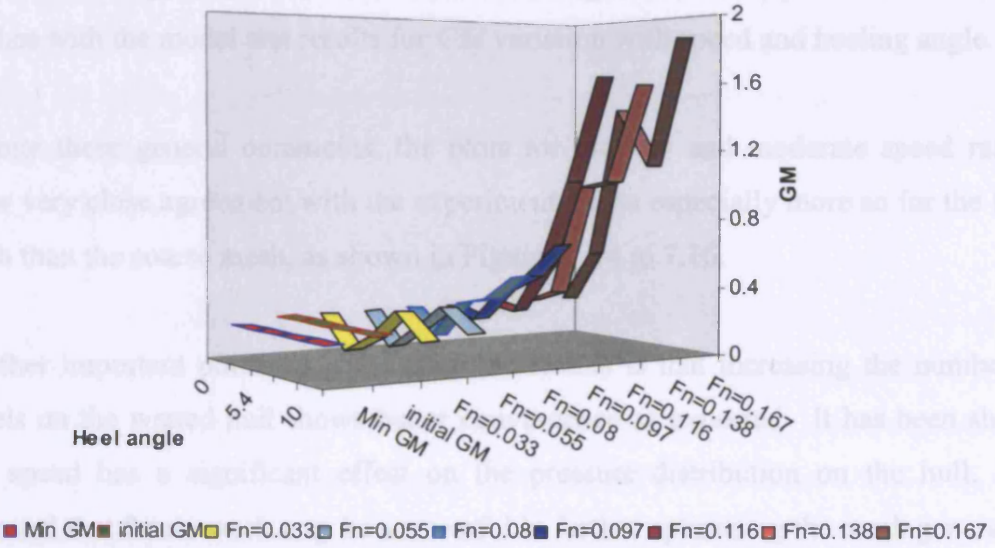

Figure 7.18a Variation of computed GM vs inclination angle at constant forward speed for high number of panels (1140)

The present research that is currently at an early stage has not achieved the best results in theoretical application method. This is because:

- The mesh generation computer code was developed from scratch at UCL. Although the graphical representation of the mesh may look acceptable, from the viewpoint of computations CFD results must be explicitly meaningful. The results generally show a minimum 2% difference with experimental data. Therefore for future modification of the mesh generation code proper attention should be paid to all comments given in Sections 7.2, and 8.2 part I.
- With regard to the solver, the steady CFD code, although the panel method has succeeded for most other engineering designs and simulations to a very good standard, there are a significant number of issues that are highlighted in Section 8.2 which should be taken into account for future work to modify the solver.

Figures 7.12 and 7.13 show the theoretical *GM* results of the prototype for small and high number of panels respectively. Evidently in general there is no close matching of the theoretical (CFD) solutions for either the high number of panels or the coarse meshes with the model test results for *GM* variation with speed and heeling angle.

Despite these general comments, the plots for the low and moderate speed ranges show very close agreement with the experimental data especially more so for the finer mesh than the coarse mesh, as shown in Figures 7.14 to 7.16.

Another important point observed from the results is that increasing the number of panels on the wetted hull shows better convergence as expected. It has been shown that speed has a significant effect on the pressure distribution on the hull. It is expected that future work may be successful in further optimising the mesh generation code, and with the availability of faster processors that more accurate and numerous results may be obtained.

8. CONCLUSIONS AND RECOMMENDATIONS

Increasing demands for speed in marine transports have expanded the interest in vessels having some part of their weight supported by dynamic forces. Hydrodynamic lift force increases as speed increases. The resulting lifted hull has a reduced wetted surface leading to some changes on stabilities characteristic of the ship in a seaway. Additionally, during the study, it has been shown that unbalanced pressure distributed on the wetted area of the hull leads the ship to heel and / or trim to one side, even for the low speed range. It may increase with increasing speed or may decrease. For a better understanding of the situation a series of experiments has been conducted in the towing tank at UCL. The experimental data are presented in Chapters 6 and 7 in detail.

The results of theoretical method, that are efforts of the CFD and the mesh generation codes, have been obtained only for one set of offsets (bodylines) that was available to the research. The offsets were derived from a scaled drawing, Figure 5.1, which may be one source of cause of difference between the experimental data and theoretical results. However, suitability of the numerical modelling of the research has been proved by comparison between the CFD results with the validated results in Chapters 4, 5 and 7 in details.

The computed results of the test case (hemi-sphere) and the Wigley hull have shown good agreement with analytical and validated results as shown in Chapters 4 and 7. The meshing procedure, for the purpose of the research, has been discussed in Chapter 5. The mesh code is able to map the triangular panels on the wetted surface of a ship according to loading conditions such as draft and inclination angle. Although, modification is required in some parts as discussed in section 8.1 the results of the meshing are unique.

Specific judgement on the CFD technique requires more sets of bodylines for simulation. Although the preliminary results of theoretical applied method are not yet promising it may improve with modification of the mesh generation and the panel

method as the solver of the steady CFD code. On the other hand, the experimental data has shown very clearly significant effect of speed on stability. Comparison between the results of both applied methods, theoretical and experimental, of the research may be classified as follows:

1. Bottom pressures distributed on the wetted surface of the ship's hull support the weight of the ship. As Froude number increases hydrodynamic effects cause redistribution of the pressure redistributing the buoyancy that can lead to a reduction or raising in the metacentric height, resulting in a decrease or increase of stability of the hull operating relatively at, or slightly above, low speed.
2. Bottom pressures on the wetted area of ships mostly are not balanced in respect to the centre-plane and / or to mid-ship section or both. This causes a ship to trim and / or steady inclination angle or a combination of these. As has been shown the angle will be increase or decrease depending on a hull form and speed range.
3. Generally, for small steady inclination low and moderate speed may be a safe speed range for navigation. High speed range for any inclined angle transversely or longitudinally is better avoided.

Considering some points arising from this work the following should be noted:

A. The experiments reported herein are denoted as low, medium, and high speed. This is in the context of the speeds achieved using the available test tank and capability of the model. In the wider context of speeds which today's vessels may in general achieve, these are at the low end of the range.
B. It should be noted that the value of GM used in the model tests was chosen to be very small (2.35mm) so that a significant response could be detected. Whilst the value is small it has been accurately determined from an inclining experiment in which it was possible to accurately control the values of mass and linear dimension to achieve the GM to the accuracy indicated.
C. Confidence in the results of the experiments conducted is high since although only data for single runs for the method using potentiometers

has been presented herein, each of these tests was performed three times by this method with equivalent results. Similar results were also obtained by the strain-gauged transducer method, and also by optical tracking.

D. Under some experimental conditions the model which was forced to heel to one side performed a rolling motion with very small amplitude. For a constant forward speed it is expected that the heeling angle may reach a constant value. However, the experimental data show very small oscillation of the heeling angle at a given constant forward speed. Such oscillatory motion may decay to zero in a longer towing tank. It is possible that the source of the oscillations may be related to the bow forming wave or (less likely) some external effect such as vibrations from the carriage's wheels. For a very low forward speed it is expected the bow forming wave should be negligible. However, very small amplitudes were detected. It would be beneficial if these effects could be investigated in more detail in some future research. Such future experimental research would of course benefit from larger testing facilities in which steady state conditions could be established for longer runs, and the decay (or otherwise) of oscillatory effects be observed better. It would be more representative of a vessel in a seaway if future experiments were conducted with a self-propelled model. If this were to be done it would be beneficial to use a light-tracking method to measure the motions behaviour.

E. The comparison between the results of other researchers with the results of the UCL-ASD code on the validated meshes of the Wigley hull from SSRC showed fairly consistent agreement across a wide range of Froude numbers. According to Figures 4.10 and 4.21, the wave making resistance for the Wigley hull form in the low speed range is linear (with no peaks or troughs). For the UCL-ASD analysis this was not so for the real ship shape as shown in Figures 4.13 and 4.17 (which are for low Froude numbers). This suggests that more attention should be paid to modification of the mesh generation code.

F. For the validation of the code only two sets of the Wigley hull form meshes were available, which were provided by the SSCR. It would be

beneficial in future research to extend this analysis to examine the effect of increasing the number of panels to approach an optimum.

G. Waves have significant effect on the ships stability. With wave crests at the bow and aft regions and a trough at the midship part of the hull, a reduction in stability occurs. As pressures are distributed on the wetted hull and varied with forward speed in calm water the generated surface wave decreases the ship stability. The variations of pressure distributions along the hull near to the waterline at different forward speeds are compared in Figure 7.5. High pressures are found at the ends and low pressures distributed in the midship. The effect is more pronounced for high Fn.

H. On page 181.

8.1 FUTURE WORK

There is considerable opportunity to extend the theoretical approach of research pursued herein in many aspects. In particular:

I. The mesh generation may be modified:
   - To control the number of panels along the waterline as well as in the draft direction.
   - To apply an appropriate method for controlling size, aspect ratio, and skewness of the triangular panels.
   - To control sufficiently high resolution of the mesh on the curved part of the hull.

II. The panel method is applied as a solver in the CFD code. As it has proven to be successful in aerodynamics and hydrodynamics applications. Modification to this application should include:
   - Improve the performance of the present CFD code for a modified mesh generation code
   - Modify the Green's function solution to achieve the two important goals, of accuracy of results, and reduced CPU time
   - Examine higher order methods.
   - Testing the idea of the research with other validated CFD codes available in other research centres.

III. Graphical output improvements, as a part of post-processing will lead to better interpretation of results.

In the theoretical methodology of the research a simple form of stability analysed to reach the actual stability evaluation it is required to add the effect of trim in the mesh generation code, and not only sailing in calm water option but also adding travelling in waves option in the solver.

Performance of a new design and / or modification of an existing ship may be checked with available and validated CFD codes, but still they can not replace towing tank. Therefore model testing facilities are needed to check performances of ships. Consequently the current experimental approach may be used to provide more benchmarks for validation of the present theoretical approach. It is suggested that different ships' hulls, regarding size and block coefficient, may be conducted in longer tanks, with more advanced facilities.

To improve stability evaluation, a modified version of the theoretical approach of the current research may lead to a new method for preliminary stability assessments of a ship in a seaway.

8.2 CONCLUSIONS

The research presented describes effects of forward speed on stability of ships, theoretically and experimentally. A new application of the panel method has been coded to evaluate stability of a ship in a seaway, and a novelty is the mesh generation computer code developed for this purpose. The study also includes unique experimental results. To sum up the finding of the research the following conclusion may be drawn:

1. Although rules and regulations may guarantee a level of safety in some sea states and loading conditions, the level of safety must be improved in accordance with demands of transportation (high speed) currently and in the future.

2. Nowadays, a very important factor of marine transportation is speed, especially according to the results of the current research; it is shown that speed plays a significant role on stability of a ship in any circumstance.
3. Due to robust computer available on board of ships and design offices, then a modified version of the theoretical method of the research may be used as an alternative. Designers and operators need more accurate and rapid methods to evaluate ship stability, which take into account speed of the ship.
4. Distribution of pressure on the wetted surface of the hull is different for a moving ship compared with its stationary condition. Generally the distribution of the pressure is not symmetric.
5. The panel method has been applied to compute pressure distribution on the wetted surface of a ship's hull, due to forward speed of the ship.
6. The unbalanced pressure distribution on the wetted hull surface causes a heeling angle. It will generally change in a seaway due to variation of either speed or wetted hull surface and its appendages, including angle of rudder. Consequently, it introduces rolling motion even in calm water, and the rolling may develop as shown from the experimental data in Figure 6.42.
7. Another important result is that in order to recover stability (restoring moment) in some cases it may be possible to do so by increasing the speed of the ship. However due to limitations of power of the ship this cannot be done in all conditions. Additionally in some cases, as the results here have shown, increasing of the speed may have a detrimental effect causing an increase in inclination angle, and increased risk of capsizing. Then loss of stability is a function of speed and any cause of developing unbalanced pressure distributed on the wetted hull surface.
8. Refer to Figure 6.42, it is a summary of the experimental data, showing dangerous conditions of the model at different speeds and loading conditions. Such plots may in future be provided as part of useful stability documentation of a ship during its design stage and finally after trials. It would provide an indication of the minimum improvement for operators to complete a safe voyage.
9. The CFD code results show the capability the applied method, as the computed results of the Wigley hull form have proved it, and also the comparison between the CFD results and the experimental data of the

container model supported. The most important issues of results of the method show that the calculations are very sensitive to the panels.

10. It is worthwhile to modify the mesh generation code, as the most significant results show the differences between the validated and the computed results are raised by weakness of the panels (aspect ratio, skew, sizing and density of the triangular panels).
11. The chosen Green's function solution is very complicated and very expensive from the point of computing. It may be possible to avoid and replace this with alternatives, which may offer better accuracy and cheaper calculation time.

It is hoped that these ideas will contribute to developing a practical improved method to assess stability and thereby improve safety in all conditions, in particular where speed is an objective. In the longer term it may be possible to replace the towing tank which is costly and time consuming specially for optimisation or as a minimum to the reduce cost of experimental tests of a new design.

H. Threshold of small heeling angle depends on a ship body lines. It becomes very important for inclination test. According to the body lines of the model, which have been shown on Figure 4.2, most part of the hull form is the rectangular shape. Then the threshold is about 15 degree as it has shown on Figure 6.2. above this angle the curve is no longer a straight line.

REFERENCES

Abbott I H, and Doenhoff V, 1959, "Theory of Wing Sections", Dover publications, New York.

Abramowitz M, and Stegun I A, "Handbook of Mathematical Functions", Dover Publications, 19th edition, New York.

Alexander G H, 1994, "The Automation of Ship Motion Recording and Analysis", MSc Dissertation project, Department of Mechanical Engineering UCL.

Andrew R N, Baar J J M and Price W G, 1987, "Prediction of Ship Wave-making Resistance and Other Steady Flow Parameters Using Neumann-Kelvin Theory", RINA Transactions 1988.

Atwood, 1796, "Disquisition on the Stability of Ship", Philosophical Transactions of the Royal Society of London.

Baar J J M and Price W G, 1988, "Evaluation of the Wavelike Disturbance in the Kelvin Wave Source Potential", Journal of Ship Research, Vol. 32, No. 1, March.

Baar J J M and Price W G, 1988, "Developments in the Calculation of the Wave Making Resistance of Ships", Proc. R. Soc. London A 416, pp115-147.

Baba E, 1975, "A Study on the Free Surface Flow Around Bow of Slowly Moving Full Forms", Journal Society of Naval Arch. Japan, Vol. 137.

Bai K J, and Yeung R W, 1974 "Numerical Solution to Free Surface Flow Problems", 10th Symposium on Naval Hydrodynamics, Hamburg.

Batchelor G, 1973, "An Introduction to Fluid Dynamics", Cambridge University Press, ISBN 0521663962, London.

Bhattacharyya R, 1987, "Dynamics of Marine Vehicles", Publisher John Wiley and Sons Inc. ISBN 0-471-07206-0.

Bird M and Morrall A, 1986, "Research Towards Realistic Stability Criteria", Proceedings RINA, London Toro Hotel, 9-10 June.

Bishop R E D 1986 "Dynamics in Ship Design" The Naval Architect, July-August.

Blount D L, Codega L T. (1992, "Dynamic Stability of Planing Boats", Marine Technology, Vol. 29 No. 1, Jan 1992, pp 4-12.

BMT, 1994, "News: The Loss of Estonia", British Maritime Technology, November.

Bouguer, 1746, "Traite du Navire de la Construction et de les Mouvements", Paris.

Brard R, 1972 "The Representation of a Given Ship Form by Singularity Distribution when the Boundary Condition on the Free Surface is Linearized", Journal Ship Research, Vol. 16, No. 1, pp 79 – 92.

Burcher R K, 1972, "Developments in Ship Manoeuvrability", Transaction RINA.

Burcher R K,1980, "The Influence of Hull Shape on Transverse Stability", Transaction RINA.

Burcher R K, 1990, "Experiments into the Capsize of Ship in Head Seas", STAB90, Transactions RINA, pp82-89, Italy.

Clement 1982, "The BP Dynaplane High Speed Research Boat", High Speed Surface Exabition and Conference, High Speed Surface Craft Publicatiion Association Midlsex, UK, 1982.

Cohen H S, and Blount D L, 1986, "Research Plan for the Investigation of Dynamic Instability of Small High Speed Craft", SNAME Transactions, Vol 94, pp 197-214.

Comstock J P, 1986, "Principles of Naval Architecture", 7th reprinting, Library of congress catalogue card No. 67-20738, December, USA.

Dallinga J J et al, 1998, "Excessive Rolling of Cruise Ships in Head and Following Waves", Int. conf. on Ship Motions RINA, 18 – 19 February, London

Dawson C W, 1977, "A Practical Computer Method for Solving Ship Wave Problem" 2nd Int. Conference Numerical Ship Hydrodynamic Berkeley.

Deakin B, 1990, "The Development of Stability Standards for UK Sailing Vessels", RINA.

Dommermuth D G and Yue D K P, 1987, "Numerical Simulations of Nonlinear Axisymmetric Flows with a Free Surface", Journal of Fluid Mechanic, Vol 178, pp 195-219.

Dudziak J, 1975, "Safety of a Vessel in Beam Seas", Ship Research Institute Gdansk Technical University Poland, Proceedings of International Conference on Stability of Ships and Ocean Vehicles, March, Glasgow Scotland.

Emerson A, 1967, "The Calculation of Ship Resistance - an Application of Guilloton's Method", Proceedings RINA, Vol. 109, No. 3, July, pp241 - 248.

Evans, 1992, "Fluid Mechanics and its Applications", Publisher Kluwer Academic, ISBN 0792316681.

Faltinsen O M, 1990, "Sea Loads on Ships and Offshore Structures", Cambridge Univ. Press, ISBN 0521 37285 2.

Falzarano J M and Troesch A W, 1990, "Application of Modern Geometric for Dynamical to the Problem of Vessel Capsizing with Water on Deck", 4th Int. Conf. on Stability of Ship and Ocean Vehicles, STAB90, September, Naples Italy.

Ferguson A M and Conn C, 1970, "The Effect of Forward Speed Motion on the Transverse Stability of a Displacement Vessel", The Institution of Naval Architecture paper No. 13, 13th January.

Gadd G E, 1975, "A Method of Computing the Flow and Free Surface Wave Pattern Around Full Forms", Transactions RINA, pp207 - 219.

Ha T. B., 2000, "A Three Dimensional Prediction of the Seakeeping Performance of High Speed Marine Vehicles", SSRC University of Strathclyde, Glasgow.

Haskind M D, 1953, "The Hydrodynamic Theory of the Oscillation of a Ship in Waves" Technical Research Bulletin No. 1-12, pp 3-43, transactions of the Society of Naval Architects and Marine Engineers, Vol 78, pp 250-287.

Havelock, 1923, "Studies in Wave Resistance", Published by the Office of Naval Research, Washington D.C. 1966, pp 3-38.

Hendrix D and Noblesse F, 1995, "Effect of Hull Discretization on Steady Free Surface Flow Calculations", Journal of Ship Research, Vol. 39, No. 1, March, pp 42 - 52.

Hess and Smith, 1962, "Calculation of Non-Lifting Potential Flow about Arbitrary Three Dimension Bodies", Douglas Aircraft Division Report No. E.S. 40622.

Hess and Smith, 1964, "Calculation of Non-lifting Potential Flow About Arbitrary 3D Bodies", Journal of Ship Research, September.

Hess and Smith, 1967, "Calculation of Potential Flow about Arbitrary Bodies", Progress in Aeronautical Sciences, Vol. 8, 1st edition 1967.

Hunt J C R, 1995a, "Practical and Fundamental Developments in the Computational Modelling of Fluid Flows", Journal of Mechanical Engineering Science, Vol. 209, p297-314.

Hunt J C R, 1995b, "Practical and Fundamental Developments in the Computational Modelling of Fluid Flows", 81st Thomas Hawksley Memorial Lecture, Proc Inst. Mech. Engrs Vol. 209, p397.

Ikeda and Katayama, 1996, "A Study on Transverse Instability of Planing Craft at High Speed in Calm Water", Proceedings of 3rd Korea-Japan Joint Workshop on Ship and Marine Hydrodynamics. 117-124.

Ikeda and Katayama, 2000, "Stability 9f High Speed Craft", Contemporary Ideas on Ship Stability ELSEVIR Science Ltd., pp401-409.

ITTC 21st, 1996, Workshop on Stability of the 19th international Towing Tank Conference, Norwegian Marine Technology, Norway, 5-11 Sep. 1996

ITTC 22nd, 1999, "Specialist Committee on Ship Stability", proceeding of the 22nd international Towing Tank Conference, Seoul and Shanghai.

ITTC 23rd, 2002, proceeding of the 23rd international Towing Tank Conference, Vol. II, Venice Italy Sep 8-14 2002.

Kaps H and Kastner S, 1990, "On the Determination of Ship Stability During Service", STAB 90, RINA Proceedings, pp226-231, Naples, Italy.

Kara F, 2000, "Time Domain Hydrodynamic and Hydroelastic Analysis of Floating Bodies with Forward Speed", SSRC University of Strathclyde, Glasgow.

Kara F and Vassalos D, 2005, "Time Domain Computation of the Wave-Making Resistance of Ship", Journal of Ship Research, Vol. 49, No. 2, June 2005, pp 144-158.

Kastner S, 1986, "Operational Stability of Ship and Safe Transport Cargo" Inter. Confe. On Stability of Ship and Ocean Vehicles, Gdansk, Sep. 1986.

Katz J O de, 1990, "The Numerical Modelling of the Ship Motions and Capsizing in Severe Seas", Journal of Ship Research, Vol. 34, No.4, Dec, pp289-301.

Katz J and Plotkin A, 1991, "Low Speed Aerodynamics from Wing Theory to Panel Methods", Mc Graw Hill International, ISBN 0-07-100876-4.

Kim K J and Jang Y, 1996, "Investigation of the Effect of Bulbous Bows on the Ship Wave Characteristics by CFD", KOJAM' 96, Daejeon.

Kim K J and Kim H C, 1997, "Application of CFD in Ship Design", International Conference, Ulsteinvik.

Kirsi K T and Paulling R, 1990, "Prediction of Critical Wave Conditions for Extreme Vessel Response in Random Seas", STAB 90, RINA Proceedings, pp386-394, Naples Italy.

Kobylinski L, 1975, "Rational Stability Criteria and Probability of Capsizing", STAB 75, RINA Proceedings, Gdansk Poland.

Kobylinski and Jens, 1986, "IMO Activities in Respect of International Requirements for the Stability of Ships", 3rd STAB Conference, Gdansk Poland.

Kobylinski L, 1990, "On the Possibility of Establishing Rational Stability Criteria", STAB 90, RINA Proceeding, pp501-511, Naples Italy.

Kroukovsky B V and Jacops W R, 1657, "Pitching and Heaving Motions of a Ship in Regular Waves" Transactions of the Society of Naval Architects and Marine Engineers, Vol 65, pp 590-632.

Kuo C and Odabsi Y, 1974, "Alternative Approaches to Ship and Ocean Vehicle Stability Criteria", The Naval Architect, July.

Kuo C, Vassalos D, J G Alexander and D A Barrie, 1986, "In Corroborating Theoretical Advances in usable Ship Stability Criteria", The Safe-ship Project International Conference, RINA, May.

Kuo C, 1997, "Application of the Safety Case Concept to High Speed Craft", Fast Ship 97, pp 381-389.

Kupras L K, 1981, "Optimisation Method and Parametric Study in Precontracted Ship Design", International Shipbuilding Progress, Vol. 23.

Larsson L, 1998, "Will Computational Fluid Dynamics Completely Take the Role of Model Testing", Int. Conference in Hydrodynamics, WEMT 98, the Netherlands.

Lewis V E, 1988, "Principles of Naval Architecture", 2nd revision Vol. I, published by SNAME, ISBN 0-939773-00-7.

Liangzi C and Hsiung C C, 1990, "A Simple Method of Computing Wave Resistance, Wave Profile and Sinkage and Trim of Transom Stern Ships", 19th International Towing Tank Conference, September, Madrid, Spain.

Lundgren and Storch 1984 "Small Fish Boat Stability A Case Study", Marine Technology, Vol. 21, No. 4, Oct 1984.

Lyon T D and Mistre F, 1985, "A Computer Based Method for the Preliminary Design of Ships", Journal of Ship Research, Vol. 29, No. 4, Dec, pp 251-269.

Mascio A Di, Landrini M and Compana E, 1996, "On the Modelling of the Flow Past a Free Surface Piercing Flat Plate", Institute Nazionale per Studi ed Esperienze di

Architettura Navale, 21st Symposium on Naval Hydrodynamics, July, pp177 – 184, Italy.

Michell J H, 1898, "The Wave Resistance of a Ship", Philosophical Magazine, London, Seris. 5, Vol. 45, pp 100-123.

Miyata H, 1997, "Time Marching CFD Simulation for Moving Boundary Problems", 21st Symposium on Naval Hydrodynamics, Tokyo.

Morral A, 1980, "The Gaul Disaster An Investigation into the Loss of a Large Stern Trawler", Transactions of RINA.

Moseley C, 1850, "On Dynamical Stability and the Oscillation of Floating Bodies", Philosophical Transactions of RINA.

Newman J N, 1978, "Marine Hydrodynamics", 2nd edition, published by Halliday Lithograph Corp. USA, ISBN 0-262-14026-8.

Newman J N, 1987, "Evaluation of the Wave Resistance Green Function: Part 1- The Double Integral", Journal of Ship Research, Vol. 31, No. 2, July, pp 79-90.

Newman J N, 1987, "Evaluation of the Wave Resistance Green Function: Part 2 - The Single Integral on the Centerplane", Journal of Ship Research,Vol. 31, No. 3, Sept.

Newman J N, 1998 "Evaluation of the Wave Resistance Green Function Near the Singular Axis", 3rd International Workshop on Water and Floating Bodies, April, pp145-150.

Noblesse F, 1981, "Alternative Integral Representations for the Green Function of the Theory of Ship Wave Resistance", Journal of Engineering Mathematics, Vol. 15, No. 8, pp 241 – 265.

Noblesse F and Chen C Y, 1983, "Preliminary Numerical Study of a New Slender Ship Theory of Wave Resistance", Journal of Ship Research, Vol. 27, No. 3, September, pp172 - 186.

Noblesse F, 1984, "Convergence of a Sequence of Slender Ship Low Froude Number Wave Resistance Approximations", Journal of Ship Research, Vol. 28, Sept pp155-162.

Ohkusu M and Iwashita H, 1989, "Hydrodynamic Forces on a Ship Moving at Forward Speed in Waves", J.S.N.A. Japan, Vol. 166, pp 88 – 109.

Ogilvie T F, 1968, "Wave Resistance the Low Speed Limit", Report No. 002 Dep. Naval Arch. Eng. Univ. Michigan.

Ogilive T F and Tuck E O, 1969, "A Rational Strip Theory for Ship Motions, Part 1" Report No. 013, The Department of Naval Architecture and Marine Engineering University of Michigan Ann Arbor.

Paulling J R and Wood P A, 1975, "Ship Capsizing in Heavy Seas The Correlation of Theory and Experiments", International Conference on Stability of Ships and Ocean Vehicles, University of Strathclyde.

Percival S, Hendrix D and Noblesse F, 2001, "Hydrodynamic Optimization of Ship Hull Forms", Applied Ocean Research, Vol. 23, November, pp 337- 355.

Proshaska C W, 1951, "Influence of Ship Form on Transfers Stability", Transactions RINA.

Proshaska C W, 1947, "Residual Stability", Transactions RINA.

Putnam N, 1994, "The Effects of Loading and Trim on the Manoeuvring Characteristics of a Ship", B.Eng. Dissertation project, Department of Mechanical Engineering, UCL.

Rahola, 1939, "The Judging of Stability of Ships and Determination of the Minimum of Stability", PhD thesis, University of Helsinki.

Rawson K J and Tupper E C 1983, "Basic Ship Theory", Vol. 1, 3rd Edition, Publisher Longman Group Ltd, ISBN 0582-30528-4.

RINA, 1996, "Marine Software for small craft", One Day Workshop, London.

RINA, 1997, "Marine Software for small craft", One Day Workshop, London.

RINA, 1998, "Marine Software for small craft", One Day Workshop, London.

RINA, 1999, "Marine Software for small craft", One Day Workshop, Southampton.

RINA, 2000, "Marine Software for small craft", One Day Workshop, Southampton.

RINA, 2001, "Marine Software for small craft", One Day Workshop, Southampton.

Shahrbaf A, 1992, "Stability criteria for Sea going Cargo Ships", MSc Dissertation, Department of Ship Research, Technical University of Gdansk.

Shuanxing D, Hudson D A, Price W G and Temarel P, 1999, "Comparison of Numerical Evaluation Techniques for the Hydrodynamic Analysis of a Ship Traveling in Waves" Transactions RINA, paper 214.

Skaribas N, 1994, "Transverse Stability of Vessels with Large Changes of Draught and Trim", BEng Dissertation project, Department of Mechanical Engineering, UCL, April.

Tim D and Mistre F, 1985, "A Computer Based Method for the Preliminary Design of Ships" Journal of Ship Research, Vol. 29, December, pp 251-269.

Tupper E, 1991, "Naval Architecture", published by Reed Educational and Professional Ltd, ISBN 0 7506 25295.

Ursell F, 1960, "On Kelvin's Wave Patetern", Journal Fluid Mechanics, Vol. 8, pp 418 – 431.

Ursell F, 1988, "On the Theory of the Kelvin Ship Wave Source: Asymptotic Expansion of an Integral", Proc. Royal Society of London, A 418, pp 81 – 93.

Ursell F, 2000, "The Metacentre in The Stability of Ships, Some Difficulties", 15th Int. Workshop on Water Wave and Floating Bodies.

Vassalos D and Kuo C, 1990, "Advances in the Stability Assessment of Semi-Submersibles", The Royal Institute of Naval Architecture, STAB 90, Naples Italy, pp527-534.

Vassalos D, 1996, Workshop on Stability of the 19th international Towing Tank Conference, Norwegian Marine Technology, Norway, 5-11 Sep. 1996, pp 121-131.

Vassalos D, 1998, "Shaping Ship Safety: The Face of the Future", Inaugural lecture delivered at the University of Strathclyde Glasgow, 5th of March.

Vassalos D, Ha T B, Kara F, 2000, "A Comparative Study of three Dimension Frequency Domain and Time Domain Approaches to Hydrodynamic Loads of HSC", Report SSRC University of Strathclyde, Glasgow.

Walkeling B. P., Sproston J. L., and Millward A., 1984, "Transverse stability of a Fast Round Bilge Hull", International Conference on Design Considerations foe Small Craft, 13-15 Feb 1984

Walker F W, 2002, "The Capsizing of S S Daphne in 1883 the World's Worst Launching Tragedy and Its Consequences", Int. Conf. RINA, 13 – 14 March, London.

Wehausen J V and Laiton E V, 1960, "Surface Wave", In Handbuch des physik, vol. 9 pp. 446-778 Berlin, Springer-Verlag.

Wu G X, 1994, "Hydrodynamic Forces on a Submerged Sphere Undergoing Large Amplitude Motion", Journal of Ship Research, Vol. 38, No. 4, pp 272-277.

Zienkiewicz O C, Lewis R W and Stagg K G, "Numerical Methods in Offshore Engineering", A Wiley – Interscience publication, ISBN 0 471 995916.

APPENDIX A

A.1 INTERACTION OF THE STATIC FORCES

Static stability is well understood and is described in many textbooks, for example Rawson and Tupper (1983), and Lewis (1988). To draw attention to sensitivity of ship stability due to any changes, and basic definitions of key words that have been used in the thesis, they are briefly reviewed in Sections A.1. to A.5.

The weight (W) of any freely floating body, which is wholly or partially immersed in a fluid, is supported by the summation of all hydrostatic pressure components acting on the wetted surface area of the body. The vertical force caused by displacement of the fluid is called buoyancy force (D). In other words, a freely floating body obeys *Archimedes Principle,* indicating that the buoyancy force increases as the weight of the floating body increases. By using this principle, it can easily be seen that a change in the buoyancy force is equal to a corresponding change on the vessel load. This principle applies to both submarines and ships.

Generally the weight of a freely floating body, which passes downward through the centre of gravity (C of G), must be equal to the buoyancy or the resultant force, which passes upward through the centre of buoyancy (B) along the same vertical line. Providing no external forces or moments act on the body, the condition is known as *static equilibrium*, and the body remains *stable* as shown in Figure A.1a.

Assuming that the positions of the masses in the floating body are not changed, a slight rotation from the static equilibrium condition will produce a moment on the body. The case where this moment tends to return the body to its original position is called a *righting moment*. The righting moment relates to the location of the body's *metacentre* point (M) as well as the corresponding *righting arm* (GZ). The righting arm or righting lever (GZ) is the horizontal distance parallel to the new water line between the centre of gravity and the new direction of the buoyancy force as shown in Figure A.1b.

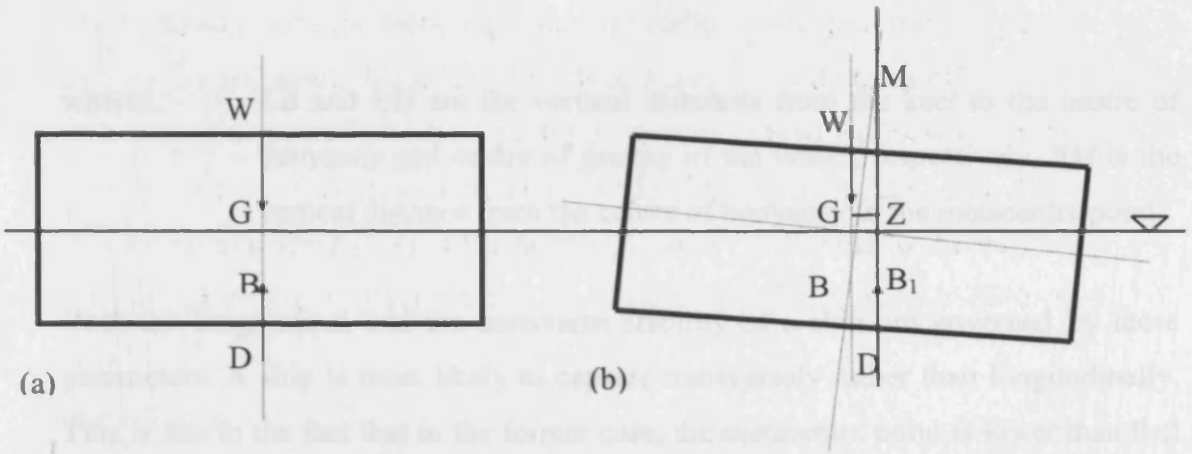

Figure A.1 Transverse cross section of a mid-ship, (a) Hydrostatic equilibrium (b) inclined by a small heel angle

Referring to the above figure, it can be seen that the centre of rotation (M) is the intersection point between the directions of the original buoyancy force (passing through B) and the new buoyancy force direction (passing through B_1). This is due to the inclined body causing a new distribution of pressures, which act on the wetted surface of the body, although the total force is the same. It is therefore evident that the metacentre position with respect to the centre of gravity (GM) will determine the stability of the body. In other words, if the location of the metacentre point is below the centre of gravity, the moment produced by the weight will tend to increase the inclination angle. In this condition the body will not necessarily capsize, and in fact will often come to rest at angle of heel called the angle of *loll*. In this case, the condition is known as *Negative Stability*. Where the centre of gravity is located on the metacentre point of the body is known as *Neutral Stability*. For ships this condition can only be maintained for very small heel angles, if the initial shape of the vessel is regarded as being a cylinder having a diameter equal to the breadth of the vessel. Alternatively, if the position of the metacentre point is above the centre of gravity such that the moment will tend to decrease the inclination angle, which in turn may return the body to its original position, this condition is known as *Positive Stability*.

Therefore, the distance of the metacentre point (M) from the centre of gravity (G) is known as m*etacentric height* and normally denoted as either H or GM. The metacentric height provides an indication of the stability of any floating body.

$$GM = KB + BM - KG \qquad \text{(A.1)}$$

where: KB and KG are the vertical distances from the keel to the centre of buoyancy and centre of gravity of the vessel, respectively. BM is the vertical distance from the centre of buoyancy to the metacentre point.

Both the longitudinal and the transverse stability of a ship are governed by these parameters. A ship is most likely to capsize transversely rather than longitudinally. This is due to the fact that in the former case, the metacentre point is lower than that of the latter case. In addition, the parameters that dictating the transverse stability of the ship vary much more rapidly than those of the longitudinal case. The parameters are explained in the following sections.

A.2 ASSESSMENT OF INITIAL METACENTRIC HEIGHT

Consider a vessel of length L, breath b and draft d, which is floating at waterline W_oL_o. Now suppose that the vessel is inclined by a small angle φ to waterline W_1L_1 as shown in Figure A.2. Since the vessel is wall-sided, W_oL_o and W_1L_1 must intersect on the centre line. A wedge of buoyancy will move across the vessel, and the centroid of the wedge will move from g_0 to g_1. If the underwater volume of the vessel is ∇ and the volume of the wedge of buoyancy is v then the horizontal distance between B_0 and B_1 is:

$$B_0B_1 = \frac{vg_0g_1}{\nabla} \qquad \text{(A.2)}$$

or, equally, equation 1.2 can be written as:

$$B_0B_1 = B_0M\sin\varphi \qquad \text{(A.3)}$$

where: the φ is a small inclination angle.

Eliminating B_0B_1 from equations A.2 and A.3, assuming for $\varphi \leq 10^\circ$ approximately, $\tan\varphi \approx \sin\varphi \approx \varphi$.

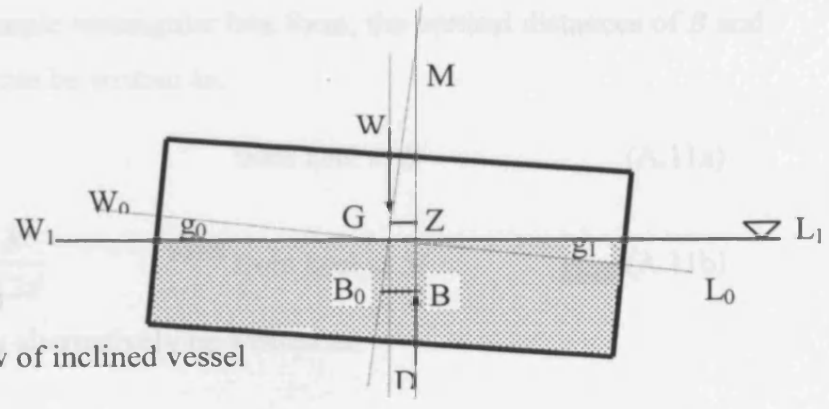

Figure A.2 Transverse view of inclined vessel

The horizontal distance between the centres of volume of two wedges, and the volume of each wedge can be obtained from:

$$g_0g_1 = 2 * \frac{2}{3} * \frac{b}{2} = \frac{2b}{3} \qquad \text{(A.4)}$$

$$v = \frac{1}{2} * \frac{b}{2} * \frac{b}{2} * \tan\varphi * L = \frac{2b^2L}{8}\tan\varphi \qquad \text{(A.5)}$$

respectively.

The moment of volume v about the longitudinal axis is:

$$g_0g_1 * v = \frac{2b}{3} * \frac{Lb^2}{8}\tan\varphi = \frac{Lb^3}{12}\tan\varphi \qquad \text{(A.6)}$$

Note that $\frac{Lb^3}{12}$ is the second moment of area of a rectangle about the axis through the centriod. Substituting equation A.6 into A.2, we obtain:

$$B_0B_1 = \frac{Lb^3}{12}\tan\varphi\frac{1}{\nabla} \qquad \text{(A.7)}$$

Since ∇ is the underwater volume of the vessel which is equal to $L*b*d$ equation A.7 becomes:

$$B_0B_1 = \frac{b^2}{12d}\tan\varphi \qquad \text{(A.8)}$$

By inserting this expression for B_0B_1 into 1.3 the transverse metacentric height BM can then be found:

$$B_0M = \frac{b^2}{12d}\frac{\tan\varphi}{\sin\varphi} \qquad \text{(A.9)}$$

which, based on the small φ angle approximation, can be written as:

$$B_0M = \frac{b^2}{12d} \qquad \text{(A.10)}$$

Using the geometry of a simple rectangular box form, the vertical distances of B and M measured from the keel can be written as:

$$KB = \frac{d}{2} \qquad \text{from keel to } B \qquad \text{(A.11a)}$$

$$KM = \frac{d}{2} + \frac{B^2}{12d} \qquad \text{from keel to } M \qquad \text{(A.11b)}$$

The second expression may alternatively be written as:

$$KM = \frac{d}{2} + \frac{I}{\nabla} \qquad \text{(A.11c)}$$

where: I denotes the second moment of area about the longitudinal axis. Therefore, according to KB (A.11a) and equation A.9, for small angle φ the general form of the formula for KM (A.11c) can be written as:

$$KM = KB + BM \qquad \text{(A.11)}$$

Considering equation 1.11 for a rectangular box shape, the effect of changing draft on the position of the metacentre can be written as:

$$KM = \frac{d}{2} + \frac{b^2}{12d} \qquad \text{(A.11d)}$$

To show the effect of geometry and loading condition on the position of metacentre from either the equation A.11d or equation A.11, it can be observed that when the draft d is small, a large value of BM occurs. Whilst for large draft the value of KB will also be large, BM steadily becomes smaller. Hence for very large draft we have approximately:

$$KM = \frac{d}{2} = KB$$

Since $\mathrm{BM} \approx 0$

For a complex shape such as for a ship, the calculation of KB, BM, and KG is more complicated. The volume transferred from one side to the other side in an element wedge of length δL with beam b can be written as:

$$\delta v = \delta L(\frac{1}{2} * \frac{b}{2} * \frac{b}{2} \tan\varphi) \qquad \text{(A.12)}$$

$$\delta v = (\frac{b^2}{8} \tan\varphi)\delta L \qquad \text{(A.13)}$$

The moment of the transferred volume of this wedge in a direction parallel to WL is given by:

$$dv = \frac{2b}{3} * \frac{b^2}{8} \tan\varphi dL \qquad \text{(A.14)}$$

and hence, the horizontal component shift BB' and the vertical shift $B'B_1$ of B to the new position are:

$$BB' = \frac{1}{\nabla}\int_0^L \frac{b^3}{12}\tan\varphi dL$$
$$BB' = BM\tan\varphi \tag{A.15}$$

and:

$$B'B_1 = \frac{1}{\nabla}\int_0^L \frac{b^2}{8}\tan\varphi\frac{1}{3}b\tan\varphi dL$$
$$B'B_1 = \frac{I}{2\nabla}\tan^2\varphi = \frac{BM}{2}\tan^2\varphi \tag{A.16}$$

For a wall-sided ship, by projection of new position of B on to a plane parallel to W_1L_1 the righting arm can be obtained as:

$$\begin{aligned} GZ &= BB'\cos\varphi + B'B_1\sin\varphi - BG\sin\varphi \\ &= BM(\sin\varphi + \frac{\tan^2\varphi}{2}\sin\varphi) - BG\sin\varphi \\ &= \sin\varphi(BM - BG + \frac{BM}{2}\tan^2\varphi) \end{aligned} \tag{A.17}$$

Then:

$$GZ = \sin\varphi(GM + \frac{BM}{2}\tan^2\varphi) \tag{A.18}$$

These values can be determined using numerical methods such as Simpson's Rule. More details can be found in Lewis (1988), Rawson and Tupper (1983) and, Tupper (1991) and others.

A.3 INFLUENCE OF GEOMETRY ON *B* AND *GM*

As discussed in the section (A.1), a ship is most likely to capsize transversely rather than longitudinally. Therefore the main geometric parameters of body form that affect transverse stability are discussed in the following sections.

A.3.1 VARIATION OF BEAM

An increase in beam may result in a small increase in draft due to added weight of structure however, the difference in displacement between two water lines (new and original) is equal to the added displacements of port and starboard. Then the

waterline area is increased too, and the *BM* will increase proportional to the square of beam in accordance with equation A.9. Therefore, the righting arm (*GZ*) increases as shown in equation A.18. When the inclination angle is small, according to equation A.18, the metacenteric height and consequently the righting moment increase. Figure A.3 shows this effect, that B_1 moves to B_2, therefore GM_2 is greater than GM_1. But they are not affected at large angles of inclination, where either the deck touches the water or the bottom comes out of the water, since the projected beam becomes smaller than the initial condition.

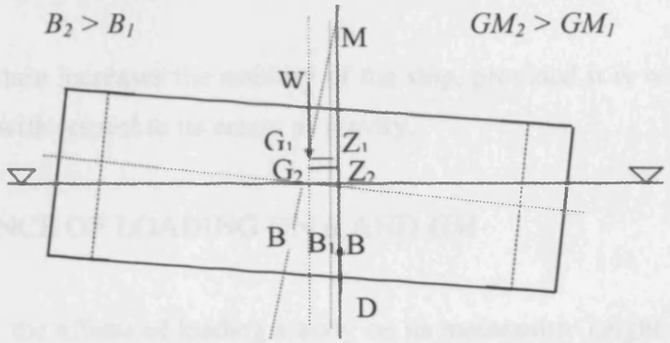

Figure A.3 Effect of beam on righting arm

A.3.2 VARIATION OF DEPTH

An increase in depth of the hull will cause an increase in the weight of the structure. Consequently, draft and the *C* of *G* rise up and at all inclination angles the righting arms *GZ* decrease, due to the upward shift of the *C* of *G* caused by the added weight of the structure. Additionally, superstructure and other topside items will increase this effect further. Thus the net effect of increasing depth on righting arm and metacentric height is to decrease these significantly, by the amount that the *C* of *G* is increased, until the deck edge is immersed. This is illustrated in Figure A.4. The new position of G_1 is higher than *G* due to the new depth, therefore GZ_1 is smaller than *GZ*.

$KG_1 > KG$ then $G_1Z_1 < GZ$

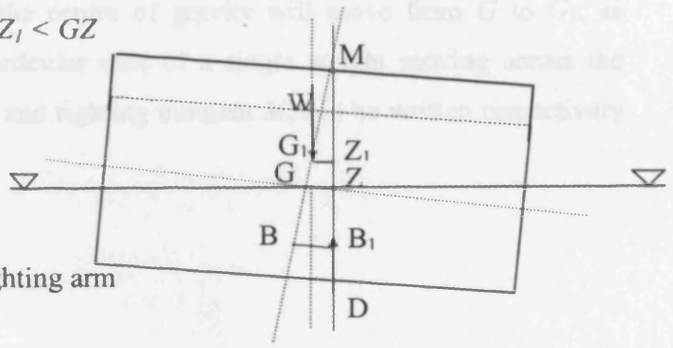

Figure A.4 Effect of depth on righting arm

A.3.3 CHANGE OF FORM ABOVE THE WATERLINE

In the upright position, changes above the waterline such as increasing flare can affect the stability in a similar way as change in beam, except that a major effect on the righting arm will be delayed until larger angles of heel are reached. Then increasing flare increases the righting arm at larger angles. Alternatively, the stability can decrease by underwater change of body usually at bow and stern. More details of this are given in Burcher (1980) and Lewis (1988).

The superstructure increases the stability of the ship, provided it is watertight. Care must be taken with respect to its centre of gravity.

A.4 INFLUENCE OF LOADING ON *B* AND *GM*

In this section, the effects of loading a body on its metacentric height are discussed. A small load is added on board of a ship on the centreline exactly above the ship's *C* of *G*. Hence, both *C* of *B* and *C* of *G* rose due to increasing draft. At this time, this weight is assumed to be a part of the ship's weight, and it may be shifted transversally (both horizontally and vertically). In addition, it is assumed that the added weight is very small in comparison with the ship's weight, and also the water plane area is not changed due to a small increase of the draft.

A.4.1 WEIGHT SHIFTED HORIZONTALLY ON THE DECK

Consider a vessel of weight W with centre of gravity G on the centreline and centre of buoyancy at B, with transverse metacentre at M. If a small weight w is moved across the vessel horizontally, the centre of gravity will move from G to G_1, as shown in Figure A.5. In the particular case of a single weight moving across the vessel, then heeling moment M_h and righting moment M_r can be written respectively as:

$$M_h = w * y * \cos\varphi$$
$$M_R = W * GG_1 \qquad \text{(A.19)}$$

where the angle is small and the position of M can be regarded as fixed. GG_1 is parallel with the waterline of the vessel:

$$GG_1 = GM \sin\varphi \qquad \text{(A.20)}$$

Then as the heeling moment is equal to the righting moment, the heeling angle satisfies:

$$\tan\varphi = \frac{w * y}{W * GG_1} \qquad \text{(A.21)}$$

A more practical approach is to consider different weights being moved transversally at various points away from the centreline of the ship.

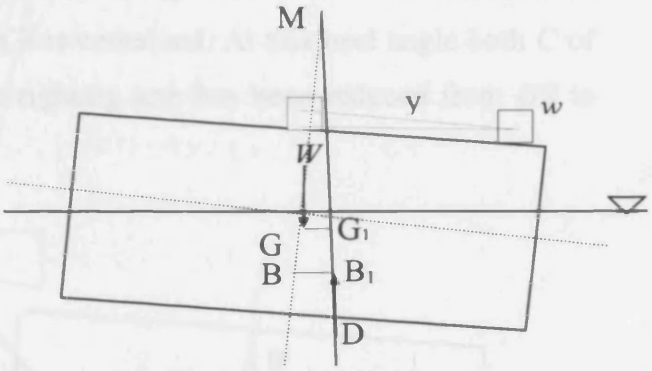

Figure A.5 Effect of shifting weight on C of G and C of B

If the small weight w is moved longitudinally, G_L will move to G_{1L} and the vessel will rotate about the Y-axis. The state depending upon being aft or fore is referred to the vessel as trimmed, *trim Aft* or *trim Fore*.

A.4.2 WEIGHT SHIFTED VERTICALLY

It is assumed that, if the small weight w on the deck of the ship, is displaced vertically, from the deck into a hatch, then the C of G of the ship will change downward from G to G_1. If Z denotes the height difference from the deck Z_1 to the hatch Z_2, then GG_1 can be obtained from:

$$\frac{GG_1}{Z} = \frac{w}{W} \qquad \text{(A.22a)}$$

then:
$$GG_1 = \frac{w}{W}(Z_2 - Z_1) \qquad \text{(A.22)}$$

Hence for any vertical downward movements of weight, *GM* increases, whereas the GM decreases for any upward movements.

A.4.3 FREE SURFACE OF LIQUID IN TANK

If a tank of a ship is not full, where the liquid is free to move continuously as a result of the vessel being heeled by any force, the centre of gravity of the liquid will move from *g* to g_2. Hence the *G* shifts to G_2 as shown in Figure A.6. The lower case is used to denote the liquid in the tank in which it is contained. At this heel angle both *C* of *G* and the *C* of *B* have moved, and the righting arm has been reduced from *GZ* to G_2Z.

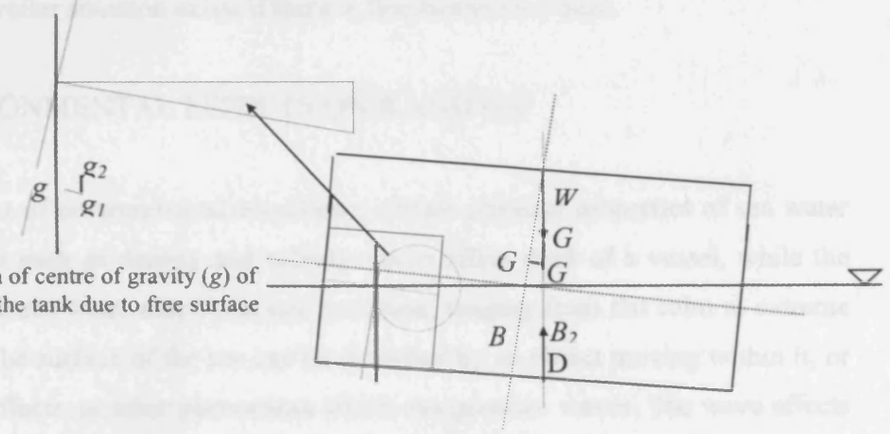

Variation of centre of gravity (*g*) of liquid in the tank due to free surface

Figure A.6 Effect of free surface in a tank on centre of gravity

At small angles of inclination, the liquid in the tank has a metacentre located at a distance equal to i / v above its centre of gravity in the upright position, where *i* is the moment of inertia of the surface of the liquid and *v* is the volume of the displaced liquid. Due to movement of wedges of the liquid from one side to anther, a moment results in horizontal and vertical movement of *g*. referring to Figure A.6 and equations A.4 to A.6 this can be written as:

$$gg_1 = \frac{i}{v}\tan\varphi \qquad \text{for horizontal movement} \qquad (A.23)$$

$$g_1g_2 = \frac{i}{2v}\tan^2\varphi \qquad \text{for vertical movement} \qquad (A.24)$$

Hence C of G for the ship will move to G_2, which can be obtained from

$$GG_1 = \frac{i}{v}\tan\varphi(\rho\frac{v}{\nabla}) = \rho\frac{i}{\nabla}\tan\varphi \qquad \text{(A.25)}$$

$$G_1G_2 = \rho\frac{i}{2\nabla}\tan^2\varphi \qquad \text{(A.26)}$$

The free surface effect is always independent of the volume of liquids on board or in the tank. Even a very small amount of liquid can have a large effect if the free surface is large. It is also independent of the position of the tank, either vertically or horizontally. As it is obvious, the effect is highly dependent on the size of the free surface especially on the width, in the same way that ship beam has a large effect on the *GM*. A similar situation exists if there is floodwater on a deck.

A.5 ENVIRONMENTAL EFFECTS ON *B* AND *GM*

In the context of environmental conditions, certain physical properties of sea water are important such as density and salinity which affect draft of a vessel, while the surface of the sea water may be in any condition, ranging from flat calm to extreme roughness. The surface of the sea can be disturbed by an object moving within it, or on it, wind effects, or other phenomena which can generate waves. The wave effects on seagoing vessels may generally be categorised as head, beam, quartering, or following seas depending on the direction in which they act. Other important wave factors are amplitude, period and length. Further environmental phenomena include icing and wind. They can seriously effect the locations of C of *B* and height of *GM*.

APPENDIX B

B.1 THE TRANSFORMATION MATRIX:

In order to use equations (3.43) to (3.48) a transformation of data is required. Referring to Figure 4.1 there are two coordinates systems, the Global coordinate system (GCS), and a Local coordinate system (LCS), which shows orientation of the panel with respect to the GCS. It is assumed that the LCS is fixed on the centre of the panel and at least one of its axes is parallel to one side of the panel. Therefore, the nodes of the panel should transfer from the GCS to the LCS on the panel. There are linear and rotational transformations for data from the GCS to the LCS, and subsequently for results from LCS to GCS.

The linear transformation is from the GCS to the centre of each panel. There is only a linear transformation and it can be defined as a distance of centre of a panel to the GCS. The centre of the panel can be determined from the three corresponding nodes of the panel.

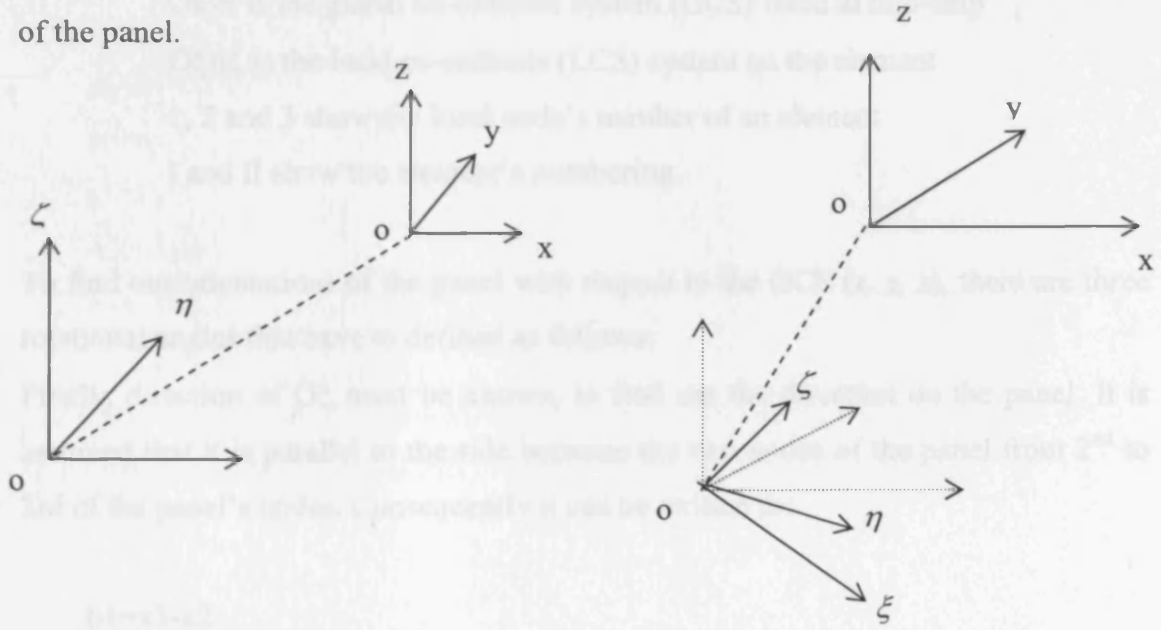

Figure B.1 Showing liner and rotational transformation

The rotational transformation is in the form of a transformation matrix to transfer the corresponding coordinates of all nodes of a panel from the GCS to the LCS on the panel, which is assumed to be fixed on the centre of the panel. Therefore the procedure can be defined as follows:

First of all a panel is a triangular shape, which in any circumstances three nodes in space make a flat shape. These three nodes are located on the ship hull, as they chosen in the mesh generation technique from tabulated hull offsets, and it is explained in detail in Chapter 5. Secondly, the origin of the LCS (ξ, η, ζ) is assumed on the centre of the panel. Two axes of the LCS are assumed parallel with two sides of the panel as shown on Figure B.2, and the third one is perpendicular of the panel outwards.

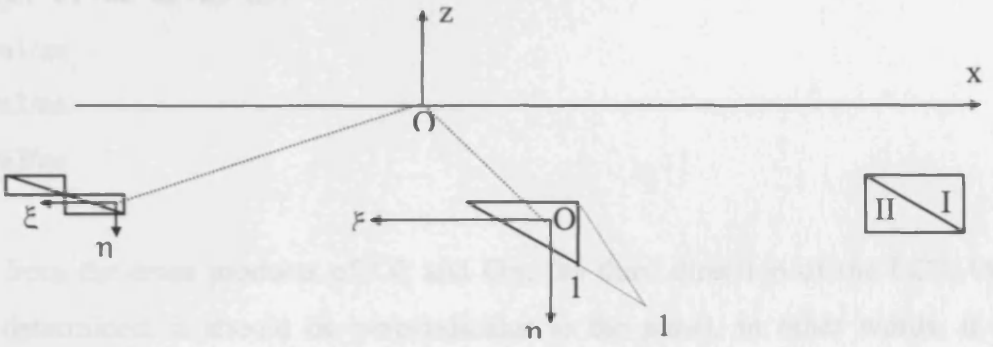

Figure B.2 axes coordinates systems

Where:

Oxyz is the global co-ordinate system (GCS) fixed at mid-ship

Oξηζ is the local co-ordinate (LCS) system on the element

1, 2 and 3 show the local node's number of an element

I and II show the element's numbering.

To find out orientations of the panel with respect to the GCS (x, y, z), there are three rotational angles that have to defined as follows:

Firstly, direction of Oξ must be known, to find out the direction on the panel. It is assumed that it is parallel to the side between the two nodes of the panel from 2nd to 3rd of the panel's nodes. Consequently it can be written as:

b1=x3-x2

b2=y3-y2

b3=z3-z2

bb=(b1*b1+b2*b2+b3*b3)$^{1/2}$

b1=b1/bb

b2=b2/bb

b3=b3/bb

Secondly, the same method as above may be used to find Oη direction. It is assumed that the direction is parallel to side between the two nodes of the panel from 2nd to the 1st of the panel. Therefore it may be written as:

a1=x1-x2

a2=y1-y2

a3=z1-z2

aa=(a1*a1+a2*a2+a3*a3)$^{1/2}$

a1=a1/aa

a2=a2/aa

a3=a3/aa

Thirdly, from the cross products of Oξ and Oη, the third direction of the LCS, Oζ, may be determined, it should be perpendicular to the panel, in other words, it is normal to the plane Oξη, and it must be checked.

c1=a2*b3-a3*b2

c2=a3*b1-a1*b3

c3=a1*b2-a2*b1

cc=(c1*c1+c2*c2+c3*c3)$^{1/2}$

c1=c1/cc

c2=c2/cc

c3=c3/cc

Once all the elements of the transformation matrix for the panel are ready with the same number as the panel number it can be stored.

$$tr = \begin{Bmatrix} t_{11} & t_{12} & t_{13} \\ t_{21} & t_{22} & t_{23} \\ t_{31} & t_{32} & t_{33} \end{Bmatrix} = \begin{Bmatrix} a_1 & a_2 & a_3 \\ b_1 & b_2 & b_3 \\ c_1 & c_2 & c_3 \end{Bmatrix}$$